UNIVERSITY OF CALIFORNIA SAN DIEGO

Investigations into the nootropic effects of ethylene glycol derivatives of benzothiazole aniline

A dissertation submitted in partial satisfaction of the
requirements for the degree Doctor of Philosophy

in

Chemistry

by

Kyle Robert Berg

Committee in charge:

Professor Jerry Yang, Chair
Professor Seth Cohen
Professor Kevin Corbett
Professor Vivian Hook
Professor Stan Opella

2021

The dissertation of Kyle Robert Berg is approved, and it is acceptable in quality and form for publication on microfilm and electronically.

University of California San Diego

2021

DEDICATION

This dissertation is dedicated to my wife, Heidi Berg, who has been more loving, more patient, and more wonderful than I deserve.

EPIGRAPH

“To those who have eyes to see and ears to hear, it is clear that the Father and the Son are giving away the secrets of the universe!”

Neal A Maxwell

“I [the Lord] will give unto the children of men line upon line, precept upon precept, here a little and there a little; and blessed are those who hearken unto my precepts, and lend an ear unto my counsel, for they shall learn wisdom; for unto him that receiveth I will give more.”

2 Nephi 28:30

The Book of Mormon

TABLE OF CONTENTS

LIST OF FIGURES

LIST OF TABLES

LIST OF SUPPLEMENTARY FILES

Supplementary file 1: Data sheet for pulldowns and tandem mass tag mass spectrometry

LIST OF ABBREVIATIONS

3xTg	A model mouse organism exhibiting Alzheimer's Disease like symptoms
A137	Alanine at position 137
A137K	Alanine at position 137 mutated to Lysine
AD	Alzheimer's Disease
AMPA	A postsynaptic glutamate receptor
AP2	The Adapter Protein2 Complex
Aβ	beta amyloid
BL21	A bacterial cell line used for expression of recombinant proteins
BSA	Bovine Serum Albumin
BTA	Benzothiazole Aniline
BTA-EG_4	An analog of Benzothiazole aniline including a tail of four ethylene glycol repeats
BTA-EG_6	An analog of Benzothiazole aniline including a tail of six ethylene glycol repeats
CA	Alpha carbon
CB	Beta Carbon
CBCAHN	NMR Experiment where magnetization is passed from the Beta carbon to the alpha carbon, and then to the amide NH

CD	Circular Dichroism
Cfa	An engineered intein with high reaction rates named off of the cystein-phenylalanine-alanine consensus sequence among fast reacting inteins
CMV	Cytomegalovirus
CRISPR	Clustered regularly interspaced short palindromic repeats
DE3-BL21	A bacterial cell line used for the expression of recombinant proteins using the T7 promotor
DIV	Days in vitro
DMEM:F12	Dubelco's Modified Eagle's Medium mixed with Ham's F12 supplement at a 1:1 ratio
DMSO	Dimethyl Sulfoxide
DNA	Deoxyribonucleic acid
DTT	Dithiothreitol
EDTA	Ethylenediaminetetraacetic acid
EG	Ethylene glycol
FG12	Control plasmid for mammalian expression of GFP
Fiji	Fiji is just ImageJ
G393	Glycine at position 393
G393E	Glycine at position 393 mutated to glutamic acid

GAPDH	Glyceraldehyde-3-phosphate-dehydrogenase
GEP	Refers to the glycine-glutamic acid-proline loop that allows for promiscuity in Cfa inteins
GFP	Green fluorescent protein
Grb2	Protein involved in focal adhesion signaling
GST	Glutathione-s-transferase
HEPES	4-(2-hydroxyethyl)-1-piperazineethanesulfonic acid
HN(CO)CA	NMR experiment where magnetization is passe from the N-H amide to the carbonyl carbon, and then to the alpha carbon of an amino acid.
HSQC	Heteronuclear single quantum coherence
IPA	Isopropyl Alcohol or Isopropanol or 2-propanol
K_d	Dissociation constant
LCMS2/MS3	Liquid Chromatography followed by tandem or triple mass spectrometry
LEMO BL21	A bacterial strain designed for the expression of insoluble constructs
MDCK	A cell line derived from dog kidney cells
M	Molar
MHz	Mega hertz
mM	millimolar
µM	micromolar

MOI	Multiplicity of infection
mRNA	Messenger ribonucleic acid
NEB	New England Biolabs
N-H	Refers to the amide N-H of a given amino acid
NIH 3T3	A human fibroblast cell line
NMDA	N-methyl-d-Aspartate
NMR	Nuclear magnetic resonance
PBS	Phosphate buffered saline solution
PBS-MC	Phosphate buffered saline solution supplemented with magnesium and calcium
PC12	A rat cell line studied for its neuronlike properties
PEG	Polyethylene glycol
pGEX-5x-2	A plasmid used for the expression of Fascin1 found in Appendix A
ppm	Parts per million
Rab 35	A master regulator protein involved in vesicle trafficking
RNA	Ribonucleic acid
RPM	Revolutions per minute
SDS-PAGE	Sodium Dodecyl Sulfate Polyacrilamide Gel Electrophoresis
shRNA	Short hairpin RNA

SHSY-5Y	A human neuroblastoma cell line
siRNA	short interfering RNA
Src	A protein involved in focal adhesion signaling
TBST	Tris buffered saline solution with 0.1% tween-20
TCEP	Tris(2-carboxyethyl)phosphine
TMT	Tandem mass tag
TROSY	Transverse relaxation optimized spectroscopy
UCSD	University of California San Diego
WT	Wild type

ACKNOWLEDGEMENTS

I would like to thank the many people who made my studies possible at the University of California San Diego.

First, my wife Heidi Berg, who was crazy enough to follow me away from family to San Diego with our (then) two small children in tow to start my PhD studies. She has been so supportive of me in my efforts and has spent many long days caring for and supporting our family while I have been away in lab. Raising a family with three children in a two-bedroom apartment with no laundry machines or dishwashers in the apartment week after week was without question much more difficult than the summed total of work I did in lab. Heidi is the true hero in the story of my PhD completion. I cannot thank her enough, and I feel more loved by her than I can express with words.

Next, my three children, Jocelyn (age 7), Kaden (age 5), and Luke (age 2) who let the whole world know when Daddy leaves for work from the balcony of our apartment with a chorus of “BYE DADDY” and exuberant hugs and excited screams when I come home. They have all been so patient with Daddy, and not too disappointed, when early mornings and late nights at work sometimes makes them go all day without seeing me. They make sure I know I am loved and missed when I am gone. Our puppy Dash also makes sure I know he missed me when I get home from lab too.

I would like to thank all the members of the Yang lab, but most especially Aashish Shivkumar, who, when life and work was too much for me, picked up the slack, and cheered me up. I simply could not have accomplished what I did without his help. A special mention goes to Meihan Li who was always a good friend to bounce ideas off of, Geoffray Leriche who was one of my first mentors in lab, and Kristine Teppang for editing

my dissertation. I am also thankful for the edits and feedback on my dissertation from my brother, Brad Berg, who helped me see many areas that needed further explanation. I am very grateful to Carla Espinosa, who worked under me as an undergraduate. She expressed mounds of Fascin1 protein and helped me develop a Fascin1 overexpression system. I am also thankful for games of Super Smash Brothers with Sascha, Rachel, Kristine, and Alex, that helped me to blow off some steam, and to Lauren, who was always fun to chat with and who let me mentor her in cell culture, even when I was pretty new to cell culture myself.

I am very grateful to Dr. Jerry Yang, who I am certain had to be extremely patient with my many shortcomings as I grew as a scientist. He was very supportive in allowing me to balance my work and family life and for that I am very grateful.

I am thankful for my committee who supported me, provided ideas, and steered me in the right directions when needed. I am especially thankful for Dr. Kevin Corbett, who, outside of Dr. Yang, was my primary mentor and was always willing to take time out of whatever he was doing to support me.

This work would not have been possible without many collaborators. I would like to thank Lara Dozier of the Patrick lab at UCSD and Jacob Wozniak of the Gonzalez lab, for their help in completing experiments that would not have been possible in the Yang lab alone. Prof. Kevin Corbett was instrumental in helping me complete protein crystallography. I would also like to thank Prof. Galia Debelouchina, Prof. Stanley Opella, Dr. Sang Ho Park, Haley Siddiqi, and Daniela Castro for their help in designing and completing protein NMR experiments.

Chapters 2 and 3 are currently being prepared for submission for publication of the material. Kyle R. Berg, Aashish Shivkumar, Kevin C. Sibucao, Geoffray Leriche, Carla A. Espinoza, Lara Dozier, Gentry Patrick, Zied Gaieb, Christian Seitz, Rommie E. Amaro, Hyun-Hee Park, Hyang-Sook Hoe, Jacob Wozniak, David Gonzalez. The dissertation author is a primary researcher and author for that manuscript.

Chapter 4 is currently being prepared for submission for publication of the material. Kyle R. Berg, Aashish Shivkumar, Sang-Ho Park, Galia Debelouchina, Xuemei Huang, Stanley J. Opella. The dissertation author is a primary researcher for that manuscript.

Perhaps most importantly, I am thankful for my Heavenly Father, and his son Jesus Christ. I saw many miracles in my personal and professional life over the course of my PhD that I recognize as answers to my prayers. I am also grateful for a living prophet, President Russel M. Nelson. Because of his counsel I was able to make changes in my life that have allowed me to transform into a better person in all aspects of life. I am also grateful for the blessings that President Nelson promised, and that I have seen realized in my life. During the hard times as a PhD student, my relationship with my Heavenly Father sustained me and lifted me, and I am so grateful for his love.

VITA

2014 Bachelor of Science, Biology, Utah State University, Logan

2014 Bachelor of Science, Biochemistry, Utah State University, Logan

2016 Master of Science, Biology, Utah State University, Logan

2021 Doctor of Philosophy, Chemistry, University of California San Diego

ABSTRACT OF THE DISSERTATION

Investigations into the nootropic effects of ethylene glycol derivatives of benzothiazole aniline

by

Kyle Robert Berg

Doctor of Philosophy in Chemistry

University of California San Diego, 2021

Professor Jerry Yang, Chair

Neurodegenerative diseases such as Alzheimer's disease (AD) are becoming more prevalent as the average human lifespan increases. Despite decades of research, no therapeutics exist that can slow the progress of AD. One of the hallmark symptoms that best correlates with symptoms of AD is synapse loss at the cellular level. Ethylene glycol (EG) analogs of benzothiazole aniline (BTA) improve memory and learning in mice by increasing the number of postsynaptic connection sites or dendritic spines in neurons. These compounds interact with the protein Fascin1. Through a combination of knockdown and overexpression studies, I show that Fascin1 levels affect dendritic spine density. Using tandem mass tag mass spectrometry pulldowns using human brain cortex lysate, I identify Fascin1-protein interactions that change in the presence of BTA-EG_4 and BTA-EG_6. I identify changes in focal adhesions, or sites at which the cell creates an attachment to the extracellular matrix, by immunofluorescence as a method by which BTA-EG_4 and BTA-EG_6 may be impacting dendritic spine density. I also provide structural evidence for the binding pocket between Fascin1 and BTA-EG_6 using solution protein nuclear magnetic resonance (NMR) and site-directed mutagenesis.

Chapter 1

Introduction: The impact of spinogenic molecules on neurodegeneration

1.1 Alzheimer's Disease

The brain is an incredible organ. It is the center of emotions, providing joy, fear, love, and anger. It is the center of both conscious and unconscious thought. On a cellular level, neurons in the brain create a complex network consisting of millions of neurons and billions of connections. Through these connections, neurons speak to one another by sending tiny chemical messengers across a gap between neurons, known as the synapse. If the collective input of many connections to a single neuron is strong enough to reach a threshold, the neuron fires and sends an electric signal known as an action potential down its axon to other neurons which can then respond in kind. Amazingly, the overall firing of neurons in the brain can coordinate the actions of an animal many orders of magnitude larger than a single neural cell.

Unfortunately, as the average human lifespan increases, more people are experiencing age related neurological disorders. Most prevalent among them is Alzheimer's Disease(AD), first described by Alois Alzheimer in 1907[1,2]. Symptoms of AD begin with memory problems such as impaired judgment, and difficulties with spatial reasoning. A person may eventually be unable to do simple tasks, such as dressing, has problems recognizing friends and family, and may begin to hallucinate or have delusions. With time, the person may no longer be able to communicate, and will be in bed nearly all the time[3–5]. AD affects over 6 million people in the United States[6]. The costs associated with caring for someone affected by AD are enormous, due largely to the long-term (sometimes over a decade) cost of care for someone with declining mental health.

The estimates for total payments for people over age 65 with dementia in 2021 are around 355 billion dollars[6].

Decades of research have gone into studying AD since it was identified as a common cause of death in the United States in 1976[7]. One of the most prevalent theories about the progression of AD is known as the amyloid cascade hypothesis[8]. In brief, it states that AD is caused by improper cleavage of the amyloid precursor protein leading to abnormally high levels of β-amyloid which aggregate to form extracellular plaques in the brain and cause neurotoxicity. The hypothesis has since been modified to the amyloid cascade-inflammatory hypothesis, which states that extracellular β-amyloid activates an inflammatory response mediated by microglia[9]. Protein interactions with β-Amyloid lead to a host of problems that wreak havoc on neurons and destroy synapses as the inflammatory response continues in the brain[10–13].

The amyloid cascade hypothesis does not fully explain all the features of AD and its accuracy has been questioned in recent years[14–17]. Despite many years of research studying the amyloid cascade hypothesis, a therapeutic to slow or halt AD has not yet been discovered and approved for treatment[6]. However, some trends in the progression of AD are clear. For example, cognitive decline can be traced to changes in the brain at the cellular level, such as a loss of synaptic connections between the neurons[18,19]. In fact, synapse loss is the best indicator of cognitive decline in Alzheimer's disease[20] and synaptic connections are constantly made or pruned through remodeling of the neuron's cytoskeleton[21]. Preserving the synapses of the brain could therefore be an alternate approach to treating Alzheimer's Disease.

1.2 The cytoskeleton is of particular importance to neurons

Neurons have a very unusual cell shape (Figure 1). Many cells that do not have a rigid cell wall adopt a three-dimensional shape that is roughly spherical. A spherical shape minimizes a cell's surface area to volume ratio meaning that if a cell can maintain a spherical shape, it will maximize the amount of space within the cell for organelles and other features, while expending a minimum amount of energy to maintain the shape of its cellular membrane. Adopting any other shape requires a physical scaffold from the cells internal cytoskeleton, or adhesions to an extracellular scaffold[22].

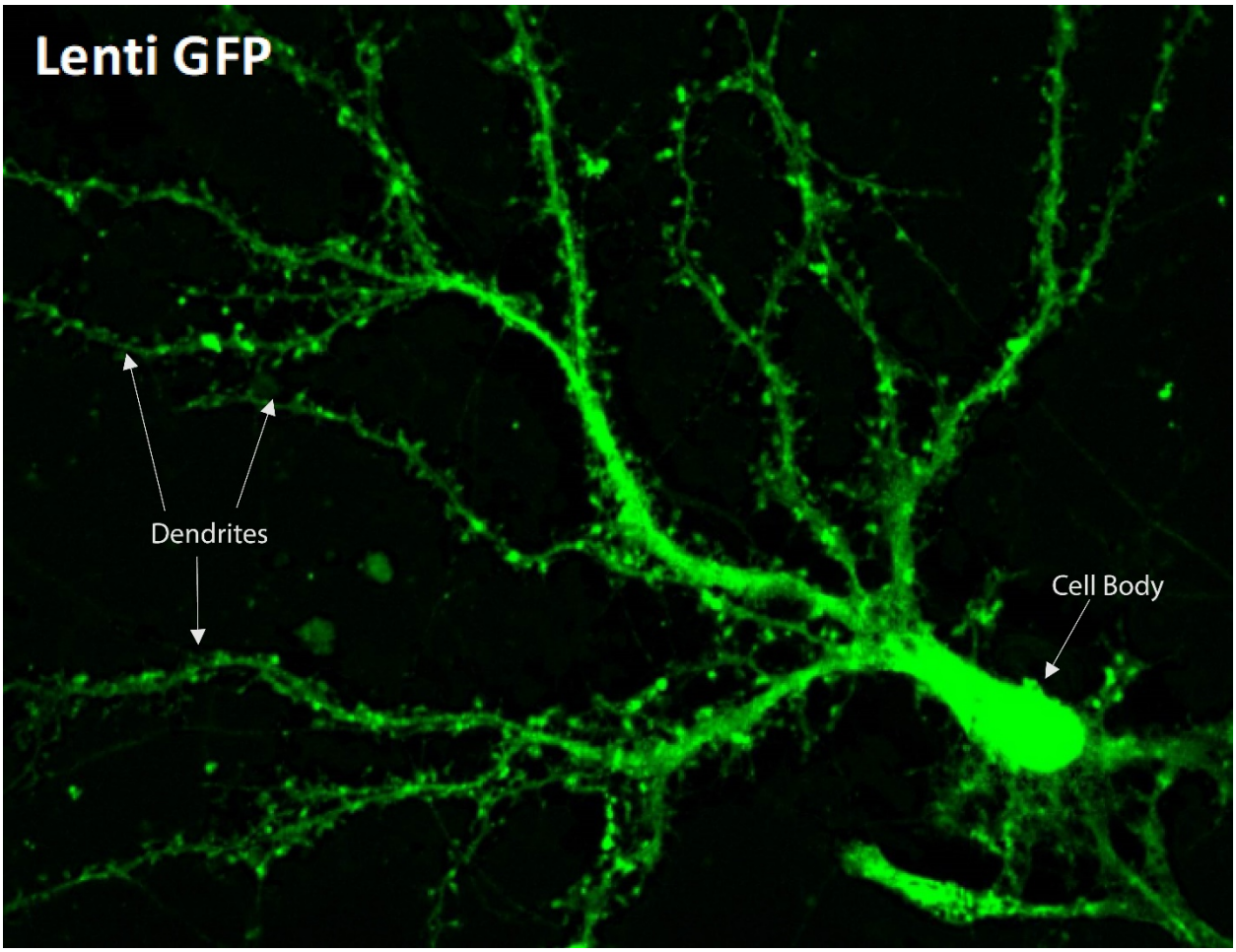

Figure 1. An image of a neuron filled with a green fluorescent protein produced by a lentiviral filler (LentiGFP), allowing visualization of the neruon. The cell body and several dendrites are labeled.

Neurons do not maintain a typical cell shape (Figure 1) because the function of a neuron is to communicate across large distances. Neurons expend a large amount of energy to create a cytoskeletal scaffold that permits the long extension of axons and an arborization amongst dendrites for sending and receiving signals[23]. The dendrites and axons extending so far from the cell body is one reason that neurons require a host of supporting glial cells in order to function properly[24].

The neuron's dependence on the cytoskeleton is not limited to the large-scale structures of the neuron. The neuron also makes use of the cytoskeleton to make vital structures used both in development and communication with other neurons[25]. The growth cone at the growing end of an elongating axon assists the axon in finding its target by utilizing numerous cytoskeletal structures including actin-rich lamellipodia and traditional filopodia[26]. In the dendrites, actin-rich structures called dendritic filopodia (distinct from traditional filopodia in internal structure) protrude from the dendrites and mature to form post synaptic connection sites known as dendritic spines[27–29]. Dendritic spines are constantly remodeled in the process of making, strengthening, or pruning synaptic connections[30].

1.3 Previous studies on oligo ethylene glycol (EG) derivatives of benzothiazole aniline (BTA) BTA-EG_4 and BTA-EG_6

The hallmark feature of patients with AD is the formation of β-amyloid plaques in the brain. As discussed previously, these extracellular plaques interact with other proteins and microglia that lead to inflammation in the brain[9]. In an attempt to reduce β-amyloid induced inflammation, the Yang lab previously synthesized BTA-EG_4 and BTA-EG_6 (Figure 2). These molecules could both bind β-amyloid plaques and prevent other

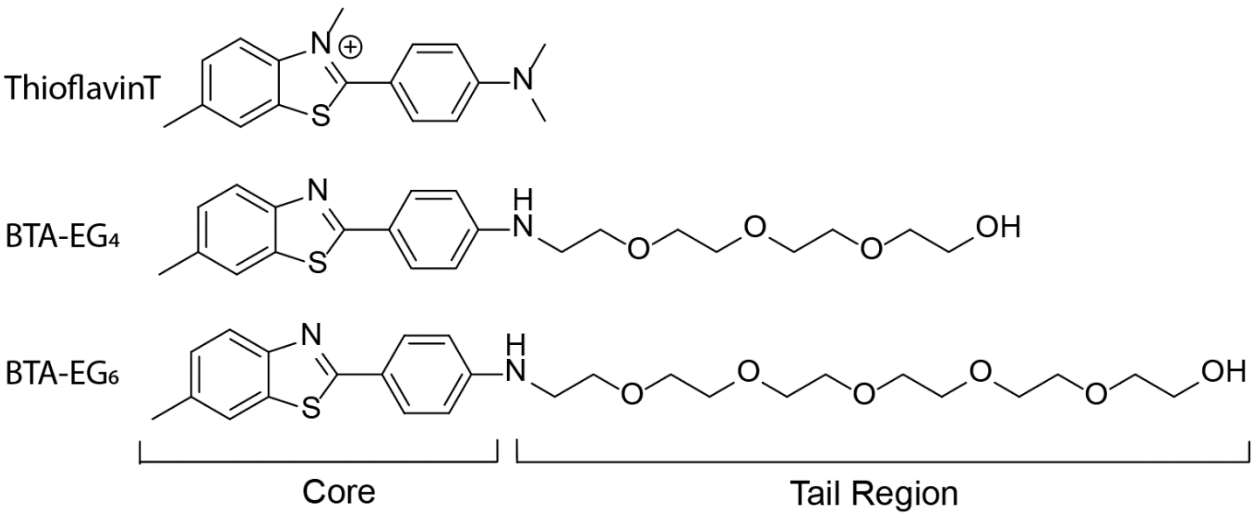

Figure 2. Illustration of the chemical structures of Thioflavin T, BTA-EG_4, and BTA-EG_6 with the core and tail regions identified.

proteins from interacting with the plaques, thereby reducing inflammation in the brain[31]. BTA-EG_4 and BTA-EG_6 are derivatives of thioflavinT, a traditional fluorescent dye used to stain β-amyloid (Figure 2)[32,33].

In order to improve biocompatibility, the Yang lab rationally designed chemical modifications to ThiflavinT to improve the biocompatibility of the molecule. First, the methyl group on the nitrogen in the benzothiazole (BTA) core was removed, eliminating the formal charge on the molecule and allowing the molecule to cross biological membranes. In addition, an ethylene glycol (EG) tail was added to one end of the molecule[34]. At first glance the ethylene glycol tail is an unusual selection to use in modifying the compound, as it increases its total number of rotatable bonds. The number of rotatable bonds in a molecule generally decrease the efficacy of a compound as a therapeutic, due to the increased entropy of the unbound molecule[34,35]. However, the addition of polyethylene glycol, or pegylation, has become increasingly common, as the rotatable tail is often not involved in the binding of a therapeutic to its target and generally

still has freedom of rotation even when the core of the therapeutic is bound[36,37]. In BTA-EG_4 and BTA-EG_6 the tail serves two purposes. From a chemical standpoint, the poly-ethylene glycol tail increases the solubility of the molecule in aqueous solution by incorporating polar oxygen atoms that can hydrogen bond with water in solution. For this reason, the longer tail on BTA-EG_6 makes it more soluble in aqueous solution than BTA-EG_4. From a biochemical standpoint, pegylation, or attaching one or more polyethylene glycol to a protein has a well-known characteristic of decreasing protein-protein interactions[38,39]. We hypothesize that the nonpolar BTA core interacts with the plaques, while the polyethylene glycol tail extends out of the protein into the nearby solvent to ward off would-be protein interactors. In this manner these molecules have been shown to decrease β-amyloid induced synapse loss in neurons[40]. BTA-EG_4 and BTA-EG_6 were found to successfully reduce the binding of antibodies[31] and cellular proteins[40] to aggregated β-amyloid and reduce amyloid-protein interactions in semen[41].

BTA-EG_4 was next investigated in a mouse model for their effect on cognitive behavior. Importantly, the molecule BTA-EG_4 was found to cross the blood brain barrier in mice[31] which is important for a therapeutic intended to act in the brain. Consistent with the theoretical conclusion described above, the 3xTg AD mouse model mice showed improved memory and learning and rescued synapse loss when treated with BTA-EG_4[42].

BTA-EG_4 was also surprisingly found to have a *non-pathological* response leading to improved memory and learning, even in wild-type (WT) mice. BTA-EG_4 treated WT mice showed improved cognitive performance in both a Morris water maze and a fear conditioning test[43]. Our collaborators investigated neurons in both 3xTg and WT mice

and found that when treated with BTA-EG_4 , the dendrites of the neurons showed an increased density of dendritic spines[43].

Dendritic spines are tiny mushroom-like structures located on the dendrites of neurons and can work as the receiving, or postsynaptic, end of a synaptic connection[44,45]. The majority of excitatory synapses in the brain form with a dendritic spine as the post synaptic connection site between neurons[44]. The experiments discussed above were the first time that the nootropic effects of BTA-EG_4 were identified *in vivo*. Since then, the spinogenic properties of BTA-EG_4 or its derivatives have also been demonstrated in rat primary neurons[46] and human neuronal induced pluripotent stem cells[47].

1.4 Photoaffinity labeling identifies the protein Fascin1 as a target for BTA-EG_4

To further understand the nootropic effects of BTA-EG_4 and BTA-EG_6, the Yang lab investigated the protein targets of these compounds. In his doctoral dissertation work, Kevin Sibucao (a former student in the Yang lab) used a chemical biology approach to identify potential protein targets for BTA-EG_4[48]. A brief overview is presented here as it is applicable to the work of this dissertation.

Dr. Sibucao synthesized an analog of BTA-EG_4 (Compound **1**, Figure 3) with modifications that would allow Compound **1** to both attach to, and extract proteins that interact with it[48]. This was accomplished by replacing a methyl group on the core of the molecule with a trifluoromethyl diazirine, and biotinylating the polyethylene glycol tail (Figure 3). The biotinylation of the tail provides a convenient handle for both identification using a streptavidin horseradish peroxidase and for isolation using neutravidin agarose

beads. The trifluoromethyl diazirine can be activated upon stimulation by ultraviolet light, resulting in the excision of N_2 gas and the production of a carbene at that location[49,50].

The carbene can then nonspecifically insert into a neighboring covalent bond, creating a new covalent adduct between the BTA-EG_4 analog and other interacting biomolecules (Figure 3). If the molecule is exposed to solvent at the time of ultraviolet light activation, the carbene can insert into a bond in the solvent molecule (e.g. between the hydrogen and oxygen atoms of water if it is used as the solvent). If the molecule is buried in a protein pocket, the resulting covalent bond can form between the molecule

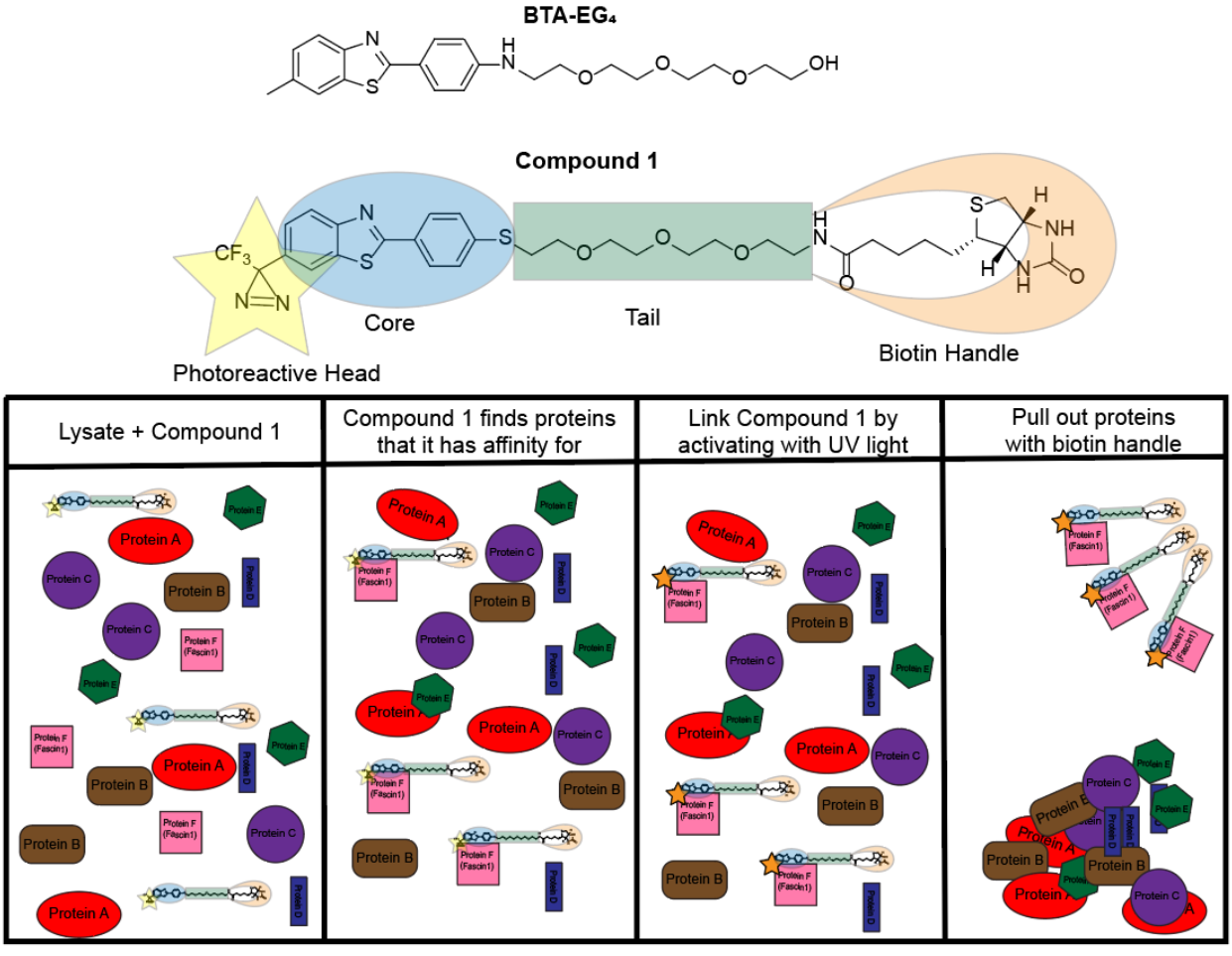

Figure 3. Illustration of the photoaffinity labeling and pulldown process by which Dr. Sibucao identified Fascin1 as a binder of the BTA-EG_4 analog Compound **1**

and the protein, covalently linking them together (Figure 3). The photoactivation of the compound was carried out in lysates SHSY-5Y neuroblastoma cells, 3xTg mouse midbrain, and human cortex. Proteins were pulled down using the biotinylated tail of the protein and neutravidin agarose beads, separated by size using SDS-PAGE gel electrophoresis, and discrete bands were cut out and proteins identified using tandem mass spectrometry. This work uncovered a list of proteins that were pulled down in this fashion, including the lead hit Fascin1[48].

1.5 Overview of the work presented in this dissertation

The findings from Dr. Sibucao's work leave several questions that I attempt to address in this dissertation:

1) Is Fascin1 on pathway and responsible for the observed effects of BTA-EG_4 and BTA-EG_6, specifically the increase in dendritic spine density upon treatment with those compounds?
2) Are there any confirmable mechanistic links between Fascin1 and dendritic spines that are consistent with our current understanding of how these compounds affect dendritic spine density?
3) Is it possible to obtain structural confirmation as to the location of the binding site of our compounds on Fascin1?

Answering these questions will afford a better understanding into novel therapeutic compounds and targets that may be exploited to reverse the synaptic loss seen in AD and other forms of dementia, as well as provide insight into ways these molecules may be modified to enhance their properties.

Chapter 2

Fascin1 expression levels affect dendritic spine density

2.1 Do BTA-EG_4 and BTA-EG_6 affect dendritic spine density *through* Fascin1 binding?

The key question addressed in this chapter is whether Fascin1 is on pathway for the observed dendritic spine increase in primary neurons when treated with BTA-EG_4 or BTA-EG_6. Dr. Sibucao previously showed that his photoreactive analog of BTA-EG_4 binds to Fascin1, and that it can be outcompeted by the addition of BTA-EG_4[48]. The binding of BTA-EG_6 to Fascin1 has been confirmed in our lab by isothermal titration calorimetry with a dissociation constant of 4.86μM. However, binding to a protein target does not necessarily signify a direct link to the observed cellular response. The experiments described in this chapter involve the measurement of changes in dendritic spine density of primary neurons as a result of modulated Fascin1 expression. Performing these experiments tests our hypothesis that Fascin1 plays a role in dendritic spine dynamics.

2.2 Fascin1 is primarily known for bundling actin in filopodia, however it has many other functions as well.

Fascin 1 is a pseudo-symmetric protein that consists of four β-trefoil domains (Figure 4)[51]. The human gene for Fascin1 is conserved with high sequence similarity to its homolog in the evolutionarily distant fruit fly *D. melanogaster*[51]. In humans Fascin1 is expressed in a variety of tissues in the developing embryo. However, as an adult Fascin1 is restricted to neurons, immune cells, the glomerulus, mesenchymal cells, the adrenal gland, and the basal layer of the skin. Its expression is very low or undetectable in most

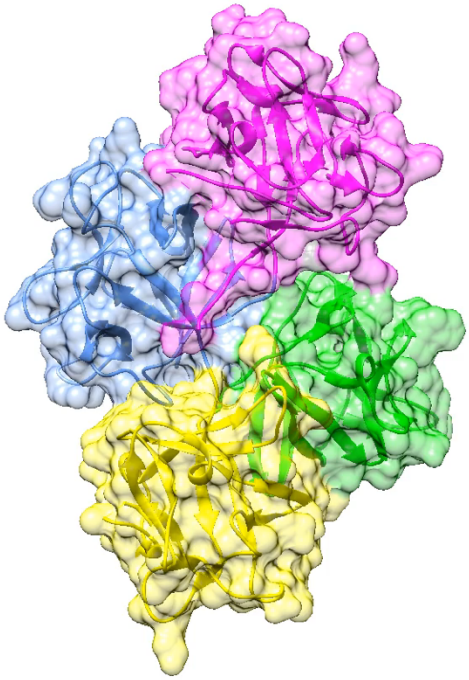

Figure 4. Illustration of the structure of Fascin1. B-trefoils 1, 2, 3, and 4 are colored pink, blue, yellow, and green respectively. PDB entry 1DFC[51].

other healthy tissues[52]. Fascin1 is best known for its function as an actin bundling protein present in traditional filopodia and invadopodia, or extrusions that protrude from the leading edge of the cell to explore the immediate environment surrounding the cell[53,54]. Filopodia contain parallel Fascin1-bundled actin and have a distinct composition from the branched actin containing dendritic filopodia that will be discussed later. Fascin1 supports filopodia structurally by taking individual strands of actin and holding them together, making the entire arrangement more rigid. Unlike other bundlers of actin such as various isoforms of α-Actinin, Fascin1 bundles are limited in size *in vitro* to approximately 20 bundles of actin per bundle[55,56].

Fascin1 has been used for decades as a prognostic biomarker for cancer with high Fascin1 expression in the cancerous tissue correlated to a poor prognosis for survival[57–61]. This is often attributed to Fascin1's role in the creation and maintenance traditional filopodia and invadopodia, which aid cancer cells in migration and metastasis[62–64]. These

cellular structures are thin fingerlike extensions that probe the cells environment and are often involved in cell migration[65]. However, some studies have shown Fascin1 expression to positively correlate with migration and invasion in a filopodia-independent manner, or to promote migration in some other way outside Fascin1's role as an actin-bundling protein[64,66–70].

Because of the relevance of Fascin1 to cancer, it has been extensively studied in that context[64]; however, Fascin1 also has several other known functions. Fascin1 stabilizes focal adhesions[71], which are locations at which the cell anchors itself to the extracellular matrix through stress fibers. Fascin1 plays two roles at the site of focal adhesions. 1) Fascin1 prevents the severing of stress fiber filaments by cofilin and 2) Fascin1 maintains the size of stress fibers. Fascin1 knockdown in fibroblasts causes a global change in cytoskeletal structure by significantly thickening the stress fibers compared to normal fibroblasts[71]. Fascin is also implicated in various other cellular processes and features including retrograde transport[72], and formation of extracellular vesicles[73]. Fascin1 is also transported to the nucleus where it acts as a transcription factor[74].

2.3 Fascin1 and dendritic spines

Korobova and Svitkina reported in 2009 that Fascin1 was not found in dendritic filopodia of young neurons at 10 days *in vitro* (DIV)[75]. Dendritic filopodia are thin finger-like protrusions that extend from a dendrite and can mature into mushroom shaped dendritic spines[27,44]. Between revealing that Fascin1 is not present in dendritic filopodia of 10 DIV neurons and the fact that the majority of actin in dendritic filopodia is branched[29,75], Fascin1 was presumed not to play a role in the formation, creation, and

maintenance of dendritic spines. Fascin1 has since largely been disregarded in the study of the cytoskeletal dynamics of dendritic spines. However, if it is true that BTA-EG_4 and BTA-EG_6 are binding Fascin1, and dendritic spine density is being affected as a result, then we hypothesize that Fascin1 is modulating the dendritic spines of neurons in a way that has hitherto been unsupported. Immunofluorescent images that I have acquired for staining of Fascin1 in primary neurons indicate that Fascin1 is present throughout fully mature neurons at 21 days in vitro (Figure 5) including localization to numerous areas which are consistent with dendritic spines.

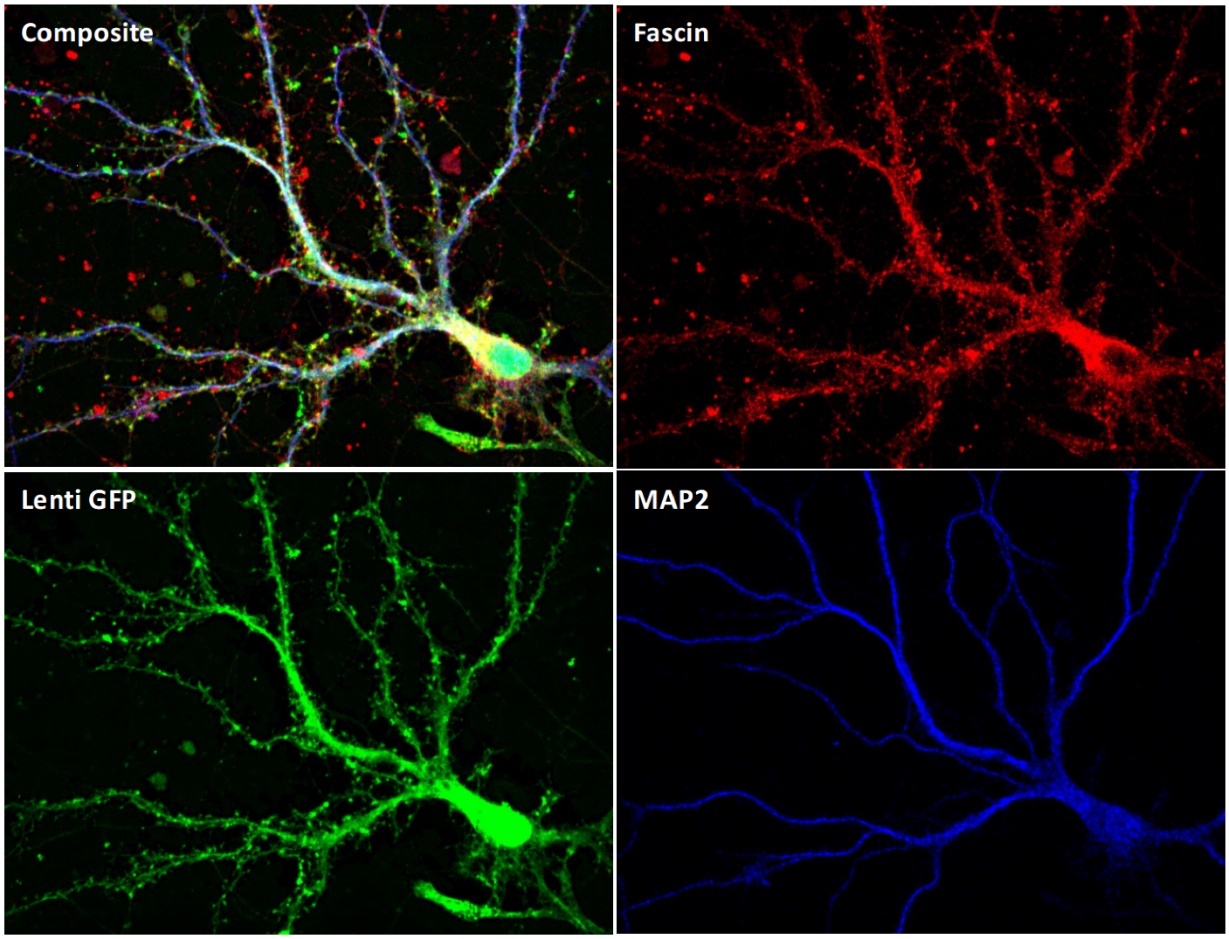

Figure 5. Immunofluorescent image of a rat neuron expressing a filler green fluorescent protein (Lenti GFP) stained for a microtubule associated protein used to identify dendrites (MAP2), and stained for Fascin1 (Fascin).

2.4 Identifying a method for Fascin1 knockdown or knockout, and overexpression in primary rat neurons

To determine whether Fascin1 is on pathway, or responsible for the increased spine density in neurons treated with our BTA-EG_4 or BTA-EG_6, I first needed to establish a method to knockdown or knockout Fascin1 expression in primary neurons.

The three common methods used to knockdown or knockout a protein in cells are short interfering RNA (siRNA), short hairpin RNA (shRNA), and clustered regularly interspaced short palindromic repeats (CRISPR)-Cas9 genome editing technology. Each of the methods has its own advantages and disadvantages. For example, the CRISPR-Cas9 system allows for complete removal of a target protein and can thus effectively eliminate expression. However complete elimination can be fatal to the cells, and off target cuts by the system must be taken into account[76–78]. By contrast, siRNA and shRNA both reduce target protein levels by utilizing native cellular machinery to cut the messenger RNA of a particular protein sequence. By providing an appropriate double stranded RNA that has a complementary sequence to the target mRNA the RNA induced silencing complex of the cell can be guided to degrade the mRNA of Fascin1[79,80].

While both siRNAs and shRNAs can be delivered via lipofectamine, siRNAs have an advantage in delivery, in that they only need to be delivered to the cell cytoplasm to be functional. shRNAs must be delivered to the nucleus, where they interact with the host DNA and are eventually expressed, producing a short hairpin RNA that is processed by the cell as previously described. siRNAs have a significant disadvantage in that their effect is transitory, while the effect of shRNAs is longer lasting due to the constant

expression of the shRNA when paired with a strong promotor such as the cytomegalovirus (CMV) promoter.[79]

In the end, I selected the shRNA system, because the long-lasting effects would be particularly useful when dealing with primary neurons, which generally are studied over the course of 1-3 weeks *in vitro*. CRISPR-Cas9 was left as a backup option if we were unable to get results using other methods of proteome manipulation.

Since our collaborators in the Patrick lab provide rat neurons for the experiments discussed here, all the vectors I designed in this chapter were made to be compatible with rat cells. While Rat and Human Fascin1 are 96% identical with 98% similarity at the protein sequence level[81], they are only about 90% identical at the DNA level[82], meaning that a ~20 nucleotide shRNA designed against the human sequence may present complications in rat cells or vice versa.

In addition to knocking out Fascin1, I also determined a method for its overexpression. I designed a Fascin1 expression lentiviral vector with a promotor designed to overexpress Fascin1. Since expression is promotor driven, it was possible to design a vector that would express well in most mammalian cell lines. Although many promoters are available, I used the cytomegalovirus promoter for the overexpression of Fascin1, since it is a strong promotor for various cell lines and well established in the literature[83,84]. The vector also included the expression of GFP under the cytomegalovirus promoter at a separate location on the plasmid as a reporter for positive transfection or transduction.

The successful overexpression and knockdown vectors were designed using Vectorbuilder inc. (Appendix A) These vectors can be delivered to cells in two different methods, both of which are used in this dissertation. The first method, lentiviral delivery, involves the vector packaged in a lentivirus that infects the cells. Delivering in this method allows for integration into the cell's genome. One advantage to lentiviral delivery is that the delivered DNA will be copied during replication and all daughter cells will receive a copy of the infected DNA. However, a limitation is that the insertion method is nonspecific, and can insert into other genes or regulatory elements in the DNA, which may complicate analysis. The second method, transient transfection, can also be used to deliver DNA plasmids to cells by lipid encapsulation of the DNA[85] or the formation of a calcium phosphate DNA precipitate[86] that is internalized into the cells. A limitation of transient transfection is that the DNA does not always get passed to daughter cells during replication. Both options are viable, especially since dendritic spine analysis is done in primary neurons, which do not divide. Vectorbuilder provided the DNA plasmids I designed in bacteria for purification and use in transient transfection and packaged the vectors in lentiviruses for lentiviral delivery or transduction.

2.5 Knockdown of Fascin1 in PC12 cells

Once I established a mechanism of knockdown and overexpression, I tested their efficacy in cells. The knockdown vector was first assessed in PC12 cells, a rat cell line that mimics many neuronal features such as neurite outgrowth and neuronsecretion[87–90]. It was not prudent to test in primary neurons first, because rats must be sacrificed to provide primary neurons. Moreover, testing in primary neurons is not advantageous because they cannot be passaged, do not grow quickly, and do not divide like the PC12

cells. PC12 cells were infected with packaged lentiviral particles. I found that a multiplicity of infection (or virus to cell ratio) of greater than or equal to 10 afforded a high transduction

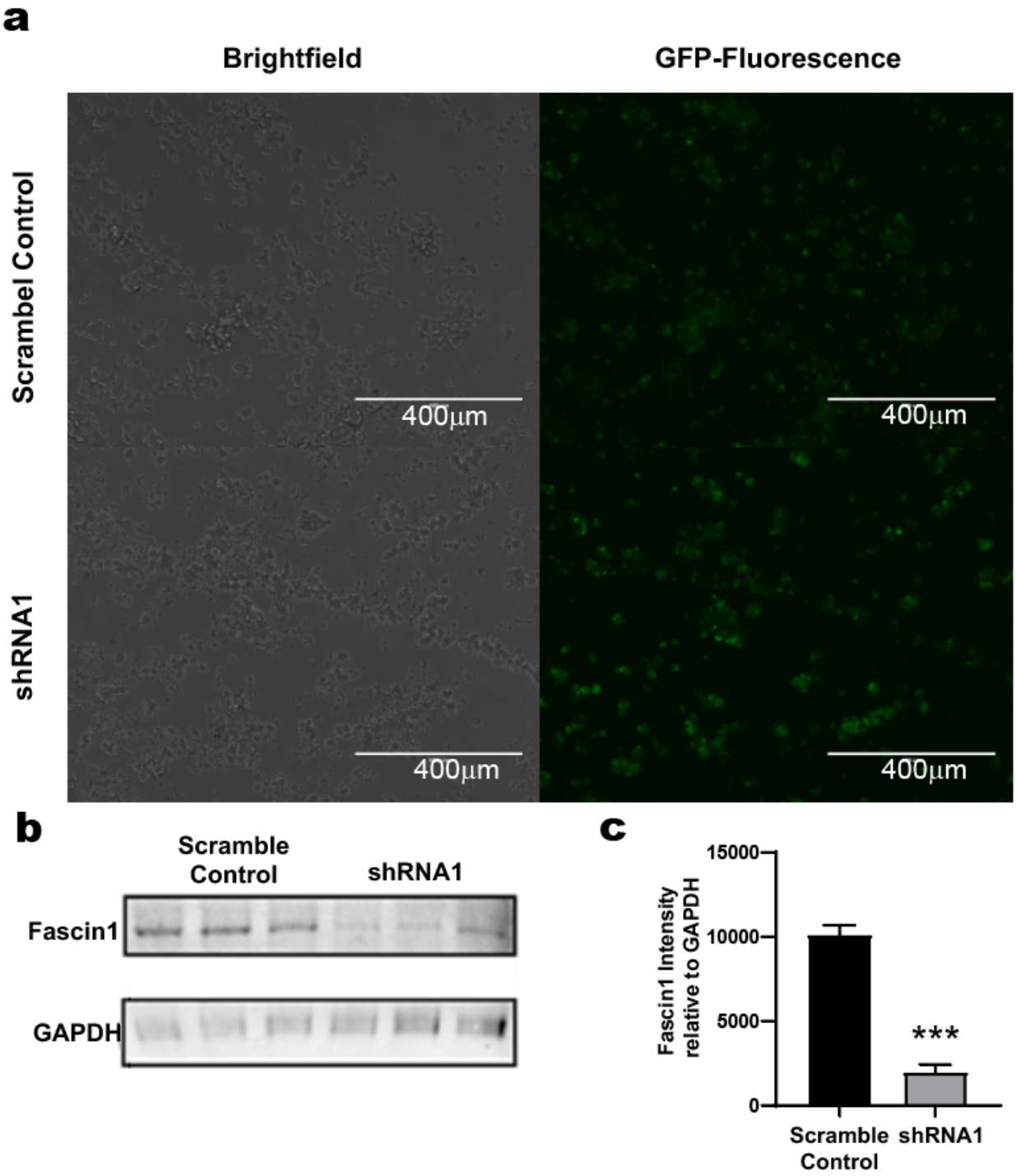

Figure 6. Verification of Fascin knockdown in PC12 cells. **a)** Overall lentiviral infection levels of shRNA1 and scramble control verified by a GFP reporter gene. **b)** Quantitative western blot of Fascin1 levels compared to a GAPDH Control. **c)** Graphical analysis of the Fascin1 intensities relative to the GAPDH Control. ***P-value ≤ 0.001 as assessed by student T-test.

efficiency of around 95% estimated visually by comparing the number of cells expressing the GFP reporter gene to the total number of cells in brightfield (Figure 6a). Due to high transduction efficiency, it was not necessary to select for infected cells.

I assessed Fascin1 expression using a quantitative western blot normalized to a GAPDH control. PC12 cells transduced with virus at a multiplicity of infection of 10 were found on average to have an approximate 80% reduction in Fascin1 expression compared to the uninfected controls (Figures 6b and 6c).

2.6 Knockdown and overexpression of Fascin 1 in primary rat neurons

After establishing that the shRNA was functioning properly in the PC12 secondary cell line, I tested the knockdown efficiency in primary neurons. All work in maintaining, growing, and imaging primary neurons was done in collaboration with Lara Dozier in the Patrick lab at UCSD. Primary neurons were cultured in a 24 well plate format and infected

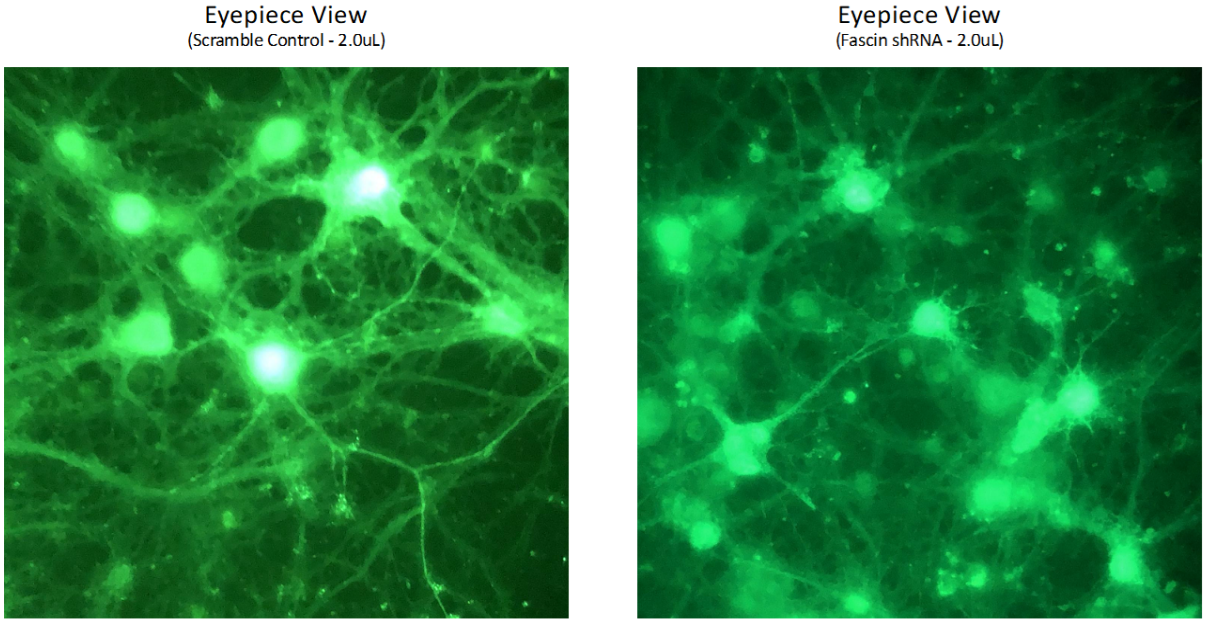

Figure 7. Eyepiece view images taken to show overall transduction efficiency of primary rat neurons when treated with the scramble control lentivirus (left) or Fascin1 shRNA lentivirus (right). In both cases 2 uL of virus in a 24 well plate format infected nearly all of the primary neurons in the well.

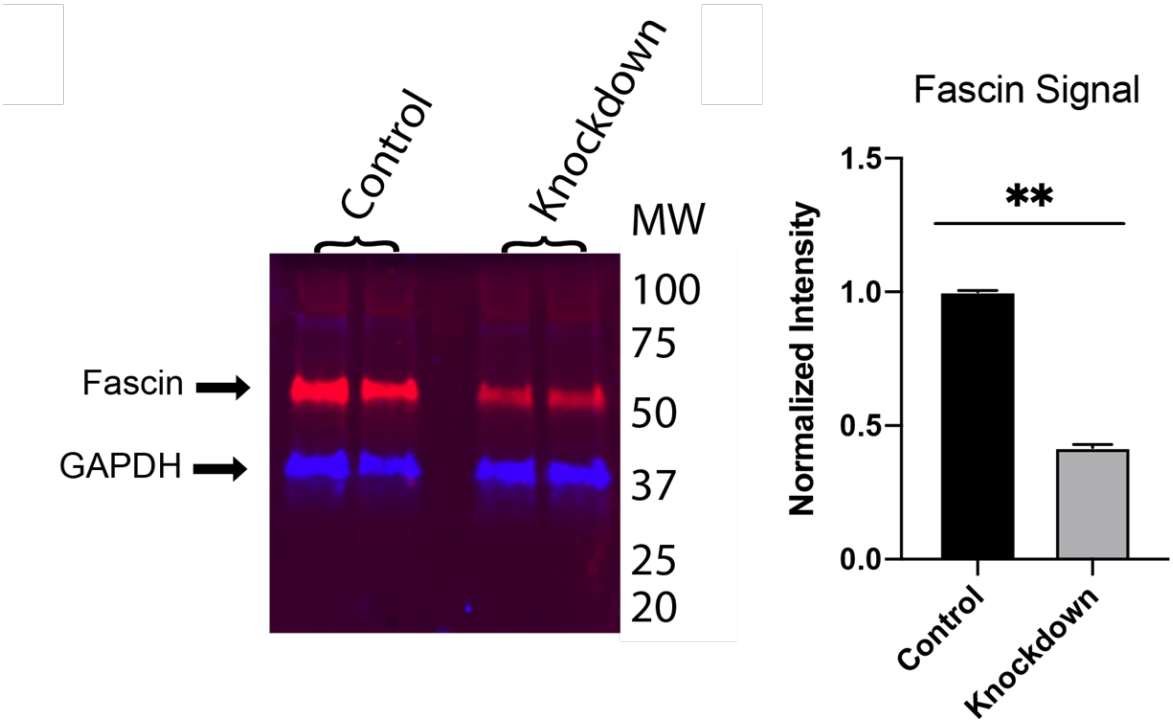

Figure 8. Knockdown of Fascin1 assessed by quantitative Western blot and image analysis. Neurons treated with a lentiviral package of Fascin1 knockdown shRNA showed an approximate 60% reduction in Fascin1 expression compared to the scramble control using GAPDH as a housekeeping gene. **p-value ≤0.01

with the shRNA vector packaged with lentivirus on DIV 14. We found that 2µL of lentivirus or $8.7x10^5$ viral particles per well afforded a high transduction efficiency (Figure 7). Some wells were infected with the scramble control vector as a negative control. The cells were harvested on DIV 21. By quantitative western blot we found that the neurons infected with the shRNA lentivirus had an approximate 60% reduction in Fascin1 expression (Figure 8).

One limitation to infection using lentiviral particles with the knockdown vector was that the GFP filler/reporter gene was not expressed strongly enough for dendritic spine analysis. To obtain clear visible spines, co-transduction with a sindbis virus with a plasmid membrane linked mCherry fluorophore is standard protocol in the Patrick lab. Although

this method achieves a very clear outline of the neurons, the sindbis virus leads to toxicity over time, and neurons must be fixed and stained within one day of infection. To avoid this issue, we performed transient transfection of the shRNA plasmid using the calcium phosphate method, which infected a smaller percentage of cells, but resulted in clearly countable spines without the need for co-transduction, and these neurons were used for dendritic spine analysis in section 2.7.

The overexpression of Fascin1 was tested directly in primary neurons due to excess availability from the Patrick lab. When transducing with lentivirus, nearly all the cells infected were glial cells, and not the primary neurons. By switching to transient transfection using the calcium phosphate method, we were able to infect the primary neurons, but at a low efficiency which would make quantitative changes in expression difficult to visualize with western blot. Therefore, functionality of the overexpression vector was assessed by immunofluorescent image analysis. The cells were fixed and

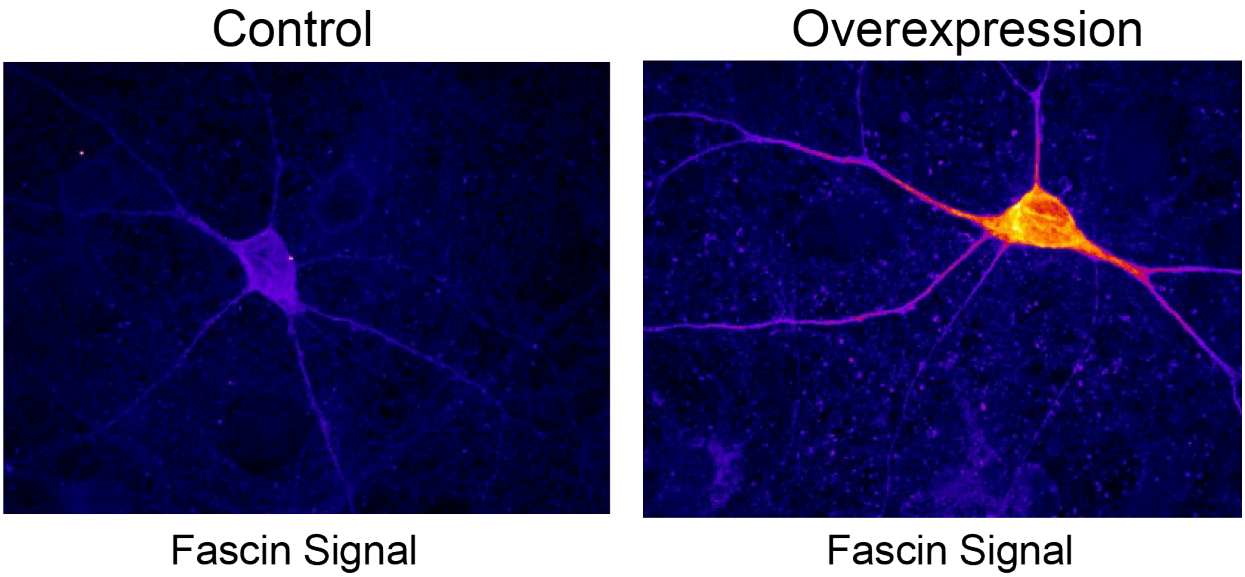

Figure 9. Overexpression of Fascin1 assessed by image analysis using the ImageJ fyre filter. Representative control neurons (left) were infected with an FG12 GFP expressing plasmid, while representative overexpression infected cells (right) were infected with a plasmid encoding both GFP and overexpression of Fascin1.

stained for Fascin1 using immunofluorescence (Figure 9). We were able to assess Fascin1 overexpression qualitatively examining a large number (~20) of infected neurons compared to controls. By qualitative image analysis, it was clear that infected neurons had an increase in Fascin1 expression compared to controls.

2.7 Spine density analysis of overexpression and knockdown neurons

To compare results between overexpression and knockdown I used an infection method consistent between both Fascin1 overexpression and knockdown neurons. Since lentiviral particles did not infect neurons with the overexpression vector, and knockdown with lentiviral particles required co-transduction with a sindbis virus as discussed previously, using lentiviral particles would introduce too many confounding variables to allow direct comparison between lentiviral infected Fascin1 knockdown and transient transfected Fascin1 overexpression neurons. I therefore performed dendritic spine analysis comparing overexpression and knockdown using only the calcium phosphate transfection method because identification and counting of spines was achievable in neurons transfected by the calcium phosphate method in both overexpression and knockdown. Neurons were transfected with plasmids at DIV 14, then fixed and stained on DIV 21. Images were taken in a single session for a given experiment and all images were taken with the same laser intensity. The analysis of spine density was blinded, meaning that all images were taken by our collaborator Lara Dozier in the Patrick Lab while I analyzed the images, unaware as to which images were treatment or control. Not until after analysis was complete was the identity of each sample treatment revealed.

Neurons were analyzed by image analysis (Figure 10)[91,92]. Secondary dendritic shafts were selected using the straighten macro[93], then cropped to 30μM segments.

Dendrites along the dendritic shaft were measured manually and counted using a spine counting macro developed in the Patrick Lab that records the length, width, and number of measured spines.

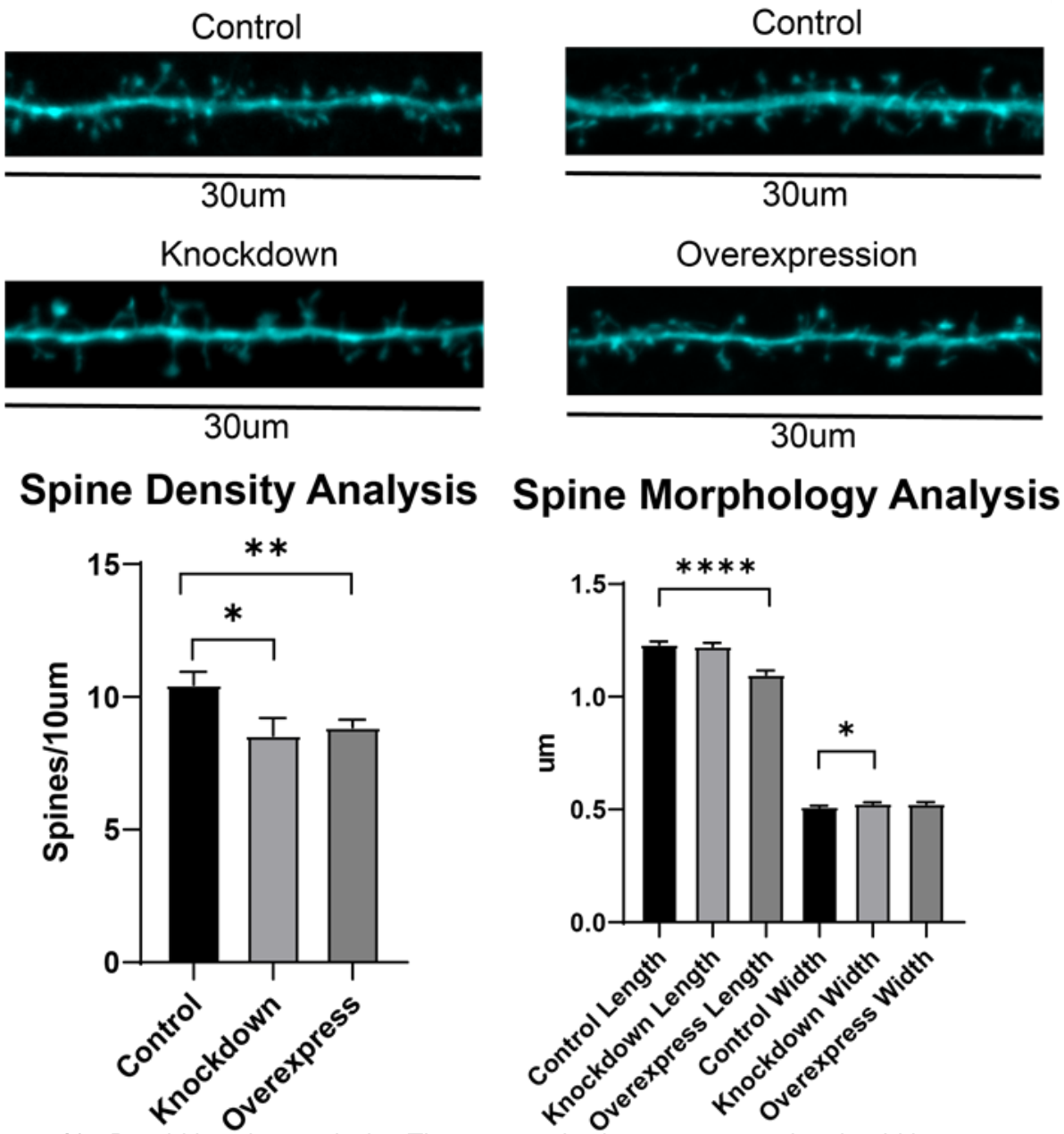

Figure 10. Dendritic spine analysis. The top panels show representative dendritic segments of dendritic spine analysis from control, Fascin1 knockdown, and Fascin 1 overexpression treatments. All samples express GFP. Both knockdown and overexpression of Fascin1 decrease dendritic spine density by approximately 20%. Overexpression of Fascin 1 caused a decrease in spine length, while knockdown caused a small, but significant change in spine width. Significance at *p<0.05, **p<0.01, ****p<0.0001 were assessed by student t-test.

Because of the observed increase in spine density resulting from treatment with BTA-EG$_4$ and BTA-EG$_6$, we predicted that Fascin1 overexpression and knockdown would have opposite effects on spine density, and that one of the two treatments would mimic the effects seen by the compounds BTA-EG$_4$ and BTA-EG$_6$. We were, therefore, surprised when we found that in both Fascin1 knockdown and Fascin1 overexpression neurons there was an approximate 20% decrease in dendritic spine density (Figure 10). This decrease in dendritic spine density does not eliminate the possibility of a logical explanation, and I, thus, performed further investigation. I performed an additional experiment treating neurons with 5μM BTA-EG$_4$ and BTA-EG$_6$ on DIV 20, harvesting 24 hours later. I analyzed the Fascin1 expression levels by quantitative western blot and found that there were no significant changes upon treatment with BTA-EG$_4$ and BTA-EG$_6$ (Figure 11). Simply changing the Fascin1 expression levels does not adequately mimic

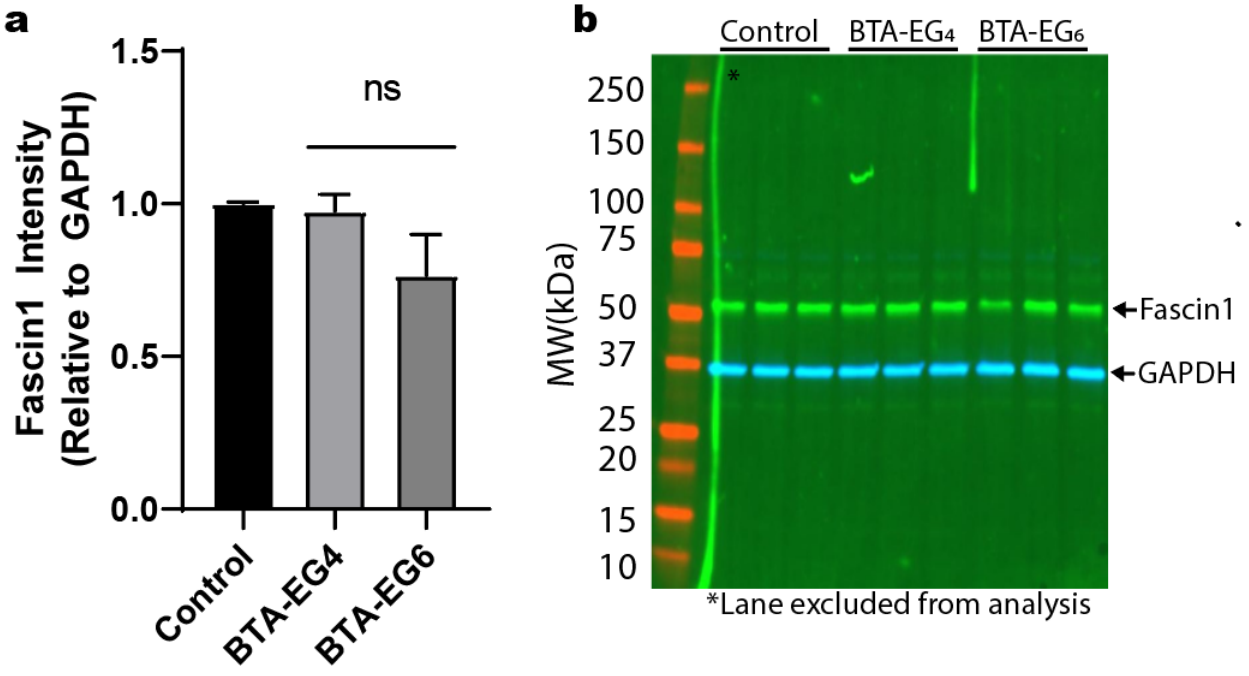

Figure 11. Fascin1 expression levels are not significantly different between neurons treated with vehicle control (DMSO), BTA-EG$_4$, and BTA-EG$_6$.

the response seen by the addition of BTA-EG_4 and BTA-EG_6, and their interactions with Fascin1.

These experiments demonstrate that Fascin1 affects spine dynamics of mature neurons, but both overexpression and knockdown of Fascin1 leads to an overall decrease in spine density. This is an important discovery, because as mentioned previously, Fascin1 has largely been disregarded in recent years as playing a role in dendritic spine dynamics.

In summary, in this chapter I showed that treatment of neurons with BTA-EG_4 and BTA-EG_6 has an opposite effect on spine density compared to both overexpression and knockdown of Fascin1. Since neither overexpression nor knockdown of Fascin1 mimics the effects observed with treatment of BTA-EG_4 and BTA-EG_6, I was interested in exploring how targeting Fascin1 with small molecules could affect spine dynamics without changing expression levels. We postulated that the small molecules could affect the interaction of Fascin1 with other cellular proteins that are involved with spine regulation. Since Fascin1 is a structural protein, modifying how and where Fascin1 binds to actin and other protein binding partners may lead to the phenotypic changes that we have seen in neurons in the presence of BTA-EG_4 and BTA-EG_6. Studies towards exploring this possibility are the subject of Chapter 3.

2.8 Methods

PC12 Cell Culture:

PC12 Cells were maintained in a 37º humidified incubator with 5% CO_2 in Modified Eagle's Medium (Gibco) supplemented with 10% heat inactivated horse serum (Gibco)

and 5% FBS (Gibco). Cells were passaged 24 hours prior to infection and plated to be around 70% confluent upon infection. Lentiviral particles were added at various multiplicities of infection (MOI) to determine transduction efficiency and added at a MOI of 10 determine Fascin1 knockdown. Fascin1 knockdown was confirmed by harvesting cells 3 days after infection using IP lysis buffer (Pierce) and following the manufacturer's protocol.

Quantitative Western Blots:

Quantitative western blots were accomplished by normalizing total protein concentration using the Pierce BCA assay and following the manufacturer's protocol. Identical quantities of total protein were loaded onto an 4-20% SDS-PAGE gel (BioRad) and run for 35 minutes at 190V. The protein was then transferred to an activated low fluorescence PVDF membrane (BioRad) using the TransBlot Turbo system (BioRad). Blots were incubated for 1hour at room temperature in 2% Membrane Blocking Agent (Cytivia) in Tris buffered Saline Solution with 0.1% Tween-20 (v/v) (TBST), followed by overnight incubation with primary antibody (1:10,000 dilution) in 2% Membrane Blocking Agent at 4ºC. The blot was then washed three times for 5 minutes each in TBST at room temperature. Secondary antibody (1:5000) was added to 2% Membrane Blocking Agent in TBST and allowed to incubate at room temperature for 1 hour. The membrane was then washed three times for 5 minutes each in TBST at room temperature, rinsed in MilliQ water three times and then imaged using the Amersham 680 RGB (Cytivia).

Neuronal Cell Culture:

Dissociated neurons from Sprague Dawley® one day old (P1) rat pups including both sexes were prepared as previously described[94–96].

Knockdown of Fascin1 in Primary Neurons:

For determining knockdown efficiency, cultured neurons were infected with lentiviral particles at 14 DIV. Harvesting of neurons for western blot were determined using the Pierce IP Lysis buffer at 21 DIV according to the manufacturer's protocol. Fascin expression was determined as described above for quantitative western blots.

Overexpression of Fascin1 in Primary Neurons:

Neurons at 14 DIV were transfected using CalPhos (Clontech 631312) with 1ug of lentiviral overexpression plasmid DNA per coverslip or FG 12 lentiviral negative control. Neurons were fixed and stained on DIV 21 as described below for immunostaining of primary neurons.

Dendritic Spine Analysis:

For dendritic spine analysis Neurons at 14 DIV were transfected using CalPhos (Clontech 631312) with 1ug of lentiviral knockdown plasmid, lentiviral overexpression plasmid DNA per coverslip, or FG 12 lentiviral negative control. Neurons were fixed and stained on DIV 21 as described below.

Immunostaining of Primary Neurons:

Neurons were fixed using 4% Paraformaldehyde/sucrose solution at room temperature for 10 minutes. Neurons were then permeabilized with 2% BSA and 0.25% Triton X-100 at room temperature for 20 minutes. Blocking was done for 6 hours at 4˚ C in 5% BSA. Primary antibodies for anti-fascin (Millipore MAB3582 1:1000), anti-MAP2 (Abcam5392 1:1000 or 1:5000), or anti GFP (Life Technologies A11122 1:1000). Nuclei were stained using Hoechst stain (Sigma B2261). Each set of images for a given trial

were acquired in one imaging session with identical exposure times, gain and power at 63x magnification.

Confocal Microscopy Imaging:

PC 12 cells were imaged on an EVOS FL (Life technologies) inverted microscope using either the Brightfield or GFP filter.

Neurons were imaged with a Leica DMI6000 inverted microscope with the following specifications: A Yokogawa Nipkon spinning disk confocal head. Orca ER high resolution Black and white cooled CCD camera (6.45 um/pixel at 1x). Plan Apochromat 63x/1.4 numerical aperture objective. An argon/krypton air-cooled laser for 405nm/140mW1oomW 561/140mW 637nm lasers.

Image Analysis:

Images were analyzed in a blinded fashion using ImageJ[97] or Fiji[91,92] (Fiji is just ImageJ). Dendritic shafts were selected using the GFP reporter/filler signal, avoiding any primary dendritic shafts. The shafts were straightened using a straighten algorithm[93] then cropped to 30um in length. The spines along the shaft were manually counted and measured as reported previously[46].

2.9 Acknowledgements

I would like to acknowledge the support I received from Professor Gentry Patrick, and Lara Dozier in the Patrick lab for their support in teaching me primary neuronal culture techniques and for providing and maintaining the many primary neurons I used.

Chapters 2 and 3 are currently being prepared for submission for publication of the material. Kyle R. Berg, Aashish Shivkumar, Kevin C. Sibucao, Geoffray Leriche, Carla

A. Espinoza, Lara Dozier, Gentry Patrick, Zied Gaieb, Christian Seitz, Rommie E. Amaro, Hyun-Hee Park, Hyang-Sook Hoe, Jacob Wozniak, David Gonzalez. The dissertation author is a primary researcher and author for that manuscript.

Chapter 3

Unraveling the web of Fascin1's protein interactions

3.1 Introduction to protein-protein interactions

Cellular proteins form a vast web of interactions that are highly regulated by the cell. A major goal in the field of biochemistry is to deconvolute biochemical interactions. Protein interactions are complex since proteins can have relevant physiological interactions with many other binding partners and the binding partners can vary between cell types. Fascin1 is an excellent example of this. Its primary known purpose of bundling actin is regulated and can be turned "on" or "off" by phosphorylation at a serine residue by protein kinase C. In addition, Fascin1 interacts with a host of other proteins. Some of those proteins, similar to Fascin1, play a role in cytoskeletal dynamics, while others participate in a plethora of molecular functions and biological processes. According to the Uniprot Database, one of the proteins known to interact with Fascin1, β-catenin, has 20 molecular functions and is involved with over 60 biological processes[98].

Investigating the protein-protein interactions of Fascin1 in the presence and absence of BTA-EG_4 and BTA-EG_6 was a logical next step for two reasons: First, upon treatment with BTA-EG_6, our lab found an increase of dendritic spine density in primary rat neurons within hours of treatment, which returns to normal dendritic spine density levels (i.e. density levels equivalent to untreated control cells) within 24 hours of compound removal[46]. This timescale led us to believe that changes in protein-protein interactions plays a pivotal role on the effects of BTA-EG_4 and BTA-EG_6. An alternate explanation, a change in the array of protein expression levels, seems unlikely because

an upstream change in protein expression levels often takes 1-3 days for noticeable effects to occur. Therefore, the observed changes that are seen in neurons within hours happen too quickly for changes in protein expression to be the primary reasoning for the observed effects of increased spine density. Second, the observed effect of treatment with BTA-EG_4 and BTA-EG_6 represents a structural change in the cell. Since Fascin1 is a cytoskeletal-modifying actin-bundling protein it is likely that the effect Fascin1 has on spine density is a result of changes in cytoskeletal dynamics. Changes in the cytoskeleton are in essence a change in protein-protein interactions.

In this chapter, I investigate the protein-protein interactions of Fascin1 in the presence and absence of BTA-EG_4 and BTA-EG_6 to connect the phenotypic morphological changes observed to what is occurring at the cellular biochemical level.

3.2 Previous work concerning the interactions of Fascin1 and other proteins

In his doctoral dissertation, Dr. Kevin Sibucao investigated Fascin1's protein interactions by using pulldowns in human brain cortex lysate to probe for protein-protein interactors that are pulled down in different proportions between controls and the addition of BTA-EG_4 and BTA-EG_6[48]. He then used western blot to determine the presence or absence of known protein interactors. Dr. Sibucao's lead hit was a disruption between the interactions of Fascin1 and Rab35, a master regulator protein that can recruit Fascin1 to the cellular membrane[72]. He hypothesized that when treated with BTA-EG_4 or BTA-EG_6, the interaction between Fascin1 and Rab35 was disrupted, causing an increased availability of actin near the neuronal membrane for creating branched actin networks common to dendritic spines[48].

A western blot approach to investigating Fascin1 protein interactions has several limitations. First, the approach is reductionist, and relies on probing for known interactions which limits the scope of the assay. Second, western blotting limits the number of trials and probes that can be used by the number of gels and lanes that can be run in a single experiment. While stripping and re-probing of western blots allows for investigation of multiple proteins, very few proteins can be imaged simultaneously, and cross-interactions can become a problem if a primary antibody is not completely removed due to incomplete stripping. Third, comparing results across different blots can be inconsistent, leading to complications in data interpretation. I therefore sought a more holistic approach to identify the Fascin1-protien interactions that were affected by BTA-EG_4 or BTA-EG_6.

3.3 A non-reductionist approach to protein-protein interactions: Tandem mass tag mass spectrometry.

For the studies presented here, I augment Dr. Sibucao's data and seek new protein-protein interactions that are modified by BTA-EG_4 and BTA-EG_6 by using the non-reductionist approach of tandem mass tag (TMT) mass spectrometry[99]. TMT mass spectrometry utilizes tags that have two properties: Tags can covalently link to specific nitrogen or carbon atoms in a protein with high efficiency and specificity, and they have signature fragmentation patterns by tandem mass spectrometry. The labeling of each treatment, control, and replicate with TMTs and identification of the proteins by tandem mass spectrometry allows for the quantification of the proteins that are identified between samples when compared to the appropriate databases.

This approach liberated me from the requirement of solely investigating proteins that were already known to interact with Fascin1. This approach also made it possible to evaluate hundreds of proteins simultaneously, rather than a small selection of proteins individually.

I first repeated the experiment as described in Dr. Sibucao's work[48] where I pulled down Fascin1-interacting proteins in brain lysate from healthy human brain tissue, which was provided as a generous gift from the Shiley-Marcos Alzheimer's Disease Research Center at UCSD. Fascin1 expressed as a fusion protein covalently linked to Glutathione-S-transferase (GST) was pre-loaded onto magnetic glutathione beads. A negative control was also prepared by loading GST alone onto magnetic beads. Brain lysate was obtained by mechanical homogenization in a hypotonic buffer using a Dounce homogenizer. The soluble fraction was collected and incubated with the pre-loaded beads at 1mg/mL of protein in the presence or absence of BTA-EG_4 and BTA-EG_6 at 100μM for 2 hours. The beads were subsequently washed in PBS +0.1% Triton-X100 three times, followed by elution using 8M Urea 50mM HEPES pH 8.0. The elutions were collected and frozen at -80°C until they were delivered to Jacob Wozniak of the Gonzales Lab for tandem mass tagging and mass spectrometry analysis.

The experiment detected 557 unique proteins that were pulled down in the presence of GST or Fascin1-GST. 100 proteins out of the 557 detected proteins showed an increased affinity for Fascin1-GST loaded magnetic beads (Figure 12). Those 100 proteins were then split into four clusters. Cluster 1 included 15 proteins that showed a further increased interaction with Fascin1-GST in the presence of BTA-EG_4 and BTA-EG_6 compared to the absence of the molecules. Cluster 2 included 8 proteins that showed

complete dissociation from Fascin1-GST in the presence of BTA-EG_4 and BTA-EG_6 compared to the absence of the molecules similar to the values obtained in the negative control. Cluster 3 included 28 proteins that had decreased interaction with Fascin1-GST in the presence of BTA-EG_4 and BTA-EG_6 compared to the absence of the molecules, but not complete dissociation as in Cluster 2. Cluster 4 were proteins that were pulled down with equal affinity in both the presence and absence of compounds. The full dataset is provided in Appendix B and Supplementary File 1.

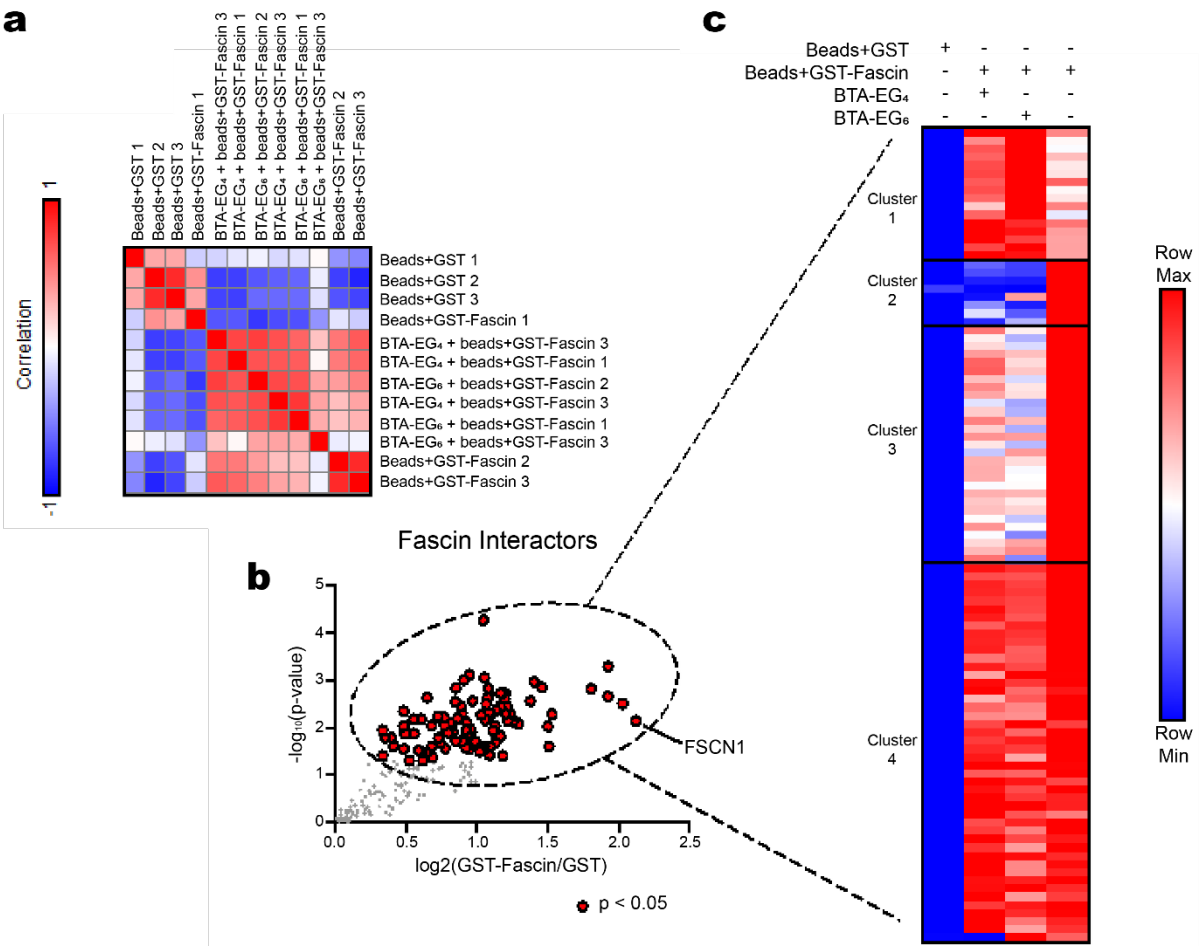

Figure 12. Tandem mass tag data and analysis. a) Correlation plot shows good clustering of related samples. b) Volcano plot highlighting the 100 proteins that showed a significant interaction with Fascin1-GST beads over the GST beads control. c) A heat map of the relative amount of protein pulled down between each sample with blue indicating a low presence of the protein and red indicating a high presence of the protein. Each row represents a single protein. The far-left column represents the amount of a given protein pulled down by the negative control (GST-beads). The far-right column represents the amount of a given protein pulled down by the Fascin-GST beads. The center two columns represent the amount of a given protein that was pulled down by Fascin-GST beads in the presence of$BTA\text{-}EG_4$ or $BTA\text{-}EG_6$.

It is also important to note that the overall profiles of $BTA\text{-}EG_4$ and $BTA\text{-}EG_6$ are similar (Figure 12c), meaning that both $BTA\text{-}EG_4$ and $BTA\text{-}EG_6$ cause a similar change with which proteins are pulled down in increased abundance, and which are pulled down in decreased abundance. This fact strengthens the data by giving it redundancy and solidifies the idea that these two compounds (although slightly different) cause similar

changes to Fascin1-protein interactions, which is consistent with their similar effect on dendritic spine density changes in primary neurons[43].

3.4 BTA-EG$_4$ and BTA-EG$_6$ increase Fascin1's interactions with some actin related proteins, but decrease its interactions with other actin related proteins

In order to find the protein candidates that could be responsible for the effects on spine density by BTA-EG$_4$ and BTA-EG$_6$, I identified the proteins in clusters 1-3 (Figure 12) that were either directly cytoskeletal or interacted closely with the cytoskeleton.

The first key finding was in cluster 1, where actin itself was pulled down in greater abundance in the presence of compounds BTA-EG$_4$ and BTA-EG$_6$. Importantly, this included both the cytoplasmic beta and gamma isoforms of actin, which are most relevant to neurons.

A second related finding was an apparent trend that many proteins that directly bind actin were also pulled down in greater abundance. These included Gelsolin, Drebrin, and subunits of the ARP2/3 complex (Table 1). The increased presence of these proteins can be explained solely by the fact that Fascin1 showed increased affinity to actin. In the case of a pulldown, the lysate is full of numerous proteins that are interacting in a complex manner. Since actin forms filamentous strands, it is entirely possible that Fascin1 may be linked to one part of an actin strand, and many of the actin associated proteins could be connected by associating with actin along another part of the strand and are pulled down by their association with actin, not necessarily by associating directly with Fascin1.

This trend, however, did not hold for all actin associated proteins. Two in particular, α-actinin1 and α-actinin4, showed decreased pulldown in the presence of BTA-EG$_4$ and

BTA-EG_6, despite the overall increase in pulldown of actin itself (Table 1). Further analysis of this peculiarity is provided in the following sections.

Table 1. Summary of select actin-related proteins that were both pulled down by Fascin1 and had a significant change in pulldown level in the presence of BTA-EG_4 and BTA-EG_6

Protein	Percent change of pulldown in the presence of BTA-EG_4	Percent change of pulldown in the presence of BTA-EG_6
Gamma Actin	64.6	93.8
Beta Actin	56.5	83.5
Actin related protein 3	45.1	81.1
Drebrin	69.4	102.9
Gelsolin	77.0	120.1
α-actinin1	-49.1	-61.6
α-actinin4	-37.4	-41.3

Decrease in Pulldown | No Change in Pulldown | Increase in Pulldown

3.5 Fascin1 and α-actinin both bundle parallel actin strands

Because of the observations made from the TMT data (i.e., a general increase in actin and actin associated proteins, but a decrease in the actin associated proteins α-actinins 1 and 4), I investigated how Fascin1 and α-actinin are reported to interact in the literature. Both Fascin1 and α-actinin are actin bundling proteins[61,100–104], meaning that the proteins hold two strands of actin together. However, the distance between strands is very different—approximately 8nm apart for Fascin and 35nm apart for α-actinin[56]. Each protein can bind at multiple locations along a strand of actin, and the strands can be bundled together into larger parallel bundles of actin. The number of filaments in Fascin1-bundled actin are limited to approximately 20 strands due to the geometry of binding and bundling, while α-actinin-bundled actin does not appear to have any such constraints[55,56].

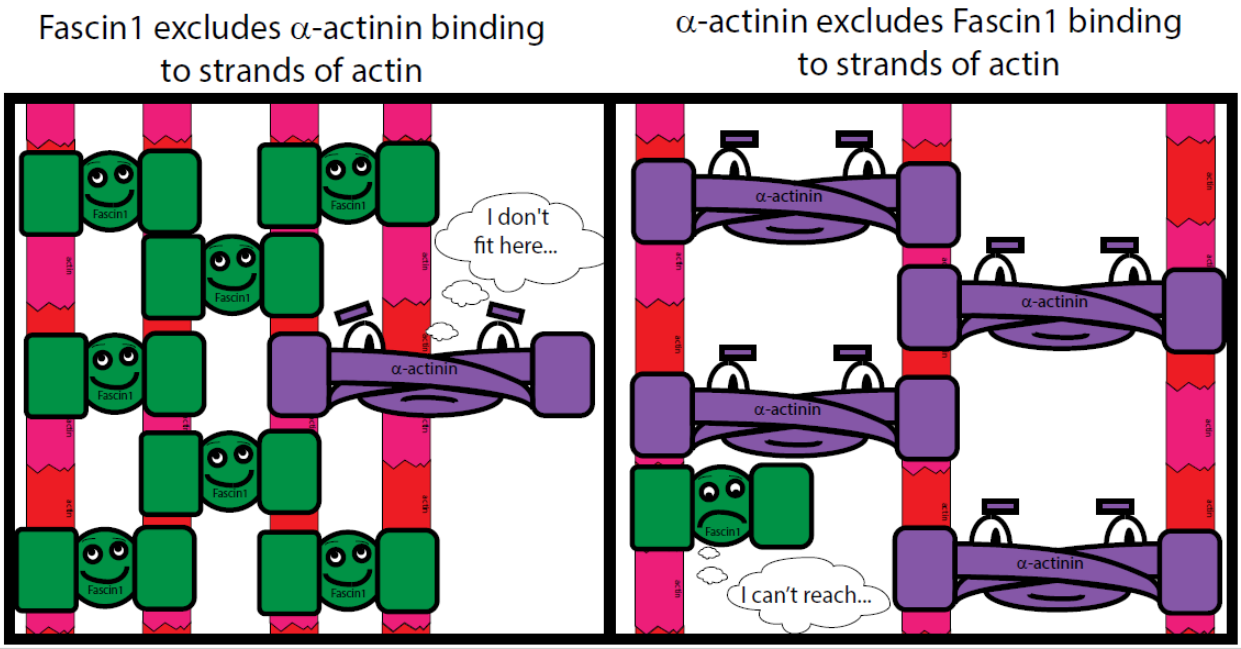

Figure 13. A cartoon diagram illustrating how Fascin1 and α-actinin each promote their own bundling to strands of actin while excluding the other.

When Fascin1 and α-actinin bundle actin *in vitro,* each promotes its own bundling while excluding the other due to the distance between strands[56] (Figure 13). Fascin1 would only reach one of the two strands of actin if it tried to bundle within a segment already bundled by α-actinin, and α-actinin would not fit between strands that were already bundled by Fascin1. Therefore, Fascin1 and α-actinin bundle actin in discrete domains[56].

3.6 Fascin1 and α-actinin work together to regulate focal adhesions

Both Fascin and α-actinin regulate focal adhesions. Focal adhesions are locations where the cell creates an attachment to the extracellular substrate through integrins which are bridging proteins that cross the plasma membrane[105]. Focal adhesions begin as smaller nascent adhesions, that eventually change to become larger mature focal adhesions[106]. On the interior of the cell the integrins interact with a host of "adhesome" proteins including Focal Adhesion Kinase, Paxillin, Vinculin, Zyxin, Espin, Talin, and

others which create a binding location for stress fibers.[105,107] Stress fibers are long parallel strands of actin that are bundled by α-actinin and myosin2[108]. Fascin1 also bundles the stress fibers, and is located adjacent to the focal adhesion at the barbed ends of the actin filaments[71]. The barbed end is the location where actin monomers are preferentially added to the filament[109,110].

Interestingly, when Fascin1 is knocked down in NIH 3T3 fibroblast cells, the stress fibers in the cell undergo a gross morphological change, where focal adhesions and stress fibers become thicker[71]. Because Fascin1 limits the number of actin filaments in a bundle, it is presumed that Fascin1 also moderates the thickness of stress fibers by bundling at the barbed end of stress fibers, where actin monomers are added[71].

Fascin inhibits focal adhesion degradation by preventing the activity of cofilin, an actin severing protein[71]. Cofilin is heavily regulated in dendritic spines and ins involved in the enlargement of spines during long term potentiation, spine pruning during in long term depression, synaptic availability of glutamate receptors, and synaptic vesicle exocytosis[111]. The Yang lab has previously shown that BTA-EG_6 decreases the ratio of active to inactive cofilin in neurons that have been treated with amyloid beta.[46] For focal adhesion turnover, Fascin must disassociate from the focal adhesion before the actin strands can be severed by cofilin.[71]

α-actinin is also involved in the regulation of stress fibers and focal adhesions, however their precise function is disagreed upon in the literature[112–118]. While many papers have published on actin bundle stabilization by α-actinin *in vitro*, their function becomes more complex in the cellular environment where many different proteins are competing for actin filament binding. Several studies have shown by RNAi that α-actinin

is involved in the assembly and maintenance of stress fibers[112–115], yet others have shown that when α-actinin is depleted, stress fiber mass increases.[116,117] In MDCK kidney epithelial cells, α-actinin was shown to suppress actin stress fibers by permitting actin filament turnover.[118]

Juxtaposing the scientific literature with the data collected from the TMT pulldown experiment, I hypothesized that BTA-EG_4 and BTA-EG_6 are acting to stabilize focal adhesions in their premature, nascent state. The two key conclusions from the TMT pulldown experiment that led me to this hypothesis were: 1) Fascin1 increases its interaction with actin in the presence of BTA-EG_4 and BTA-EG_6, and 2) α-actinin pulldown is decreased in the presence of BTA-EG_4 and BTA-EG_6, despite an increase in pulldown of other actin associated proteins. Stabilized focal adhesions can also lead to an increase in dendritic spines as will be discussed in the next section.

3.7 Focal adhesion and integrin signaling play a role in the formation and maintenance of dendritic spines

Since this work focuses on the implications of BTA-EG_4 and BTA-EG_6 on dendritic spine density, it is also important to consider the effect of focal adhesions on dendritic spines. Focal adhesions are centered on integrins, which bridge the cellular membrane, forming a link between the extracellular matrix and stress fibers on the interior of the cell[105]. An entire review article has been published on how integrins affect neural connectivity, both on the presynaptic bouton of the axon, and the postsynaptic dendritic spine[119]. Integrin activation induces the formation of dendritic spines by assisting the maturation of dendritic filopodia to dendritic spines through a signaling complex including focal adhesion kinase, Src, Grb2, and paxillin, which are all traditionally associated with

the focal adhesion complex as a whole[120]. Focal adhesion Kinase specifically is involved with the maintenance of dendritic spines by regulating cofilin activity, and is proposed to be involved with the formation of new spines.[121]

3.8 Confirmation of Fascin1's apparent increase in affinity to actin in the presence of BTA-EG$_4$ and BTA-EG$_6$

To test my hypothesis that Fascin1 is stabilizing focal adhesions in a nascent state by binding more tightly to actin, I designed some preliminary experiments. In collaboration with Aashish Shivkumar, another doctoral student in the Yang lab, we attempted to confirm the TMT data showing that Fascin1 better binds to or bundles actin in the presence of BTA-EG$_4$ and BTA-EG$_6$. Accordingly, we performed an actin bundling assay with and without BTA-EG$_4$ and BTA-EG$_6$. We also used the compound G2, a known inhibitor of actin bundling by Fascin1, as a negative control. However, because we wanted to identify both increases and decreases in actin bundling, we first identified conditions in which actin was not the limiting reagent. We therefore conducted a slow speed actin bundling and sedimentation assay at a constant 20uM Actin and varied the Fascin1 concentration. We identified 0.4μM Fascin1 as a concentration at which bundling was significant compared to the controls but did not yet saturate the amount of actin found in the pellet. The experiment was then repeated at 0.4μM Fascin1 with the addition of compounds BTA-EG$_4$, BTA-EG$_6$, and G2. Actin bundles were pelleted by centrifugation, and then resuspended in an equal volume of 1x sample buffer.

The actin bundling was significantly increased by coincubation with BTA-EG_4 and BTA-EG_6, while actin bundling was eliminated by G2 (Figure 14). This result corroborates my earlier finding that Fascin interacts more strongly with actin in the presence of BTA-EG_4 and BTA-EG_6 as discussed in section 3.4.

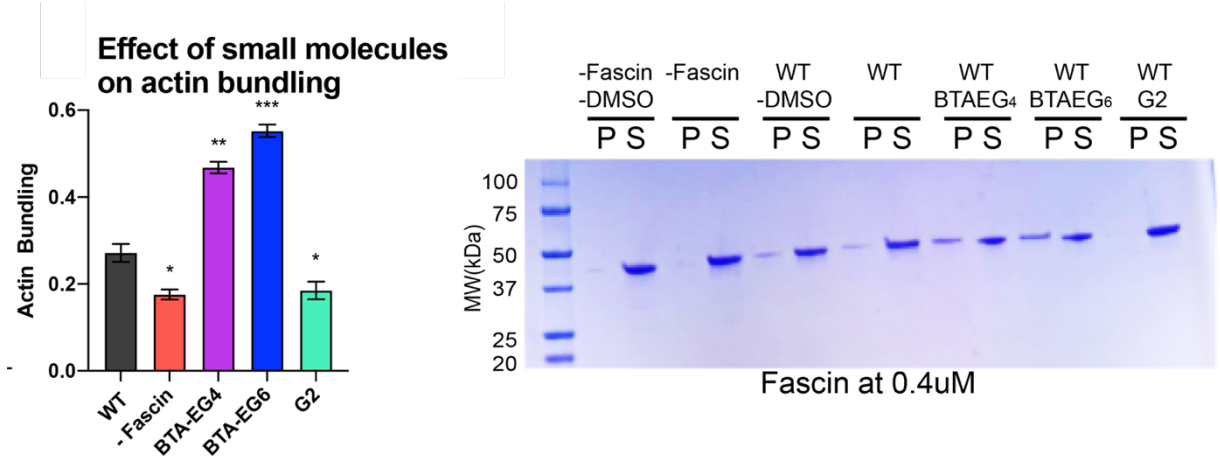

Figure 14. The effects of small molecules BTA-EG_4, BTA-EG_6, and G2 on the actin bundling activity of Fascin1. BTA-EG_4 and BTA-EG_6 increase actin bundling by Fascin1, while G2 eliminates actin bundling by Fascin1.

3.9 Immunofluorescent microscopy reveals a change in focal adhesions of SHSY-5Y cells treated with BTA-EG_4 and BTA-EG_6, causing the focal adhesions to maintain a pre-mature state

Next, I established a cellular assay to investigate focal adhesions by immunofluorescence. I seeded SHSY-5Y cells on poly-d-lysine coated coverslips at between 50-70% confluency. The following day I treated the cells with BTA-EG_4, BTA-EG_6, or vehicle control (DMSO), with small molecule compounds at a concentration of 10μM. After 24 hours, cells were fixed and stained for actin by a fluorescent phalloidin conjugate and stained for paxillin (a common reporter of focal adhesions) with a mouse

anti-paxillin primary antibody and a Alexafluor488 conjugated goat anti-mouse secondary antibody. (Figure 15)

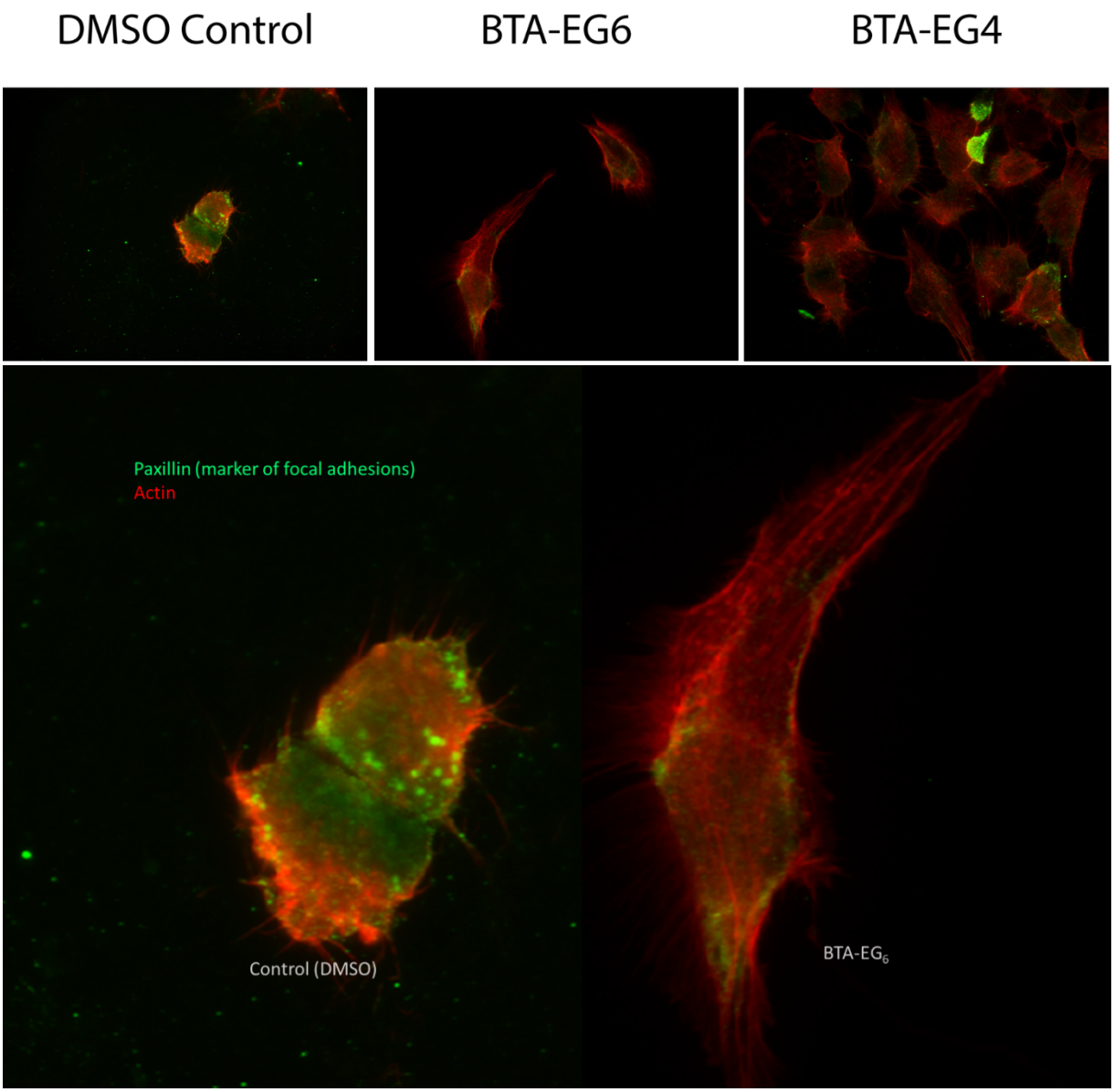

Figure 15. Immunofluorescent microscopy of undifferentiated SHSY-5Y cells treated with BTA-EG_4, BTA-EG_6, or vehicle control DMSO (top panels). Enlarged side by side comparison of DMSO treated and BTA-EG_6 treated cells. Mature focal adhesions appear to maintain their nascent state when cells are treated with BTA-EG_4 and BTA-EG_6.

The control samples looked as expected, with each cell containing many small nascent adhesions and several larger mature focal adhesions. In contrast, the large focal

adhesions completely disappeared in cells treated with BTA-EG_6, and the cells exhibited a stretched or spread-out phenotype (Figure 15). The cells treated with BTA-EG_4 were also stretched or spread-out, but the focal adhesions appeared to take on an intermediate form, somewhere in between the control and BTA-EG_6 treated cells. These preliminary findings indicate that the focal adhesions are not being disassembled as the neuroblastoma cells attempt to migrate.

These results are consistent with my hypothesis that BTA-EG_4 and BTA-EG_6 stabilize focal adhesions causing them to maintain a pre-mature state. The stretched-out phenotype that cells treated with BTA-EG_4 and BTA-EG_6 exhibit also supports this hypothesis, because the focal adhesions are stabilized, preventing detachment from the substrate as the cell attempts to move/migrate.

3.10 Other possible Fascin1 related pathways that could be affected by BTA-EG_4 and BTA-EG_6 leading to changes in dendritic spines

In addition to the findings described in section 3.9, the TMT tandem mass spectrometry approach identified other protein interactions that changed with the coincubation of BTA-EG_4 and BTA-EG_6 that may be in part responsible for the Fascin1 mediated increase in dendritic spine density. These leads are a great starting point for future research into the effects of BTA-EG_4 and BTA-EG_6 on dendritic spine density, as well as Fascin1's role in dendritic spine formation or maintenance.

A collection of proteins that showed up repeatedly in the TMT data as having decreased binding to Fascin1 in the presence of BTA-EG_4 and BTA-EG_6, were proteins that are involved in clathrin coated pit mediated endocytosis. These proteins included 4 subunits of the AP2 adaptor protein complex (α1, α2, β, and μ), and snap91, a clathrin

coat assembly protein. The AP2 complex serves as a mediator between a clathrin coated pit vesicle and other proteins in the cell and forms a cage around the endocytosed vesicle[122].

The AP2 complex facilitates the endocytosis and recycling of many postsynaptic receptors found on the dendritic spine. These include NMDA and AMPA receptors which are both involved in dendritic spine dynamics and plasticity, and long term potentiation, as well as the GABAA receptors involved in fast synaptic inhibition[95,123–125]. The AP2 complex can also selectively endocytose integrins[126], which have already been discussed in section 3.7. Because a large number of membrane-bound proteins can be recycled in this way, further experiments would need to be conducted in order to identify specific proteins that may be affecting dendritic spines through a BTA-EG_4 and BTA-EG_6 induced pathway through Fascin1. Interestingly, microtubule dependent disassembly of focal adhesions through clathrin coated pits, (presumably mediated by the AP2 complex) have already been shown to be Fascin1 dependent in NIH 3T3 cells using a nocodazole washout experiment[71] and Fascin1 has been shown to mediate interactions between actin and microtubules[127].

Microtubules occasionally invade dendritic spines for 1-5 minute intervals[128]. The purpose for this invasion, has been debated within the literature[128–130]. Although some cargos have been identified that are delivered to dendritic spines via microtubule transport in this manner, no specific cargo has yet been identified that is transported out of dendritic spines by this method[129]. Further experiments would be needed to address whether Fascin1 and cargo transport in clathrin coated pits are involved in this process.

A final group of proteins that I found have decreased interaction with Fascin1 in the presence of BTA-EG_4 and BTA-EG_6 are those involved in retrograde transport and endosomal trafficking. These proteins include RAB6A and RAB6B, as well as the dynein light chain 1. Perhaps in concert with the AP2 complex, these proteins could be regulating vesicle transport out of the dendritic spine for recycling to a newly formed dendritic spine or tagged for degradation by the proteosome.

3.11 Methods

Expression of Fascin1-GST for pulldowns:

Fascin 1 was grown by transforming the Fascin1 pGEX-5X-2 plasmid cloned by Dr. Kevin Sibucao[48] into DE3-BL21 cells (NEB) following the manufacturer's instructions. Cells were plated on selection agar plates containing100µg/mL ampicillin. A colony was selected for growth overnight in 50mL LB broth with 100µg/mL ampicillin with shaking at 220 RPM and 37ºC. The culture was then transferred to a 1L culture containing YT broth (pre-warmed to 37ºC) and 100µg/mL ampicillin. The culture was allowed to grow to an OD of 0.8-1.0 at which point the temperature was reduced to 17ºC and the culture was induced with 0.5mM IPTG. The culture was allowed to incubate overnight, and the bacteria were harvested by centrifugation at 3000x gravity for 30 minutes and frozen at -80ºC.

Purification of Fascin1

Fascin1 was purified by lysing the bacteria by resuspending the bacterial pellets in 30-40mL resuspension buffer (20mM Tris pH8, 150mM NaCl, 1mM DTT) , with 50mg lysozyme and 2uL Benzonase Nuclease (MilliporeSigma) per liter of bacterial culture.

The resuspension was then sonicated on ice for 10 minutes at 60% power with a pules sequence of 3 seconds on and 3 seconds off (20 minutes total time). The lysate was then centrifuged at 18500x gravity for 45-60 minutes. The supernatant was filtered twice to remove any residual membranous material first by a 0.45μM and then a 0.22 μM pore size filter (Genesee Scientific), then incubated with 5mL Glutathione Sepharose 4b beads (Cytivia) for at least 2 hours at 4ºC with rotation. The beads were then collected by gravity flow filtration and washed with approximately 75mL of resuspension buffer. Fascin1-GST was eluted by the addition of elution buffer (10mM reduced glutathione 50mM Tris, 150mM NaCl pH8), then concentrated with a 30kDa cutoff centrifugal concentrator (Millipore) to a total volume of less than 1mL, dialyzed into PBS, then diluted to the appropriate concentrations for pulldowns in brain lysate.

Fascin1-GST pulldowns in brain lysate

Glutathione magnetic beads were washed three times in hypotonic lysis buffer (20mM Tris pH 8). Fascin1-GST or GST were loaded onto magnetic beads. Protein was added to the beads such that there was16μL of 25% slurry glutathione magnetic beads (Pierce), and 20μg Fascin1-GST per trial. An equimolar amount of GST was prepared per control. The beads and protein were allowed to incubate while preparing the lysate (around 2 hours) at 4ºC. After incubation, the beads were pulled to the side of the tube using a magnet and washed once with hypotonic lysis buffer immediately before being resuspended in an appropriate volume (~25μL per sample) before being added to lysate.

Lysate was prepared by removing approximately 1g brain tissue from storage at -80ºC and resuspending the tissue in 3-5mL cold hypotonic lysis buffer with protease inhibitor cocktail (C0mplete EDTA Free Protease Inhibitors Cocktail Roche) and allowed

to incubate for 30 minutes. Tissue was then homogenized by mechanical disruption using a Dounce homogenizer. The tissue was ground extensively with first the loose and then the tight homogenizer rods on ice. Lysate was centrifuged at 18,000xg for 20 minutes and the soluble fraction collected. Concentration was verified by BCA assay (Pierce) following the manufacturer's protocol and the lysate was diluted to 1mg/mL total protein.

BTA-EG_4, BTA-EG_6, or DMSO (control) were added to the lysate to a final concentration of 100uM compound and 0.1%DMSO. Pre-loaded beads were then added to the lysate and allowed to incubate at 4ºC for 2 hours. The beads were washed 3 times using cold wash buffer (0.1% Triton x-100 in PBS) using a magnet to pull the beads to the side of the tube prior to each wash. Samples were eluted by adding 25µL of 8M Urea 50mM HEPES pH 8 to the beads, agitating slightly by flicking gently, then pulling the beads to the side with a magnet and collecting the protein solution that was eluted off the beads. The elution step was repeated three times.

Protein samples were then frozen at -80 until being sent for tandem mass tagged mass spectrometry.

TMT mass spectrometry

Trypsin digestion, tandem mass tag labeling and fractionation, and LC MS2/MS3 analysis were performed as described previously[131].

Cell culture:

SH-SY5Y cells were grown in DMEM:F12 1:1 media and maintained in a humidified incubator at 37ºC. Cells were seeded in a 24 well plate on poly-d-lysine coated glass coverslips to be around 50-70% confluent. The following day the cells were

subjected to treatment with BTA-EG_4, BTA-EG_6, or DMSO control to a final concentration of 10μM compound with 0.1% DMSO. Cells were fixed and stained 24 hours after treatment with compounds

Fixing and immunostaining of cells:

Cells were washed once with 300μL PBS supplemented with magnesium and calcium (PBS-MC). Cells were then fixed for 10 minutes with 300μL of 4% paraformaldehyde and 4% sucrose in PBS-MC. Cells were carefully and slowly rinsed three times with PBS-MC. Cells were permeabilized/blocked for 20 minutes in 2% BSA, 0.25% Triton x-100 in PBS-MC. Cells were rinsed 3x with PBS-MC, then blocked with 5% BSA in PBS-MC for 4+ hours. The blocking solution was removed and mouse anti paxillin antibody was added at a 1:100 dilution in 2% BSA in PBS-MC. The cells were incubated overnight at 4ºC, then carefully and slowly rinsed 3x with PBS MC. Goat anti mouse AF-488 (Invitrogen) at a 1:1000 dilution in 2% BSA/PBS-MC was added together with phalloidin conjugated iFluor555 (Abcam) at 1x concentration, added to each well and allowed to incubate for 1 hour at room temperature. The wells were carefully and slowly rinsed 3x with PBS-MC and placed on an orbital shaker for 15 minutes on the last rinse (less than 60 rpm). Cells were mounted on microscope slides using ProLong Glass mounting media (Thermofisher) and sealed with clear fingernail polish after the mounting media had set. The slides were kept in the dark until the slides were imaged by a Keyence All-in-One Fluorescence Microscope BZ-X800. All images were acquired at 100x during the same session with identical laser intensities.

3.12 Acknowledgements

I would like to thank Dr. Kevin Corbett for helping me identify TMT mass spectrometry as a tool for identifying changes in protein-protein interactions in the presence of BTA-EG_4 and BTA-EG_6, and Dr. Vivian Hook for connecting me to the Gonzalez lab. I would like to thank Dr. David Gonzalez, and Dr. Jacob Wozniak from the Gonzalez lab for their assistance in tandem mass tagging and tandem mass spectrometry of my brain tissue samples.

Chapters 2 and 3 are currently being prepared for submission for publication of the material. Kyle R. Berg, Aashish Shivkumar, Kevin C. Sibucao, Geoffray Leriche, Carla A. Espinoza, Lara Dozier, Gentry Patrick, Zied Gaieb, Christian Seitz, Rommie E. Amaro, Hyun-Hee Park, Hyang-Sook Hoe, Jacob Wozniak, David Gonzalez. The dissertation author is a primary researcher and author for that manuscript.

Chapter 4

Structural studies to identify key interactions for the binding of BTA-EG_6 to Fascin1

4.1 Introduction

The development of a compound that improves memory and learning in mice and has the potential to combat symptoms of neurodegenerative disease is scientifically and medically groundbreaking. Understanding exactly how a compound binds to its specific protein target can lead to a better understanding of its mechanism of action, and lead to the creation of new compounds that bind with higher affinity that are better candidates for clinical trials. This chapter identifies key residues that are involved with the binding of BTA-EG_6 to Fascin1. BTA-EG_4 was not studied in this chapter because of its low solubility; however, I have collected evidence in Chapter 3 to demonstrate that BTA-EG_4 and BTA-EG_6 cause a similar perturbation of binding partners to Fascin1. The two compounds also cause a similar cellular response which is an observed increase in dendritic spine density[43]. Accordingly, it is likely that the results for BTA-EG_6 reported in this chapter also apply to BTA-EG_4.

In this chapter I utilize both protein crystallography and protein NMR to provide experimental evidence for the binding pocket of BTA-EG_6 to Fascin1.

4.2 Previous Work

As mentioned previously, Dr. Kevin Sibucao carried out photoaffinity labeling studies in the Yang lab to identify Fascin1 as the target of BTA-EG_4 and its analogs. Aashish Shivkumar, a PhD student in the Yang lab, confirmed the binding of BTA-EG_6 to

Fascin1 by isothermal titration calorimetry and found the binding/dissociation constant (K_d) of BTA-EG_6 to Fascin1 to be 4.86μM (data in preparation for publication). He also performed *in silico* docking studies supported by site directed mutagenesis to identify a potential binding pocket for BTA-EG_6 (Figure 16).

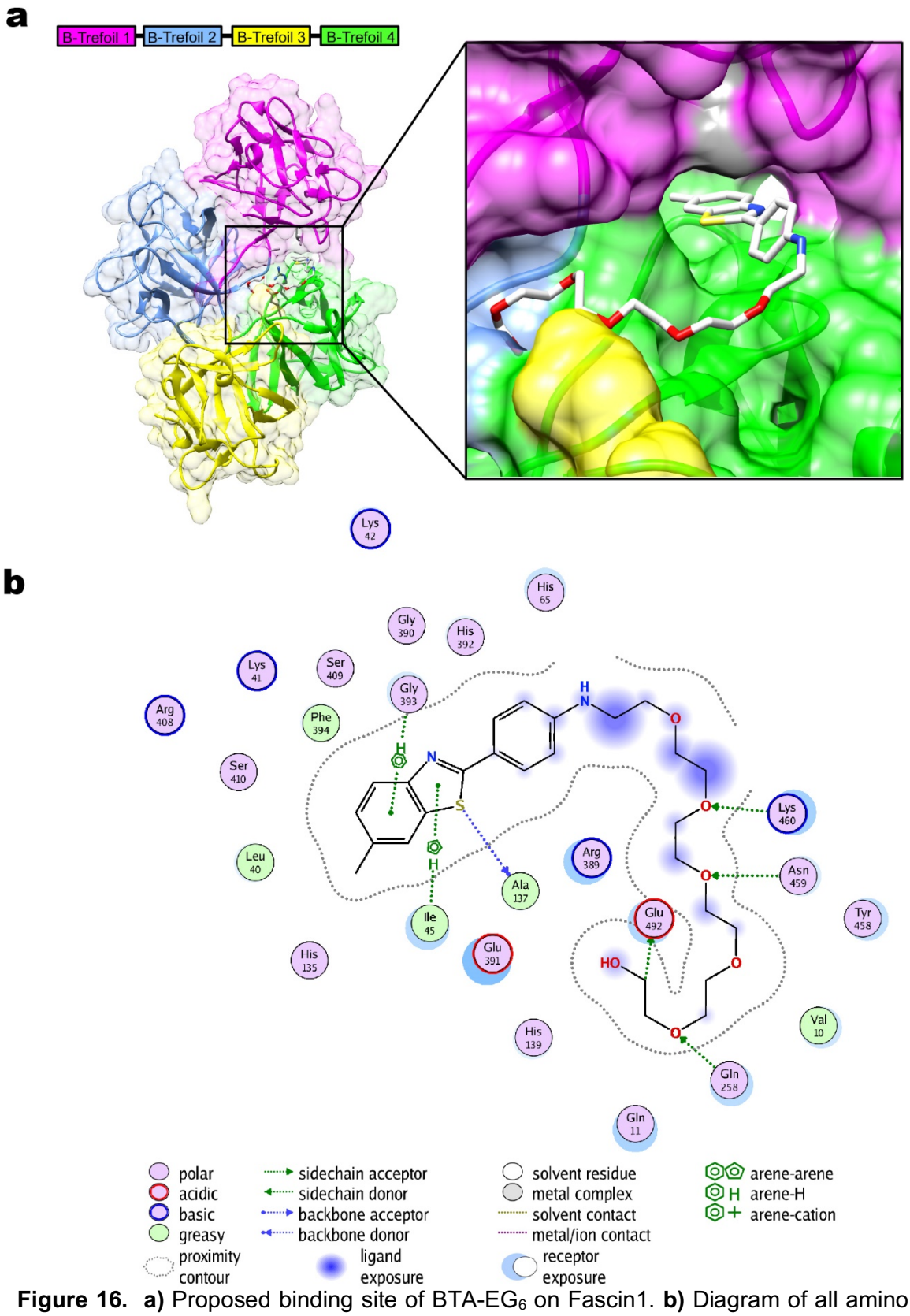

Figure 16. **a)** Proposed binding site of BTA-EG$_6$ on Fascin1. **b)** Diagram of all amino acids that interact directly with BTA-EG$_6$ in the proposed binding site

I build on these studies to provide additional structural evidence as to the binding pocket BTA-EG_6.

4.3 X-ray crystallography and protein NMR: advantages and disadvantages

The two methods that I chose for this analysis are x-ray crystallography and NMR of proteins in solution. These two techniques are complimentary and provides different information; however, the utility of each technique is dependent on the protein studied. Some proteins that are suitable for analysis by protein NMR may not have known crystallization conditions or may not crystallize well. Conversely, proteins that crystallize may not give resolved spectra by protein NMR. X-ray crystallography relies on the diffraction of an x-ray beam to reveal the three-dimensional structure of the electron clouds within the crystal lattice, while protein NMR reveals information about individual nuclei by using a strong magnetic field. Both techniques give insights into protein-ligand interactions, which could allow for the elucidation of interactions between BTA-EG_6 and Fascin1.

X-ray crystallography is not limited by the size of the protein being investigated, and it is relatively inexpensive and straightforward to produce a crystal when crystallization conditions are known. It can yield high atomic resolution and gives a direct indication of the three-dimensional structure of the protein. Its limitations are that the sample must be crystallizable and a single crystal must be obtained with a single lattice to procure good data. Many proteins exist where conditions for crystallization simply have not been found. Additional drawbacks to crystallography are that it provides a static representation of the protein, and that the conditions used to induce crystal formation may not accurately represent the native environment of the protein. Because of this it is

possible that the resulting “snapshot” of the protein may not represent a native conformation and is therefore not accurately depicting intermolecular and intramolecular interactions. The high-energy x-rays used for diffraction also destroy the sample.

The primary advantage of protein NMR is that it is a dynamic technique, meaning it provides a representation of different conformations and fluctuations that a protein may take at a high structural resolution. Protein NMR can give an idea of different intramolecular interactions and conformations the protein may take. The technique is noninvasive and non-destructive, assuming that the protein is stable in the solution. A limitation of protein NMR is the complexity of data interpretation. This is especially true of proteins with a molecular weight greater than or equal to 30kDa. Fascin1 a 55KDa protein, is larger than what is usually done in protein NMR. Finally, in order to achieve a high signal to noise ratio, a large amount of pure protein must be acquired. For context, the amount of Fascin1 I used for a single NMR experiment is equivalent to the amount needed for 300 wells of crystallization.

4.4 Screening x-ray protein crystallography conditions for Fascin1

Since crystallization conditions of Fascin1 are already published[54,132–135], I began with x-ray crystallography. In literature, most published papers use Fascin1 at a concentration of around 14mg/mL in a protein buffer including 20mM Tris, 40mM KBr, and 0.5M EDTA pH 8 for crystallization[54,132,135]. The Fascin1 is then mixed into crystallization buffers including 15-20% Polyethylene Glycol (PEG) of various molecular weights between 3500 and 8000, HEPES or Tris at 100mM pH 8, and 1mM DTT at a 1:1 ratio[33,132,133,135]. The final published conditions occasionally include additives such as 1-2.5% isopropanol[54,132,135], 4 % glycerol[133,134], or 200mM lithium acetate[134].

I was able to produce crystals of Fascin1 without the addition of BTA-EG_6 under a series of conditions via the hanging drop method[136]. Two sets of trays were prepared, one to test the pH from 6-8 at 14-24% of PEG 4000, and another to test glycerol, isopropanol, 1,4-butanediol, and 2-Methyl-2,4-pentanediol as additives at 3% (V/V) at a constant pH of 8.0 in HEPES buffer. Concentrated Fascin1 in protein buffer was added to crystallization buffer at a 1:1 ratio (2μL each). I found that Fascin1 often crystalizes more quickly along one axis, resulting in long toothpick shaped crystals. These crystals are not ideal, as I found that short thicker crystals are better for getting a good diffraction pattern. In my pH test, I found crystals in most wells, however at lower pH values the crystals became thin fragile-looking sheets which were not ideal for diffraction. The best crystals that I collected were found in HEPES at pH 8. For additives I found the most promising crystals in 3% isopropanol at PEG 4000 concentrations of 18% and 22%. I also found crystals in 3% 2-Methyl-2,4-pentanediol at PEG 4000 concentrations of 18% and 22% and in 3%1,4-butanediol at 22% PEG4000.

4.5 Crystallizing the protein Fascin1 in the presence of BTA-EG_6

I next attempted to crystalize Fascin1 in the presence of BTA-EG_6. BTA-EG_6 was added to 14mg/mL Fascin1 in protein buffer at a concentration of 2mM (near the maximum solubility of BTA-EG_6 in aqueous solution). The crystal conditions had a constant 100mM HEPES pH8, 1mM DTT. The range of PEG 4000 was 14-24% PEG4000 Each condition was run in duplicate with 6 conditions containing 3% isopropanol, and 6 conditions containing no isopropanol.

I found crystals in many of the conditions. Crystals were exchanged into cryo buffer (crystallization conditions plus additional glycerol for a final concentration of 30% cryoprotectant) to inhibit ice crystal formation upon flash-freezing, collected in loops and frozen in liquid nitrogen. Crystals were sent to the synchrotron at Argonne National Lab. Diffraction data collection was performed by remote control of the beamline at that location. Data was reduced with XDS package utilities[137], molecular replacement was performed with PHASER[138], then iterative refinement and building was performed with Coot[139] and phenix.refine[140]. Many of the crystals collected diffracted well, but the best resolution crystal came from the condition containing 18% PEG 4000, 100mM HEPES pH 8.0, 3% IPA, 1mM DTT. The crystal structure was found to belong to the C2 space group and was solved with a resolution of 2.1 angstroms (Figure 17).

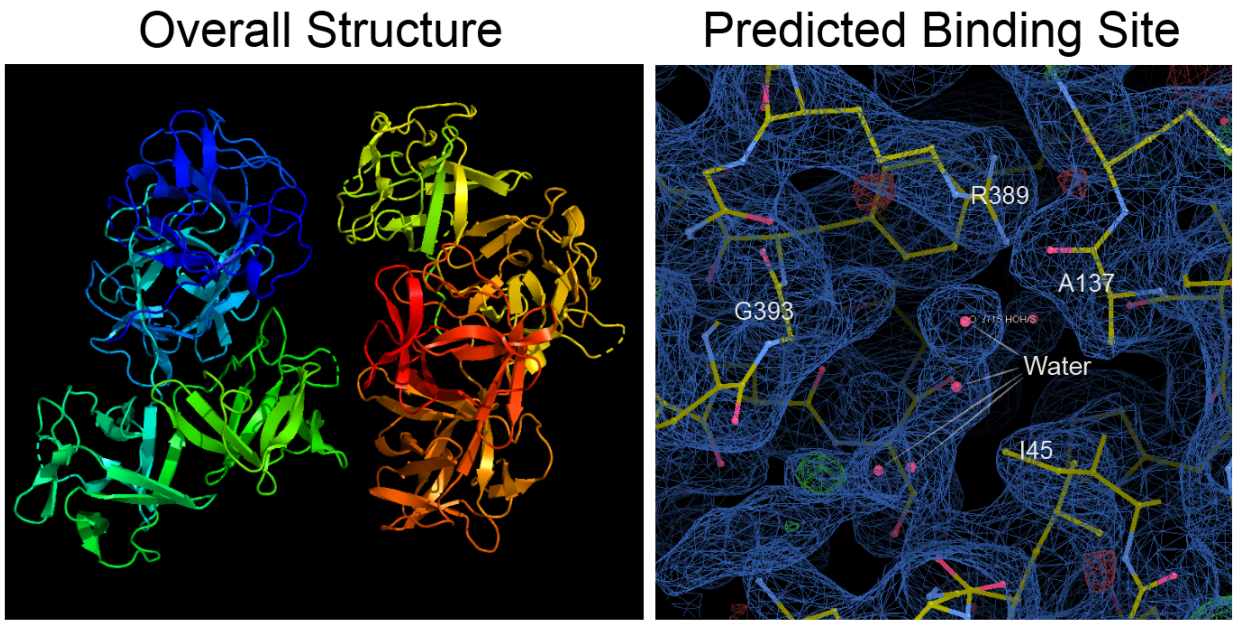

Figure 17. X-ray crystallography of Fascin1. Finished image of the 2.1 angstrom structure that I obtained showing both Fascin1 proteins in the repeating unit of the crystal (left panel). Electron density map at the proposed binding pocket of BTA-EG_6 (right panel). Images were obtained using Pymol2 and Coot.

Unfortunately, from this experiment no clear electron density corresponding to BTA-EG_6 was found in the structure (Figure 17). Several factors could have caused this

result. First, it is possible that the crystal lattice excludes the binding of BTA-EG_6. Second, the crystallization solvent could potentially interact with BTA-EG_6 and prevent its binding to Fascin1 in one of two ways. Complications could have arisen because BTA-EG_6 has a polyethylene glycol (PEG) tail and the crystallization solvent contains 18% PEG. The solubility of the compound is likely reduced in the crystallization solvent due to the PEG crowding agents in the crystallization conditions. Another potential complication is that the polyethylene glycol from the solvent could competitively exclude the compound from binding to the protein. This means that, because PEG and BTA-EG_6 have a polyethylene glycol moiety, the PEG, which is at solvent level concentrations (18% in this case) is more likely to bind to the protein and prevent BTA-EG_6 from binding. And if a large percentage of the binding pocket of BTA-EG_6 on the protein is occupied by PEG, it would prevent the visualization and identification of the electron density of the much smaller fraction bound by BTA-EG_6.

Although I found several water molecules in the proposed binding pocket (Figure 17), Jansen and co-workers published a structure of Fascin1 in the literature that has a number of small molecule electron densities including the labeling of PEG, and glycerol molecules[134]. Within the crystal lattice at the proposed binding pocket of BTA-EG_6 near Arginine 389 is a molecule of PEG, giving structural evidence to the hypothesis that PEG might be able to competitively exclude our compound from binding[134] (Figure 18).

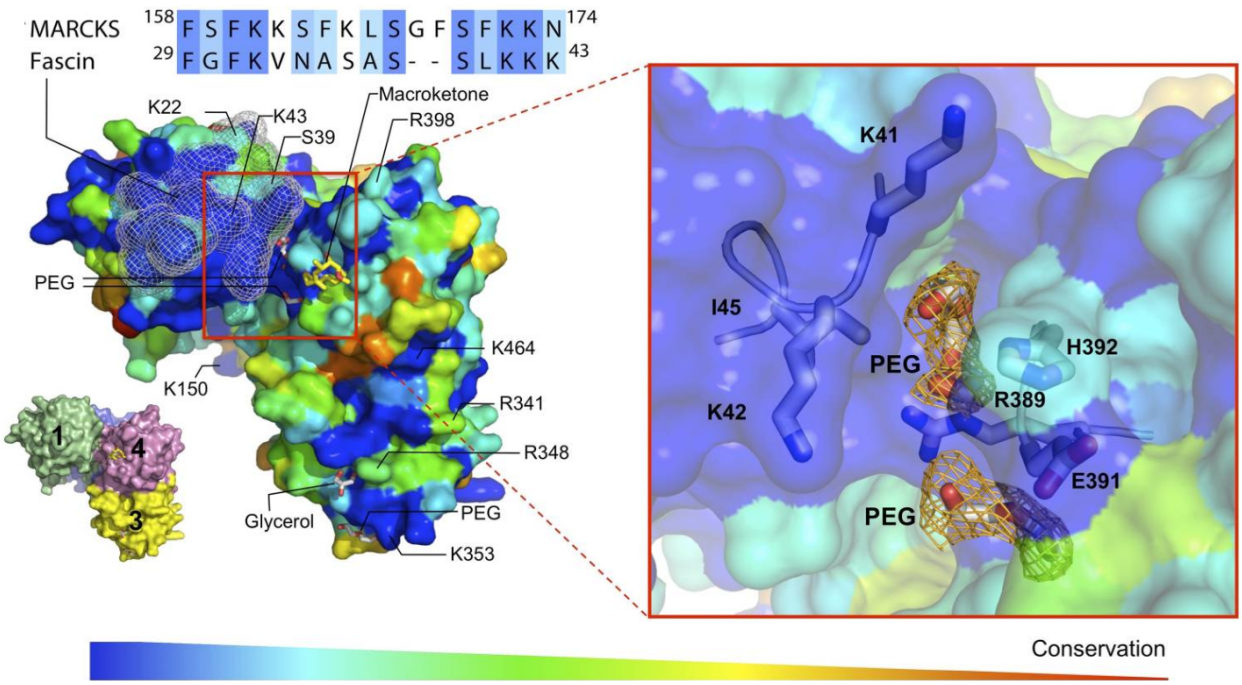

Figure 18. *A*, surface representation of the actin-binding site in β-trefoil-1 colored by residue conservation (*left*) and an enlarged view (*right*) showing molecules of PEG bound in the cleft formed at the interface between β-trefoil domains 1 and 4. Residue conservation decreases from *blue* to *red* as indicated by the *bar* at the *bottom* of the figure. Reproduced from Jansen *et al*[134].

Despite this setback, I attempted to find new crystallization conditions for Fascin1 that did not include PEG. I screened several libraries totaling hundreds of crystallization conditions but did not find any condition in which I could crystalize Fascin1 without PEG. To provide an alternate avenue for obtaining structural information about the binding of BTA-EG_6 to Fascin1, I explored the complementary technique of protein NMR.

4.6 Introduction to protein NMR

Solution protein NMR relies on identifying the amide N-H on the backbone of the polypeptide chain of the protein[141]. Since each N-H corresponds to a single amino acid, the number of peaks seen in a two-dimensional NMR analysis of ^{15}N ^{1}H protein should correspond to the number of amino acids in the protein, minus the prolines, which do not

have the N-H common to most amino acids. The starting methionine can often be removed during expression and processing by the host organism and is therefore not visible as well. Taking this into account, a protein like Fascin1 with 493 amino acids, 15 prolines, and a starter methionine should have 477 total N-H peaks.

In order for the amide nitrogen to appear in the NMR spectra, it must have the proper atomic spin[141], therefore the predominant form of nitrogen ^{14}N must be enriched with ^{15}N. Likewise, carbon atoms must be isotopically enriched with ^{13}C rather than the predominant natural occurring ^{12}C. The predominant form of Hydrogen ^{1}H does not need to be isotopically enriched. In fact, because this signal is present in so many molecules, the ^{1}H signal often needs to be suppressed by utilizing deuterium ^{2}H.

Each isotope produces a unique protein NMR signal and has its own unique one-dimensional spectrum. In addition, two-dimensional and three-dimensional NMR experiments allow for the correlation of nuclei that are nearby to each other. There are a number of experimental methods that can be employed to take advantage of the signals each nucleus provides by protein NMR. Heteronuclear single quantum coherence (HSQC) spectroscopy is the most common two-dimensional experiment, which correlates the N-H amide peaks as previously described[141]. Other three-dimensional experiments (named for the atoms and order in which the magnetization is passed) such as the HNCA correlate an N-H peak (HN) to the alpha carbon signal(CA)[142,143], and the HNCACB experiment correlates the N-H signal (HN) to both the alpha (CA) and beta carbons (CB) of a given amino acid[144]. Each experiment gives additional data because the alpha carbon chemical shifts are unique to some amino acids, and beta carbon chemical shifts are unique to even more amino acids, allowing for the correlation between a given N-H

peak and its amino acid identity. Transverse relaxation optimized spectroscopy (TROSY) experiments tend to give better signal and resolution for large proteins[145]. I utilize a combination of these experiments to provide evidence for a binding site of BTA-EG_6 to Fascin1.

4.7 Two-dimensional solution NMR of Fascin1

Since the x-ray crystallography experiment showed no evidence of BTA-EG_6 bound to Fascin1, I began experimenting with protein NMR of Fascin1. This method started out as an unlikely candidate for studying Fascin1 simply because it is considered to be too large for analysis by solution protein NMR. As mentioned previously, solution NMR tends to become too complicated with proteins of a size larger than 30kDa because many peaks begin to overlap. Since Fascin1 is a 54.5kDa protein, it seemed unlikely that Fascin1 would produce a viable NMR spectrum, as too many peaks would overlap one another. Despite these theoretical limitations, I was curious to see what information could be obtained through NMR methods.

I expressed and purified Fascin1 in Mengli minimal media with 15N labeled ammonium chloride. I initially attempted the analysis in a buffer containing 50mM HEPES pH 7.4, 100mM NaCl, and 1mM DTT with 100μM Fascin1, which gave excellent resolution in the NMR spectra. Since more peaks are visible at lower pH due to a slower exchange rate of the amide hydrogen with the solution, I later optimized my conditions to 40mM HEPES pH6, 90mM NaCl, 3mM TCEP, and 0.1%DMSO (deuterated) with 300μM Fascin1 and 10% deuterium oxide. The TROSY-HSQC spectrum showed excellent resolution for a protein of this size (Figure 19). Further analysis and assignment of peaks will be discussed in later sections of this chapter. All data in the NMR spectra of this chapter

were collected at 37ºC on a Bruker Avance Neo 800MHz spectrometer, and data was processed using NMRPIPE[146] and analyzed with Bruker Topspin4(www.bruker.com). Images were produced using the Bruker Topspin4 software and Adobe Illustrator.

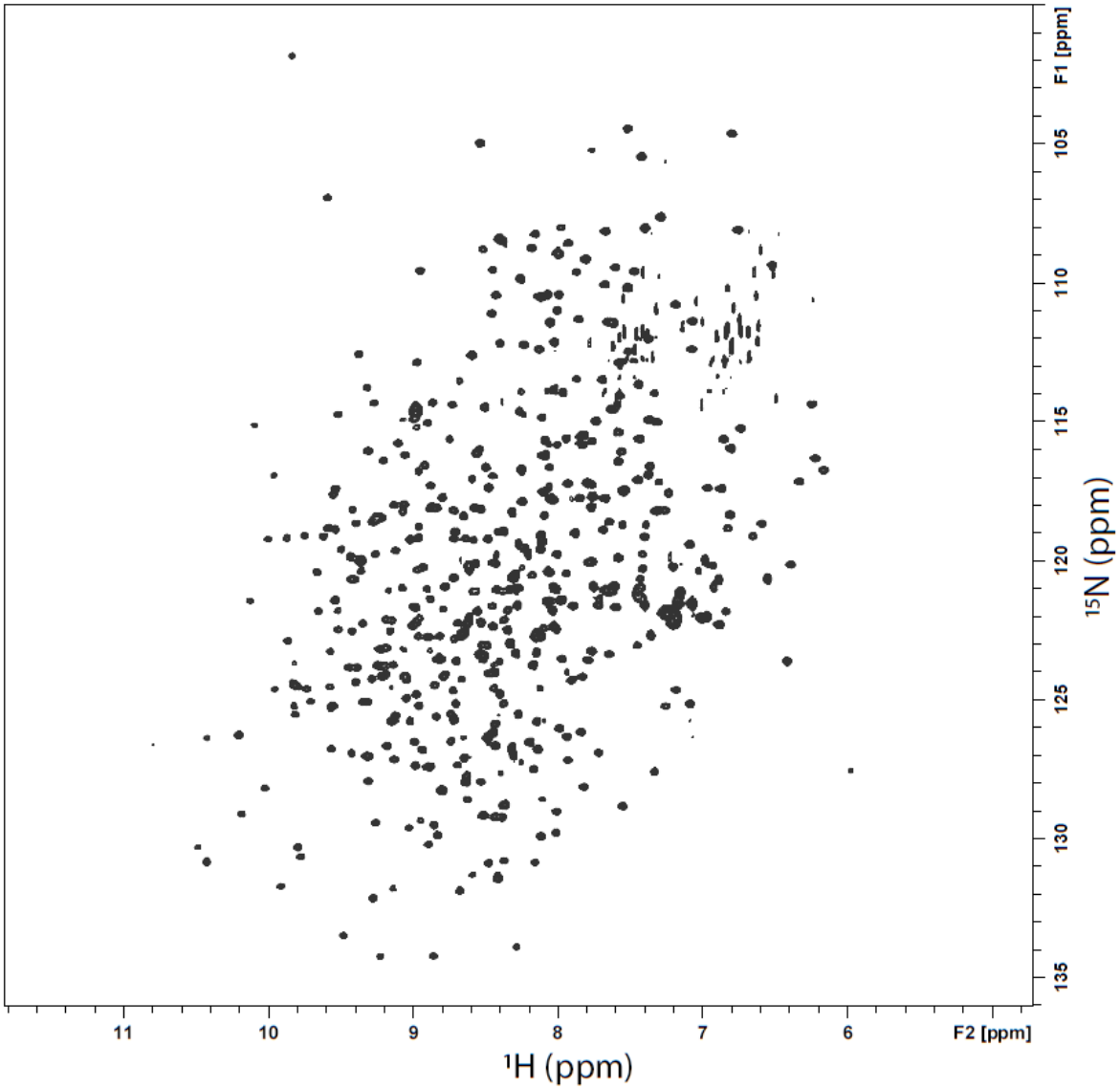

Figure 19. TROSY-HSQC of Fascin1 in solution. 463 out of 477 expected peaks were visualized for 97% coverage. Image produced using Topspin4 and Adobe Illustrator.

Glutamine and asparagine residues also have N-H signals from their sidechains that can appear in the same region as the N-H signals from the backbone. Since the sidechain peaks do not correlate to the amide N-H signal that I am studying, they must

be removed from peak counting for identifying coverage. In my spectra they appear in the range of δ6-8 ppm on the H axis and δ105-115ppm on the N axis in the spectra I collected and appear elongated in the nitrogen dimension. After accounting for the glutamine and asparagine sidechains, the spectrum was found to contain 463 out of the 477 expected peaks of Fascin1, representing 97% coverage. There is excellent resolution for most peaks with relatively few overlapping signals which makes it very high quality for a protein of this size.

After completing the experiments on Fascin without BTA-EG_6, I ran the TROSY-HSQC experiment in the same conditions with the addition of 600μM BTA-EG_6 (a 2:1 small molecule to protein ratio) to look for perturbations in the spectrum that might correlate to the amino acids that interact with BTA-EG_6. I then overlayed the spectrum with the apo protein spectrum (Figure 20). While most of the peaks overlap well between the two spectra, there are approximately 50 peaks with a clear chemical shift. These peaks likely correspond to amino acid residues that shifted due to compound binding through proximity to BTA-EG_6. The peak shifts could also be a result of a conformational change that happens when BTA-EG_6 binds Fascin1.

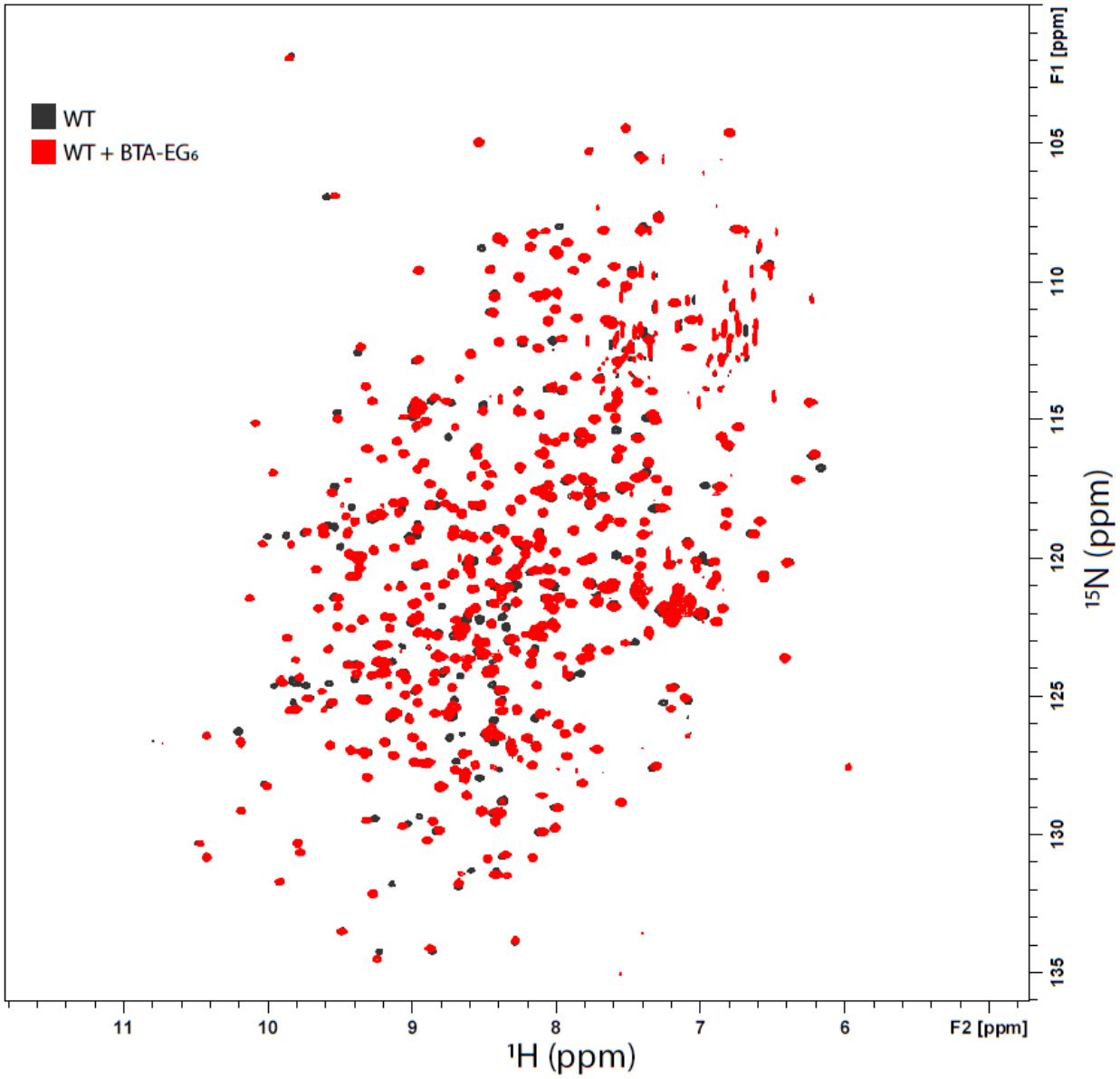

Figure 20. TROSY-HSQC of Fascin1 in solution (black) overlayed with TROSY-HSQC of Fascin1 with 600uM BTA-EG_6(red). Most of the peaks are precisely overlayed, however there are approximately 50 peaks with a noticeable change in chemical environment. Image produced using Topspin4 and Adobe Illustrator.

4.8 Attempts to assign peaks by three-dimensional NMR Analysis

To assign each peak to an amino acid residue, I used three-dimensional NMR analysis in an attempt to assign the peaks that I had seen in my previous two-dimensional

NMR analysis with the amino acids of the primary sequence of Fascin1. This can be accomplished by growing protein in media that is enriched for both ^{13}C and ^{15}N. The protein can be analyzed by a TROSY coupled HNCA experiment[145,147]. With this method, each N-H signal is coupled to the alpha carbon signal on the amino acid in question (residue i), and is also coupled to the alpha carbon of the previous residue on the amino acid chain (residue i-1) resulting in a weaker peak that is vertically aligned on the ^{1}H-^{13}C spectra for a given 15N plane (Figure 21).[148] The weaker signal will have a corresponding strong signal to the i-1 residue with an identical 13C shift. This allows "walking" along the

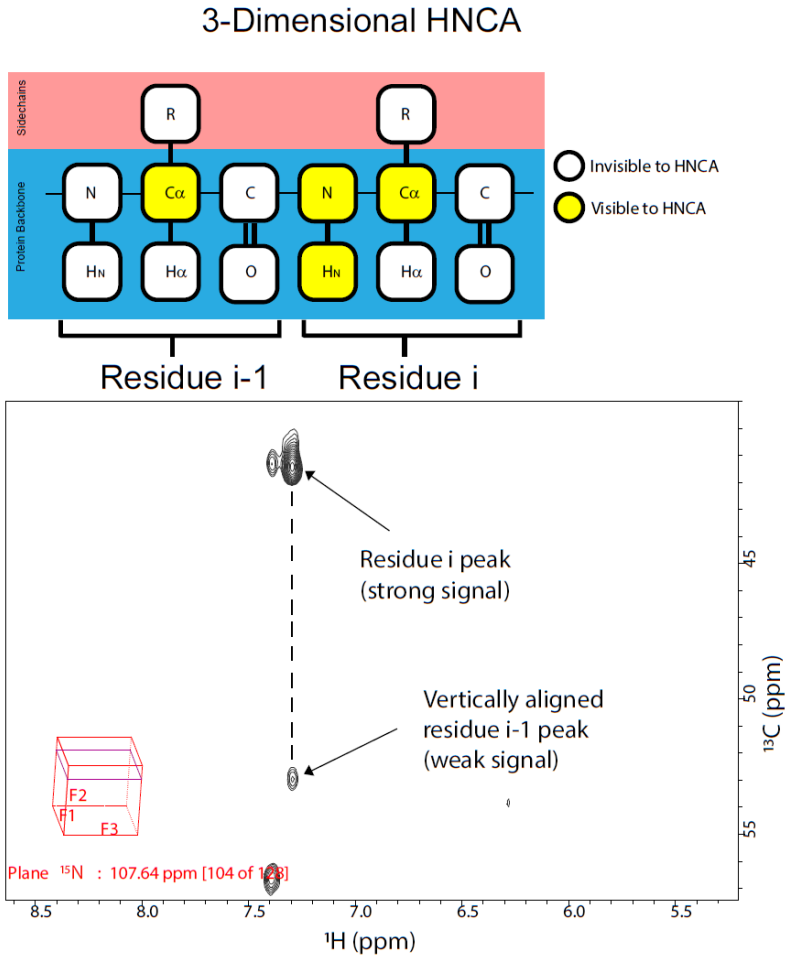

Figure 21. Example of a ^{15}N plane (107.64ppm) from the Fascin1 3D HNCA data demonstrating protein assignment by "walking" along the backbone of the protein. For a single N-H residue peak there will be a strong peak corresponding to that residue (i) and a vertically aligned weak peak corresponding to the previous residue (i-1). Spectrum produced using Topspin4 and Adobe Illustrator

backbone of the protein from residue to residue to identify the NH peaks that are adjacent to one another in the primary sequence of the protein. Although many amino acids have nondescript chemical shifts, certain amino acids like glycine have unique chemical ^{15}N and ^{13}C shifts that are distinct because the side chain of glycine attached to the α-carbon is a hydrogen, while all other amino acids contain a β-carbon attached to the α-carbon[149]. By comparing the identifiable amino acids to the primary amino acid sequence, it becomes possible to assign each NH peak.

However, I found that because Fascin1 was so large, I was only able to assign a few peaks in this manner. While navigation in the periphery of my spectra was manageable, I was unable to definitively "walk" along the backbone of my protein when the peaks were more densely packed because too many signals had identical ^{13}C shifts, which complicated analysis. Attempts to address this issue by selective labeling and truncation of Fascin1 will be discussed in section 4.9. I also attempted to collect additional three-dimensional NMR data including an HNCACB[144], CBCAHN[144], and HN(CO)CA[150], to give additional data to assist in the positive identification of residues, however in each case at 300μM Fascin1 there was not sufficient signal to collect a spectrum of useful quality.

Although my initial attempt to fully assign the protein by three-dimensional NMR analysis was unsuccessful, the HNCA spectrum allowed for identification of specific residues involved in the binding of BTA-EG_6 which will be discussed in later sections of this chapter.

4.9 Using the Cfa intein to selectively label Fascin1

Since I was unable to identify the residues of the full-length Fascin1 protein, I attempted reduce the amount of data in the NMR spectrum by partial isotopic labeling of Fascin1 utilizing an intein reaction strategy. Inteins are a class of enzyme that catalyze the splicing of two amino acid sequences together[151]. The advantages of using an intein to splice together two protein sequences in NMR is that the two halves of the protein can be grown separately, meaning that one of the sequences can be labeled with isotopes for visualization by two and three-dimensional NMR analyses, while the other can be unlabeled, rendering it undetectable by NMR (Figure 22b). This reduction in data makes peak assignments easier to deconvolute. Specifically, the Cfa_{GEP} intein, engineered from the Cysteine-Phenylalanine-Alanine (CFA) consensus sequence among naturally occurring, DnaE inteins[152] and modified to include a glycine-glutamic acid-proline loop (GEP)[153] (hereon referred to as Cfa), was selected for use in these experiments because it is fast reacting, only leaves a single amino acid "scar" between the two spliced sequences, and is promiscuous, meaning that it functions well regardless of the two protein sequences being spliced together[153]. If the Cfa segments are histidine tagged, initial purification of the intein reactants can be accomplished by nickel affinity chromatography, then after the intein reaction has taken place purification of the spliced protein product from the Cfa proteins can be accomplished by reverse nickel affinity chromatography (Figure 22a). Fascin1 natively contains a cysteine on the linker between β-trefoil 2 and β-trefoil 3, meaning that I could accomplish the labeling reaction without even leaving a scar on the protein (Figure 22c).

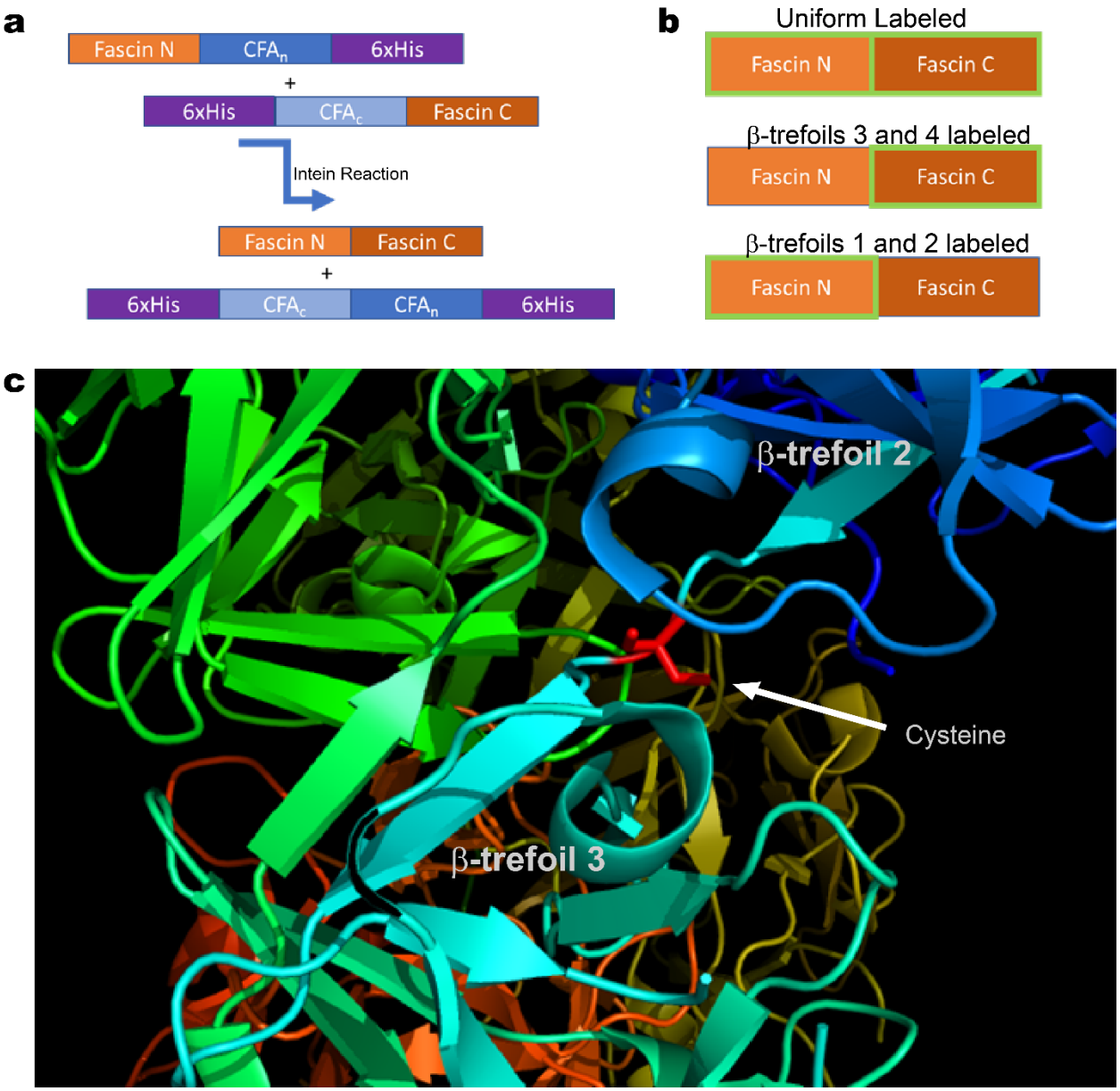

Figure 22. Design of Cfa constructs. **a)** Purification scheme using nickel affinity chromatography for purification the Cfa constructs, and reverse nickel affinity chromatography to separate the final product from the Cfa proteins. **b)** Diagram comparing uniform labeled protein to the half-labeled products that can result from segmental labeling. Green outlines indicate isotopically labeled sections. **c)** Image of the protein Fascin1 with β-trefoil 2, β-trefoil 3 and the native cysteine residue(red) on the linker between the two trefoils. Image rendered in PyMol2 from PDB entry 3llp[133].

I designed two constructs that I named CfaC-FascinC, and FascinN-CfaN, where C refers to belonging to the c-terminal half of the Fascin1 protein/construct and N refers

to the n-terminal half of the Fascin1 protein/construct. Unfortunately, I found that FascinN-CfaN expressed solely into the inclusion bodies, meaning that purification would require a denaturing reagent such as urea, followed by a post-translational protein refolding step since urea denatures the protein. Fortunately, both nickel affinity chromatography and the intein reaction work in the presence of urea. I purified both constructs and added them to a final concentration of 15μM each in an initial 6M urea that was slowly dialyzed out as the intein reaction proceeded.

Due to the kinetics of the reaction the Cfa intein works better at warmer temperatures; however, urea can modify proteins at warmer temperatures by carbamylating the lysine and arginine residues. I therefore tested the intein reaction at both 37ºC and at 4ºC. After verifying by SDS-PAGE that both temperatures achieved formation of full length Fascin1 product (Figure 23), I proceeded with using only the reacted protein at 4ºC, to protect the protein from carbamylation. I then purified the solution using a reverse-nickel column and used dialysis to remove the remaining urea. The removal of urea caused most of the protein to become insoluble. Fortunately, there was sufficient protein in the soluble fraction for purification by anion exchange chromatography. Two peaks of pure Fascin eluted off the column. Electrostatic differences in the protein are responsible for the presence of two peaks. I tested these two peaks by circular dichroism (CD) spectroscopy to check if the folding of the protein in the peaks matched the folding of wild-type Fascin1. Both peaks did not match the wild-type Fascin-1 peak, meaning that the overall folding of the proteins in the two peaks were different from natively folded Fascin1 (Figure 23). Since the protein was misfolded there was no reason to collect sufficient sample for NMR.

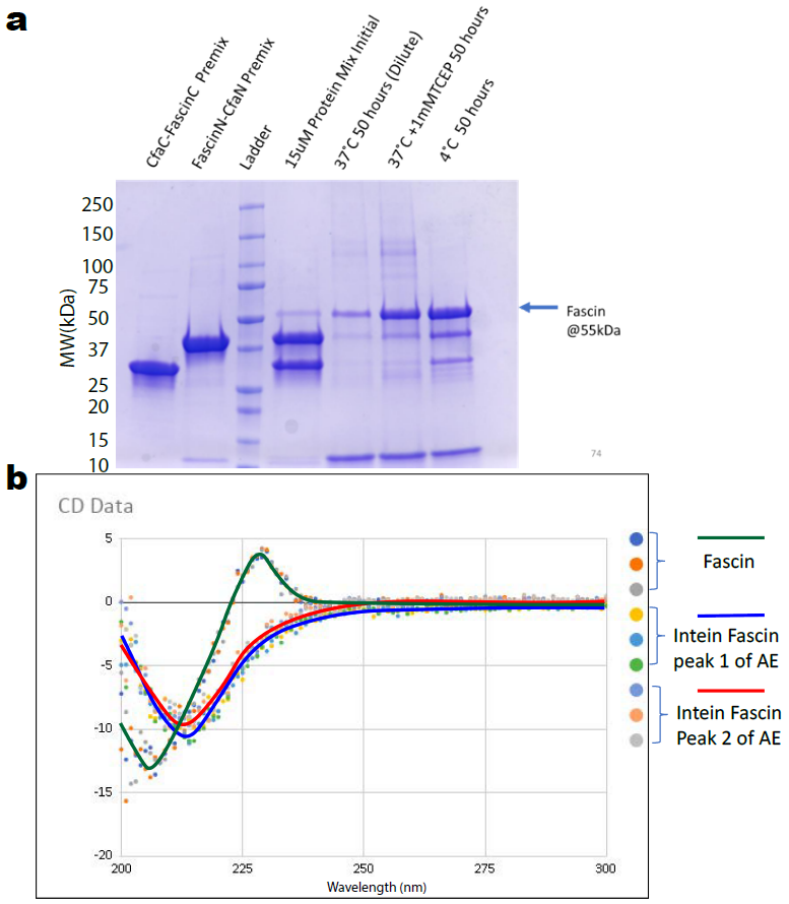

Figure 23. **a)** Intein reaction monitored by SDS-PAGE and Coomassie blue staining. **b)** circular dichroism spectra of wild type natively folded Fascin1 (green) compared to the two peaks eluted off of the anion exchange(AE) column from intein reacted Fascin1(blue and red). The intein reacted Fascin1 does not align with natively folded Fascin1 indicating that the intein reacted Fascin1 is misfolded.

I attempted many variations on refolding the intein-generated Fascin1 protein but was unable to achieve properly folded full-length product. I also redesigned and subcloned the intein to splice between β-trefoil 1 and β-trefoil 2, and between β-trefoil 3 and β-trefoil 4, rather than my initial attempts to splice halfway through the protein between β-trefoil 2 and β-trefoil 3. Each of these attempts resulted in protein that required refolding and gave similar results of improperly folded Fascin1 product as the initial attempt.

I also attempted variations on truncating the protein coupled to GST, however the protein either expressed poorly or precipitated out of solution before or after the cleavage of the GST tag. These studies led me to conclude that Fascin1 needs to remain intact to maintain a properly folded conformation. The removal of a β-trefoil domain during expression and purification was problematic because this potentially exposed too many natively buried hydrophobic residues to the polar solvent environment, which destabilized the protein and caused it to precipitate out of solution.

4.10 Identification of residues involved in the binding pocket of BTA-EG_6 by a combination of selective isotope labeling and site-directed mutagenesis.

Since assigning the residues of full-length Fascin1 was not feasible by the methods previously employed, I shifted my focus to identification of key residues involved in the binding of BTA-EG_6 using a combination of selective amino acid labeling and site directed mutagenesis.

With the help of Prof. Stanley Opella, Prof. Galia Debelouchina, and Dr. Sang Ho Park (all experts on protein NMR at UCSD), I selected two residues to identify in the NMR spectrum that were proposed to interact with BTA-EG_6 in the binding pocket of Fascin1, G393 and A137 (Figure16b). Aashish Shivkumar in the Yang lab had already created several mutants including G393E and A137K for the isothermal titration calorimetry experiments discussed in section 4.2. These mutants expressed well and matched the folding of wild-type Fascin1 as assessed by CD. Therefore, I selected the mutants G393E (glycine to glutamic acid) and A137K (alanine to lysine) for identification and further analysis.

4.11 Identification of the peak belonging to G393

I expressed and purified ^{15}N uniform labeled G393E mutant protein for two-dimensional NMR analysis by TROSY-HSQC. I overlayed the mutated spectrum and wild-type spectra for further analysis (Figure 24). Since glutamic acid contains a negatively charged sidechain at the experimental conditions, I expected this amino acid mutation to cause a large perturbation in the chemical shifts of nearby residues, larger than that seen by BTA-EG_6 binding, because BTA-EG_6 does not contain a formal charge. This was confirmed with around 60 peaks showing a visible chemical shift. I also anticipated the disappearance of one residue (corresponding to G393) and the appearance of a new residue (corresponding to mutated E393). The disappearance of the G393 residue is the clearest indication of the identity of the peak belonging to G393 in the wild-type spectrum.

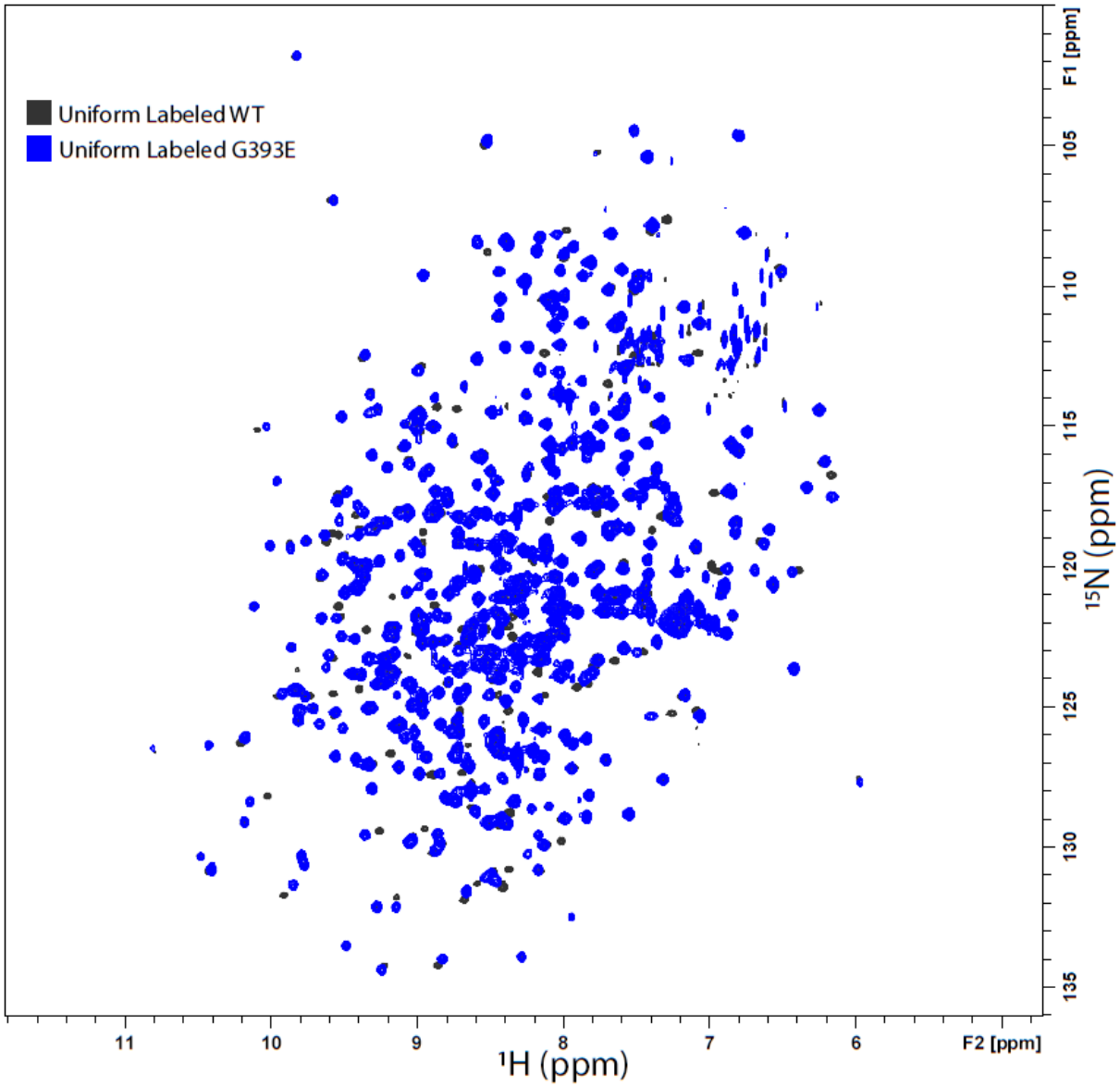

Figure 24. Overlay of the TROSY-HSQC for uniform labeled wildtype Fascin1 (black) with the TROSY-HSQC of uniform labeled G393E (blue). Image produced using Topspin4 and Adobe Illustrator.

Selective glycine labeling was not requried for identification of glycine peaks because glycine residues contain a characteristic α-carbon chemical shift and I had previously collected α-carbon data when completing the three-dimensional HNCA experiments. Glycine residues, with a hydrogen R-group, have a unique α-carbon chemical shift that is upfield, averaging around 45.378ppm. All 19 other common amino

acids have a β-carbon adjacent to the α-carbon, which is a significant change in chemical environment. These other amino acids, therefore, have an average α-carbon chemical shift ranging from 53-63ppm[149]. I inspected the HNCA three-dimensional spectrum correlating the N-H peaks to the α-carbon and found a peak that disappeared from the G393E spectrum, without a corresponding new peak appearing nearby (Figures 24 and 25). This could have been caused by the disappearance of one of two nearby peaks, which I will refer to as peak 1 and peak 2 (Figure 25). Using the three-dimensional HNCA data I obtained in section 4.8, I was able to identify peak 1 as glycine due to its signature chemical shift, while based off its chemical shift peak 2 is not glycine (Figure 25). Thus, I refer to peak 1 as peak G393 in the discussion that follows.

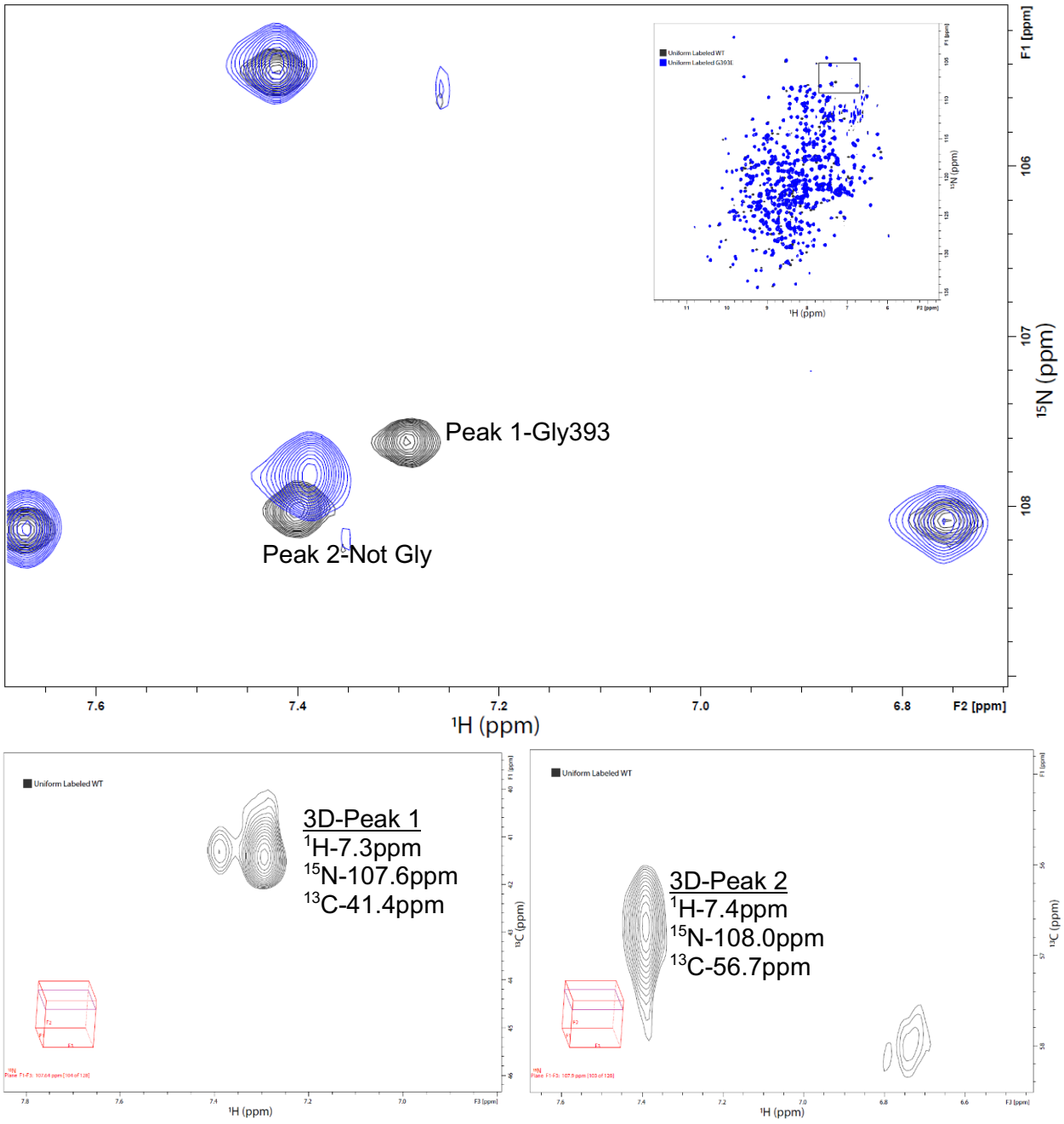

Figure 25. Zoomed in overlay of the TROSY-HSQC for uniform labeled wild-type Fascin1 (black) with the TROSY-HSQC of uniform labeled G393E (top panel). Using the three-dimensional HNCA I had previously obtained, I identified the α-carbon shift of Peak 1 to be 41.4, which is indicative of glycine (bottom left panel). Peak 2 had an α-carbon shift of 56.7, which is clearly not a glycine (bottom right panel). Spectra produced using Topspin4 and Adobe Illustrator.

I next utilized my earlier spectra at the same chemical shift values comparing Fascin1-WT and Fascin1-WT with BTA-EG_6 overlayed (Figure 20) to discover if peak G393 has a chemical shift upon the binding of BTA-EG_6. I indeed observed chemical shift of peak G393 in the presence of BTA-EG_6 (Figure 26), supporting the idea that G393 may be present in the binding pocket of BTA-EG_6 to Fascin1.

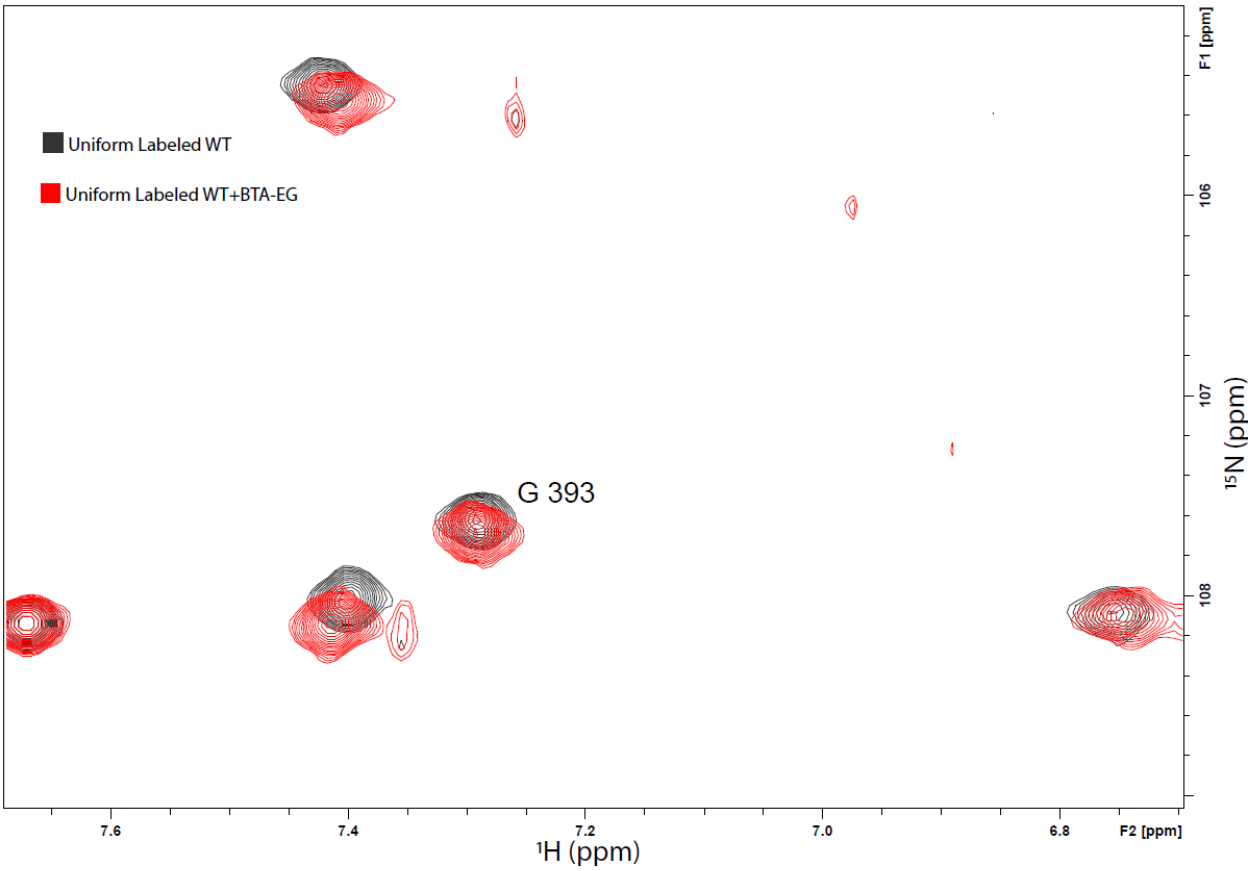

Figure 26. Zoomed in overlay of Figure 17 around G 393 showing uniform labeled WT Fascin1 with (red) and without (black) BTA-EG_6. Peak G393 shows a chemical shift upon binding to BTA-EG_6. Image produced using Topspin4 and Adobe Illustrator.

4.12 Investigation of the peak belonging to A137

Now that I had identified the peak in the Fascin1-WT spectrum belonging to G393, I turned my attention to A137, the other peak I had selected for investigation in section 4.10. I expressed and purified uniform ^{15}N labeled A137K. As in G393E, the mutation should create a perturbation larger than that caused by BTA-EG_6 binding because at the

mutated lysine introduces a formal charge. The disappearance of the A137 signal, and the appearance of the mutated K137 signal are also expected in the mutated spectrum. I expressed and purified A137K mutant Fascin1 and overlayed the spectrum with wild type Fascin1 as before (Figure 27). As in the previous mutation there is good convergence between the two spectra with approximately 60 peaks that do not overlap.

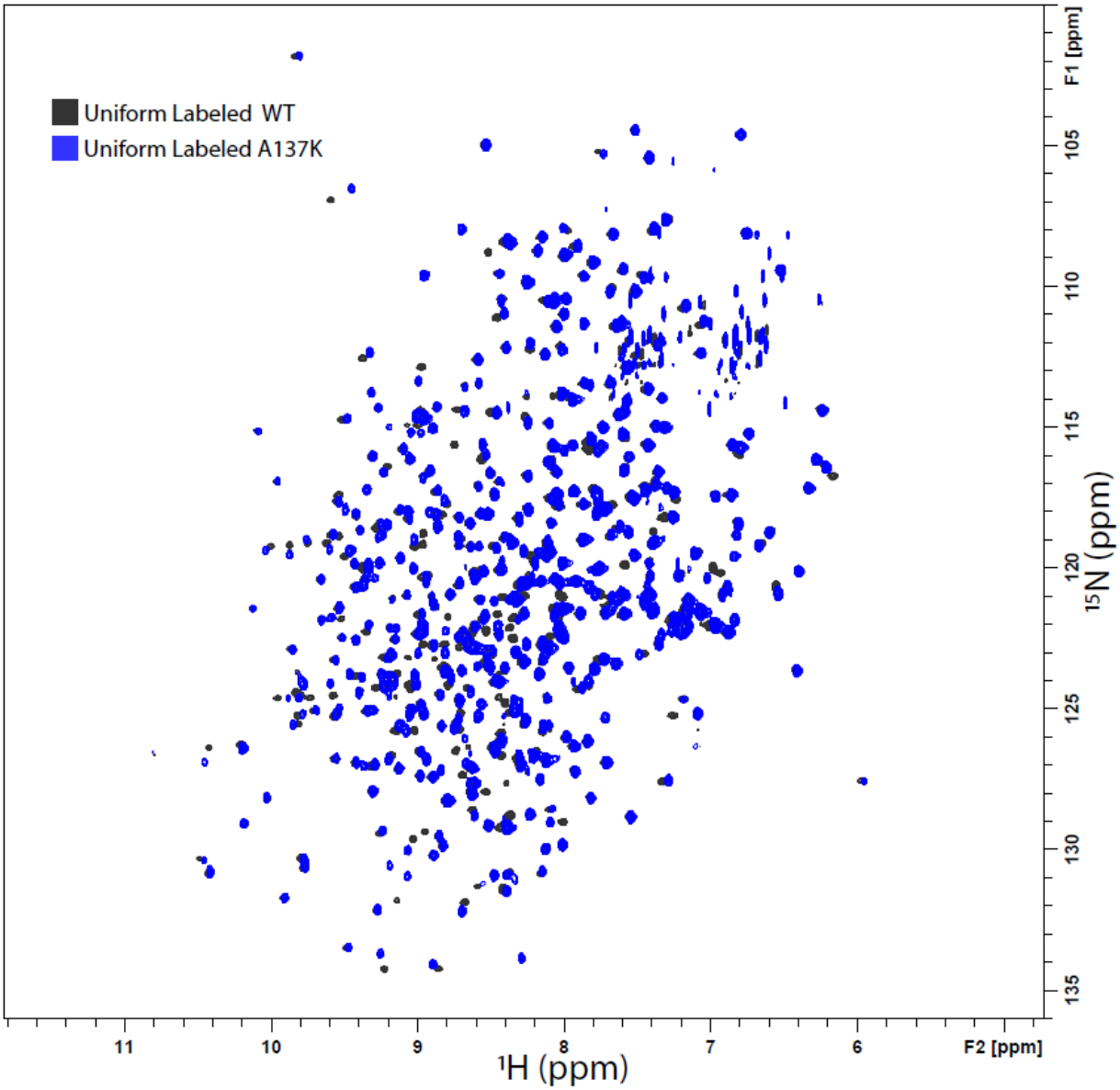

Figure 27. Overlay of the TROSY-HSQC for uniform labeled wildtype Fascin1 (black) with the TROSY-HSQC of uniform labeled A137K (blue). Image produced using Topspin4 and Adobe Illustrator

Unlike glycine, alanine does not contain a unique average chemical shift. I began to search for A137 by selectively labeling alanine residues of my wild-type and mutant proteins. This is accomplished by growing bacteria without any labels for incorporation into the proteins, and then spiking the media with the ^{15}N labeled alanine and the 19 other unlabeled common amino acids prior to induction. Providing all the amino acids suppresses the interconversion of amino acids through the bacteria's natural metabolic pathways for a short time. For this reason, expression can only be induced for a few hours, and usually at 37°C. Fascin1 is normally expressed into inclusion bodies at 37°C and to mitigate this problem it is normally induced overnight at 17ºC. Therefore, it was necessary to optimize Fascin1 expression for the incorporation of alanine labels.

I completed a series of small-scale experiments and tested various bacterial strains and expression for 2 hours at 37ºC, 2.5 hours at 30ºC, and 3 hours at 20ºC. I found the greatest expression of Fascin1 into the supernatant with the use of LEMO BL21s[154] with 100µM rhamnose to slightly activate the T7 Lysozyme expression that is included in this strain of BL21 cells.

I expressed and purified sufficient protein to perform a TROSY-HSQC experiment with Fascin1 at 190µM. The resulting spectrum overlapped well with the spectrum of full-length uniform labeled Fascin1 protein (Figure 28).

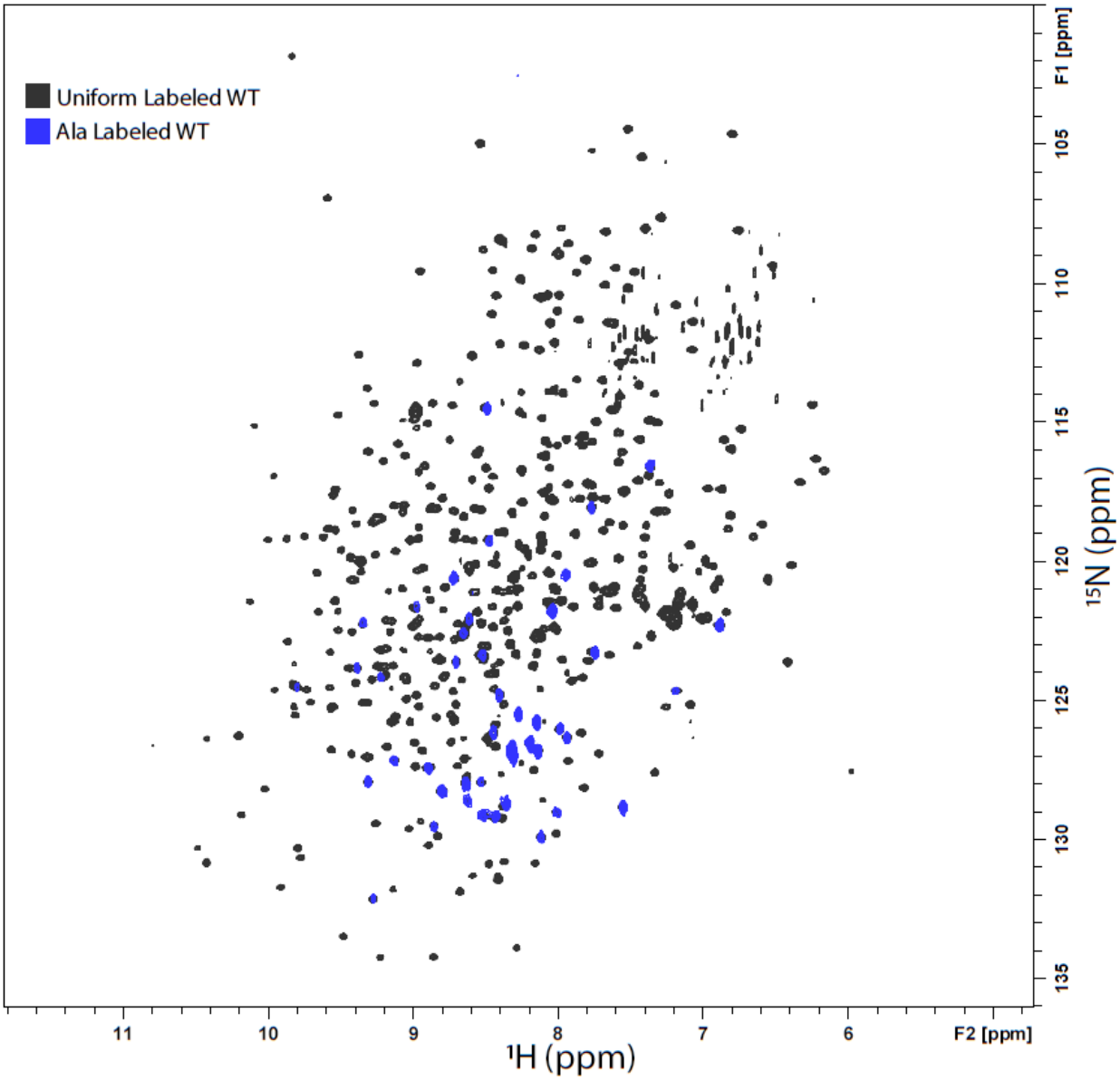

Figure 28. Overlay of the TROSY-HSQC for uniform labeled wild-type Fascin1 (black) with the TROSY-HSQC of alanine labeled wild-type Fascin1 (blue). Image produced using Topspin4 and Adobe Illustrator.

I found 45 peaks out of 49 expected total alanine residues in the protein sequence for 92% coverage, which is reasonably close to the 97% overall coverage for uniform-labeled Fascin1. Combining the alanine labeled Fascin1 spectrum with the uniform labeled WT Fascin1 and A137K Fascin1 spectra, it was easier to identify alanine residues

that disappeared in the A137K spectrum. The most promising candidates were in a cluster of four residues, three of which were alanine. (Figure 29) I will refer to them as $P1_A$, $P2_A$, P3, and $P4_A$ with the subscript A denoting an alanine identified from the alanine labeled WT-Fascin1 spectrum (Figure 28).

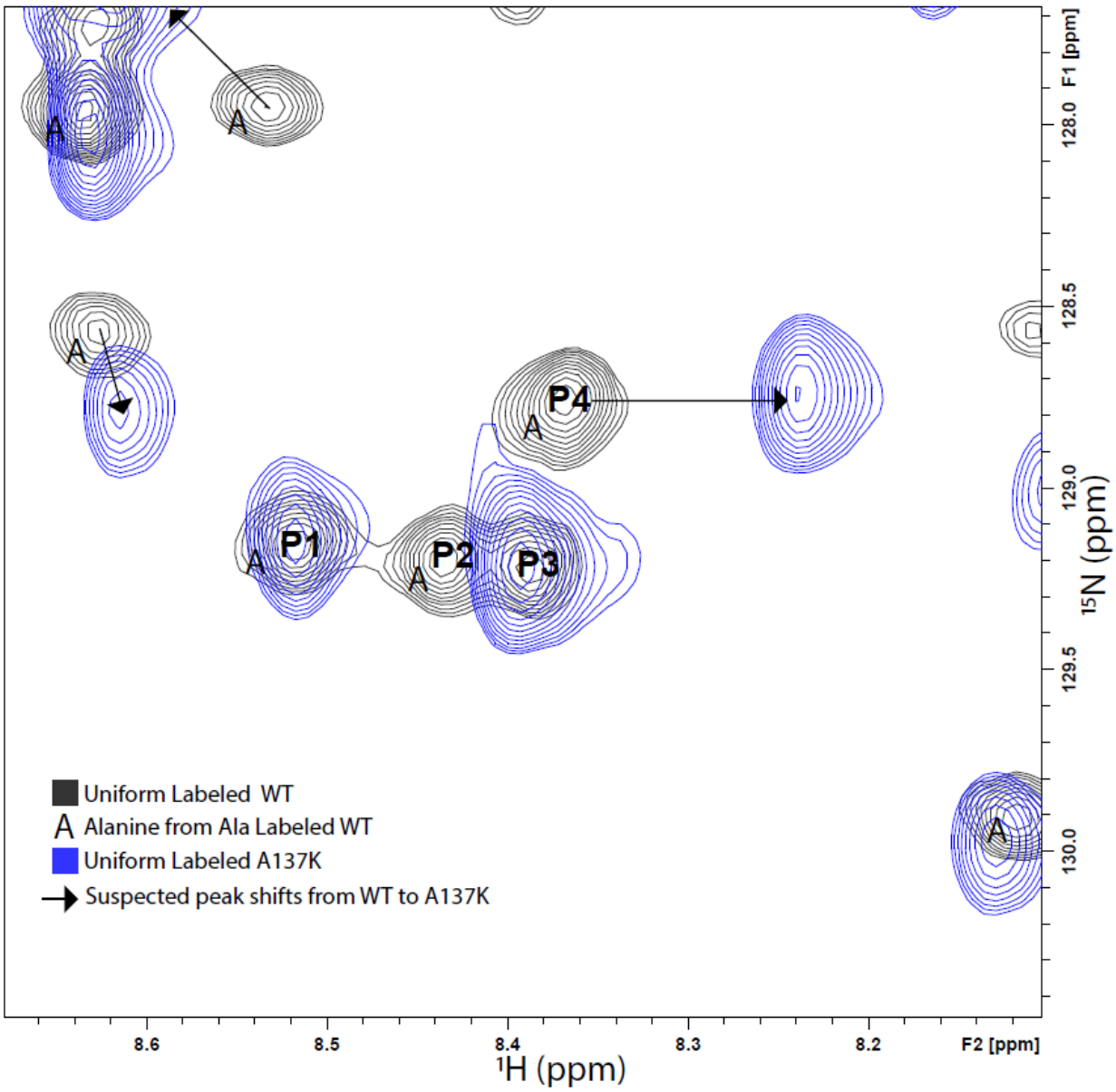

Figure 29. Zoomed in overlay of the TROSY-HSQC for uniform labeled wild-type Fascin1 (black) with the TROSY-HSQC of alanine labeled wild-type Fascin1 (blue). Alanine residues from alanine labeled WT-Fascin1 are labeled with "A" and arrows denote suspected peak shifts from WT to A137K Fascin1. Image produced using Topspin4 and Adobe Illustrator.

The overlayed spectra show that $P1_A$ and P3 do not show changes in chemical shift, $P4_A$ shifts upfield in the hydrogen dimension, and $P2_A$ disappears, suggesting that $P2_A$ is A137. However, P3 increases in intensity, making the shift of $P2_A$ underneath P3 possible (Figure 29). To investigate this possibility, I expressed and purified alanine labeled A137K Fascin1. The spectrum overlayed well with the A137K uniform labeled spectrum (Figure 30).

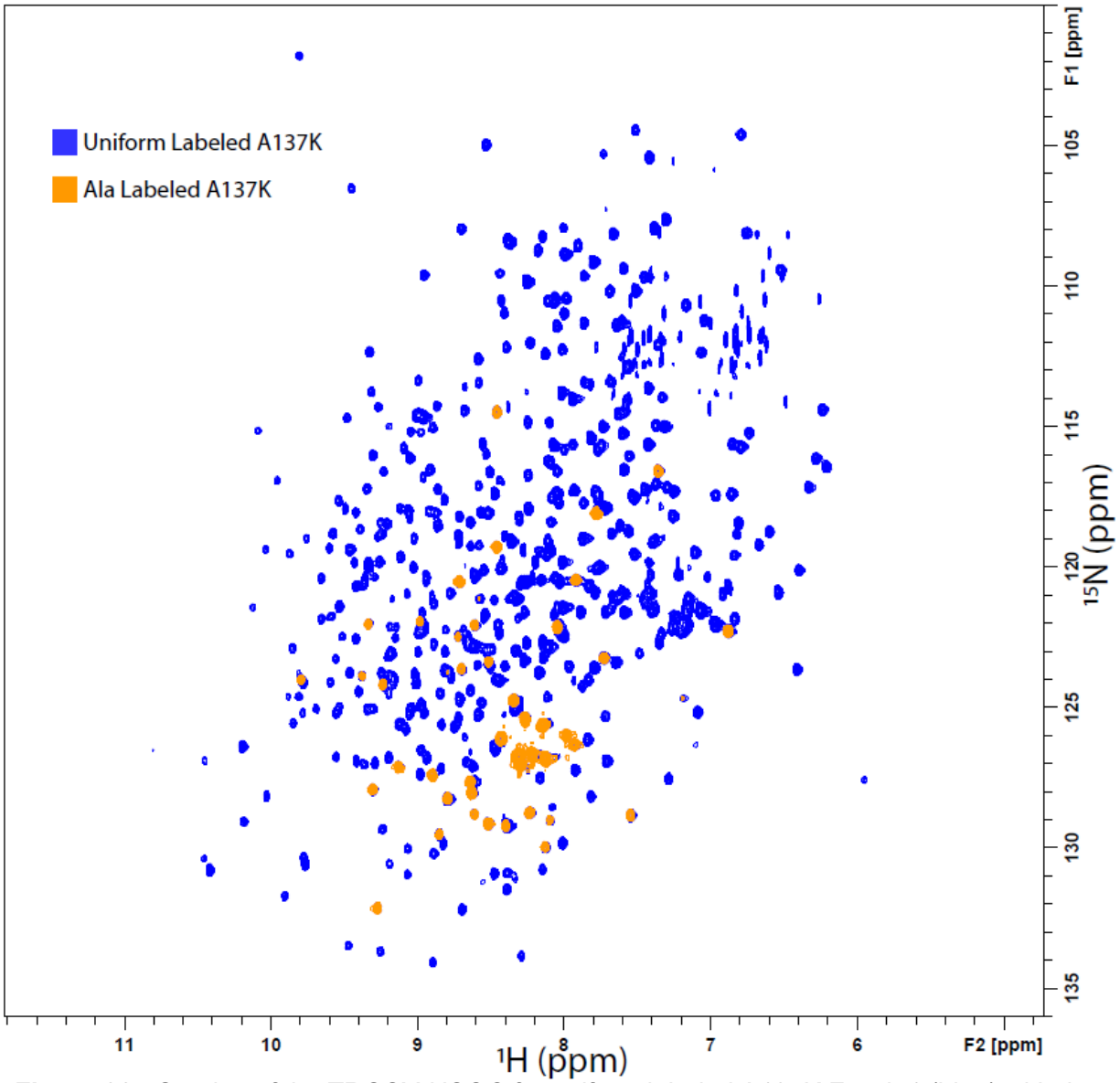

Figure 30. Overlay of the TROSY-HSQC for uniform labeled A137K Fascin1 (blue) with the TROSY-HSQC of alanine labeled A137K Fascin1 (orange). Image produced using Topspin4 and Adobe Illustrator.

The alanine labeling of A137K Fascin1 showed that $P2_A$ shifted underneath P3 as a result of the alanine to lysine mutation, explaining both the disappearance of $P2_A$ and the increased intensity of P3 in the A137K spectrum (Figure 31). $P2_A$ therefore cannot be A137.

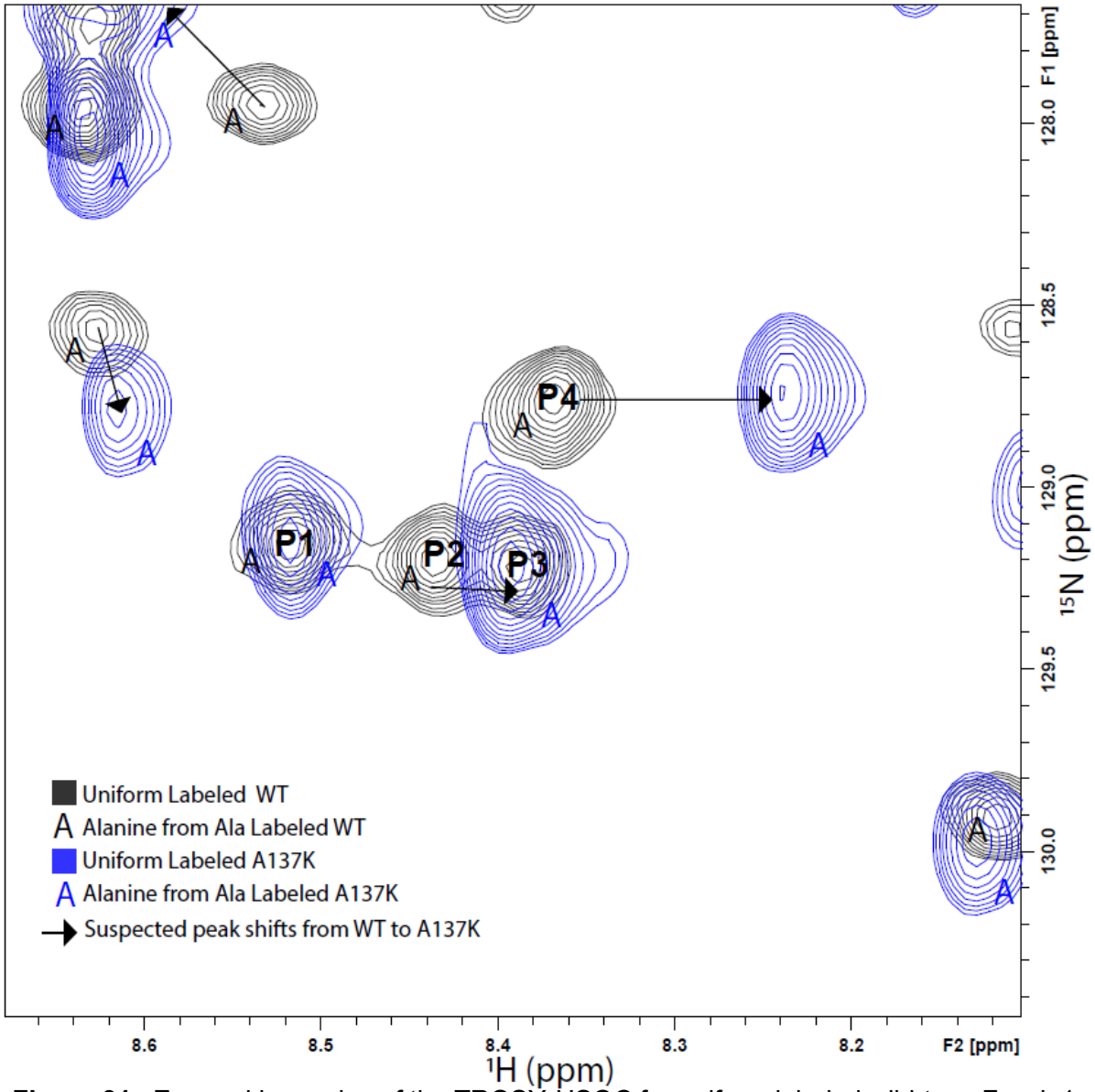

Figure 31. Zoomed in overlay of the TROSY-HSQC for uniform labeled wild-type Fascin1 (black) with the TROSY-HSQC of alanine labeled wild-type Fascin1 (blue). Alanines from alanine labeled WT-Fascin1 are labeled with a black "A". Alanines from A137K are labeled with a blue "A". Arrows denote suspected peak shifts from WT to A137K Fascin1. Image produced using Topspin4 and Adobe Illustrator.

To seek another candidate for A137, I overlayed the alanine labeled A137K spectrum with the alanine labeled WT Fascin1 spectrum. After closely inspecting each of the 45 signals from the alanine labeled WT Fascin1 spectrum and comparing to the

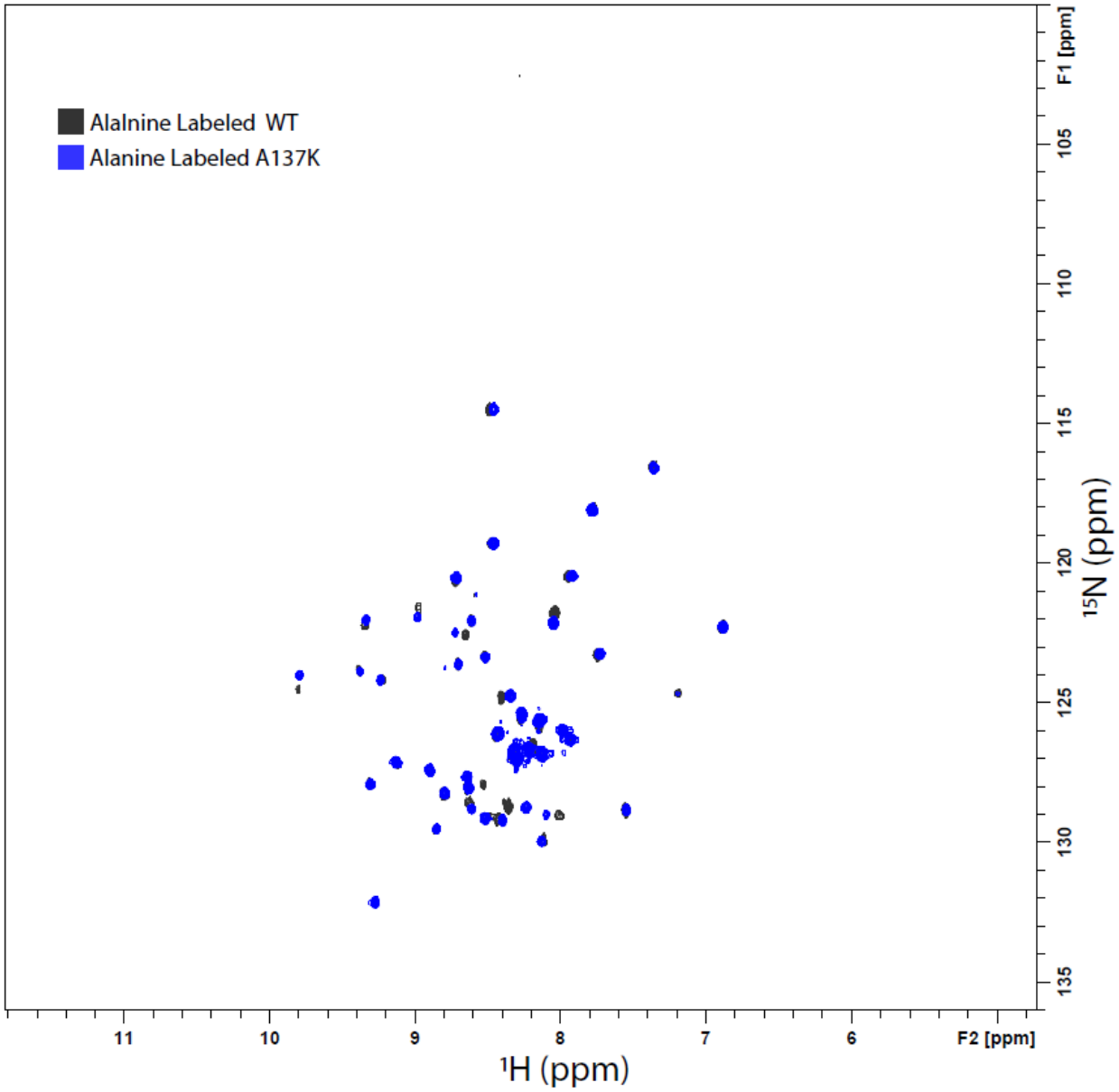

Figure 32. Overlay of the TROSY-HSQC for alanine labeled WT-Fascin1 (black) with the TROSY-HSQC of alanine labeled A137K Fascin1 (blue). Image produced using Topspin4 and Adobe Illustrator.

alanine labeled A137K Fascin1 spectrum, I concluded that each alanine peak from the wild-type spectrum has a corresponding peak in the A137K spectrum (Figure 32).

The alanine labeled WT-Fascin1 spectrum showed 45 out of the expected 49 alanine signals for Fascin1. As a result of investigations into the alanine labeled WT and A137K Fascin1 spectra, I concluded that A137 must be one of the four alanine signals that does not appear in the alanine labeled WT spectrum. The residue corresponding to G393 was identified and determined to shift upon the binding of BTA-EG_6 to Fascin1 supporting previous studies that identified G393 as a participant in the binding pocket of BTA-EG_6.

These experiments lay the groundwork for additional studies to identify specific residues that are involved in the binding of BTA-EG_6 to Fascin1 and for the full assignment of the WT-Fascin1 spectrum. These experiments will also aid research into future therapeutics that target Fascin1 in the context of both neurodegenerative disorders and cancer by providing an alternative to crystallization for the structural determination of therapeutic binding.

4.13 Methods

Expression of Fascin1 for crystallography:

Fascin 1 was grown by transforming the Fascin1 pGEX-5X-2 plasmid cloned by Dr. Kevin Sibucao[48] into DE3-BL21 cells (NEB) following the manufacturer's instructions. Cells were plated on selection agar plates containing100µg/mL ampicillin. A colony was selected for growth overnight in 50mL LB broth with 100µg/mL ampicillin with shaking at 220 RPM and 37ºC. The culture was then transferred to a 1L culture containing YT broth

(pre-warmed to 37ºC) and 100µg/mL ampicillin. The culture was allowed to grow to an OD of 0.8-1.0 at which point the temperature was reduced to 17ºC and the culture was induced with 0.5mM IPTG. The culture was allowed to incubate overnight, and the bacteria were harvested by centrifugation at 3000x gravity for 30 minutes and frozen at -80ºC.

Purification of Fascin1

Fascin1 was purified by lysing the bacteria by resuspending the bacterial pellets in 30-40mL resuspension buffer (20mM Tris pH8, 150mM NaCl, 1mM DTT) , with 50mg lysozyme and 2uL Benzonase Nuclease (MilliporeSigma) per liter of bacterial culture. The resuspension was then sonicated on ice for 10 minutes at 60% power with a pules sequence of 3 seconds on and 3 seconds off (20 minutes total time). The lysate was then centrifuged at 18500x gravity for 45-60 minutes. The supernatant was filtered twice to remove any residual membranous material first by a 0.45µM and then a 0.22 µM pore size filter (Genesee Scientific), then incubated with 5mL Glutathione Sepharose 4b beads (Cytivia) for at least 2 hours at 4ºC with rotation. The beads were then collected by gravity flow filtration and washed with approximately 50mL of resuspension buffer followed by 25 mL thrombin cleavage buffer (20mM Tris, 150mM NaCl, 1mM DTT, 2mM $CaCl_2$. 50-100 units of thrombin were added to the beads at a 30-50% bead slurry in thrombin cleavage buffer and allowed to incubate with rotation overnight at 4ºC. The flowthrough was collected and washed with about 3 bead volumes of thrombin cleavage buffer, then concentrated with a 30kDa cutoff centrifugal concentrator (Millipore) to a total volume of less than 1mL. The protein was then purified by S200 size exclusion chromatography in protein buffer (20mM Tris, 40mM KBr, and 0.5M EDTA pH 8) for crystallography or NMR

buffer (40mM HEPES, 90mM 1mM TCEP NaCl pH6) for protein NMR. The protein was then concentrated using a 30kDa cutoff (Millipore) to the desired concentration for experimentation.

Crytallography of Fascin1

Crystals for diffraction were obtained by mixing 2 µL14mg/mL Fascin in protein buffer (20mM Tris, 40mM KBr, and 0.5M EDTA pH 8 2mM BTA-EG_6) with 2µL crystallization buffer (14-24% PEG 4000 100mM HEPES pH8, 1mM DTT) on a glass coverslip and sealed over a well containing 1mL crystallization buffer. Crystals formed over the course of 3 days. Crystals were exchanged into cryo buffer (crystallization conditions plus additional glycerol for a final concentration of 30% cryoprotectant) to inhibit ice crystal formation upon flash-freezing, collected in loops and frozen in liquid nitrogen. Crystals were sent to the synchrotron at Argonne National Lab. Diffraction data collection was performed by remote control of the beamline at that location. Data was reduced with XDS package utilities[137], molecular replacement was performed with PHASER[138], then iterative refinement and building was performed with Coot[139] and phenix.refine[140].

Expression of uniform ^{15}N labeled Fascin1 and mutants for HSQC NMR

Plasmids were transformed into DE3-BL21 cells as previously described. A colony was selected for growth for 5 hours in 2-3mL LB broth with 100µg/mL ampicillin with shaking at 220 RPM and 37ºC. 200uL of the culture was then transferred into a 50mL culture containing M9 or Mengli minimal media containing 1g of either ^{15}N labeled ammonium chloride or ammonium sulfate and 8g unlabeled glucose. The culture was

then transferred to a 1L culture containing Mengli media (pre-warmed to 37ºC) and 100µg/mL ampicillin. The culture was allowed to grow to an OD of 0.8-1.0 at which point the temperature was reduced to 17ºC and the culture was induced with 0.5mM IPTG. The culture was allowed to incubate overnight, and the bacteria were harvested by centrifugation at 3000x gravity for 30 minutes and frozen at -80ºC. Purification proceeded as previously described in 4.13 methods.

Expression of uniform ^{15}N ^{13}C labeled Fascin1 for HNCA NMR

Plasmids were transformed into DE3-BL21 cells as previously described. A colony was selected for growth for 5 hours in 2-3mL LB broth with 100µg/mL ampicillin with shaking at 220 RPM and 37ºC. 200uL of the culture was then transferred into a 50mL culture containing M9 or Mengli minimal media containing 1g of ^{15}N labeled ammonium chloride and 2g of ^{13}C labeled glucose. The culture was then transferred to a 1L culture containing Mengli media (pre-warmed to 37ºC) and 100µg/mL ampicillin. The culture was allowed to grow to an OD of 0.8-1.0 at which point the temperature was reduced to 17ºC and the culture was induced with 0.5mM IPTG. The culture was allowed to incubate overnight, and the bacteria were harvested by centrifugation at 3000x gravity for 30 minutes and frozen at -80ºC. Purification proceeded as previously described in 4.13 methods.

Expression of alanine labeled Fascin1 and mutants for HSQC NMR

Plasmids were transformed into Lemo DE3-BL21 (NEB) cells following the manufacturer's protocol. A colony was selected for growth for 5 hours in 2-3mL LB broth with 100µg/mL ampicillin and 30µg/mL chloramphenicol with shaking at 220 RPM and

37ºC. 200uL of the culture was then transferred into a 50mL culture containing M9 media with 100µg/mL ampicillin and 30µg/mL chloramphenicol containing 1g of unlabeled ammonium chloride and 5g unlabeled glucose. The culture was then transferred to a 1L culture containing M9 media (pre-warmed to 37ºC) with 100µg/mL ampicillin and 30ug/mL chloramphenicol. The culture was allowed to grow to an OD of 0.4-0.5 at which point 100mL of amino acid suspension containing 0.1g ^{15}N Alanine and 0.2-0.5g of the remaining 19 common amino acids. At an OD of 0.6-0.8 Rhamnose was added to a final concentration of 100µM to induce expression of the T7 Lysozyme and the culture was plunged into an ice bath with shaking for 5 minutes. The cultures were returned to the incubator at a temperature of 20ºC and the culture was induced with 0.5mM IPTG. The culture was allowed to incubate for 3 hours, and the bacteria were harvested by centrifugation at 3000x gravity for 30 minutes and frozen at -80ºC. Purification proceeded as previously described in 4.13 methods.

NMR experiments

All protein NMR experiments were recorded at 37 °C on Bruker Avance Neo 800MHz spectrometers equipped with a TXO 1H/13C/15N cryoprobes. ^{1}H/^{15}N TROSY-HSQC data was recorded with 2k and 256 complex points. The NMR data were processed with NMRPIPE and analyzed with Bruker Topspin 4 (www.bruker.com).

Cloning of intein constructs and Fascin1 truncations

Primers were designed using the CfaCFascinC and CfaNFascinN plasmids as a template for intiein constructs (Appendix A) and against Fascin_pGEX-5X-2 (Appendix

A). All cloning was done using the Gibson Assembly® Master Mix NEB E2611L and following the manufacturer's protocol.

Cloning of GSG onto the CfaCFascinC construct upstream of the polyhistidine tag to promote expression was accomplished by using the following primers and CfaCFascinC (Appendix A) as a template:

Forward: TGGTCATCACCATCACCATCAC

Reverse: GAGCCCATGGTATATCTCCTTCTTAAAG

Cloning of intein split fascin1 between β-trefoils 1 and 2 and between β-trefoils 3 and 4 was accomplished by using the following primers using CfaC-FascinC as a template:

CfaC Reverse: ATTGCTTGCAACCAGACC

Trefoil 3 Forward Trefoil 2 overhang:
TGAACTGTTTGCACTGGAACAGAGCTGTCAGGTTGTTCTGCAG

CfaC Reverse (w/scar Cys): ACAATTGCTTGCAACCAG

Trefoil 3 Forward: TGTCAGGTTGTTCTGCAG

Trefoil 3 Reverse-CfaN overhang:
GAATTTCGGTATCATAGCTCAGACAAATCAGTTTCATCAGAAACAGTTC

Trefoil 4 Forward: CGTCCGATTATTGTGTTTCG

CfaCFascinC Trefoils 3 and 4 Reverse: ATATTCCCACAGGCTTGC

CfaCFascinC Trefoils 3 and 4 Forward: GGATCCGCTGCTAACAAAG

Cloning of intein split fascin1 between β-trefoils 1 and 2 and between β-trefoils 3 and 4 was accomplished by using the following primers using FascinNCfaN (Appendix A) as a template:

FascinN Trefoils 1 and 2 CfaN Reverse: CATGGTATATCTCCTTCTTAAAGTTAAAC

FascinN Trefoils 2 and 2 CfaN Forward: ACCGCAAATGGCACC

Trefoil 1 Reverse: TGCAATATGAACTGACCATTTTTC

Trefoil2 Forward ScarC Cfa Overhang:
AAATGGTCTGGTTGCAAGCAATTGTCATCCGCAGGTTAACATTTATAGC

Trefoil 2 Reverse: GCTCTGTTCCAGTGCAAAC

Trefoil 2 Reverse T3 Overhang:
TTGCTGCCTGCAGAACAACCTGACAGCTCTGTTCCAGTG

CfaN Forward: TGTCTGAGCTATGATACCGAAATTC

Cloning of Truncated Fascin-GST constructs was accomplished using the following primers and Fascin_pGEX-5x-2 (Appendix A) as a template:

GST-Fascin Trefoil 4 Reverse: GGATCCACGCGGAACC

GST-Fascin Trefoil 1 Reverse: GTGCATGGCGATGTGCAC

GST-Fascin Trefoils 1+4 Reverse: GTGCATGGCGATGTGCA

GST-Fascin Trefoils 1+2 Reverse: GCTCTGCTCCAGAGCAAAG

GST-Fascin Trefoils 3+4 Forward: TGCGCCCAGGTCGTGCTGCAGG

GST-Fascin Trefoils 1+4 Forward: ATCATCGTGTTCCGCGG

GST-Fascin Trefoil 4 Forward: ATCATCGTGTTCCGCGG

Purification of CfaCFascinC, CfaNFascinN, and reacted intein constructs:

Constructs used for intein reactions were initially purified as described by Gupta and Tycko[155]. The purified intein reacted Fascin1 protein was then further purified by HiTrap Q HP anion exchange chromatography (Cytivia) following the manufacterer's recommended protocol.

4.14 Acknowledgements

I would like to thank Dr. Kevin Corbett for the immense help he gave me in better understanding protein crystallography, and allowing me to send my protein crystals along with crystals from his lab to be diffracted at the beamline in Argonne National Labs. I would also like to thank the NMR group. Dr. Galia Debolouchina was my first mentor in interpreting protein NMR data. Dr. Xuemei Huang patiently taught me how to run my protein samples on the 800mHz NMR Spectrometer, and I was finally able to do it on my own with her instruction. I would also like to thank Dr. Stanley Opella and the other members of the Opella lab, Dr. Sang Ho Park, Haley Siddiqi, and Daniela Castro for their help in all aspects of selective labeling expression and protein NMR analysis.

Chapter 4 is currently being prepared for submission for publication of the material. Kyle R. Berg, Aashish Shivkumar, Sang-Ho Park, Galia Debelouchina, Xuemei Huang, Stanley J. Opella. The dissertation author is a primary researcher for that manuscript.

Chapter 5

Conclusions

The work of Dr. Sibucao and others in the Yang lab has resulted in an investigation of the nootropic effects of BTA-EG_4 and BTA-EG_6 and their effects through the protein Fascin1. In seeking to address if Fascin1 is on pathway and responsible for the observed effects of BTA-EG_4 and BTA-EG_6, I have provided novel insight into Fascin1 as a regulator of dendritic spines through Fascin1 knockdown and overexpression studies in primary neurons. By exploring confirmable mechanistic links between Fascin1 and dendritic spines, I have contributed novel information regarding the protein-protein interactions of Fascin1 in neuronal tissue. I have also identified the maintenance of focal adhesions in a nascent state as a direct cellular mechanism linking Fascin1 and the binding of BTA-EG_4 and BTA-EG_6 to the maintenance and formation of dendritic spines. By examining Fascin1 and the binding of BTA-EG_6 from the prospective of structural biology, I have provided direct evidence for locating the binding pocket in which BTA-EG_6 binds to fascin through solution-based protein NMR studies and have shown that solution protein NMR can be a viable tool for studying the interactions between Fascin1 and potential small molecule therapeutics.

To further investigate the effect of BTA-EG_4 and BTA-EG_6 on dendritic spines future studies in this area would include studies in both secondary and primary neuronal cells. These experiments should include both fixed and live cell imaging to further investigate the effect of BTA-EG_4 and BTA-EG_6 on focal adhesions and to investigate the interaction between Fascin1 and the AP2 complex, yet to be described in the literature.

The interactions between Fascin1 and α-actinin in the presence or absence of BTA-EG_4 and BTA-EG_6 can be studied through *in vitro* competition actin-bundling assays.

A combination of additional selective labeling experiments and the expression of labeled Fascin1 in deuterated aqueous media followed by $^{1}H/^{15}N/^{13}C$ may lead to sufficient signal for three-dimensional HNCACB experiments and allow for the full assignment of the Fascin1 NMR spectra. Additional point mutations will also aid in this effort and can further confirm the binding pocket of BTA-EG_6. While the full protein remains unassigned by protein NMR, two-dimensional HSQC analysis and mutagenesis can be used to confirm the binding and provide insight into structural changes caused by the binding of BTA-EG_4, BTA-EG_6, and other known Fascin1 binding molecules.

In conclusion, this dissertation adds another block to the construction of work done by Dr. Sibucao and other previous graduate students in the Yang Lab. My work provides a basis for further investigations and in turn my contributions will also be built upon, in the hope that these discoveries can eventually lead to therapeutics and treatments for Alzheimer's Disease and other forms of dementia.

Appendix A: Plasmids

Fascin1 Bacterial Expression Plasmid:

AGCTTATCGACTGCACGGTGCACCAATGCTTCTGGCGTCAGGCAGCCATCGGAAGCTGTGGTAT
GGCTGTGCAGGTCGTAAATCACTGCATAATTCGTGTCGCTCAAGGCGCACTCCCGTTCTGGATA
ATGTTTTTTGCGCCGACATCATAACGGTTCTGGCAAATATTCTGAAATGAGCTGTTGACAATTA
ATCATCGGCTCGTATAATGTGTGGAATTGTGAGCGGATAACAATTTCACACAGGAAACAGTATT
CATGTCCCCTATACTAGGTTATTGGAAAATTAAGGGCCTTGTGCAACCCACTCGACTTCTTTTG
GAATATCTTGAAGAAAAATATGAAGAGCATTTGTATGAGCGCGATGAAGGTGATAAATGGCGAA
ACAAAAAGTTTGAATTGGGTTTGGAGTTTCCCAATCTTCCTTATTATATTGATGGTGATGTTAA
ATTAACACAGTCTATGGCCATCATACGTTATATAGCTGACAAGCACAACATGTTGGGTGGTTGT
CCAAAAGAGCGTGCAGAGATTTCAATGCTTGAAGGAGCGGTTTTGGATATTAGATACGGTGTTT
CGAGAATTGCATATAGTAAAGACTTTGAAACTCTCAAAGTTGATTTTCTTAGCAAGCTACCTGA
AATGCTGAAAATGTTCGAAGATCGTTTATGTCATAAAACATATTTAAATGGTGATCATGTAACC
CATCCTGACTTCATGTTGTATGACGCTCTTGATGTTGTTTTATACATGGACCCAATGTGCCTGG
ATGCGTTCCCAAAATTAGTTTGTTTTAAAAAACGTATTGAAGCTATCCCACAAATTGATAAGTA
CTTGAAATCCAGCAAGTATATAGCATGGCCTTTGCAGGGCTGGCAAGCCACGTTTGGTGGTGGC

GACCATCCTCCAAAATCGGATCTGATCGAAGGTCGTGGAATTCTGGTTCCGCGTGGATCCACTG
CCACCATGACCGCCAACGGCACAGCCGAGGCGGTGCAGATCCAGTTCGGCCTCATCAACTGCGG
CAACAAGTACCTGACGGCCGAGGCGTTCGGGTTCAAGGTGAACGCGTCCGCCAGCAGCCTGAAG
AAGAAGCAGATCTGGACGCTGGAGCAGCCCCCTGACGAGGCGGGCAGCGCGGCCGTGTGCCTGC
GCAGCCACCTGGGCCGCTACCTGGCGGCGGACAAGGACGGCAACGTGACCTGCGAGCGCGAGGT
GCCCGGTCCCGACTGCCGTTTCCTCATCGTGGCGCACGACGACGGTCGCTGGTCGCTGCAGTCC
GAGGCGCACCGGCGCTACTTCGGCGGCACCGAGGACCGCCTGTCCTGCTTCGCGCAGACGGTGT
CCCCCGCCGAGAAGTGGAGCGTGCACATCGCCATGCACCCTCAGGTCAACATCTACAGCGTCAC
CCGTAAGCGCTACGCGCACCTGAGCGCGCGGCCGGCCGACGAGATCGCCGTGGACCGCGACGTG
CCCTGGGGCGTCGACTCGCTCATCACCCTCGCCTTCCAGGACCAGCGCTACAGCGTGCAGACCG
CCGACCACCGCTTCCTGCGCCACGACGGGCGCCTGGTGGCGCGCCCCGAGCCGGCCACTGGCTA
CACGCTGGAGTTCCGCTCCGGCAAGGTGGCCTTCCGCGACTGCGAGGGCCGTTACCTGGCGCCG
TCGGGGCCCAGCGGCACGCTCAAGGCGGGCAAGGCCACCAAGGTGGGCAAGGACGAGCTCTTTG
CTCTGGAGCAGAGCTGCGCCCAGGTCGTGCTGCAGGCGGCCAACGAGAGGAACGTGTCCACGCG
CCAGGGTATGGACCTGTCTGCCAATCAGGACGAGGAGACCGACCAGGAGACCTTCCAGCTGGAG
ATCGACCGCGACACCAAAAAGTGTGCCTTCCGTACCCACACGGGCAAGTACTGGACGCTGACGG
CCACCGGGGGCGTGCAGTCCACCGCCTCCAGCAAGAATGCCAGCTGCTACTTTGACATCGAGTG
GCGTGACCGGCGCATCACACTGAGGGCGTCCAATGGCAAGTTTGTGACCTCCAAGAAGAATGGG
CAGCTGGCCGCCTCGGTGGAGACAGCAGGGGACTCAGAGCTCTTCCTCATGAAGCTCATCAACC
GCCCCATCATCGTGTTCCGCGGGGAGCATGGCTTCATCGGCTGCCGCAAGGTCACGGGCACCCT
GGACGCCAACCGCTCCAGCTATGACGTCTTCCAGCTGGAGTTCAACGATGGCGCCTACAACATC
AAAGACTCCACAGGCAAATACTGGACGGTGGGCAGTGACTCCGTGGTCACCAGCAGCGGCGACA
CTCCTGTGGACTTCTTCTTCGAGTTCTGCGACTATAACAAGGTGGCCATCAAGGTGGGCGGGCG
CTACCTGAAGGGCGACCACGCAGGCGTCCTGAAGGCCTCGGCGGAAACCGTGGACCCCGCCTCG
CTCTGGGAGTACTAGGGCCGGCCCGTCCTTCCCCGCCCCTGCCCACATGGCGGCTCCTGCCAAC
CCTCCCTGCTAACCACTTCTCCGCCAGGTGGGCTCCAGGGCGGGAGGCAAGCCCCCTTGCCTTT
CAAACTGGAAACCCCAGAGAAAACGGTGCCCCCACCTGTCGCCCCTATGGACTCCCCACTCTCC
CCTCCGCCCGGGTTCCCTACTCCCCTCGGGTCAGCGGCTGCGGCCTGGCCCTGGGAGGGATTTC
AGATGCCCCTGCCCTCTTGTCTGCCACGGGGCGAGTCTGGCACCTCTTTCTTCTGACCTCAGAC
GGCTCTGAGAATTCCCGGGTCGACTCGAGCGGCCGCATCGTGACTGACTGACGATCTGCCTCGC
GCGTTTCGGTGATGACGGTGAAAACCTCTGACACATGCAGCTCCCGGAGACGGTCACAGCTTGT
CTGTAAGCGGATGCCGGGAGCAGACAAGCCCGTCAGGGCGCGTCAGCGGGTGTTGGCGGGTGTC
GGGGCGCAGCCATGACCCAGTCACGTAGCGATAGCGGAGTGTATAATTCTTGAAGACGAAAGGG
CCTCGTGATACGCCTATTTTTATAGGTTAATGTCATGATAATAATGGTTTCTTAGACGTCAGGT
GGCACTTTTCGGGGAAATGTGCGCGGAACCCCTATTTGTTTATTTTTCTAAATACATTCAAATA
TGTATCCGCTCATGAGACAATAACCCTGATAAATGCTTCAATAATATTGAAAAAGGAAGAGTAT
GAGTATTCAACATTTCCGTGTCGCCCTTATTCCCTTTTTTGCGGCATTTTGCCTTCCTGTTTTT
GCTCACCCAGAAACGCTGGTGAAAGTAAAAGATGCTGAAGATCAGTTGGGTGCACGAGTGGGTT
ACATCGAACTGGATCTCAACAGCGGTAAGATCCTTGAGAGTTTTCGCCCCGAAGAACGTTTTCC
AATGATGAGCACTTTTAAAGTTCTGCTATGTGGCGCGGTATTATCCCGTGTTGACGCCGGGCAA
GAGCAACTCGGTCGCCGCATACACTATTCTCAGAATGACTTGGTTGAGTACTCACCAGTCACAG
AAAAGCATCTTACGGATGGCATGACAGTAAGAGAATTATGCAGTGCTGCCATAACCATGAGTGA
TAACACTGCGGCCAACTTACTTCTGACAACGATCGGAGGACCGAAGGAGCTAACCGCTTTTTTG
CACAACATGGGGGATCATGTAACTCGCCTTGATCGTTGGGAACCGGAGCTGAATGAAGCCATAC
CAAACGACGAGCGTGACACCACGATGCCTGCAGCAATGGCAACAACGTTGCGCAAACTATTAAC
TGGCGAACTACTTACTCTAGCTTCCCGGCAACAATTAATAGACTGGATGGAGGCGGATAAAGTT
GCAGGACCACTTCTGCGCTCGGCCCTTCCGGCTGGCTGGTTTATTGCTGATAAATCTGGAGCCG

GTGAGCGTGGGTCTCGCGGTATCATTGCAGCACTGGGGCCAGATGGTAAGCCCTCCCGTATCGT
AGTTATCTACACGACGGGGAGTCAGGCAACTATGGATGAACGAAATAGACAGATCGCTGAGATA
GGTGCCTCACTGATTAAGCATTGGTAACTGTCAGACCAAGTTTACTCATATATACTTTAGATTG
ATTTAAAACTTCATTTTTAATTTAAAAGGATCTAGGTGAAGATCCTTTTTGATAATCTCATGAC
CAAAATCCCTTAACGTGAGTTTTCGTTCCACTGAGCGTCAGACCCCGTAGAAAAGATCAAAGGA
TCTTCTTGAGATCCTTTTTTTCTGCGCGTAATCTGCTGCTTGCAAACAAAAAAACCACCGCTAC
CAGCGGTGGTTTGTTTGCCGGATCAAGAGCTACCAACTCTTTTTCCGAAGGTAACTGGCTTCAG
CAGAGCGCAGATACCAAATACTGTCCTTCTAGTGTAGCCGTAGTTAGGCCACCACTTCAAGAAC
TCTGTAGCACCGCCTACATACCTCGCTCTGCTAATCCTGTTACCAGTGGCTGCTGCCAGTGGCG
ATAAGTCGTGTCTTACCGGGTTGGACTCAAGACGATAGTTACCGGATAAGGCGCAGCGGTCGGG
CTGAACGGGGGGTTCGTGCACACAGCCCAGCTTGGAGCGAACGACCTACACCGAACTGAGATAC
CTACAGCGTGAGCTATGAGAAAGCGCCACGCTTCCCGAAGGGAGAAAGGCGGACAGGTATCCGG
TAAGCGGCAGGGTCGGAACAGGAGAGCGCACGAGGGAGCTTCCAGGGGGAAACGCCTGGTATCT
TTATAGTCCTGTCGGGTTTCGCCACCTCTGACTTGAGCGTCGATTTTTGTGATGCTCGTCAGGG
GGGCGGAGCCTATGGAAAAACGCCAGCAACGCGGCCTTTTTACGGTTCCTGGCCTTTTGCTGGC
CTTTTGCTCACATGTTCTTTCCTGCGTTATCCCCTGATTCTGTGGATAACCGTATTACCGCCTT
TGAGTGAGCTGATACCGCTCGCCGCAGCCGAACGACCGAGCGCAGCGAGTCAGTGAGCGAGGAA
GCGGAAGAGCGCCTGATGCGGTATTTTCTCCTTACGCATCTGTGCGGTATTTCACACCGCATAA
ATTCCGACACCATCGAATGGTGCAAAACCTTTCGCGGTATGGCATGATAGCGCCCGGAAGAGAG
TCAATTCAGGGTGGTGAATGTGAAACCAGTAACGTTATACGATGTCGCAGAGTATGCCGGTGTC
TCTTATCAGACCGTTTCCCGCGTGGTGAACCAGGCCAGCCACGTTTCTGCGAAAACGCGGGAAA
AAGTGGAAGCGGCGATGGCGGAGCTGAATTACATTCCCAACCGCGTGGCACAACAACTGGCGGG
CAAACAGTCGTTGCTGATTGGCGTTGCCACCTCCAGTCTGGCCCTGCACGCGCCGTCGCAAATT
GTCGCGGCGATTAAATCTCGCGCCGATCAACTGGGTGCCAGCGTGGTGGTGTCGATGGTAGAAC
GAAGCGGCGTCGAAGCCTGTAAAGCGGCGGTGCACAATCTTCTCGCGCAACGCGTCAGTGGGCT
GATCATTAACTATCCGCTGGATGACCAGGATGCCATTGCTGTGGAAGCTGCCTGCACTAATGTT
CCGGCGTTATTTCTTGATGTCTCTGACCAGACACCCATCAACAGTATTATTTTCTCCCATGAAG
ACGGTACGCGACTGGGCGTGGAGCATCTGGTCGCATTGGGTCACCAGCAAATCGCGCTGTTAGC
GGGCCCATTAAGTTCTGTCTCGGCGCGTCTGCGTCTGGCTGGCTGGCATAAATATCTCACTCGC
AATCAAATTCAGCCGATAGCGGAACGGGAAGGCGACTGGAGTGCCATGTCCGGTTTTCAACAAA
CCATGCAAATGCTGAATGAGGGCATCGTTCCCACTGCGATGCTGGTTGCCAACGATCAGATGGC
GCTGGGCGCAATGCGCGCCATTACCGAGTCCGGGCTGCGCGTTGGTGCGGATATCTCGGTAGTG
GGATACGACGATACCGAAGACAGCTCATGTTATATCCCGCCGTTAACCACCATCAAACAGGATT
TTCGCCTGCTGGGGCAAACCAGCGTGGACCGCTTGCTGCAACTCTCTCAGGGCCAGGCGGTGAA
GGGCAATCAGCTGTTGCCCGTCTCACTGGTGAAAAGAAAAACCACCCTGGCGCCCAATACGCAA
ACCGCCTCTCCCCGCGCGTTGGCCGATTCATTAATGCAGCTGGCACGACAGGTTTCCCGACTGG
AAAGCGGGCAGTGAGCGCAACGCAATTAATGTGAGTTAGCTCACTCATTAGGCACCCCAGGCTT
TACACTTTATGCTTCCGGCTCGTATGTTGTGTGGAATTGTGAGCGGATAACAATTTCACACAGG
AAACAGCTATGACCATGATTACGGATTCACTGGCCGTCGTTTTACAACGTCGTGACTGGGAAAA
CCCTGGCGTTACCCAACTTAATCGCCTTGCAGCACATCCCCCTTTCGCCAGCTGGCGTAATAGC
GAAGAGGCCCGCACCGATCGCCCTTCCCAACAGTTGCGCAGCCTGAATGGCGAATGGCGCTTTG
CCTGGTTTCCGGCACCAGAAGCGGTGCCGGAAAGCTGGCTGGAGTGCGATCTTCCTGAGGCCGA
TACTGTCGTCGTCCCCTCAAACTGGCAGATGCACGGTTACGATGCGCCCATCTACACCAACGTA
ACCTATCCCATTACGGTCAATCCGCCGTTTGTTCCCACGGAGAATCCGACGGGTTGTTACTCGC
TCACATTTAATGTTGATGAAAGCTGGCTACAGGAAGGCCAGACGCGAATTATTTTTGATGGCGT
TGGAATT

Fascin1 Knockdown Plasmid (designed against rat mRNA)

Purchased from Vectorbuilder. ID#[VB181031-1197kmw]

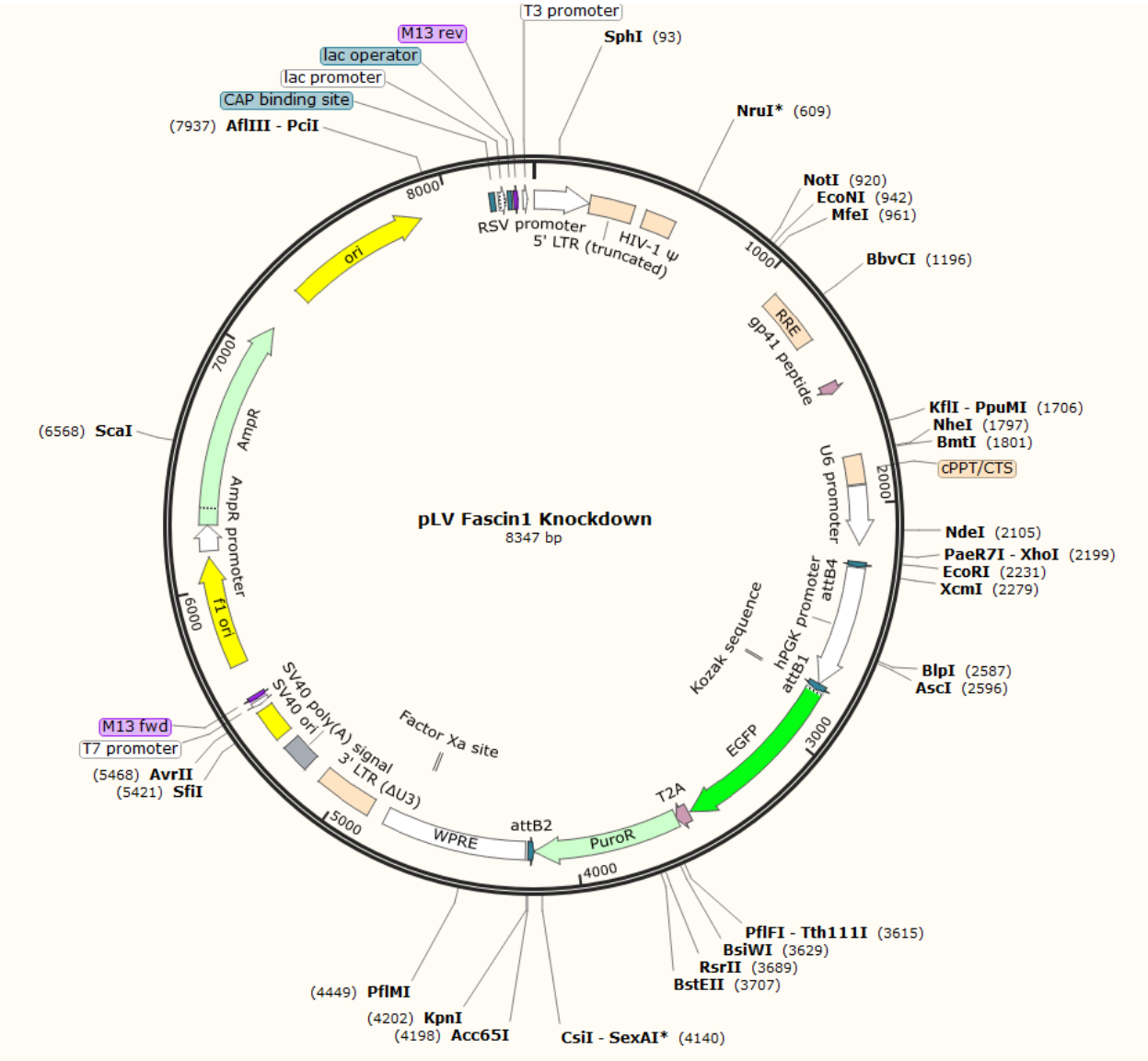

AATGTAGTCTTATGCAATACTCTTGTAGTCTTGCAACATGGTAACGATGAGTTAGCAACATGCC
TTACAAGGAGAGAAAAAGCACCGTGCATGCCGATTGGTGGAAGTAAGGTGGTACGATCGTGCCT
TATTAGGAAGGCAACAGACGGGTCTGACATGGATTGGACGAACCACTGAATTGCCGCATTGCAG
AGATATTGTATTTAAGTGCCTAGCTCGATACATAAACGGGTCTCTCTGGTTAGACCAGATCTGA
GCCTGGGAGCTCTCTGGCTAACTAGGGAACCCACTGCTTAAGCCTCAATAAAGCTTGCCTTGAG
TGCTTCAAGTAGTGTGTGCCCGTCTGTTGTGTGACTCTGGTAACTAGAGATCCCTCAGACCCTT
TTAGTCAGTGTGGAAAATCTCTAGCAGTGGCGCCCGAACAGGGACTTGAAAGCGAAAGGGAAAC
CAGAGGAGCTCTCTCGACGCAGGACTCGGCTTGCTGAAGCGCGCACGGCAAGAGGCGAGGGGCG
GCGACTGGTGAGTACGCCAAAAATTTTGACTAGCGGAGGCTAGAAGGAGAGAGATGGGTGCGAG
AGCGTCAGTATTAAGCGGGGGAGAATTAGATCGCGATGGGAAAAAATTCGGTTAAGGCCAGGGG
GAAAGAAAAAATATAAATTAAAACATATAGTATGGGCAAGCAGGGAGCTAGAACGATTCGCAGT

TAATCCTGGCCTGTTAGAAACATCAGAAGGCTGTAGACAAATACTGGGACAGCTACAACCATCC
CTTCAGACAGGATCAGAAGAACTTAGATCATTATATAATACAGTAGCAACCCTCTATTGTGTGC
ATCAAAGGATAGAGATAAAAGACACCAAGGAAGCTTTAGACAAGATAGAGGAAGAGCAAAACAA
AAGTAAGACCACCGCACAGCAAGCGGCCGCTGATCTTCAGACCTGGAGGAGGAGATATGAGGGA
CAATTGGAGAAGTGAATTATATAAATATAAAGTAGTAAAAATTGAACCATTAGGAGTAGCACCC
ACCAAGGCAAAGAGAAGAGTGGTGCAGAGAGAAAAAAGAGCAGTGGGAATAGGAGCTTTGTTCC
TTGGGTTCTTGGGAGCAGCAGGAAGCACTATGGGCGCAGCGTCAATGACGCTGACGGTACAGGC
CAGACAATTATTGTCTGGTATAGTGCAGCAGCAGAACAATTTGCTGAGGGCTATTGAGGCGCAA
CAGCATCTGTTGCAACTCACAGTCTGGGGCATCAAGCAGCTCCAGGCAAGAATCCTGGCTGTGG
AAAGATACCTAAAGGATCAACAGCTCCTGGGGATTTGGGGTTGCTCTGGAAAACTCATTTGCAC
CACTGCTGTGCCTTGGAATGCTAGTTGGAGTAATAAATCTCTGGAACAGATTTGGAATCACACG
ACCTGGATGGAGTGGGACAGAGAAATTAACAATTACACAAGCTTAATACACTCCTTAATTGAAG
AATCGCAAAACCAGCAAGAAAAGAATGAACAAGAATTATTGGAATTAGATAAATGGGCAAGTTT
GTGGAATTGGTTTAACATAACAAATTGGCTGTGGTATATAAAATTATTCATAATGATAGTAGGA
GGCTTGGTAGGTTTAAGAATAGTTTTTGCTGTACTTTCTATAGTGAATAGAGTTAGGCAGGGAT
ATTCACCATTATCGTTTCAGACCCACCTCCCAACCCCGAGGGGACCCGACAGGCCCGAAGGAAT
AGAAGAAGAAGGTGGAGAGAGAGACAGAGACAGATCCATTCGATTAGTGAACGGATCTCGACGG
TATCGCTAGCTTTTAAAAGAAAAGGGGGGATTGGGGGGTACAGTGCAGGGGAAAGAATAGTAGA
CATAATAGCAACAGACATACAAACTAAAGAATTACAAAAACAAATTACAAAAATTCAAAATTTT
ACTAGTGAGGGCCTATTTCCCATGATTCCTTCATATTTGCATATACGATACAAGGCTGTTAGAG
AGATAATTGGAATTAATTTGACTGTAAACACAAAGATATTAGTACAAAATACGTGACGTAGAAA
GTAATAATTTCTTGGGTAGTTTGCAGTTTTAAAATTATGTTTTAAAATGGACTATCATATGCTT
ACCGTAACTTGAAAGTATTTCGATTTCTTGGCTTTATATATCTTGTGGAAAGGACGAAACACCG
GAGTCAACTCTGAGCCTTATTTCTCGAGAAATAAGGCTCAGAGTTGACTTTTTTGAATTCCAAC
TTTGTATAGAAAAGTTGGGGTTGCGCCTTTTCCAAGGCAGCCCTGGGTTTGCGCAGGGACGCGG
CTGCTCTGGGCGTGGTTCCGGGAAACGCAGCGGCGCCGACCCTGGGTCTCGCACATTCTTCACG
TCCGTTCGCAGCGTCACCCGGATCTTCGCCGCTACCCTTGTGGGCCCCCCGGCGACGCTTCCTG
CTCCGCCCCTAAGTCGGGAAGGTTCCTTGCGGTTCGCGGCGTGCCGGACGTGACAAACGGAAGC
CGCACGTCTCACTAGTACCCTCGCAGACGGACAGCGCCAGGGAGCAATGGCAGCGCGCCGACCG
CGATGGGCTGTGGCCAATAGCGGCTGCTCAGCAGGGCGCGCCGAGAGCAGCGGCCGGGAAGGGG
CGGTGCGGGAGGCGGGGTGTGGGGCGGTAGTGTGGGCCCTGTTCCTGCCCGCGCGGTGTTCCGC
ATTCTGCAAGCCTCCGGAGCGCACGTCGGCAGTCGGCTCCCTCGTTGACCGAATCACCGACCTC
TCTCCCCAGGCAAGTTTGTACAAAAAAGCAGGCTGCCACCATGGTGAGCAAGGGCGAGGAGCTG
TTCACCGGGGTGGTGCCCATCCTGGTCGAGCTGGACGGCGACGTAAACGGCCACAAGTTCAGCG
TGTCCGGCGAGGGCGAGGGCGATGCCACCTACGGCAAGCTGACCCTGAAGTTCATCTGCACCAC
CGGCAAGCTGCCCGTGCCCTGGCCCACCCTCGTGACCACCCTGACCTACGGCGTGCAGTGCTTC
AGCCGCTACCCCGACCACATGAAGCAGCACGACTTCTTCAAGTCCGCCATGCCCGAAGGCTACG
TCCAGGAGCGCACCATCTTCTTCAAGGACGACGGCAACTACAAGACCCGCGCCGAGGTGAAGTT
CGAGGGCGACACCCTGGTGAACCGCATCGAGCTGAAGGGCATCGACTTCAAGGAGGACGGCAAC
ATCCTGGGGCACAAGCTGGAGTACAACTACAACAGCCACAACGTCTATATCATGGCCGACAAGC
AGAAGAACGGCATCAAGGTGAACTTCAAGATCCGCCACAACATCGAGGACGGCAGCGTGCAGCT
CGCCGACCACTACCAGCAGAACACCCCCATCGGCGACGGCCCCGTGCTGCTGCCCGACAACCAC
TACCTGAGCACCCAGTCCGCCCTGAGCAAAGACCCCAACGAGAAGCGCGATCACATGGTCCTGC
TGGAGTTCGTGACCGCCGCCGGGATCACTCTCGGCATGGACGAGCTGTACAAGGGCTCCGGAGA
GGGCAGGGGAAGTCTTCTAACATGCGGGGACGTGGAGGAAAATCCCGGCCCCATGACCGAGTAC
AAGCCCACGGTGCGCCTCGCCACCCGCGACGACGTCCCCAGGGCCGTACGCACCCTCGCCGCCG
CGTTCGCCGACTACCCCGCCACGCGCCACACCGTCGATCCGGACCGCCACATCGAGCGGGTCAC

CGAGCTGCAAGAACTCTTCCTCACGCGCGTCGGGCTCGACATCGGCAAGGTGTGGGTCGCGGAC
GACGGCGCCGCGGTGGCGGTCTGGACCACGCCGGAGAGCGTCGAAGCGGGGGCGGTGTTCGCCG
AGATCGGCCCGCGCATGGCCGAGTTGAGCGGTTCCCGGCTGGCCGCGCAGCAACAGATGGAAGG
CCTCCTGGCGCCGCACCGGCCCAAGGAGCCCGCGTGGTTCCTGGCCACCGTCGGCGTCTCGCCC
GACCACCAGGGCAAGGGTCTGGGCAGCGCCGTCGTGCTCCCCGGAGTGGAGGCGGCCGAGCGCG
CCGGGGTGCCCGCCTTCCTGGAGACCTCCGCGCCCCGCAACCTCCCCTTCTACGAGCGGCTCGG
CTTCACCGTCACCGCCGACGTCGAGGTGCCCGAAGGACCGCGCACCTGGTGCATGACCCGCAAG
CCCGGTGCCTGAACCCAGCTTTCTTGTACAAAGTGGTGGTACCCGATAATCAACCTCTGGATTA
CAAAATTTGTGAAAGATTGACTGGTATTCTTAACTATGTTGCTCCTTTTACGCTATGTGGATAC
GCTGCTTTAATGCCTTTGTATCATGCTATTGCTTCCCGTATGGCTTTCATTTTCTCCTCCTTGT
ATAAATCCTGGTTGCTGTCTCTTTATGAGGAGTTGTGGCCCGTTGTCAGGCAACGTGGCGTGGT
GTGCACTGTGTTTGCTGACGCAACCCCCACTGGTTGGGGCATTGCCACCACCTGTCAGCTCCTT
TCCGGGACTTTCGCTTTCCCCCTCCCTATTGCCACGGCGGAACTCATCGCCGCCTGCCTTGCCC
GCTGCTGGACAGGGGCTCGGCTGTTGGGCACTGACAATTCCGTGGTGTTGTCGGGGAAGCTGAC
GTCCTTTCCATGGCTGCTCGCCTGTGTTGCCACCTGGATTCTGCGCGGGACGTCCTTCTGCTAC
GTCCCTTCGGCCCTCAATCCAGCGGACCTTCCTTCCCGCGGCCTGCTGCCGGCTCTGCGGCCTC
TTCCGCGTCTTCGCCTTCGCCCTCAGACGAGTCGGATCTCCCTTTGGGCCGCCTCCCCGCATCG
GCTTTAAGACCAATGACTTACAAGGCAGCTGTAGATCTTAGCCACTTTTTAAAAGAAAAGGGGG
GACTGGAAGGGCTAATTCACTCCCAACGAAGACAAGATCTGCTTTTTGCTTGTACTGGGTCTCT
CTGGTTAGACCAGATCTGAGCCTGGGAGCTCTCTGGCTAACTAGGGAACCCACTGCTTAAGCCT
CAATAAAGCTTGCCTTGAGTGCTTCAAGTAGTGTGTGCCCGTCTGTTGTGTGACTCTGGTAACT
AGAGATCCCTCAGACCCTTTTAGTCAGTGTGGAAAATCTCTAGCAGTAGTAGTTCATGTCATCT
TATTATTCAGTATTTATAACTTGCAAAGAAATGAATATCAGAGAGTGAGAGGAACTTGTTTATT
GCAGCTTATAATGGTTACAAATAAAGCAATAGCATCACAAATTTCACAAATAAAGCATTTTTTT
CACTGCATTCTAGTTGTGGTTTGTCCAAACTCATCAATGTATCTTATCATGTCTGGCTCTAGCT
ATCCCGCCCCTAACTCCGCCCATCCCGCCCCTAACTCCGCCCAGTTCCGCCCATTCTCCGCCCC
ATGGCTGACTAATTTTTTTTATTTATGCAGAGGCCGAGGCCGCCTCGGCCTCTGAGCTATTCCA
GAAGTAGTGAGGAGGCTTTTTTGGAGGCCTAGGGACGTACCCAATTCGCCCTATAGTGAGTCGT
ATTACGCGCGCTCACTGGCCGTCGTTTTACAACGTCGTGACTGGGAAAACCCTGGCGTTACCCA
ACTTAATCGCCTTGCAGCACATCCCCCTTTCGCCAGCTGGCGTAATAGCGAAGAGGCCCGCACC
GATCGCCCTTCCCAACAGTTGCGCAGCCTGAATGGCGAATGGGACGCGCCCTGTAGCGGCGCAT
TAAGCGCGGCGGGTGTGGTGGTTACGCGCAGCGTGACCGCTACACTTGCCAGCGCCCTAGCGCC
CGCTCCTTTCGCTTTCTTCCCTTCCTTTCTCGCCACGTTCGCCGGCTTTCCCCGTCAAGCTCTA
AATCGGGGGCTCCCTTTAGGGTTCCGATTTAGTGCTTTACGGCACCTCGACCCCAAAAAACTTG
ATTAGGGTGATGGTTCACGTAGTGGGCCATCGCCCTGATAGACGGTTTTTCGCCCTTTGACGTT
GGAGTCCACGTTCTTTAATAGTGGACTCTTGTTCCAAACTGGAACAACACTCAACCCTATCTCG
GTCTATTCTTTTGATTTATAAGGGATTTTGCCGATTTCGGCCTATTGGTTAAAAAATGAGCTGA
TTTAACAAAAATTTAACGCGAATTTTAACAAAATATTAACGCTTACAATTTAGGTGGCACTTTT
CGGGGAAATGTGCGCGGAACCCCTATTTGTTTATTTTTCTAAATACATTCAAATATGTATCCGC
TCATGAGACAATAACCCTGATAAATGCTTCAATAATATTGAAAAAGGAAGAGTATGAGTATTCA
ACATTTCCGTGTCGCCCTTATTCCCTTTTTTGCGGCATTTTGCCTTCCTGTTTTTGCTCACCCA
GAAACGCTGGTGAAAGTAAAAGATGCTGAAGATCAGTTGGGTGCACGAGTGGGTTACATCGAAC
TGGATCTCAACAGCGGTAAGATCCTTGAGAGTTTTCGCCCCGAAGAACGTTTTCCAATGATGAG
CACTTTTAAAGTTCTGCTATGTGGCGCGGTATTATCCCGTATTGACGCCGGGCAAGAGCAACTC
GGTCGCCGCATACACTATTCTCAGAATGACTTGGTTGAGTACTCACCAGTCACAGAAAAGCATC
TTACGGATGGCATGACAGTAAGAGAATTATGCAGTGCTGCCATAACCATGAGTGATAACACTGC
GGCCAACTTACTTCTGACAACGATCGGAGGACCGAAGGAGCTAACCGCTTTTTTGCACAACATG

GGGGATCATGTAACTCGCCTTGATCGTTGGGAACCGGAGCTGAATGAAGCCATACCAAACGACG
AGCGTGACACCACGATGCCTGTAGCAATGGCAACAACGTTGCGCAAACTATTAACTGGCGAACT
ACTTACTCTAGCTTCCCGGCAACAATTAATAGACTGGATGGAGGCGGATAAAGTTGCAGGACCA
CTTCTGCGCTCGGCCCTTCCGGCTGGCTGGTTTATTGCTGATAAATCTGGAGCCGGTGAGCGTG
GGTCTCGCGGTATCATTGCAGCACTGGGGCCAGATGGTAAGCCCTCCCGTATCGTAGTTATCTA
CACGACGGGGAGTCAGGCAACTATGGATGAACGAAATAGACAGATCGCTGAGATAGGTGCCTCA
CTGATTAAGCATTGGTAACTGTCAGACCAAGTTTACTCATATATACTTTAGATTGATTTAAAAC
TTCATTTTTAATTTAAAAGGATCTAGGTGAAGATCCTTTTTGATAATCTCATGACCAAAATCCC
TTAACGTGAGTTTTCGTTCCACTGAGCGTCAGACCCCGTAGAAAAGATCAAAGGATCTTCTTGA
GATCCTTTTTTTCTGCGCGTAATCTGCTGCTTGCAAACAAAAAAACCACCGCTACCAGCGGTGG
TTTGTTTGCCGGATCAAGAGCTACCAACTCTTTTTCCGAAGGTAACTGGCTTCAGCAGAGCGCA
GATACCAAATACTGTTCTTCTAGTGTAGCCGTAGTTAGGCCACCACTTCAAGAACTCTGTAGCA
CCGCCTACATACCTCGCTCTGCTAATCCTGTTACCAGTGGCTGCTGCCAGTGGCGATAAGTCGT
GTCTTACCGGGTTGGACTCAAGACGATAGTTACCGGATAAGGCGCAGCGGTCGGGCTGAACGGG
GGGTTCGTGCACACAGCCCAGCTTGGAGCGAACGACCTACACCGAACTGAGATACCTACAGCGT
GAGCTATGAGAAAGCGCCACGCTTCCCGAAGAGAGAAAGGCGGACAGGTATCCGGTAAGCGGCA
GGGTCGGAACAGGAGAGCGCACGAGGGAGCTTCCAGGGGGAAACGCCTGGTATCTTTATAGTCC
TGTCGGGTTTCGCCACCTCTGACTTGAGCGTCGATTTTTGTGATGCTCGTCAGGGGGGCGGAGC
CTATGGAAAAACGCCAGCAACGCGGCCTTTTTACGGTTCCTGGCCTTTTGCTGGCCTTTTGCTC
ACATGTTCTTTCCTGCGTTATCCCCTGATTCTGTGGATAACCGTATTACCGCCTTTGAGTGAGC
TGATACCGCTCGCCGCAGCCGAACGACCGAGCGCAGCGAGTCAGTGAGCGAGGAAGCGGAAGAG
CGCCCAATACGCAAACCGCCTCTCCCCGCGCGTTGGCCGATTCATTAATGCAGCTGGCACGACA
GGTTTCCCGACTGGAAAGCGGGCAGTGAGCGCAACGCAATTAATGTGAGTTAGCTCACTCATTA
GGCACCCCAGGCTTTACACTTTATGCTTCCGGCTCGTATGTTGTGTGGAATTGTGAGCGGATAA
CAATTTCACACAGGAAACAGCTATGACCATGATTACGCCAAGCGCGCAATTAACCCTCACTAAA
GGGAACAAAAGCTGGAGCTGCAAGCTT

Fascin1 Mammalian Overexpression Plasmid:

Purchased from Vectorbuilder ID# VB190307-1132dnt

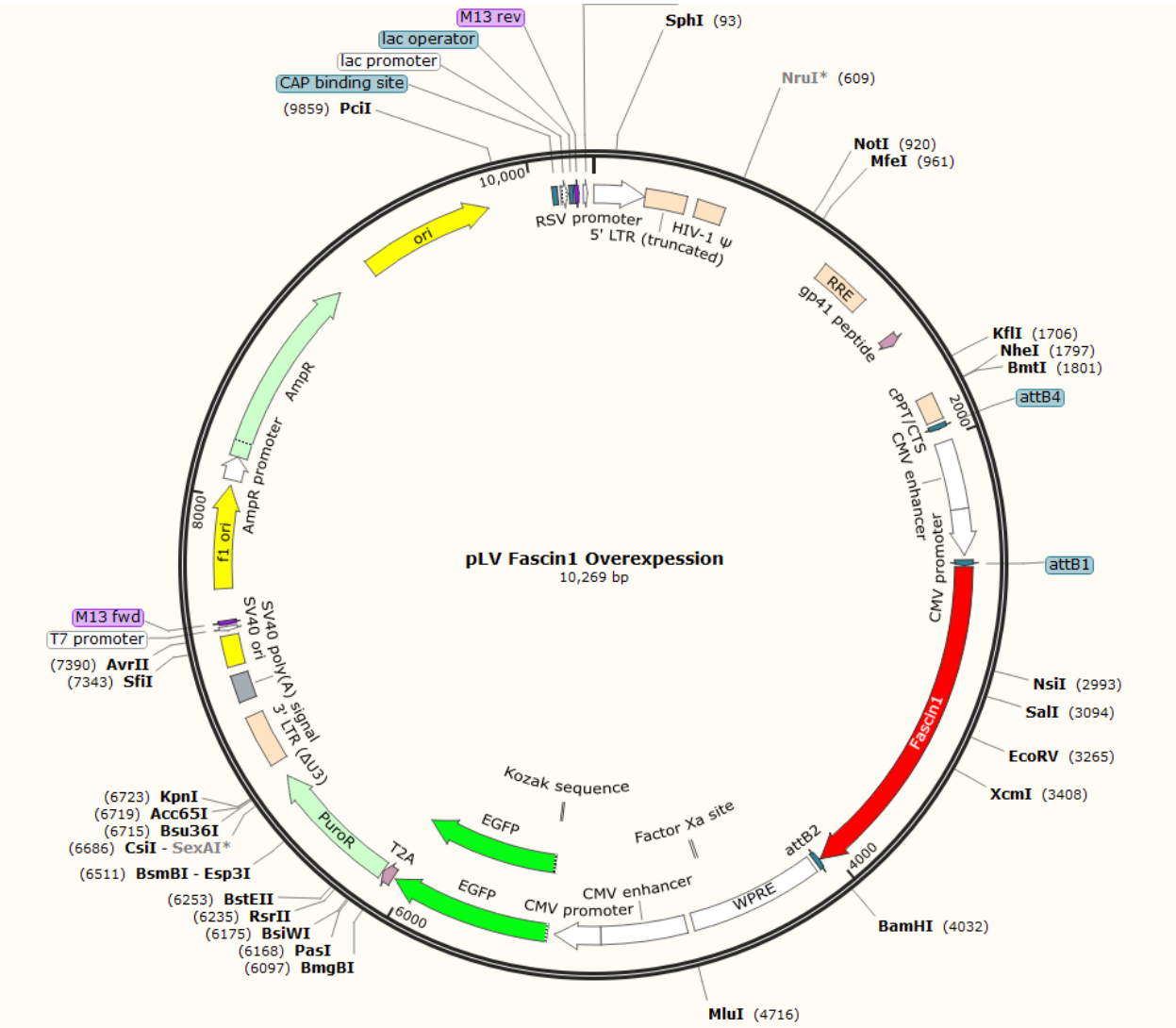

AATGTAGTCTTATGCAATACTCTTGTAGTCTTGCAACATGGTAACGATGAGTTAGCAACATGCC
TTACAAGGAGAGAAAAAGCACCGTGCATGCCGATTGGTGGAAGTAAGGTGGTACGATCGTGCCT
TATTAGGAAGGCAACAGACGGGTCTGACATGGATTGGACGAACCACTGAATTGCCGCATTGCAG
AGATATTGTATTTAAGTGCCTAGCTCGATACATAAACGGGTCTCTCTGGTTAGACCAGATCTGA
GCCTGGGAGCTCTCTGGCTAACTAGGGAACCCACTGCTTAAGCCTCAATAAAGCTTGCCTTGAG
TGCTTCAAGTAGTGTGTGCCCGTCTGTTGTGTGACTCTGGTAACTAGAGATCCCTCAGACCCTT
TTAGTCAGTGTGGAAAATCTCTAGCAGTGGCGCCCGAACAGGGACTTGAAAGCGAAAGGGAAAC
CAGAGGAGCTCTCTCGACGCAGGACTCGGCTTGCTGAAGCGCGCACGGCAAGAGGCGAGGGGCG
GCGACTGGTGAGTACGCCAAAAATTTTGACTAGCGGAGGCTAGAAGGAGAGAGATGGGTGCGAG
AGCGTCAGTATTAAGCGGGGGAGAATTAGATCGCGATGGGAAAAAATTCGGTTAAGGCCAGGGG
GAAAGAAAAAATATAAATTAAAACATATAGTATGGGCAAGCAGGGAGCTAGAACGATTCGCAGT
TAATCCTGGCCTGTTAGAAACATCAGAAGGCTGTAGACAAATACTGGGACAGCTACAACCATCC
CTTCAGACAGGATCAGAAGAACTTAGATCATTATATAATACAGTAGCAACCCTCTATTGTGTGC

ATCAAAGGATAGAGATAAAAGACACCAAGGAAGCTTTAGACAAGATAGAGGAAGAGCAAAACAA
AAGTAAGACCACCGCACAGCAAGCGGCCGCTGATCTTCAGACCTGGAGGAGGAGATATGAGGGA
CAATTGGAGAAGTGAATTATATAAATATAAAGTAGTAAAAATTGAACCATTAGGAGTAGCACCC
ACCAAGGCAAAGAGAAGAGTGGTGCAGAGAGAAAAAAGAGCAGTGGGAATAGGAGCTTTGTTCC
TTGGGTTCTTGGGAGCAGCAGGAAGCACTATGGGCGCAGCGTCAATGACGCTGACGGTACAGGC
CAGACAATTATTGTCTGGTATAGTGCAGCAGCAGAACAATTTGCTGAGGGCTATTGAGGCGCAA
CAGCATCTGTTGCAACTCACAGTCTGGGGCATCAAGCAGCTCCAGGCAAGAATCCTGGCTGTGG
AAAGATACCTAAAGGATCAACAGCTCCTGGGGATTTGGGGTTGCTCTGGAAAACTCATTTGCAC
CACTGCTGTGCCTTGGAATGCTAGTTGGAGTAATAAATCTCTGGAACAGATTTGGAATCACACG
ACCTGGATGGAGTGGGACAGAGAAATTAACAATTACACAAGCTTAATACACTCCTTAATTGAAG
AATCGCAAAACCAGCAAGAAAAGAATGAACAAGAATTATTGGAATTAGATAAATGGGCAAGTTT
GTGGAATTGGTTTAACATAACAAATTGGCTGTGGTATATAAAATTATTCATAATGATAGTAGGA
GGCTTGGTAGGTTTAAGAATAGTTTTTGCTGTACTTTCTATAGTGAATAGAGTTAGGCAGGGAT
ATTCACCATTATCGTTTCAGACCCACCTCCCAACCCCGAGGGGACCCGACAGGCCCGAAGGAAT
AGAAGAAGAAGGTGGAGAGAGAGACAGAGACAGATCCATTCGATTAGTGAACGGATCTCGACGG
TATCGCTAGCTTTTAAAAGAAAAGGGGGGATTGGGGGGTACAGTGCAGGGGAAAGAATAGTAGA
CATAATAGCAACAGACATACAAACTAAAGAATTACAAAAACAAATTACAAAAATTCAAAATTTT
ACTAGTGATTATCGGATCAACTTTGTATAGAAAAGTTGTAGTTATTAATAGTAATCAATTACGG
GGTCATTAGTTCATAGCCCATATATGGAGTTCCGCGTTACATAACTTACGGTAAATGGCCCGCC
TGGCTGACCGCCCAACGACCCCCGCCCATTGACGTCAATAATGACGTATGTTCCCATAGTAACG
CCAATAGGGACTTTCCATTGACGTCAATGGGTGGAGTATTTACGGTAAACTGCCCACTTGGCAG
TACATCAAGTGTATCATATGCCAAGTACGCCCCCTATTGACGTCAATGACGGTAAATGGCCCGC
CTGGCATTATGCCCAGTACATGACCTTATGGGACTTTCCTACTTGGCAGTACATCTACGTATTA
GTCATCGCTATTACCATGGTGATGCGGTTTTGGCAGTACATCAATGGGCGTGGATAGCGGTTTG
ACTCACGGGGATTTCCAAGTCTCCACCCCATTGACGTCAATGGGAGTTTGTTTTGGCACCAAAA
TCAACGGGACTTTCCAAAATGTCGTAACAACTCCGCCCCATTGACGCAAATGGGCGGTAGGCGT
GTACGGTGGGAGGTCTATATAAGCAGAGCTGGTTTAGTGAACCGTCAGATCCAAGTTTGTACAA
AAAAGCAGGCTGCCACCATGACAGCCAACGGAACAGCTGAGGCCGTGCAGATCCAGTTCGGCCT
GATCAACTGCGGCAACAAGTACCTGACAGCCGAGGCCTTCGGATTCAAAGTGAACGCCTCTGCC
AGCAGCCTGAAGAAGAAGCAGATCTGGACCCTGGAACAGCCTCCTGACGAAGCCGGATCTGCTG
CCGTGTGTCTGAGAAGCCACCTGGGAAGATACCTGGCCGCCGACAAGGACGGAAACGTGACATG
CGAGAGAGAGGTGCCAGGACCTGACTGCAGATTCCTGATCGTGGCCCACGACGACGGAAGATGG
TCCCTGCAGTCTGAGGCCCACAGAAGATACTTCGGCGGCACCGAGGACAGGCTGTCTTGTTTCG
CTCAGACCGTGTCTCCCGCCGAGAAGTGGAGTGTGCATATCGCCATGCATCCCCAAGTGAACAT
CTACAGCGTGACCAGAAAGAGATACGCCCACCTGTCTGCCAGACCTGCCGATGAGATTGCCGTG
GACAGAGATGTGCCTTGGGGCGTCGACTCCCTGATCACACTGGCTTTTCAGGACCAGAGGTACA
GCGTGCAGACCGCCGACCACAGATTTCTGAGGCACGATGGAAGGCTGGTGGCCAGACCAGAACC
TGCCACAGGCTACACCCTGGAATTCAGATCTGGCAAGGTGGCCTTCAGGGACTGCGAGGGGAGA
TATCTGGCTCCTTCTGGACCTAGCGGCACACTGAAGGCCGGCAAGGCTACCAAAGTGGGCAAAG
ACGAGCTGTTCGCCCTCGAGCAGTCTTGTGCTCAGGTTGTGCTGCAGGCCGCCAACGAGAGAAA
CGTGTCCACCAGACAAGGCATGGACCTGAGCGCCAACCAGGACGAGGAAACCGACCAAGAGACA
TTCCAGCTCGAGATCGACAGGGACACCAAGAAGTGCGCCTTCAGAACCCACACCGGCAAGTACT
GGACACTGACAGCTACAGGCGGCGTGCAGTCTACCGCCTCTAGCAAGAACGCCAGCTGCTACTT
CGACATCGAGTGGCGGGACAGAAGGATCACCCTGAGAGCCAGCAACGGCAAGTTCGTGACCTCC
AAGAAGAACGGACAGCTGGCCGCCTCTGTGGAAACAGCCGGCGATTCTGAGCTGTTCCTGATGA
AGCTGATCAACAGGCCCATCATCGTGTTCAGGGGCGAGCACGGCTTCATCGGCTGCAGAAAAGT
GACAGGCACCCTGGACGCCAACAGGTCCTCTTACGATGTGTTTCAGCTCGAGTTCAACGACGGC

GCCTACAACATCAAGGACAGCACAGGGAAGTATTGGACCGTGGGCTCTGACAGCGCCGTGACAT
CTTCTGGCGATACCCCTGTGGATTTCTTCTTCGAATTCTGCGACTACAACAAGGTCGCCATCAA
AGTCGGCGGCAGATACCTGAAGGGCGATCATGCTGGCGTGCTGAAGGCTTCTGCTGAGACAGTG
GATCCTGCCAGCCTGTGGGAGTACTGATGAACCCAGCTTTCTTGTACAAAGTGGTGATAATCGA
ATTCCGATAATCAACCTCTGGATTACAAAATTTGTGAAAGATTGACTGGTATTCTTAACTATGT
TGCTCCTTTTACGCTATGTGGATACGCTGCTTTAATGCCTTTGTATCATGCTATTGCTTCCCGT
ATGGCTTTCATTTTCTCCTCCTTGTATAAATCCTGGTTGCTGTCTCTTTATGAGGAGTTGTGGC
CCGTTGTCAGGCAACGTGGCGTGGTGTGCACTGTGTTTGCTGACGCAACCCCCACTGGTTGGGG
CATTGCCACCACCTGTCAGCTCCTTTCCGGGACTTTCGCTTTCCCCCTCCCTATTGCCACGGCG
GAACTCATCGCCGCCTGCCTTGCCCGCTGCTGGACAGGGGCTCGGCTGTTGGGCACTGACAATT
CCGTGGTGTTGTCGGGGAAGCTGACGTCCTTTCCATGGCTGCTCGCCTGTGTTGCCACCTGGAT
TCTGCGCGGGACGTCCTTCTGCTACGTCCCTTCGGCCCTCAATCCAGCGGACCTTCCTTCCCGC
GGCCTGCTGCCGGCTCTGCGGCCTCTTCCGCGTCTTCGCCTTCGCCCTCAGACGAGTCGGATCT
CCCTTTGGGCCGCCTCCCCGCATCGGGAATTCCCGCGGTTCGAACGCGTTGACATTGATTATTG
ACTAGTTATTAATAGTAATCAATTACGGGGTCATTAGTTCATAGCCCATATATGGAGTTCCGCG
TTACATAACTTACGGTAAATGGCCCGCCTGGCTGACCGCCCAACGACCCCCGCCCATTGACGTC
AATAATGACGTATGTTCCCATAGTAACGCCAATAGGGACTTTCCATTGACGTCAATGGGTGGAG
TATTTACGGTAAACTGCCCACTTGGCAGTACATCAAGTGTATCATATGCCAAGTACGCCCCCTA
TTGACGTCAATGACGGTAAATGGCCCGCCTGGCATTATGCCCAGTACATGACCTTATGGGACTT
TCCTACTTGGCAGTACATCTACGTATTAGTCATCGCTATTACCATGGTGATGCGGTTTTGGCAG
TACATCAATGGGCGTGGATAGCGGTTTGACTCACGGGGATTTCCAAGTCTCCACCCCATTGACG
TCAATGGGAGTTTGTTTTGGCACCAAAATCAACGGGACTTTCCAAAATGTCGTAACAACTCCGC
CCCATTGACGCAAATGGGCGGTAGGCGTGTACGGTGGGAGGTCTATATAAGCAGAGCTCTCTGG
CTAACTAGAGAACCCACTGCGCCACCATGGTGAGCAAGGGCGAGGAGCTGTTCACCGGGGTGGT
GCCCATCCTGGTCGAGCTGGACGGCGACGTAAACGGCCACAAGTTCAGCGTGTCCGGCGAGGGC
GAGGGCGATGCCACCTACGGCAAGCTGACCCTGAAGTTCATCTGCACCACCGGCAAGCTGCCCG
TGCCCTGGCCCACCCTCGTGACCACCCTGACCTACGGCGTGCAGTGCTTCAGCCGCTACCCCGA
CCACATGAAGCAGCACGACTTCTTCAAGTCCGCCATGCCCGAAGGCTACGTCCAGGAGCGCACC
ATCTTCTTCAAGGACGACGGCAACTACAAGACCCGCGCCGAGGTGAAGTTCGAGGGCGACACCC
TGGTGAACCGCATCGAGCTGAAGGGCATCGACTTCAAGGAGGACGGCAACATCCTGGGGCACAA
GCTGGAGTACAACTACAACAGCCACAACGTCTATATCATGGCCGACAAGCAGAAGAACGGCATC
AAGGTGAACTTCAAGATCCGCCACAACATCGAGGACGGCAGCGTGCAGCTCGCCGACCACTACC
AGCAGAACACCCCCATCGGCGACGGCCCCGTGCTGCTGCCCGACAACCACTACCTGAGCACCCA
GTCCGCCCTGAGCAAAGACCCCAACGAGAAGCGCGATCACATGGTCCTGCTGGAGTTCGTGACC
GCCGCCGGGATCACTCTCGGCATGGACGAGCTGTACAAGGGCTCCGGAGAGGGCAGGGGAAGTC
TTCTAACATGCGGGGACGTGGAGGAAAATCCCGGCCCCATGACCGAGTACAAGCCCACGGTGCG
CCTCGCCACCCGCGACGACGTCCCCAGGGCCGTACGCACCCTCGCCGCCGCGTTCGCCGACTAC
CCCGCCACGCGCCACACCGTCGATCCGGACCGCCACATCGAGCGGGTCACCGAGCTGCAAGAAC
TCTTCCTCACGCGCGTCGGGCTCGACATCGGCAAGGTGTGGGTCGCGGACGACGGCGCCGCGGT
GGCGGTCTGGACCACGCCGGAGAGCGTCGAAGCGGGGGCGGTGTTCGCCGAGATCGGCCCGCGC
ATGGCCGAGTTGAGCGGTTCCCGGCTGGCCGCGCAGCAACAGATGGAAGGCCTCCTGGCGCCGC
ACCGGCCCAAGGAGCCCGCGTGGTTCCTGGCCACCGTCGGCGTCTCGCCCGACCACCAGGGCAA
GGGTCTGGGCAGCGCCGTCGTGCTCCCCGGAGTGGAGGCGGCCGAGCGCGCCGGGGTGCCCGCC
TTCCTGGAGACCTCCGCGCCCCGCAACCTCCCCTTCTACGAGCGGCTCGGCTTCACCGTCACCG
CCGACGTCGAGGTGCCCGAAGGACCGCGCACCTGGTGCATGACCCGCAAGCCCGGTGCCTGAGG
TACCTTTAAGACCAATGACTTACAAGGCAGCTGTAGATCTTAGCCACTTTTTAAAAGAAAAGGG
GGGACTGGAAGGGCTAATTCACTCCCAACGAAGACAAGATCTGCTTTTTGCTTGTACTGGGTCT

CTCTGGTTAGACCAGATCTGAGCCTGGGAGCTCTCTGGCTAACTAGGGAACCCACTGCTTAAGC
CTCAATAAAGCTTGCCTTGAGTGCTTCAAGTAGTGTGTGCCCGTCTGTTGTGTGACTCTGGTAA
CTAGAGATCCCTCAGACCCTTTTAGTCAGTGTGGAAAATCTCTAGCAGTAGTAGTTCATGTCAT
CTTATTATTCAGTATTTATAACTTGCAAAGAAATGAATATCAGAGAGTGAGAGGAACTTGTTTA
TTGCAGCTTATAATGGTTACAAATAAAGCAATAGCATCACAAATTTCACAAATAAAGCATTTTT
TTCACTGCATTCTAGTTGTGGTTTGTCCAAACTCATCAATGTATCTTATCATGTCTGGCTCTAG
CTATCCCGCCCCTAACTCCGCCCATCCCGCCCCTAACTCCGCCCAGTTCCGCCCATTCTCCGCC
CCATGGCTGACTAATTTTTTTTATTTATGCAGAGGCCGAGGCCGCCTCGGCCTCTGAGCTATTC
CAGAAGTAGTGAGGAGGCTTTTTTGGAGGCCTAGGGACGTACCCAATTCGCCCTATAGTGAGTC
GTATTACGCGCGCTCACTGGCCGTCGTTTTACAACGTCGTGACTGGGAAAACCCTGGCGTTACC
CAACTTAATCGCCTTGCAGCACATCCCCCTTTCGCCAGCTGGCGTAATAGCGAAGAGGCCCGCA
CCGATCGCCCTTCCCAACAGTTGCGCAGCCTGAATGGCGAATGGGACGCGCCCTGTAGCGGCGC
ATTAAGCGCGGCGGGTGTGGTGGTTACGCGCAGCGTGACCGCTACACTTGCCAGCGCCCTAGCG
CCCGCTCCTTTCGCTTTCTTCCCTTCCTTTCTCGCCACGTTCGCCGGCTTTCCCCGTCAAGCTC
TAAATCGGGGGCTCCCTTTAGGGTTCCGATTTAGTGCTTTACGGCACCTCGACCCCAAAAAACT
TGATTAGGGTGATGGTTCACGTAGTGGGCCATCGCCCTGATAGACGGTTTTTCGCCCTTTGACG
TTGGAGTCCACGTTCTTTAATAGTGGACTCTTGTTCCAAACTGGAACAACACTCAACCCTATCT
CGGTCTATTCTTTTGATTTATAAGGGATTTTGCCGATTTCGGCCTATTGGTTAAAAAATGAGCT
GATTTAACAAAAATTTAACGCGAATTTTAACAAAATATTAACGCTTACAATTTAGGTGGCACTT
TTCGGGGAAATGTGCGCGGAACCCCTATTTGTTTATTTTTCTAAATACATTCAAATATGTATCC
GCTCATGAGACAATAACCCTGATAAATGCTTCAATAATATTGAAAAAGGAAGAGTATGAGTATT
CAACATTTCCGTGTCGCCCTTATTCCCTTTTTTGCGGCATTTTGCCTTCCTGTTTTTGCTCACC
CAGAAACGCTGGTGAAAGTAAAAGATGCTGAAGATCAGTTGGGTGCACGAGTGGGTTACATCGA
ACTGGATCTCAACAGCGGTAAGATCCTTGAGAGTTTTCGCCCCGAAGAACGTTTTCCAATGATG
AGCACTTTTAAAGTTCTGCTATGTGGCGCGGTATTATCCCGTATTGACGCCGGGCAAGAGCAAC
TCGGTCGCCGCATACACTATTCTCAGAATGACTTGGTTGAGTACTCACCAGTCACAGAAAAGCA
TCTTACGGATGGCATGACAGTAAGAGAATTATGCAGTGCTGCCATAACCATGAGTGATAACACT
GCGGCCAACTTACTTCTGACAACGATCGGAGGACCGAAGGAGCTAACCGCTTTTTTGCACAACA
TGGGGGATCATGTAACTCGCCTTGATCGTTGGGAACCGGAGCTGAATGAAGCCATACCAAACGA
CGAGCGTGACACCACGATGCCTGTAGCAATGGCAACAACGTTGCGCAAACTATTAACTGGCGAA
CTACTTACTCTAGCTTCCCGGCAACAATTAATAGACTGGATGGAGGCGGATAAAGTTGCAGGAC
CACTTCTGCGCTCGGCCCTTCCGGCTGGCTGGTTTATTGCTGATAAATCTGGAGCCGGTGAGCG
TGGGTCTCGCGGTATCATTGCAGCACTGGGGCCAGATGGTAAGCCCTCCCGTATCGTAGTTATC
TACACGACGGGGAGTCAGGCAACTATGGATGAACGAAATAGACAGATCGCTGAGATAGGTGCCT
CACTGATTAAGCATTGGTAACTGTCAGACCAAGTTTACTCATATATACTTTAGATTGATTTAAA
ACTTCATTTTTAATTTAAAAGGATCTAGGTGAAGATCCTTTTTGATAATCTCATGACCAAAATC
CCTTAACGTGAGTTTTCGTTCCACTGAGCGTCAGACCCCGTAGAAAAGATCAAAGGATCTTCTT
GAGATCCTTTTTTTCTGCGCGTAATCTGCTGCTTGCAAACAAAAAAACCACCGCTACCAGCGGT
GGTTTGTTTGCCGGATCAAGAGCTACCAACTCTTTTTCCGAAGGTAACTGGCTTCAGCAGAGCG
CAGATACCAAATACTGTTCTTCTAGTGTAGCCGTAGTTAGGCCACCACTTCAAGAACTCTGTAG
CACCGCCTACATACCTCGCTCTGCTAATCCTGTTACCAGTGGCTGCTGCCAGTGGCGATAAGTC
GTGTCTTACCGGGTTGGACTCAAGACGATAGTTACCGGATAAGGCGCAGCGGTCGGGCTGAACG
GGGGGTTCGTGCACACAGCCCAGCTTGGAGCGAACGACCTACACCGAACTGAGATACCTACAGC
GTGAGCTATGAGAAAGCGCCACGCTTCCCGAAGAGAGAAAGGCGGACAGGTATCCGGTAAGCGG
CAGGGTCGGAACAGGAGAGCGCACGAGGGAGCTTCCAGGGGGAAACGCCTGGTATCTTTATAGT
CCTGTCGGGTTTCGCCACCTCTGACTTGAGCGTCGATTTTTGTGATGCTCGTCAGGGGGGCGGA
GCCTATGGAAAAACGCCAGCAACGCGGCCTTTTTACGGTTCCTGGCCTTTTGCTGGCCTTTTGC

TCACATGTTCTTTCCTGCGTTATCCCCTGATTCTGTGGATAACCGTATTACCGCCTTTGAGTGA
GCTGATACCGCTCGCCGCAGCCGAACGACCGAGCGCAGCGAGTCAGTGAGCGAGGAAGCGGAAG
AGCGCCCAATACGCAAACCGCCTCTCCCCGCGCGTTGGCCGATTCATTAATGCAGCTGGCACGA
CAGGTTTCCCGACTGGAAAGCGGGCAGTGAGCGCAACGCAATTAATGTGAGTTAGCTCACTCAT
TAGGCACCCCAGGCTTTACACTTTATGCTTCCGGCTCGTATGTTGTGTGGAATTGTGAGCGGAT
AACAATTTCACACAGGAAACAGCTATGACCATGATTACGCCAAGCGCGCAATTAACCCTCACTA
AAGGGAACAAAAGCTGGAGCTGCAAGCTT

FascinN-CfaN Plasmid:

Purchased from Vectorbuilder. ID# [VB181221-1147qzj]

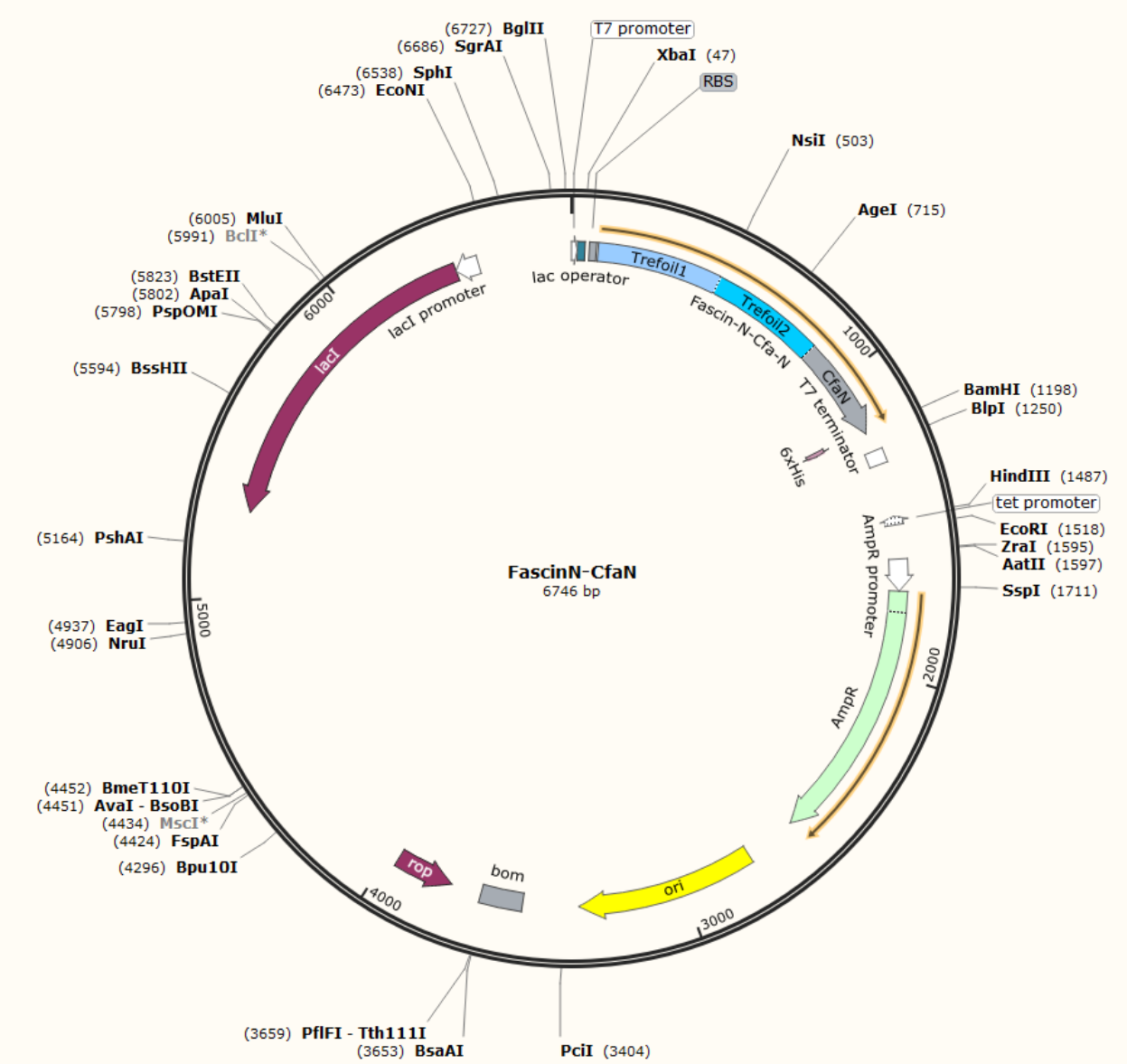

TAATACGACTCACTATAGGGGAATTGTGAGCGGATAACAATTCCCCTCTAGAAATAATTTTGTT
TAACTTTAAGAAGGAGATATACCATGACCGCAAATGGCACCGCAGAAGCAGTTCAGATTCAGTT
TGGTCTGATTAATTGCGGCAACAAATATCTGACAGCAGAAGCCTTTGGCTTTAAAGTTAATGCA
AGCGCAAGCAGCCTGAAAAAAAAGCAGATTTGGACCCTGGAACAGCCTCCGGATGAAGCAGGTA
GCGCAGCAGTTTGTCTGCGTAGCCATCTGGGTCGTTATCTGGCAGCCGATAAAGATGGTAATGT
TACCTGTGAACGTGAAGTTCCGGGTCCTGATTGTCGTTTTCTGATTGTTGCACATGATGATGGT
CGTTGGAGCCTGCAGAGCGAAGCACATCGTCGTTATTTTGGTGGCACCGAAGATCGTCTGAGCT
GTTTTGCACAGACCGTTAGTCCGGCAGAAAAATGGTCAGTTCATATTGCAATGCATCCGCAGGT
TAACATTTATAGCGTTACCCGTAAACGTTATGCACATCTGAGCGCACGTCCTGCAGATGAAATT
GCAGTTGATCGTGATGTTCCGTGGGGTGTTGATAGCCTGATTACCCTGGCATTTCAGGATCAGC
GTTATAGCGTGCAGACCGCAGATCACCGTTTTCTGCGTCATGATGGCCGTCTGGTTGCACGTCC
GGAACCGGCAACCGGTTATACACTGGAATTTCGTAGCGGTAAAGTTGCCTTTCGTGATTGTGAA
GGACGCTATCTGGCACCGTCAGGTCCGAGCGGCACCCTGAAAGCAGGTAAAGCAACCAAAGTTG
GTAAAGATGAACTGTTTGCACTGGAACAGAGCTGTCTGAGCTATGATACCGAAATTCTGACCGT
GGAATATGGCTTTCTGCCGATTGGTAAAATTGTGGAAGAACGTATTGAATGCACCGTGTATACC
GTGGATAAAAACGGTTTTGTTTATACCCAGCCGATTGCACAGTGGCATAATCGTGGTGAACAAG
AAGTTTTTGAGTACTGTCTGGAAGATGGTAGCATTATTCGTGCGACCAAAGATCACAAATTTAT
GACCACCGATGGTCAGATGCTGCCGATCGATGAAATTTTTGAACGTGGTCTGGATCTGAAACAG
GTTGATGGTCTGCCTGGTAGCGGTCATCATCATCACCATCACTAAGGATCCGCTGCTAACAAAG
CCCGAAAGGAAGCTGAGTTGGCTGCTGCCACCGCTGAGCAATAACTAGCATAACCCCTTGGGGC
CTCTAAACGGGTCTTGAGGGGTTTTTTGCTGAAAGGAGGAACTATATCCGGATATCCCGCAAGA
GGCCCGGCAGTACCGGCATAACCAAGCCTATGCCTACAGCATCCAGGGTGACGGTGCCGAGGAT
GACGATGAGCGCATTGTTAGATTTCATACACGGTGCCTGACTGCGTTAGCAATTTAACTGTGAT
AAACTACCGCATTAAAGCTTATCGATGATAAGCTGTCAAACATGAGAATTCTTGAAGACGAAAG
GGCCTCGTGATACGCCTATTTTTATAGGTTAATGTCATGATAATAATGGTTTCTTAGACGTCAG
GTGGCACTTTTCGGGGAAATGTGCGCGGAACCCCTATTTGTTTATTTTTCTAAATACATTCAAA
TATGTATCCGCTCATGAGACAATAACCCTGATAAATGCTTCAATAATATTGAAAAAGGAAGAGT
ATGAGTATTCAACATTTCCGTGTCGCCCTTATTCCCTTTTTTGCGGCATTTTGCCTTCCTGTTT
TTGCTCACCCAGAAACGCTGGTGAAAGTAAAAGATGCTGAAGATCAGTTGGGTGCACGAGTGGG
TTACATCGAACTGGATCTCAACAGCGGTAAGATCCTTGAGAGTTTTCGCCCCGAAGAACGTTTT
CCAATGATGAGCACTTTTAAAGTTCTGCTATGTGGCGCGGTATTATCCCGTGTTGACGCCGGGC
AAGAGCAACTCGGTCGCCGCATACACTATTCTCAGAATGACTTGGTTGAGTACTCACCAGTCAC
AGAAAAGCATCTTACGGATGGCATGACAGTAAGAGAATTATGCAGTGCTGCCATAACCATGAGT
GATAACACTGCGGCCAACTTACTTCTGACAACGATCGGAGGACCGAAGGAGCTAACCGCTTTTT
TGCACAACATGGGGGATCATGTAACTCGCCTTGATCGTTGGGAACCGGAGCTGAATGAAGCCAT
ACCAAACGACGAGCGTGACACCACGATGCCTGCAGCAATGGCAACAACGTTGCGCAAACTATTA
ACTGGCGAACTACTTACTCTAGCTTCCCGGCAACAATTAATAGACTGGATGGAGGCGGATAAAG
TTGCAGGACCACTTCTGCGCTCGGCCCTTCCGGCTGGCTGGTTTATTGCTGATAAATCTGGAGC
CGGTGAGCGTGGGTCACGCGGTATCATTGCAGCACTGGGGCCAGATGGTAAGCCCTCCCGTATC
GTAGTTATCTACACGACGGGGAGTCAGGCAACTATGGATGAACGAAATAGACAGATCGCTGAGA
TAGGTGCCTCACTGATTAAGCATTGGTAACTGTCAGACCAAGTTTACTCATATATACTTTAGAT
TGATTTAAAACTTCATTTTTAATTTAAAAGGATCTAGGTGAAGATCCTTTTTGATAATCTCATG
ACCAAAATCCCTTAACGTGAGTTTTCGTTCCACTGAGCGTCAGACCCCGTAGAAAAGATCAAAG
GATCTTCTTGAGATCCTTTTTTTCTGCGCGTAATCTGCTGCTTGCAAACAAAAAAACCACCGCT
ACCAGCGGTGGTTTGTTTGCCGGATCAAGAGCTACCAACTCTTTTTCCGAAGGTAACTGGCTTC
AGCAGAGCGCAGATACCAAATACTGTCCTTCTAGTGTAGCCGTAGTTAGGCCACCACTTCAAGA
ACTCTGTAGCACCGCCTACATACCTCGCTCTGCTAATCCTGTTACCAGTGGCTGCTGCCAGTGG

CGATAAGTCGTGTCTTACCGGGTTGGACTCAAGACGATAGTTACCGGATAAGGCGCAGCGGTCG
GGCTGAACGGGGGGTTCGTGCACACAGCCCAGCTTGGAGCGAACGACCTACACCGAACTGAGAT
ACCTACAGCGTGAGCTATGAGAAAGCGCCACGCTTCCCGAAGGGAGAAAGGCGGACAGGTATCC
GGTAAGCGGCAGGGTCGGAACAGGAGAGCGCACGAGGGAGCTTCCAGGGGGAAACGCCTGGTAT
CTTTATAGTCCTGTCGGGTTTCGCCACCTCTGACTTGAGCGTCGATTTTTGTGATGCTCGTCAG
GGGGGCGGAGCCTATGGAAAAACGCCAGCAACGCGGCCTTTTTACGGTTCCTGGCCTTTTGCTG
GCCTTTTGCTCACATGTTCTTTCCTGCGTTATCCCCTGATTCTGTGGATAACCGTATTACCGCC
TTTGAGTGAGCTGATACCGCTCGCCGCAGCCGAACGACCGAGCGCAGCGAGTCAGTGAGCGAGG
AAGCGGAAGGGCGCCTGATGCGGTATTTTCTCCTTACGCATCTGTGCGGTATTTCACACCGCAA
TGGTGCACTCTCAGTACAATCTGCTCTGATGCCGCATAGTTAAGCCAGTATACACTCCGCTATC
GCTACGTGACTGGGTCATGGCTGCGCCCCGACACCCGCCAACACCCGCTGACGCGCCCTGACGG
GCTTGTCTGCTCCCGGCATCCGCTTACAGACAAGCTGTGACCGTCTCCGGGAGCTGCATGTGTC
AGAGGTTTTCACCGTCATCACCGAAACGCGCGAGGCAGCTGCGGTAAAGCTCATCAGCGTGGTC
GTGAAGCGATTCACAGATGTCTGCCTGTTCATCCGCGTCCAGCTCGTTGAGTTTCTCCAGAAGC
GTTAATGTCTGGCTTCTGATAAAGCGGGCCATGTTAAGGGCGGTTTTTTCCTGTTTGGTCACTG
ATGCCTCCGTGTAAGGGGGATTTCTGTTCATGGGGGTAATGATACCGATGAAACGAGAGAGGAT
GCTCACGATACGGGTTACTGATGATGAACATGCCCGGTTACTGGAACGTTGTGAGGGTAAACAA
CTGGCGGTATGGATGCGGCGGGACCAGAGAAAAATCACTCAGGGTCAATGCCAGCGCTTCGTTA
ATACAGATGTAGGTGTTCCACAGGGTAGCCAGCAGCATCCTGCGATGCAGATCCGGAACATAAT
GGTGCAGGGCGCTGACTTCCGCGTTTCCAGACTTTACGAAACACGGAAACCGAAGACCATTCAT
GTTGTTGCTCAGGTCGCAGACGTTTTGCAGCAGCAGTCGCTTCACGTTCGCTCGCGTATCGGTG
ATTCATTCTGCTAACCAGTAAGGCAACCCCGCCAGCCTAGCCGGGTCCTCAACGACAGGAGCAC
GATCATGCGCACCCGTGGCCAGGACCCAACGCTGCCCGAGATGCGCCGCGTGCGGCTGCTGGAG
ATGGCGGACGCGATGGATATGTTCTGCCAAGGGTTGGTTTGCGCATTCACAGTTCTCCGCAAGA
ATTGATTGGCTCCAATTCTTGGAGTGGTGAATCCGTTAGCGAGGTGCCGCCGGCTTCCATTCAG
GTCGAGGTGGCCCGGCTCCATGCACCGCGACGCAACGCGGGGAGGCAGACAAGGTATAGGGCGG
CGCCTACAATCCATGCCAACCCGTTCCATGTGCTCGCCGAGGCGGCATAAATCGCCGTGACGAT
CAGCGGTCCAATGATCGAAGTTAGGCTGGTAAGAGCCGCGAGCGATCCTTGAAGCTGTCCCTGA
TGGTCGTCATCTACCTGCCTGGACAGCATGGCCTGCAACGCGGGCATCCCGATGCCGCCGGAAG
CGAGAAGAATCATAATGGGGAAGGCCATCCAGCCTCGCGTCGCGAACGCCAGCAAGACGTAGCC
CAGCGCGTCGGCCGCCATGCCGGCGATAATGGCCTGCTTCTCGCCGAAACGTTTGGTGGCGGGA
CCAGTGACGAAGGCTTGAGCGAGGGCGTGCAAGATTCCGAATACCGCAAGCGACAGGCCGATCA
TCGTCGCGCTCCAGCGAAAGCGGTCCTCGCCGAAAATGACCCAGAGCGCTGCCGGCACCTGTCC
TACGAGTTGCATGATAAAGAAGACAGTCATAAGTGCGGCGACGATAGTCATGCCCCGCGCCCAC
CGGAAGGAGCTGACTGGGTTGAAGGCTCTCAAGGGCATCGGTCGAGATCCCGGTGCCTAATGAG
TGAGCTAACTTACATTAATTGCGTTGCGCTCACTGCCCGCTTTCCAGTCGGGAAACCTGTCGTG
CCAGCTGCATTAATGAATCGGCCAACGCGCGGGGAGAGGCGGTTTGCGTATTGGGCGCCAGGGT
GGTTTTTCTTTTCACCAGTGAGACGGGCAACAGCTGATTGCCCTTCACCGCCTGGCCCTGAGAG
AGTTGCAGCAAGCGGTCCACGCTGGTTTGCCCCAGCAGGCGAAAATCCTGTTTGATGGTGGTTA
ACGGCGGGATATAACATGAGCTGTCTTCGGTATCGTCGTATCCCACTACCGAGATATCCGCACC
AACGCGCAGCCCGGACTCGGTAATGGCGCGCATTGCGCCCAGCGCCATCTGATCGTTGGCAACC
AGCATCGCAGTGGGAACGATGCCCTCATTCAGCATTTGCATGGTTTGTTGAAAACCGGACATGG
CACTCCAGTCGCCTTCCCGTTCCGCTATCGGCTGAATTTGATTGCGAGTGAGATATTTATGCCA
GCCAGCCAGACGCAGACGCGCCGAGACAGAACTTAATGGGCCCGCTAACAGCGCGATTTGCTGG
TGACCCAATGCGACCAGATGCTCCACGCCCAGTCGCGTACCGTCTTCATGGGAGAAAATAATAC
TGTTGATGGGTGTCTGGTCAGAGACATCAAGAAATAACGCCGGAACATTAGTGCAGGCAGCTTC
CACAGCAATGGCATCCTGGTCATCCAGCGGATAGTTAATGATCAGCCCACTGACGCGTTGCGCG

AGAAGATTGTGCACCGCCGCTTTACAGGCTTCGACGCCGCTTCGTTCTACCATCGACACCACCA
CGCTGGCACCCAGTTGATCGGCGCGAGATTTAATCGCCGCGACAATTTGCGACGGCGCGTGCAG
GGCCAGACTGGAGGTGGCAACGCCAATCAGCAACGACTGTTTGCCCGCCAGTTGTTGTGCCACG
CGGTTGGGAATGTAATTCAGCTCCGCCATCGCCGCTTCCACTTTTTCCCGCGTTTTCGCAGAAA
CGTGGCTGGCCTGGTTCACCACGCGGGAAACGGTCTGATAAGAGACACCGGCATACTCTGCGAC
ATCGTATAACGTTACTGGTTTCACATTCACCACCCTGAATTGACTCTCTTCCGGGCGCTATCAT
GCCATACCGCGAAAGGTTTTGCGCCATTCGATGGTGTCCGGGATCTCGACGCTCTCCCTTATGC
GACTCCTGCATTAGGAAGCAGCCCAGTAGTAGGTTGAGGCCGTTGAGCACCGCCGCCGCAAGGA
ATGGTGCATGCAAGGAGATGGCGCCCAACAGTCCCCCGGCCACGGGGCCTGCCACCATACCCAC
GCCGAAACAAGCGCTCATGAGCCCGAAGTGGCGAGCCCGATCTTCCCCATCGGTGATGTCGGCG
ATATAGGCGCCAGCAACCGCACCTGTGGCGCCGGTGATGCCGGCCACGATGCGTCCGGCGTAGA
GGATCGAGATCTCGATCCCGCGAAAT

CfaC-FascinC Plasmid:

Purchased from Vectorbuilder. ID: VB181221-1149zrp

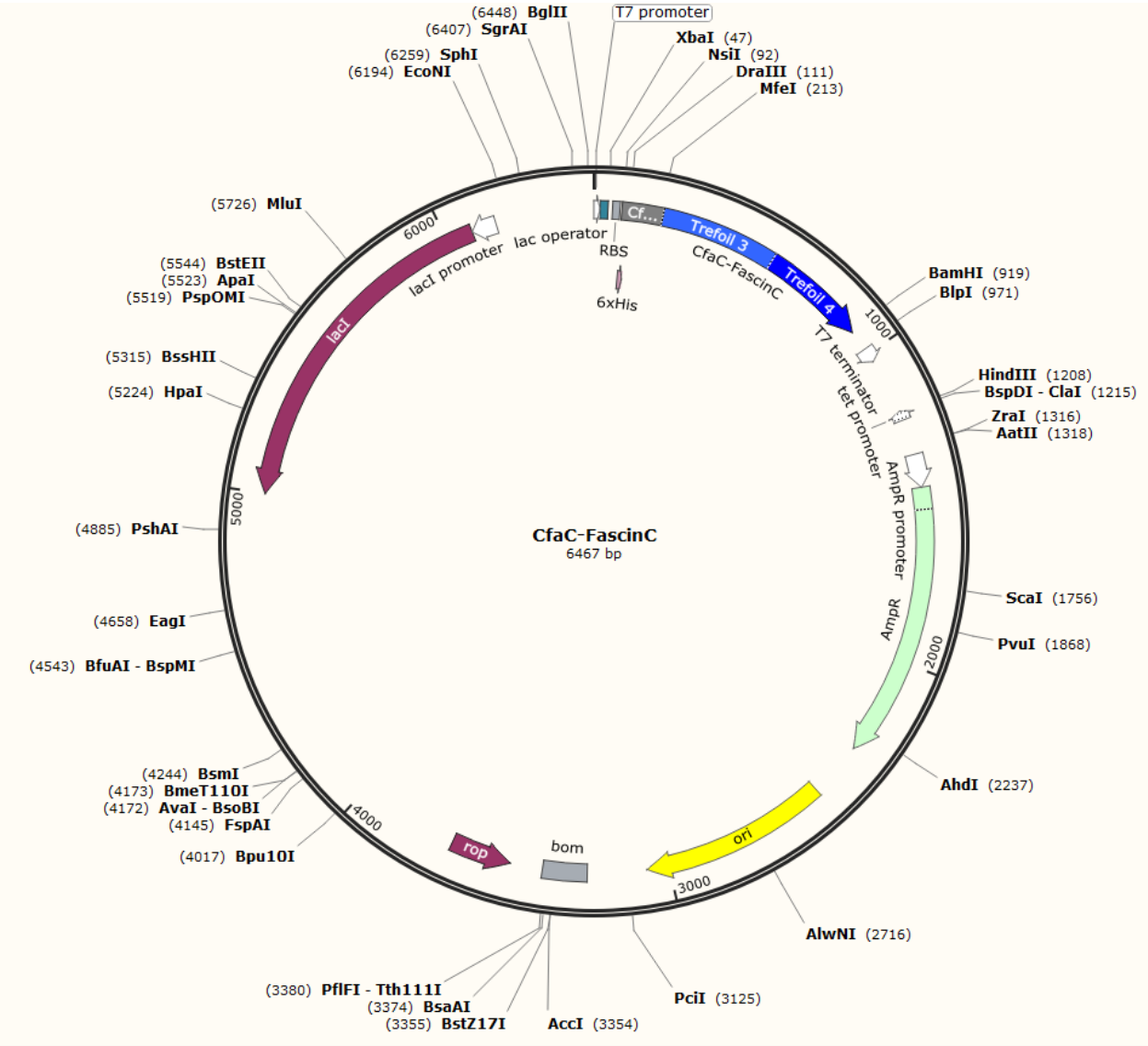

TAATACGACTCACTATAGGGGAATTGTGAGCGGATAACAATTCCCCTCTAGAAATAATTTTGTT
TAACTTTAAGAAGGAGATATACCATGCATCACCATCACCATCACATGGTGAAAATCATTAGCCG
TAAAAGCCTGGGCACCCAGAATGTTTATGATATTGGTGTTGGTGAACCGCACAACTTTCTGCTG
AAAAATGGTCTGGTTGCAAGCAATTGTCAGGTTGTTCTGCAGGCAGCAAATGAACGTAATGTTA
GCACCCGTCAAGGTATGGATCTGAGCGCAAATCAGGATGAAGAAACCGATCAAGAAACCTTTCA
GCTGGAAATTGATCGCGATACCAAAAAATGTGCATTTCGTACCCATACCGGTAAATATTGGACC
CTGACCGCAACCGGTGGTGTTCAGAGCACCGCAAGCAGCAAAAATGCAAGCTGTTATTTTGATA
TCGAATGGCGTGATCGTCGTATTACCCTGCGTGCCAGCAATGGCAAATTTGTTACCAGCAAAAA
AAACGGTCAGCTGGCAGCAAGCGTTGAAACCGCAGGCGATAGCGAACTGTTTCTGATGAAACTG
ATTAACCGTCCGATTATTGTGTTTCGTGGTGAACATGGTTTTATTGGTTGCCGTAAAGTTACCG
GTACACTGGATGCAAATCGTAGCAGCTATGATGTTTTTCAGCTTGAGTTTAACGATGGTGCCTA

CAACATTAAAGATAGCACAGGCAAATACTGGACCGTTGGTAGCGATAGCGCAGTGACCAGCAGC
GGTGATACACCGGTTGATTTTTTCTTTGAATTCTGCGACTATAACAAAGTGGCCATTAAAGTTG
GTGGTCGCTATCTGAAAGGTGATCATGCCGGTGTTCTGAAAGCAAGCGCAGAAACCGTTGATCC
GGCAAGCCTGTGGGAATATTAAGGATCCGCTGCTAACAAAGCCCGAAAGGAAGCTGAGTTGGCT
GCTGCCACCGCTGAGCAATAACTAGCATAACCCCTTGGGGCCTCTAAACGGGTCTTGAGGGGTT
TTTTGCTGAAAGGAGGAACTATATCCGGATATCCCGCAAGAGGCCCGGCAGTACCGGCATAACC
AAGCCTATGCCTACAGCATCCAGGGTGACGGTGCCGAGGATGACGATGAGCGCATTGTTAGATT
TCATACACGGTGCCTGACTGCGTTAGCAATTTAACTGTGATAAACTACCGCATTAAAGCTTATC
GATGATAAGCTGTCAAACATGAGAATTCTTGAAGACGAAAGGGCCTCGTGATACGCCTATTTTT
ATAGGTTAATGTCATGATAATAATGGTTTCTTAGACGTCAGGTGGCACTTTTCGGGGAAATGTG
CGCGGAACCCCTATTTGTTTATTTTTCTAAATACATTCAAATATGTATCCGCTCATGAGACAAT
AACCCTGATAAATGCTTCAATAATATTGAAAAAGGAAGAGTATGAGTATTCAACATTTCCGTGT
CGCCCTTATTCCCTTTTTTGCGGCATTTTGCCTTCCTGTTTTTGCTCACCCAGAAACGCTGGTG
AAAGTAAAAGATGCTGAAGATCAGTTGGGTGCACGAGTGGGTTACATCGAACTGGATCTCAACA
GCGGTAAGATCCTTGAGAGTTTTCGCCCCGAAGAACGTTTTCCAATGATGAGCACTTTTAAAGT
TCTGCTATGTGGCGCGGTATTATCCCGTGTTGACGCCGGGCAAGAGCAACTCGGTCGCCGCATA
CACTATTCTCAGAATGACTTGGTTGAGTACTCACCAGTCACAGAAAAGCATCTTACGGATGGCA
TGACAGTAAGAGAATTATGCAGTGCTGCCATAACCATGAGTGATAACACTGCGGCCAACTTACT
TCTGACAACGATCGGAGGACCGAAGGAGCTAACCGCTTTTTTGCACAACATGGGGGATCATGTA
ACTCGCCTTGATCGTTGGGAACCGGAGCTGAATGAAGCCATACCAAACGACGAGCGTGACACCA
CGATGCCTGCAGCAATGGCAACAACGTTGCGCAAACTATTAACTGGCGAACTACTTACTCTAGC
TTCCCGGCAACAATTAATAGACTGGATGGAGGCGGATAAAGTTGCAGGACCACTTCTGCGCTCG
GCCCTTCCGGCTGGCTGGTTTATTGCTGATAAATCTGGAGCCGGTGAGCGTGGGTCACGCGGTA
TCATTGCAGCACTGGGGCCAGATGGTAAGCCCTCCCGTATCGTAGTTATCTACACGACGGGGAG
TCAGGCAACTATGGATGAACGAAATAGACAGATCGCTGAGATAGGTGCCTCACTGATTAAGCAT
TGGTAACTGTCAGACCAAGTTTACTCATATATACTTTAGATTGATTTAAAACTTCATTTTTAAT
TTAAAAGGATCTAGGTGAAGATCCTTTTTGATAATCTCATGACCAAAATCCCTTAACGTGAGTT
TTCGTTCCACTGAGCGTCAGACCCCGTAGAAAAGATCAAAGGATCTTCTTGAGATCCTTTTTTT
CTGCGCGTAATCTGCTGCTTGCAAACAAAAAAACCACCGCTACCAGCGGTGGTTTGTTTGCCGG
ATCAAGAGCTACCAACTCTTTTTCCGAAGGTAACTGGCTTCAGCAGAGCGCAGATACCAAATAC
TGTCCTTCTAGTGTAGCCGTAGTTAGGCCACCACTTCAAGAACTCTGTAGCACCGCCTACATAC
CTCGCTCTGCTAATCCTGTTACCAGTGGCTGCTGCCAGTGGCGATAAGTCGTGTCTTACCGGGT
TGGACTCAAGACGATAGTTACCGGATAAGGCGCAGCGGTCGGGCTGAACGGGGGGTTCGTGCAC
ACAGCCCAGCTTGGAGCGAACGACCTACACCGAACTGAGATACCTACAGCGTGAGCTATGAGAA
AGCGCCACGCTTCCCGAAGGGAGAAAGGCGGACAGGTATCCGGTAAGCGGCAGGGTCGGAACAG
GAGAGCGCACGAGGGAGCTTCCAGGGGGAAACGCCTGGTATCTTTATAGTCCTGTCGGGTTTCG
CCACCTCTGACTTGAGCGTCGATTTTTGTGATGCTCGTCAGGGGGGCGGAGCCTATGGAAAAAC
GCCAGCAACGCGGCCTTTTTACGGTTCCTGGCCTTTTGCTGGCCTTTTGCTCACATGTTCTTTC
CTGCGTTATCCCCTGATTCTGTGGATAACCGTATTACCGCCTTTGAGTGAGCTGATACCGCTCG
CCGCAGCCGAACGACCGAGCGCAGCGAGTCAGTGAGCGAGGAAGCGGAAGGGCGCCTGATGCGG
TATTTTCTCCTTACGCATCTGTGCGGTATTTCACACCGCAATGGTGCACTCTCAGTACAATCTG
CTCTGATGCCGCATAGTTAAGCCAGTATACACTCCGCTATCGCTACGTGACTGGGTCATGGCTG
CGCCCCGACACCCGCCAACACCCGCTGACGCGCCCTGACGGGCTTGTCTGCTCCCGGCATCCGC
TTACAGACAAGCTGTGACCGTCTCCGGGAGCTGCATGTGTCAGAGGTTTTCACCGTCATCACCG
AAACGCGCGAGGCAGCTGCGGTAAAGCTCATCAGCGTGGTCGTGAAGCGATTCACAGATGTCTG
CCTGTTCATCCGCGTCCAGCTCGTTGAGTTTCTCCAGAAGCGTTAATGTCTGGCTTCTGATAAA
GCGGGCCATGTTAAGGGCGGTTTTTTCCTGTTTGGTCACTGATGCCTCCGTGTAAGGGGGATTT

CTGTTCATGGGGGTAATGATACCGATGAAACGAGAGAGGATGCTCACGATACGGGTTACTGATG
ATGAACATGCCCGGTTACTGGAACGTTGTGAGGGTAAACAACTGGCGGTATGGATGCGGCGGGA
CCAGAGAAAAATCACTCAGGGTCAATGCCAGCGCTTCGTTAATACAGATGTAGGTGTTCCACAG
GGTAGCCAGCAGCATCCTGCGATGCAGATCCGGAACATAATGGTGCAGGGCGCTGACTTCCGCG
TTTCCAGACTTTACGAAACACGGAAACCGAAGACCATTCATGTTGTTGCTCAGGTCGCAGACGT
TTTGCAGCAGCAGTCGCTTCACGTTCGCTCGCGTATCGGTGATTCATTCTGCTAACCAGTAAGG
CAACCCCGCCAGCCTAGCCGGGTCCTCAACGACAGGAGCACGATCATGCGCACCCGTGGCCAGG
ACCCAACGCTGCCCGAGATGCGCCGCGTGCGGCTGCTGGAGATGGCGGACGCGATGGATATGTT
CTGCCAAGGGTTGGTTTGCGCATTCACAGTTCTCCGCAAGAATTGATTGGCTCCAATTCTTGGA
GTGGTGAATCCGTTAGCGAGGTGCCGCCGGCTTCCATTCAGGTCGAGGTGGCCCGGCTCCATGC
ACCGCGACGCAACGCGGGGAGGCAGACAAGGTATAGGGCGGCGCCTACAATCCATGCCAACCCG
TTCCATGTGCTCGCCGAGGCGGCATAAATCGCCGTGACGATCAGCGGTCCAATGATCGAAGTTA
GGCTGGTAAGAGCCGCGAGCGATCCTTGAAGCTGTCCCTGATGGTCGTCATCTACCTGCCTGGA
CAGCATGGCCTGCAACGCGGGCATCCCGATGCCGCCGGAAGCGAGAAGAATCATAATGGGGAAG
GCCATCCAGCCTCGCGTCGCGAACGCCAGCAAGACGTAGCCCAGCGCGTCGGCCGCCATGCCGG
CGATAATGGCCTGCTTCTCGCCGAAACGTTTGGTGGCGGGACCAGTGACGAAGGCTTGAGCGAG
GGCGTGCAAGATTCCGAATACCGCAAGCGACAGGCCGATCATCGTCGCGCTCCAGCGAAAGCGG
TCCTCGCCGAAAATGACCCAGAGCGCTGCCGGCACCTGTCCTACGAGTTGCATGATAAAGAAGA
CAGTCATAAGTGCGGCGACGATAGTCATGCCCCGCGCCCACCGGAAGGAGCTGACTGGGTTGAA
GGCTCTCAAGGGCATCGGTCGAGATCCCGGTGCCTAATGAGTGAGCTAACTTACATTAATTGCG
TTGCGCTCACTGCCCGCTTTCCAGTCGGGAAACCTGTCGTGCCAGCTGCATTAATGAATCGGCC
AACGCGCGGGGAGAGGCGGTTTGCGTATTGGGCGCCAGGGTGGTTTTTCTTTTCACCAGTGAGA
CGGGCAACAGCTGATTGCCCTTCACCGCCTGGCCCTGAGAGAGTTGCAGCAAGCGGTCCACGCT
GGTTTGCCCCAGCAGGCGAAAATCCTGTTTGATGGTGGTTAACGGCGGGATATAACATGAGCTG
TCTTCGGTATCGTCGTATCCCACTACCGAGATATCCGCACCAACGCGCAGCCCGGACTCGGTAA
TGGCGCGCATTGCGCCCAGCGCCATCTGATCGTTGGCAACCAGCATCGCAGTGGGAACGATGCC
CTCATTCAGCATTTGCATGGTTTGTTGAAAACCGGACATGGCACTCCAGTCGCCTTCCCGTTCC
GCTATCGGCTGAATTTGATTGCGAGTGAGATATTTATGCCAGCCAGCCAGACGCAGACGCGCCG
AGACAGAACTTAATGGGCCCGCTAACAGCGCGATTTGCTGGTGACCCAATGCGACCAGATGCTC
CACGCCCAGTCGCGTACCGTCTTCATGGGAGAAAATAATACTGTTGATGGGTGTCTGGTCAGAG
ACATCAAGAAATAACGCCGGAACATTAGTGCAGGCAGCTTCCACAGCAATGGCATCCTGGTCAT
CCAGCGGATAGTTAATGATCAGCCCACTGACGCGTTGCGCGAGAAGATTGTGCACCGCCGCTTT
ACAGGCTTCGACGCCGCTTCGTTCTACCATCGACACCACCACGCTGGCACCCAGTTGATCGGCG
CGAGATTTAATCGCCGCGACAATTTGCGACGGCGCGTGCAGGGCCAGACTGGAGGTGGCAACGC
CAATCAGCAACGACTGTTTGCCCGCCAGTTGTTGTGCCACGCGGTTGGGAATGTAATTCAGCTC
CGCCATCGCCGCTTCCACTTTTTCCCGCGTTTTCGCAGAAACGTGGCTGGCCTGGTTCACCACG
CGGGAAACGGTCTGATAAGAGACACCGGCATACTCTGCGACATCGTATAACGTTACTGGTTTCA
CATTCACCACCCTGAATTGACTCTCTTCCGGGCGCTATCATGCCATACCGCGAAAGGTTTTGCG
CCATTCGATGGTGTCCGGGATCTCGACGCTCTCCCTTATGCGACTCCTGCATTAGGAAGCAGCC
CAGTAGTAGGTTGAGGCCGTTGAGCACCGCCGCCGCAAGGAATGGTGCATGCAAGGAGATGGCG
CCCAACAGTCCCCCGGCCACGGGGCCTGCCACCATACCCACGCCGAAACAAGCGCTCATGAGCC
CGAAGTGGCGAGCCCGATCTTCCCCATCGGTGATGTCGGCGATATAGGCGCCAGCAACCGCACC
TGTGGCGCCGGTGATGCCGGCCACGATGCGTCCGGCGTAGAGGATCGAGATCTCGATCCCGCGA
AAT

Appendix B: Tandem mass tag pulldowns of Fascin1 in human brain cortex lysate

ProteinID	Gene	Cluster	pvalue GST vs GST-Fascin1	GST			GST-Fascin1+BTA-EG4			GST-Fascin1+BTA-EG4			GST-Fascin1		
				Trial 1	Trial 2	Trial 3	Trial 1	Trial 2	Trial 3	Trial 1	Trial 2	Trial 3	Trial 1	Trial 2	Trial 3
A0A087WT59	TTR	1	0.01630	67.644	67.748	57.512	93.227	88.554	99.931	111.635	88.268	78.867	88.199	76.990	88.390
A0A0G2JIW1	HSPA1B	1	0.00445	57.477	63.816	63.008	100.091	89.730	101.812	100.526	92.833	84.553	79.418	85.791	92.321
C9JLB7	OXNAD1	1	0.02466	50.136	13.646	22.314	105.451	91.521	112.812	144.092	131.074	118.629	61.095	93.433	89.944
K7EM38	ACTG1	1	0.01070	44.930	35.593	42.520	108.072	93.517	111.902	128.583	112.319	106.451	64.664	81.718	92.383
P06396	GSN	1	0.02348	27.964	47.877	42.964	108.247	84.214	114.708	133.791	105.372	113.840	67.822	66.451	90.944
P06576	ATP5F1B	1	0.04969	76.931	50.635	52.958	99.502	92.767	102.793	105.750	94.532	90.983	77.928	89.475	92.307
P48643	CCT5	1	0.00799	58.260	46.887	47.247	98.810	96.381	106.093	96.028	100.928	91.948	75.715	93.387	98.303
P60709	ACTB	1	0.00508	40.961	34.342	37.539	107.033	94.181	112.557	130.176	111.812	106.362	66.394	83.072	91.738
P61158	ACTR3	1	0.02893	34.747	47.475	43.046	99.531	89.081	104.337	122.735	99.847	111.944	71.968	66.930	101.936
P68032	ACTC1	1	0.00484	38.481	34.944	40.757	104.910	95.460	112.544	129.626	108.974	105.500	67.134	82.340	92.400
Q16643	DBN1	1	0.00938	37.764	19.776	23.084	120.271	92.092	117.946	149.358	121.909	108.472	61.480	74.382	92.186
Q16658	FSCN1	1	0.00714	34.831	11.322	14.504	112.997	106.610	116.847	121.090	114.657	101.106	65.968	95.375	102.289
Q5T9B7	AK1	1	0.02418	53.552	71.738	66.374	86.201	87.849	97.843	107.912	87.121	89.166	85.228	80.432	89.301
Q9BPX5	ARPC5L	1	0.01326	47.770	52.692	NA	NA	NA	87.162	111.224	NA	NA	NA	91.063	100.441
Q9BWD1	ACAT2	1	0.02703	29.396	48.117	56.681	93.893	89.858	95.165	92.398	119.742	97.372	69.661	100.866	105.885
Q9H3H3	C11orf68	1	0.00508	40.323	37.502	NA	NA	NA	106.205	122.307	NA	NA	NA	88.144	95.141
A0A2R8Y7X9	-	2	0.00360	30.408	61.744	65.479	68.334	65.533	64.482	66.056	54.709	62.957	124.245	122.599	118.001
E9PFW3	AP2M1	2	0.03396	49.238	79.257	76.698	96.869	71.009	69.039	63.283	65.887	82.285	95.022	120.342	104.875
P02042	HBD	2	0.00076	55.609	59.724	70.360	60.464	66.654	68.724	70.889	58.113	64.679	123.934	123.121	110.447
P07954	FH	2	0.01135	67.734	79.747	80.592	73.958	82.537	76.271	86.516	82.949	79.545	94.147	94.279	99.206
P63010	AP2B1	2	0.00915	64.191	74.836	74.010	86.414	89.146	74.298	74.218	75.360	78.271	90.776	99.188	107.752
P68871	HBB	2	0.00318	40.495	62.556	68.378	61.820	69.945	67.453	70.605	59.237	64.324	122.234	126.560	109.891
P69905	HBA1	2	0.01948	39.955	84.888	70.412	51.787	60.898	61.153	58.536	45.676	68.049	132.861	120.055	110.033
Q13424	SNTA1	2	0.02482	61.420	69.817	NA	NA	NA	66.804	92.789	NA	NA	NA	109.585	100.181
A0A087WZN1	IDH3B	3	0.00272	42.913	28.811	51.076	95.960	92.327	92.964	82.577	81.226	71.323	92.552	108.415	118.191
H3BRN4	ABAT	3	0.00192	61.951	41.408	48.385	83.458	85.630	69.950	69.270	76.017	70.513	103.605	126.696	118.874
O00410	IPO5	3	0.00050	38.142	28.615	31.704	86.967	88.461	70.005	54.798	69.305	69.853	107.953	130.720	135.382
O43707	ACTN4	3	0.00601	45.782	59.414	70.431	77.436	88.455	86.996	87.926	82.006	78.208	93.730	102.051	103.356
O60641	SNAP91	3	0.01604	80.128	69.367	72.613	97.937	88.038	84.119	83.492	79.685	75.186	86.575	99.018	98.291
O94973	AP2A2	3	0.01105	38.798	61.234	63.729	94.951	87.355	78.239	76.123	84.427	76.346	88.567	112.750	108.966
O95373	IPO7	3	0.00825	44.233	41.293	41.911	91.812	103.211	83.455	90.079	77.624	72.730	92.684	106.542	113.042
O95782	AP2A1	3	0.00890	53.700	65.376	66.841	90.647	91.012	83.858	76.304	90.249	75.938	86.185	107.820	103.650
P12814	ACTN1	3	0.00582	53.541	64.101	70.084	80.829	89.589	79.465	78.599	81.047	75.009	93.504	113.727	102.673
P20340	RAB6A	3	0.01323	76.933	65.866	63.259	82.483	88.562	83.180	85.716	94.396	82.834	87.548	105.024	97.038
P27361	MAPK3	3	0.00719	64.425	32.179	43.929	84.713	97.446	84.173	85.416	91.839	68.170	94.863	121.997	109.683
P28482	MAPK1	3	0.00563	56.143	31.484	49.675	91.299	96.961	86.369	83.765	87.899	68.937	91.668	121.930	110.867
P49327	FASN	3	0.00502	60.832	36.604	50.581	92.904	91.497	79.151	66.797	79.975	68.190	96.045	126.539	117.947
P49441	INPP1	3	0.00497	66.355	54.072	44.336	79.248	103.281	74.800	87.034	104.574	64.062	92.002	103.046	110.827
P49589	CARS	3	0.00540	65.026	45.963	44.750	90.771	91.790	79.335	84.416	84.810	78.599	92.596	117.847	106.840

ProteinID	Gene	Cluster	pvalue GST vs GST-Fascin1	GST			GST-Fascin1+BTA-EG4			GST-Fascin1+BTA-EG4			GST-Fascin1		
				Trial 1	Trial 2	Trial 3	Trial 1	Trial 2	Trial 3	Trial 1	Trial 2	Trial 3	Trial 1	Trial 2	Trial 3
P52306	RAP1GDS1	3	0.00087	60.532	49.450	49.106	87.696	88.912	76.201	72.219	77.257	70.985	99.560	114.129	115.627
P53004	BLVRA	3	0.00235	53.608	42.567	50.753	90.016	89.428	83.760	87.632	87.886	84.391	88.920	111.111	109.706
P54750	PDE1A	3	0.00147	52.621	46.278	57.490	84.908	97.457	78.290	79.025	70.355	66.060	98.962	122.208	109.527
P60891	PRPS1	3	0.00512	27.194	37.437	48.498	97.930	97.057	66.631	87.579	75.192	84.083	87.127	114.676	124.564
P63167	DYNLL1	3	0.00308	28.657	29.317	NA	NA	NA	97.479	76.047	NA	NA	NA	122.913	113.036
Q08257	CRYZ	3	0.02757	79.038	45.622	56.084	87.364	97.162	74.733	84.009	85.402	80.815	87.460	108.719	112.838
Q10567	AP1B1	3	0.02987	66.849	67.099	68.135	87.738	90.752	73.678	73.890	76.879	77.661	90.879	100.822	111.726
Q13618	CUL3	3	0.02069	66.976	39.847	38.001	87.186	106.360	80.398	67.284	100.027	87.152	81.092	116.115	119.656
Q14232	EIF2B1	3	0.02522	64.765	30.891	64.618	81.934	69.564	75.371	93.247	106.039	80.658	92.803	133.034	105.573
Q3LXA3	TKFC	3	0.00723	31.118	52.962	53.513	99.831	89.779	67.870	68.472	77.468	72.641	92.048	108.654	127.280
Q86VP6	CAND1	3	0.00150	37.250	26.931	38.947	94.659	90.075	67.044	67.201	73.146	72.659	99.559	128.063	133.054
Q9NRW1	RAB6B	3	0.02810	78.199	61.333	66.739	86.200	88.594	83.916	89.693	94.075	82.483	85.239	107.552	95.720
Q9UBB4	ATXN10	3	0.01800	78.042	53.937	39.170	96.292	88.595	60.051	88.471	80.661	77.735	94.907	115.230	110.735
Q9UI12	ATP6V1H	3	0.03184	82.614	37.396	39.309	95.548	94.398	77.695	77.415	82.384	79.409	91.387	116.381	115.043
A0A1W2PNV4	-	4	0.22602	52.216	59.126	74.132	97.366	84.908	108.361	112.928	97.937	112.943	66.357	70.999	93.245
A0A087WY85	UBE2D3	4	0.03830	40.426	55.978	NA	NA	NA	85.352	102.734	NA	NA	NA	110.341	94.879
A0A087X0R6	SNX12	4	0.00005	46.590	53.716	45.482	78.642	78.214	89.390	96.459	107.503	69.768	99.655	98.619	102.552
A0A2R8Y891	PFKM	4	0.03904	42.546	41.012	46.825	103.747	87.538	87.733	83.638	97.966	91.965	78.578	98.211	118.757
B1APG0	PRKACB	4	0.01623	65.764	53.605	53.773	102.382	97.027	90.282	83.907	94.330	80.700	78.869	107.283	101.580
B1APG3	PRKACB	4	0.01637	66.369	51.762	53.773	102.382	97.027	94.022	86.083	94.330	80.700	78.869	106.385	99.741
E7EUC7	UGP2	4	0.04999	78.865	51.414	53.500	97.510	101.465	95.912	89.027	90.782	82.043	79.691	106.426	95.548
H0Y858	-	4	0.00684	48.077	33.063	57.846	105.020	95.316	95.444	105.286	89.224	68.601	83.990	98.886	106.424
M0QYZ2	AP2S1	4	0.00140	27.835	40.077	42.191	106.349	86.435	80.897	105.579	82.759	83.160	87.832	103.709	110.766
O00154	ACOT7	4	0.01332	56.968	69.412	58.723	94.313	92.740	91.278	87.747	85.207	83.915	84.511	85.692	102.015
O75663	TIPRL	4	0.01914	39.142	56.391	58.645	95.932	97.665	92.125	103.150	103.891	78.597	77.702	108.608	91.545
O94811	TPPP	4	0.00144	54.467	57.055	41.891	98.652	88.498	97.772	99.514	87.347	84.114	88.388	91.759	96.559
P00367	GLUD1	4	0.00910	56.132	54.542	54.115	94.894	87.109	93.660	91.163	85.356	82.553	88.515	102.775	98.880
P01034	CST3	4	0.00108	26.853	39.091	45.507	97.357	86.618	98.863	101.435	84.517	85.825	89.000	100.992	104.640
P04350	TUBB4A	4	0.02515	43.942	46.907	46.278	103.392	92.276	88.357	90.634	94.922	85.327	80.511	104.085	107.837
P07437	TUBB	4	0.00358	41.845	40.871	48.354	100.952	91.818	90.172	95.853	94.896	86.234	80.816	104.774	107.564
P09417	QDPR	4	0.00097	52.750	49.696	54.363	84.130	93.952	92.059	96.921	88.819	81.684	89.243	106.909	97.959
P0CG29	GSTT2	4	0.01514	58.001	38.507	38.297	91.261	96.583	84.352	102.172	89.818	98.795	82.175	123.423	96.988
P11216	PYGB	4	0.01278	61.573	48.112	54.085	100.595	96.060	93.598	95.152	94.777	82.812	78.959	108.192	97.071
P11217	PYGM	4	0.01284	63.012	43.110	45.682	104.209	93.858	86.124	87.653	94.694	84.479	80.054	105.429	109.693
P16152	CBR1	4	0.00202	53.007	42.270	41.098	100.510	93.258	93.223	97.923	95.345	80.176	84.701	100.376	104.628
P17612	PRKACA	4	0.00758	60.389	49.163	47.018	101.524	97.947	91.159	82.568	88.131	80.585	82.784	111.090	103.186
P21291	CSRP1	4	0.03943	60.763	81.600	75.867	66.726	71.676	79.380	102.486	90.349	95.993	94.153	90.544	90.708
P21695	GPD1	4	0.00273	35.339	56.239	49.124	88.316	88.504	95.880	106.884	111.488	75.556	86.338	92.663	96.381
P23381	WARS	4	0.00662	66.150	63.003	59.845	101.931	94.684	89.695	89.559	89.032	76.878	81.716	96.348	98.965

ProteinID	Gene	Cluster	pvalue GST vs GST-Fascin1	GST			GST-Fascin1+BTA-EG4			GST-Fascin1+BTA-EG4			GST-Fascin1		
				Trial 1	Trial 2	Trial 3	Trial 1	Trial 2	Trial 3	Trial 1	Trial 2	Trial 3	Trial 1	Trial 2	Trial 3
P30043	BLVRB	4	0.02107	72.533	46.880	45.624	96.492	90.573	98.407	98.604	102.052	82.144	83.331	92.376	100.002
P30711	GSTT1	4	0.01165	49.852	30.568	60.701	90.559	89.222	87.877	108.089	79.111	89.247	86.939	117.178	100.974
P48506	GCLC	4	0.03242	74.067	54.462	55.697	82.963	99.757	87.421	87.065	94.739	94.740	79.546	95.064	106.356
P49773	HINT1	4	0.00216	30.324	21.298	28.782	106.849	98.234	92.422	105.759	88.769	90.272	81.262	114.268	109.351
P50213	IDH3A	4	0.00232	52.972	61.748	58.467	89.269	94.202	93.993	102.403	88.406	89.093	82.923	96.522	92.098
P61088	UBE2N	4	0.02663	72.769	37.751	40.318	104.674	90.975	90.719	104.897	92.755	87.965	81.819	102.604	101.224
P61764	STXBP1	4	0.00892	53.562	52.342	64.877	103.900	84.338	91.645	83.795	90.981	79.729	82.225	104.113	104.946
P61978	HNRNPK	4	0.00283	49.033	48.066	51.606	95.755	101.271	107.852	97.588	95.087	86.715	77.723	91.795	97.838
P68366	TUBA4A	4	0.00185	45.812	43.750	41.002	99.607	92.731	92.075	91.383	90.447	84.245	85.295	97.340	110.468
P68371	TUBB4B	4	0.00427	42.852	42.699	48.296	102.060	91.753	89.531	92.442	96.199	85.788	80.142	105.867	107.936
Q13509	TUBB3	4	0.00243	46.491	40.331	42.115	102.057	90.907	90.747	96.462	95.051	85.662	82.652	107.693	105.055
Q13885	TUBB2A	4	0.01587	66.156	40.180	46.564	102.137	91.328	88.114	93.602	96.288	86.540	80.438	105.302	106.770
Q14240	EIF4A2	4	0.01249	58.100	40.042	52.200	98.107	89.864	87.720	92.860	104.312	87.133	78.358	104.661	108.919
Q6PCE3	PGM2L1	4	0.00651	63.822	55.741	62.950	96.659	89.707	91.866	94.966	90.972	84.412	81.576	96.969	99.190
Q71U36	TUBA1A	4	0.00187	45.523	42.075	41.186	99.410	95.118	93.953	92.669	91.846	84.303	83.796	98.782	108.976
Q96FJ2	DYNLL2	4	0.00351	40.453	52.300	54.068	96.562	92.104	102.676	109.374	87.029	89.016	82.437	100.217	88.782
Q9BR01	SULT4A1	4	0.00909	45.128	34.593	56.588	99.845	92.398	96.028	92.569	91.812	84.030	80.674	111.370	105.747
Q9H201	EPN3	4	0.01936	41.969	67.776	42.688	88.227	80.907	92.345	89.487	87.316	83.056	96.383	119.631	85.626
Q9NPJ3	ACOT13	4	0.01203	62.702	45.234	54.283	87.411	96.199	86.066	93.418	97.396	89.357	80.926	98.390	109.134
Q9UN36	NDRG2	4	0.02979	73.561	36.574	41.454	97.540	88.874	90.844	92.451	97.109	77.956	88.118	124.293	96.940
Q9UQ03	CORO2B	4	0.04209	75.262	47.714	51.666	92.975	93.163	91.733	88.941	101.506	83.824	81.517	89.551	109.648
Q9Y2S2	CRYL1	4	0.00636	57.191	58.657	41.424	102.811	91.451	88.218	89.822	91.774	85.759	83.321	102.675	100.200
L7N2F9	-	#N/A	NA	NA	NA	131.066	76.348	70.112	NA	NA	62.932	113.363	77.430	NA	NA
A0A1B0GU03	-	#N/A	0.10329	83.232	287.129	238.676	28.587	35.166	54.294	34.657	30.350	69.788	111.901	39.852	41.222
H7BYZ3	-	#N/A	0.06621	151.007	308.516	162.840	38.408	44.919	29.757	33.719	47.250	74.687	116.820	42.918	32.264
A0A024R6I7	SERPINA1	#N/A	0.06367	101.463	193.833	158.552	46.575	57.062	66.057	69.450	54.317	85.762	102.349	59.702	59.110
A0A087WV75	NCAM1	#N/A	0.04994	106.936	217.600	168.446	65.391	51.445	58.535	72.450	66.788	74.890	94.400	60.057	46.650
A0A087WVQ6	CLTC	#N/A	0.10533	63.226	85.979	93.876	84.618	73.829	63.801	60.417	59.564	79.712	97.389	98.390	115.057
A0A087WZQ7	NAPB	#N/A	0.04638	87.117	87.560	100.212	93.404	90.138	107.832	92.438	90.006	81.064	74.166	70.917	82.579
A0A0A0MRA8	EPB41L3	#N/A	0.43576	81.374	84.147	60.539	95.889	93.079	93.270	88.815	99.319	95.476	73.827	88.110	86.791
A0A0A0MSS8	AKR1C3	#N/A	0.32667	190.827	91.232	92.021	86.493	91.105	83.609	85.317	96.375	75.792	79.003	111.612	62.649
A0A0A0MT26	ATP1A3	#N/A	0.00246	180.833	198.623	152.521	63.182	71.376	61.720	63.217	62.809	96.847	83.338	61.202	50.408
A0A0A0MT64	FDXR	#N/A	NA	NA	NA	64.536	94.701	82.273	NA	NA	112.586	135.619	57.224	NA	NA
A0A0A0MTN0	CUL2	#N/A	0.47802	136.078	48.123	50.929	89.821	90.999	65.113	88.206	70.944	79.272	95.930	105.839	108.422
A0A0A6YYG9	ARPC4- TTLL3	#N/A	0.22978	85.808	128.636	75.187	109.216	70.872	89.091	89.964	110.581	117.048	61.343	88.009	61.264
A0A0D9SF54	SPTAN1	#N/A	0.03976	93.122	123.251	108.862	79.654	73.243	87.049	68.172	76.794	93.466	84.338	74.999	83.138
A0A0D9SGF6	SPTAN1	#N/A	0.04503	92.595	124.126	108.863	79.310	73.058	87.137	67.621	76.501	93.373	84.700	74.662	83.101
A0A1B0GW77	ALDH7A1	#N/A	0.05322	119.860	279.517	235.990	19.432	30.604	48.286	37.879	40.567	75.317	112.927	55.190	34.505

ProteinID	Gene	Cluster	pvalue GST vs GST-Fascin1	GST			GST-Fascin1+BTA-EG4			GST-Fascin1+BTA-EG4			GST-Fascin1		
				Trial 1	Trial 2	Trial 3	Trial 1	Trial 2	Trial 3	Trial 1	Trial 2	Trial 3	Trial 1	Trial 2	Trial 3
A0A1C7CYX9	DPYSL2	#N/A	0.03265	133.837	265.167	210.758	33.329	42.010	46.890	43.438	42.848	82.939	105.107	47.669	43.059
A0A1W2PR46	GFAP	#N/A	0.09584	90.750	268.086	206.166	32.125	45.398	50.125	47.548	42.109	76.862	108.124	51.225	41.254
A0A2R8Y4H2	SEPTIN3	#N/A	0.32932	84.489	65.651	NA	NA	NA	97.624	77.975	NA	NA	NA	82.607	103.627
A0A2R8Y5Q8	TBCE	#N/A	0.16055	77.153	66.652	NA	NA	NA	75.294	104.956	NA	NA	NA	110.708	87.917
A0A2R8Y5V9	TPM4	#N/A	0.60538	76.016	113.976	82.088	57.748	68.185	109.120	87.666	70.235	104.207	101.059	79.041	65.690
A0A2R8Y6X2	DTD1	#N/A	0.20824	329.228	98.065	129.936	102.831	78.422	90.475	103.242	123.045	95.653	50.256	51.769	57.569
A0A2R8YDT1	GLUL	#N/A	0.03642	110.239	145.112	134.255	61.224	60.557	50.659	57.389	58.403	79.958	102.309	95.492	83.803
A0A2U3TZH3	EEF1A2	#N/A	0.09345	79.500	58.297	59.349	96.009	90.462	100.220	111.684	100.720	93.393	75.642	85.084	88.000
A0A2U3TZU2	GPI	#N/A	0.14339	75.001	310.365	197.130	29.858	44.233	43.287	28.109	41.550	82.079	110.152	44.839	35.630
A0A3B3ITF1	DLG2	#N/A	0.66944	137.117	76.514	NA	NA	NA	67.843	107.267	NA	NA	NA	99.802	82.630
A0A3B3ITK7	PGM1	#N/A	NA	NA	NA	199.096	32.958	85.485	NA	NA	52.225	79.089	87.887	NA	NA
A2A274	ACO2	#N/A	0.10851	87.254	214.866	157.359	51.207	60.878	62.152	58.011	62.707	78.242	99.338	60.857	56.136
A2A288	ZC3H12D	#N/A	0.01589	159.576	143.884	NA	NA	NA	74.871	69.685	NA	NA	NA	78.745	65.937
A6NCE7	MAP1LC3B2	#N/A	0.13571	204.705	120.831	96.037	93.705	85.393	90.845	95.228	107.143	106.005	61.455	59.674	60.788
A6PVN8	PTPA	#N/A	0.40492	143.512	78.042	106.511	81.973	93.232	52.790	83.711	109.587	89.004	66.252	95.503	104.410
B1AK88	CAPZB	#N/A	0.89051	26.119	96.658	85.427	92.681	72.722	107.911	115.523	88.350	90.522	82.888	53.563	82.278
D6RBW1	EIF4E	#N/A	0.17197	63.662	82.892	78.056	76.030	92.271	79.878	105.620	90.174	79.591	87.295	105.562	79.662
D6RER5	SEPTIN11	#N/A	0.81316	129.446	76.782	61.869	96.099	98.644	93.586	75.494	95.123	93.633	73.060	86.570	92.352
D6RGZ6	VCAN	#N/A	0.05108	103.329	212.235	156.310	64.744	57.503	65.713	66.490	66.350	92.590	88.289	53.142	52.998
E7EPK1	SEPTIN7	#N/A	0.31896	189.855	83.526	100.614	91.731	90.528	78.602	85.963	84.615	83.997	75.174	84.630	84.219
E7EQR4	EZR	#N/A	0.13204	182.522	100.711	102.747	91.509	79.607	95.700	110.209	106.295	116.755	58.970	66.940	61.321
E7ESC6	XPO7	#N/A	0.57636	308.322	75.255	51.355	94.741	95.582	73.070	58.481	78.493	74.680	91.095	96.702	84.456
E7EWW9	GSTM1	#N/A	0.19056	340.829	103.409	162.551	88.011	83.921	80.727	76.609	100.598	89.975	54.852	76.350	59.659
E9PGC8	MAP1A	#N/A	0.30793	163.826	71.226	54.552	104.948	92.163	112.966	166.666	132.920	121.183	50.474	50.838	50.036
E9PK25	CFL1	#N/A	0.85479	56.380	103.080	90.614	88.610	79.505	90.119	103.083	80.463	86.657	84.385	79.180	77.768
E9PL57	NEDD8-MDP1	#N/A	0.13456	40.445	73.159	NA	NA	NA	67.242	87.894	NA	NA	NA	124.336	95.615
E9PNQ8	THY1	#N/A	0.55134	173.556	24.861	142.166	88.274	76.557	126.612	102.327	72.793	79.088	77.198	78.775	88.151
F5GYQ1	ATP6V0D1	#N/A	0.27843	45.703	81.098	NA	NA	NA	96.913	92.672	NA	NA	NA	94.581	85.926
F8W0W8	PPP1CC	#N/A	0.00468	146.798	148.565	NA	NA	NA	72.764	90.894	NA	NA	NA	55.393	67.126
F8W1S1	KRT74	#N/A	0.30164	253.067	89.007	41.812	50.935	288.299	104.418	153.031	86.476	55.734	32.894	42.179	43.903
F8WB74	SELENOW	#N/A	0.67152	59.299	42.106	140.622	85.963	91.089	88.041	88.111	82.160	76.395	70.245	109.804	107.139
F8WF69	CLTA	#N/A	0.85793	143.550	69.209	63.108	101.780	77.649	73.739	75.458	72.398	82.173	91.671	101.010	98.981
G8JLD5	DNM1L	#N/A	0.10762	93.900	58.440	54.701	92.536	98.415	78.225	79.429	87.365	79.686	84.904	111.932	101.784
H0Y300	HP	#N/A	0.13300	72.020	353.736	214.591	30.758	45.799	36.983	29.182	42.268	77.398	105.933	29.660	21.018
H0Y8X4	DNPH1	#N/A	0.97306	43.148	124.101	105.455	82.523	74.517	72.975	86.609	60.157	70.663	98.279	93.644	78.062
H0YB09	DGLUCY	#N/A	0.43349	572.085	105.924	NA	NA	NA	68.718	69.898	NA	NA	NA	53.659	49.004
H3BR70	PKM	#N/A	0.06672	113.568	302.857	217.085	27.109	37.782	44.716	41.844	41.023	76.380	111.143	38.841	29.896
H7BY58	PCMT1	#N/A	0.15146	91.119	61.848	54.360	93.308	94.475	84.010	93.519	90.409	92.044	80.354	106.065	92.335

ProteinID	Gene	Cluster	pvalue GST vs GST-Fascin1	GST			GST-Fascin1+BTA-EG4			GST-Fascin1+BTA-EG4			GST-Fascin1		
				Trial 1	Trial 2	Trial 3	Trial 1	Trial 2	Trial 3	Trial 1	Trial 2	Trial 3	Trial 1	Trial 2	Trial 3
O95166	GABARAP	#N/A	0.27082	342.856	114.094	NA	NA	NA	96.751	90.895	NA	NA	NA	69.750	39.472
O95433	AHSA1	#N/A	0.77652	129.596	59.481	NA	NA	NA	102.106	112.139	NA	NA	NA	88.988	77.026
P00338	LDHA	#N/A	0.30808	88.711	126.488	118.046	64.873	73.858	57.426	62.058	67.722	77.513	97.324	105.131	86.460
P00352	ALDH1A1	#N/A	0.11177	76.802	368.849	245.827	14.399	42.889	15.765	39.575	21.669	101.355	102.554	29.947	17.970
P00441	SOD1	#N/A	0.91624	33.454	203.577	64.238	13.924	31.710	59.188	48.125	26.848	93.937	159.139	112.691	49.981
P00492	HPRT1	#N/A	0.13723	68.785	317.409	198.237	37.918	46.115	50.610	44.012	45.342	87.560	102.102	37.165	23.552
P00505	GOT2	#N/A	0.12482	89.466	371.657	206.089	36.208	34.571	24.101	20.624	43.310	75.139	111.467	33.049	18.116
P00558	PGK1	#N/A	0.10869	86.284	251.633	191.509	39.994	49.530	52.533	51.489	40.032	76.821	107.707	53.628	47.011
P00915	CA1	#N/A	0.13864	78.667	361.436	208.935	24.422	31.049	33.612	24.656	39.757	79.942	116.457	28.882	20.253
P00918	CA2	#N/A	0.07146	101.887	256.190	213.469	30.160	55.841	45.582	47.621	37.445	70.766	106.383	55.523	47.243
P00966	ASS1	#N/A	0.05381	84.208	45.685	28.856	101.569	89.974	86.801	80.209	91.004	84.550	88.716	118.736	101.789
P01009	SERPINA1	#N/A	0.07185	97.637	191.618	158.007	47.191	57.553	66.193	69.418	55.539	85.428	101.756	61.541	59.936
P01023	A2M	#N/A	0.09939	86.770	295.898	222.270	28.566	38.346	38.085	39.663	38.082	86.979	105.485	43.656	40.252
P01024	C3	#N/A	NA	NA	NA	50.112	112.924	86.313	NA	NA	122.708	73.941	73.512	NA	NA
P01111	NRAS	#N/A	0.01771	128.518	149.503	NA	NA	NA	87.316	86.865	NA	NA	NA	57.271	61.721
P01834	IGKC	#N/A	NA	NA	NA	124.777	80.207	53.463	NA	NA	69.504	68.427	101.008	NA	NA
P02511	CRYAB	#N/A	0.07667	71.011	63.284	45.643	96.931	93.408	87.102	82.173	95.539	111.928	71.882	90.609	106.594
P02533	KRT14	#N/A	0.19882	201.622	109.943	46.025	47.942	294.163	89.073	193.907	64.417	57.909	36.804	35.478	29.096
P02538	KRT6A	#N/A	0.15268	192.500	112.027	64.580	44.006	311.595	95.905	158.891	56.262	45.744	33.351	46.815	37.742
P02686	MBP	#N/A	0.92789	102.514	64.634	57.712	89.003	73.753	78.667	144.268	105.771	149.988	61.654	79.708	79.125
P02768	ALB	#N/A	0.04839	126.291	314.059	234.811	26.562	37.352	41.583	34.964	39.273	78.183	106.509	36.330	28.215
P02787	TF	#N/A	NA	NA	NA	251.957	23.234	45.798	NA	NA	39.540	75.040	100.679	NA	NA
P02792	FTL	#N/A	0.14677	69.453	360.003	229.302	14.626	27.209	35.058	18.388	30.457	81.147	119.259	37.105	20.533
P02794	FTH1	#N/A	0.19613	67.039	337.829	180.754	15.417	28.262	44.819	28.468	29.411	90.755	128.292	39.813	21.739
P04075	ALDOA	#N/A	0.08382	105.100	319.772	223.579	23.735	34.789	36.960	36.724	33.732	73.538	115.659	36.379	29.413
P04179	SOD2	#N/A	0.13970	77.550	332.011	213.995	17.478	25.092	37.427	37.875	33.314	77.560	123.725	30.341	28.109
P04259	KRT6B	#N/A	0.13143	198.328	113.774	75.932	46.549	288.178	96.352	160.542	53.421	47.857	39.486	43.818	36.332
P04264	KRT1	#N/A	0.04025	171.584	108.656	83.746	78.033	175.269	89.858	182.898	98.485	78.984	45.948	46.823	33.402
P04406	GAPDH	#N/A	0.12518	79.980	351.890	229.067	19.718	29.761	33.305	27.289	32.130	76.579	117.349	32.455	22.720
P05091	ALDH2	#N/A	0.06744	109.964	273.221	172.316	51.431	57.002	54.096	43.660	63.549	83.643	94.332	40.851	40.743
P05413	FABP3	#N/A	NA	NA	NA	314.584	17.128	32.105	NA	NA	30.731	69.068	97.330	NA	NA
P06733	ENO1	#N/A	0.10986	87.465	340.547	235.407	16.733	30.540	35.352	28.828	29.221	75.826	117.791	33.781	25.818
P06753	TPM3	#N/A	0.23184	102.499	123.926	82.088	57.748	68.185	107.385	82.526	70.235	104.207	101.059	75.089	61.896
P07195	LDHB	#N/A	0.15603	71.852	259.616	194.332	34.297	48.304	44.176	41.423	40.531	76.872	109.707	63.379	49.270
P07197	NEFM	#N/A	0.06814	98.889	237.537	164.804	53.273	53.807	59.523	48.610	67.333	105.677	86.787	52.427	51.859
P07737	PFN1	#N/A	0.46813	34.388	225.155	133.022	22.853	34.513	65.345	62.019	40.071	94.061	130.705	67.044	49.924
P07814	EPRS	#N/A	0.26634	83.785	49.661	NA	NA	NA	91.258	98.683	NA	NA	NA	119.790	86.475
P07900	HSP90AA1	#N/A	0.10746	87.835	112.967	90.097	83.787	81.538	89.830	89.065	82.678	86.028	85.217	74.836	77.413

ProteinID	Gene	Cluster	pvalue GST vs GST-Fascin1	GST			GST-Fascin1+BTA-EG4			GST-Fascin1+BTA-EG4			GST-Fascin1		
				Trial 1	Trial 2	Trial 3	Trial 1	Trial 2	Trial 3	Trial 1	Trial 2	Trial 3	Trial 1	Trial 2	Trial 3
P08238	HSP90AB1	#N/A	0.37153	90.586	91.477	76.890	90.024	86.503	95.920	89.923	89.311	87.914	81.076	80.389	83.045
P08670	VIM	#N/A	0.06632	117.659	253.627	183.174	41.258	42.977	49.728	50.565	32.784	74.092	115.847	55.475	42.668
P08758	ANXA5	#N/A	0.10289	80.728	252.937	202.828	31.198	46.339	62.496	54.456	54.043	85.915	101.405	48.648	42.216
P08779	KRT16	#N/A	0.18620	195.981	114.309	43.353	42.164	325.393	90.246	197.031	53.866	49.815	33.069	32.203	26.618
P09104	ENO2	#N/A	0.12790	79.268	342.169	224.598	17.445	30.371	38.292	27.697	32.147	78.911	118.326	33.197	25.155
P09211	GSTP1	#N/A	0.21428	375.561	108.135	136.883	91.776	78.642	91.478	90.765	96.915	110.306	55.570	64.366	44.567
P09382	LGALS1	#N/A	0.67189	48.204	171.862	106.756	30.837	42.307	73.504	76.299	43.191	90.114	131.721	74.475	63.868
P09471	GNAO1	#N/A	0.83388	53.006	82.155	101.407	107.600	91.944	92.209	93.385	88.244	86.643	65.300	97.505	85.117
P09497	CLTB	#N/A	0.13812	35.887	69.285	NA	NA	NA	91.959	81.365	NA	NA	NA	118.259	90.815
P09543	CNP	#N/A	0.13301	106.323	81.606	91.420	104.326	100.653	97.213	95.760	90.524	94.658	61.607	77.483	84.510
P09622	DLD	#N/A	NA	NA	NA	105.947	83.261	83.320	NA	NA	89.187	81.002	80.190	NA	NA
P09936	UCHL1	#N/A	0.53242	79.935	82.856	88.655	92.589	83.844	90.059	93.576	81.010	83.844	82.294	89.846	86.195
P09960	LTA4H	#N/A	0.00608	147.213	133.372	134.531	63.148	79.447	82.988	87.179	58.178	70.935	96.878	77.107	60.788
P09972	ALDOC	#N/A	0.08308	100.076	333.759	234.653	26.167	35.317	36.937	34.235	38.412	75.223	109.106	31.033	25.828
P10114	RAP2A	#N/A	0.07155	41.238	68.974	55.392	89.381	98.607	121.272	91.827	96.661	106.494	71.972	75.038	90.367
P10599	TXN	#N/A	0.41331	131.040	159.257	79.275	28.979	45.770	74.411	70.679	52.288	87.428	136.684	85.637	56.694
P10768	ESD	#N/A	0.22956	32.383	396.819	177.175	51.080	36.256	31.907	24.196	54.532	90.860	102.269	32.830	4.435
P10809	HSPD1	#N/A	0.00789	160.955	214.062	171.960	45.625	56.645	76.084	57.642	56.835	83.163	99.466	46.024	46.404
P11021	HSPA5	#N/A	0.30593	126.670	81.985	81.541	81.814	89.206	96.516	108.031	90.429	98.828	77.280	75.028	76.671
P11142	HSPA8	#N/A	0.79170	84.187	85.109	73.356	92.628	90.234	99.698	98.927	89.332	87.743	79.368	77.755	82.153
P11413	G6PD	#N/A	NA	NA	NA	64.574	97.540	81.480	NA	NA	89.607	87.889	83.394	NA	NA
P11766	ADH5	#N/A	0.23515	53.464	363.582	151.593	57.909	46.208	31.356	31.442	38.459	67.996	116.678	25.077	22.127
P11940	PABPC1	#N/A	0.22213	55.770	85.339	73.642	114.216	89.883	92.086	81.239	88.988	76.350	75.010	98.694	88.722
P12277	CKB	#N/A	0.30422	62.706	180.775	120.353	64.052	62.854	57.049	72.686	69.322	82.447	99.326	66.936	72.012
P13611	VCAN	#N/A	0.06826	91.947	205.270	158.972	62.502	56.583	68.775	67.954	66.740	93.986	88.215	53.748	55.867
P13639	EEF2	#N/A	0.77040	58.553	81.137	96.591	83.276	81.471	105.637	102.008	103.322	82.607	78.272	99.659	71.411
P13645	KRT10	#N/A	0.18038	192.468	111.740	56.556	83.666	168.850	97.829	167.513	119.389	82.601	45.520	41.058	35.246
P13647	KRT5	#N/A	0.07298	180.236	115.999	94.372	53.856	252.133	97.043	159.169	71.056	51.070	39.989	44.033	37.682
P13797	PLS3	#N/A	0.54058	50.339	134.039	115.500	57.990	76.203	86.059	73.926	76.766	87.157	93.017	74.587	80.234
P13804	ETFA	#N/A	0.19202	249.763	121.720	99.639	85.007	67.306	85.461	84.259	91.534	120.665	71.260	72.817	56.131
P14174	MIF	#N/A	0.07877	17.167	74.542	60.233	74.663	70.217	90.612	115.438	68.384	75.530	111.311	84.118	90.873
P14618	PKM	#N/A	0.10101	93.569	299.712	203.686	32.815	41.570	44.639	42.989	40.622	75.090	111.409	42.286	32.151
P14625	HSP90B1	#N/A	0.44784	48.401	89.065	77.146	86.789	90.711	101.779	89.279	97.199	87.386	78.155	80.504	87.137
P15121	AKR1B1	#N/A	0.07920	115.369	286.574	167.969	45.442	55.866	42.596	46.782	49.224	79.150	105.130	35.954	39.592
P16949	STMN1	#N/A	0.69735	52.689	150.435	63.768	21.095	37.990	72.709	75.860	34.727	102.514	147.364	116.420	54.759
P17174	GOT1	#N/A	0.09000	100.670	301.175	188.582	35.812	49.754	46.156	45.346	54.002	80.532	104.086	38.222	30.299
P17600	SYN1	#N/A	0.01844	92.146	92.106	99.715	83.156	84.900	87.653	95.434	83.287	89.999	79.533	77.534	85.854
P17677	GAP43	#N/A	0.22509	86.658	224.099	124.205	35.489	60.925	54.635	75.353	35.331	82.630	122.388	66.172	43.024

ProteinID	Gene	Cluster	pvalue GST vs GST-Fascin1	GST			GST-Fascin1+BTA-EG4			GST-Fascin1+BTA-EG4			GST-Fascin1		
				Trial 1	Trial 2	Trial 3	Trial 1	Trial 2	Trial 3	Trial 1	Trial 2	Trial 3	Trial 1	Trial 2	Trial 3
P17987	TCP1	#N/A	0.10894	87.003	52.544	55.727	95.709	93.301	89.120	96.337	99.904	85.244	79.118	107.558	93.236
P18669	PGAM1	#N/A	0.15105	72.875	300.114	210.873	22.499	38.035	38.643	38.358	33.387	70.121	119.778	50.544	36.354
P19338	NCL	#N/A	0.47757	102.425	102.227	84.338	90.758	84.638	66.624	67.473	88.928	81.081	82.440	83.507	102.342
P19367	HK1	#N/A	0.45279	107.815	66.312	59.831	92.557	93.301	86.325	90.560	93.269	83.264	82.319	102.116	89.661
P20336	RAB3A	#N/A	0.59784	58.644	99.387	81.866	79.465	84.974	86.210	92.876	79.057	87.171	88.548	91.219	81.047
P20339	RAB5A	#N/A	0.01053	216.847	144.322	166.811	59.506	56.287	65.243	60.438	92.028	89.061	81.142	81.201	67.072
P21266	GSTM3	#N/A	0.22756	343.790	96.709	133.153	86.530	83.194	91.878	89.354	116.055	107.910	51.515	75.721	50.336
P21281	ATP6V1B2	#N/A	0.19345	152.840	95.465	96.168	88.195	80.244	84.108	101.531	81.794	85.157	82.877	78.474	73.851
P21283	ATP6V1C1	#N/A	0.33382	82.848	79.736	86.825	108.239	81.787	83.092	81.067	68.431	90.897	78.299	98.526	93.819
P22234	PAICS	#N/A	0.17228	263.242	170.596	NA	NA	NA	75.242	68.602	NA	NA	NA	48.766	51.801
P22314	UBA1	#N/A	0.52348	84.474	98.317	94.103	83.333	90.354	86.166	81.386	82.095	84.136	81.398	99.776	79.779
P23471	PTPRZ1	#N/A	0.02754	231.017	198.463	123.497	78.564	57.540	59.190	51.566	74.303	83.181	92.671	61.436	51.178
P23526	AHCY	#N/A	NA	NA	NA	175.363	39.490	35.675	NA	NA	98.692	102.332	88.745	NA	NA
P24534	EEF1B2	#N/A	NA	NA	NA	114.583	85.339	69.492	NA	NA	95.720	97.803	73.984	NA	NA
P24752	ACAT1	#N/A	0.44877	132.175	78.103	80.029	83.608	92.266	88.610	102.504	90.913	94.711	77.111	80.698	82.823
P25705	ATP5F1A	#N/A	0.30659	105.484	49.237	48.497	107.067	87.814	90.351	94.353	94.892	87.093	79.581	92.464	100.986
P25788	PSMA3	#N/A	NA	NA	NA	154.113	44.910	70.813	NA	NA	99.536	92.576	80.584	NA	NA
P26038	MSN	#N/A	0.14182	192.154	98.633	104.168	95.672	74.380	92.815	120.541	106.101	119.867	57.892	63.011	59.516
P26640	VARS	#N/A	0.48649	236.440	88.130	53.271	108.995	89.374	76.751	80.043	99.339	82.517	77.160	72.183	85.853
P26641	EEF1G	#N/A	0.96087	127.515	66.105	60.523	95.817	95.765	95.507	106.570	95.114	82.715	79.275	93.829	77.583
P27348	YWHAQ	#N/A	0.09788	84.879	128.839	110.040	67.665	76.100	87.223	85.331	80.691	88.011	88.809	73.556	72.437
P28161	GSTM2	#N/A	0.20071	328.726	99.897	140.227	89.194	85.725	91.431	91.562	114.828	104.277	49.202	70.978	52.065
P29218	IMPA1	#N/A	NA	NA	NA	178.845	69.907	74.527	NA	NA	78.437	104.122	63.708	NA	NA
P29401	TKT	#N/A	0.05944	115.240	290.696	229.375	28.157	32.418	43.157	43.058	38.575	74.267	111.325	45.729	33.629
P30038	ALDH4A1	#N/A	NA	NA	NA	183.583	30.342	27.931	NA	NA	38.262	88.510	119.301	NA	NA
P30041	PRDX6	#N/A	0.13355	81.426	285.209	196.031	27.964	37.959	48.626	44.332	38.535	75.311	117.771	44.371	38.411
P30044	PRDX5	#N/A	0.88207	53.883	97.137	84.949	83.294	84.516	96.006	102.978	80.000	85.191	86.765	75.015	80.504
P30086	PEBP1	#N/A	0.39955	100.654	191.002	96.736	24.951	42.073	75.550	61.745	34.730	87.393	140.994	84.309	46.515
P30153	PPP2R1A	#N/A	0.85860	118.147	77.581	72.302	85.742	86.775	81.131	77.371	87.860	93.284	82.334	104.481	90.255
P30626	SRI	#N/A	0.43680	28.047	96.421	75.873	66.939	61.039	109.286	108.920	45.926	106.061	109.242	81.265	70.268
P31146	CORO1A	#N/A	0.61215	44.144	28.409	134.679	64.769	74.102	113.915	115.134	94.667	116.368	67.942	108.396	88.736
P31150	GDI1	#N/A	0.08344	94.801	261.769	185.584	41.391	53.705	51.415	56.945	51.647	87.116	98.891	46.441	41.277
P31323	PRKAR2B	#N/A	0.31842	73.122	100.516	63.844	92.914	107.259	129.253	103.398	107.003	87.006	68.884	70.285	58.692
P31946	YWHAB	#N/A	0.08634	91.310	184.022	143.915	58.513	64.333	69.733	70.440	64.269	84.174	95.488	67.370	59.698
P32119	PRDX2	#N/A	0.01661	167.358	301.484	223.064	33.611	42.309	45.240	35.458	50.349	87.351	97.188	35.886	28.002
P34932	HSPA4	#N/A	0.01210	158.053	201.761	157.248	49.690	49.125	65.469	71.561	63.399	74.614	106.427	53.807	48.910
P35080	PFN2	#N/A	0.04968	128.602	288.994	221.318	22.929	36.248	41.773	31.434	31.629	76.814	115.342	46.716	39.291
P35527	KRT9	#N/A	0.04920	161.218	89.139	93.132	80.934	167.329	88.852	202.112	68.470	81.451	54.477	51.748	34.357

ProteinID	Gene	Cluster	pvalue GST vs GST-Fascin1	GST			GST-Fascin1+BTA-EG4			GST-Fascin1+BTA-EG4			GST-Fascin1		
				Trial 1	Trial 2	Trial 3	Trial 1	Trial 2	Trial 3	Trial 1	Trial 2	Trial 3	Trial 1	Trial 2	Trial 3
P35579	MYH9	#N/A	0.06392	53.683	31.765	43.320	124.453	95.851	109.203	119.554	106.470	115.071	54.848	84.685	98.302
P35611	ADD1	#N/A	0.20658	72.379	86.914	69.628	87.586	79.943	94.164	88.614	85.470	93.901	85.821	84.937	87.613
P35813	PPM1A	#N/A	NA	NA	NA	19.026	106.400	104.737	NA	NA	103.111	68.134	85.607	NA	NA
P35908	KRT2	#N/A	0.22790	229.735	114.542	48.643	72.844	211.029	87.999	167.381	99.629	71.572	44.804	41.738	33.905
P36405	ARL3	#N/A	0.62945	52.607	113.618	115.139	91.080	68.093	81.340	90.565	85.025	95.841	76.320	96.348	74.671
P36543	ATP6V1E1	#N/A	0.01435	182.438	149.154	148.200	51.742	57.378	64.198	52.428	45.281	65.834	113.976	85.273	71.597
P37837	TALDO1	#N/A	0.08502	99.099	315.190	233.061	28.161	33.596	38.900	35.139	33.658	75.489	110.907	44.380	28.489
P37840	SNCA	#N/A	0.61671	65.069	188.891	91.997	24.675	42.625	57.782	56.740	43.638	102.483	133.088	70.046	73.209
P38606	ATP6V1A	#N/A	0.69660	90.264	88.949	77.365	89.015	83.951	82.035	85.473	84.819	92.957	81.916	92.234	88.843
P38646	HSPA9	#N/A	0.03618	115.814	122.870	95.621	93.736	89.405	97.248	81.701	83.974	90.723	73.658	70.545	69.459
P40227	CCT6A	#N/A	0.57474	108.323	68.874	65.011	90.437	89.797	86.049	81.230	95.842	89.292	80.023	89.969	99.570
P40818	USP8	#N/A	0.51187	70.372	172.175	NA	NA	NA	56.602	42.305	NA	NA	NA	67.075	92.481
P40925	MDH1	#N/A	0.11637	86.436	340.153	216.087	26.177	36.316	34.354	24.241	39.435	84.763	109.560	43.261	24.222
P40926	MDH2	#N/A	0.10939	85.047	328.398	231.065	19.686	32.364	41.849	33.113	35.878	75.831	114.739	33.856	27.357
P41250	GARS	#N/A	0.17923	85.753	110.418	143.294	43.359	88.149	81.153	85.085	64.131	94.100	87.653	90.304	78.265
P42025	ACTR1B	#N/A	0.26785	16.301	77.826	85.341	92.632	82.169	104.018	81.479	79.528	103.383	76.440	106.786	87.296
P42765	ACAA2	#N/A	0.78958	107.995	93.000	50.499	75.070	98.413	128.210	75.041	101.290	94.190	83.002	87.623	64.991
P43034	PAFAH1B1	#N/A	0.20409	87.357	208.926	99.443	65.943	86.736	61.480	71.122	67.801	76.474	96.750	58.133	54.558
P46439	GSTM5	#N/A	0.19475	318.486	98.331	150.006	90.904	87.433	88.448	82.788	105.812	95.731	51.478	75.828	58.261
P46821	MAP1B	#N/A	0.37164	89.175	57.513	43.350	102.982	92.541	131.487	189.360	140.152	127.673	49.210	46.457	47.953
P47755	CAPZA2	#N/A	0.86093	32.583	111.869	86.560	71.493	77.798	96.562	113.245	99.876	97.980	82.535	55.487	79.052
P48735	IDH2	#N/A	0.96264	79.562	99.304	115.103	76.463	80.776	58.608	83.871	69.642	63.882	95.094	105.712	91.498
P49189	ALDH9A1	#N/A	NA	NA	NA	163.597	46.925	60.389	NA	NA	59.452	82.100	99.150	NA	NA
P49368	CCT3	#N/A	0.26878	92.380	58.263	64.136	99.805	93.012	116.747	72.171	94.686	85.630	76.738	110.774	84.077
P49588	AARS	#N/A	0.99186	26.228	150.859	NA	NA	NA	49.839	75.685	NA	NA	NA	89.998	85.495
P49593	PPM1F	#N/A	NA	NA	NA	64.844	91.431	110.085	NA	NA	84.644	79.407	78.459	NA	NA
P50135	HNMT	#N/A	0.11115	13.473	58.809	84.769	73.832	116.216	78.701	105.178	75.381	72.779	83.515	112.423	98.353
P50395	GDI2	#N/A	0.03840	114.188	217.049	182.428	43.550	55.943	59.562	65.789	49.611	86.916	98.612	55.806	51.171
P50990	CCT8	#N/A	0.24254	132.115	77.290	91.332	102.615	94.096	100.033	101.594	96.309	76.852	70.602	85.520	74.595
P50991	CCT4	#N/A	0.88454	140.740	69.213	59.272	106.835	86.308	84.268	78.135	74.138	86.783	84.322	110.827	86.620
P50993	ATP1A2	#N/A	0.01509	238.458	162.214	152.521	63.182	71.376	61.144	73.820	62.809	96.847	83.338	67.272	55.951
P51148	RAB5C	#N/A	0.01125	216.847	144.322	160.944	66.286	71.705	65.243	60.438	84.338	88.350	75.928	81.201	67.072
P51149	RAB7A	#N/A	0.02581	124.552	98.334	139.927	54.677	71.710	96.512	103.077	68.430	109.746	83.178	77.509	68.442
P51157	RAB28	#N/A	0.68102	160.875	50.828	43.164	98.526	109.179	114.382	117.331	115.438	106.515	60.625	58.547	84.066
P51452	DUSP3	#N/A	0.38669	118.018	34.689	50.990	93.609	102.425	99.974	92.194	97.177	79.825	80.425	100.671	99.239
P51553	IDH3G	#N/A	0.10049	64.071	64.667	70.682	100.684	93.231	88.863	69.658	117.939	75.537	70.925	92.793	111.185
P51649	ALDH5A1	#N/A	0.02080	233.070	133.355	173.509	83.175	69.509	79.630	66.497	59.734	72.761	80.687	61.806	70.056
P52209	PGD	#N/A	0.80127	79.448	106.054	84.217	80.731	83.805	64.607	85.546	77.229	80.237	91.305	99.140	86.518

ProteinID	Gene	Cluster	pvalue GST vs GST-Fascin1	GST			GST-Fascin1+BTA-EG4			GST-Fascin1+BTA-EG4			GST-Fascin1		
				Trial 1	Trial 2	Trial 3	Trial 1	Trial 2	Trial 3	Trial 1	Trial 2	Trial 3	Trial 1	Trial 2	Trial 3
P52907	CAPZA1	#N/A	0.79844	64.954	87.074	94.574	82.038	75.180	97.076	107.047	100.007	90.166	80.125	78.019	80.679
P53041	PPP5C	#N/A	0.13315	133.564	244.719	NA	NA	NA	48.327	50.160	NA	NA	NA	57.670	45.732
P53597	SUCLG1	#N/A	0.66922	103.822	57.332	75.675	92.894	81.816	89.550	96.167	106.660	98.779	72.103	87.895	98.247
P54577	YARS	#N/A	0.62102	126.300	58.121	97.162	87.326	88.970	100.357	111.792	86.378	77.472	80.770	84.727	81.748
P54578	USP14	#N/A	0.74950	136.214	80.859	50.982	103.982	92.167	93.709	91.775	85.972	97.329	77.056	79.670	83.878
P54652	HSPA2	#N/A	0.82351	81.242	80.764	78.401	96.824	87.363	99.847	98.979	89.754	87.875	77.254	81.417	83.131
P55786	NPEPPS	#N/A	0.17371	60.168	271.370	203.359	33.212	43.838	47.536	37.005	41.608	80.489	107.806	57.618	47.211
P55809	OXCT1	#N/A	0.04586	105.928	215.456	199.798	44.196	49.852	65.958	54.438	62.918	77.985	95.479	51.703	57.723
P60174	TPI1	#N/A	0.11242	85.550	346.686	230.033	20.967	31.678	37.361	26.469	34.320	77.567	114.584	31.560	23.632
P60201	PLP1	#N/A	0.14993	71.115	192.015	189.493	66.756	61.424	79.114	79.205	63.605	104.693	72.510	57.407	52.762
P60763	RAC3	#N/A	0.00937	120.480	124.252	110.322	80.496	68.215	93.014	93.970	73.698	120.886	75.612	85.984	55.803
P60953	CDC42	#N/A	0.15358	74.858	146.709	108.031	70.251	81.323	90.444	89.878	79.042	100.246	81.519	74.453	58.274
P60981	DSTN	#N/A	0.05271	77.875	59.859	58.488	96.087	90.727	94.020	100.788	96.504	91.982	77.694	89.261	94.493
P60983	GMFB	#N/A	0.34378	32.383	184.053	198.749	45.567	52.331	60.016	69.250	55.287	75.426	97.653	73.237	70.964
P61020	RAB5B	#N/A	0.10018	216.847	144.322	116.335	76.716	85.785	65.243	60.438	97.457	93.348	71.267	81.201	67.072
P61026	RAB10	#N/A	0.01075	136.117	120.981	106.575	73.365	82.115	71.952	79.080	77.219	88.328	85.710	80.369	78.802
P61081	UBE2M	#N/A	0.42619	239.560	84.692	NA	NA	NA	80.715	75.497	NA	NA	NA	93.500	76.367
P61160	ACTR2	#N/A	0.08942	91.479	33.671	46.966	39.938	53.284	107.983	109.614	36.827	90.663	141.409	97.007	91.482
P61204	ARF3	#N/A	0.07394	81.693	54.247	58.324	91.027	88.135	88.158	97.981	93.983	90.965	82.277	112.922	89.800
P61266	STX1B	#N/A	0.24990	46.367	198.464	150.549	52.330	73.723	62.639	77.032	71.632	87.178	88.517	60.681	61.315
P61328	FGF12	#N/A	0.29129	352.641	104.976	NA	NA	NA	92.002	101.449	NA	NA	NA	58.783	46.565
P61586	RHOA	#N/A	0.78528	47.558	127.747	91.011	87.716	82.420	80.844	85.583	70.572	96.006	82.817	89.392	73.453
P61604	HSPE1	#N/A	0.50637	69.148	247.129	80.752	27.192	44.221	53.752	51.635	37.814	91.169	140.955	74.337	40.370
P61981	YWHAG	#N/A	0.08001	96.983	197.948	139.884	57.954	65.699	63.954	74.809	68.153	81.879	95.898	60.010	55.460
P62258	YWHAE	#N/A	0.12296	82.162	277.516	189.567	33.582	44.227	49.147	48.315	49.601	80.023	108.846	45.838	39.750
P62714	PPP2CB	#N/A	NA	NA	NA	68.529	58.686	70.773	NA	NA	91.142	104.128	96.419	NA	NA
P62760	VSNL1	#N/A	NA	NA	NA	110.532	76.102	103.235	NA	NA	87.972	87.912	70.811	NA	NA
P62820	RAB1A	#N/A	0.00453	149.379	153.721	130.568	63.170	56.621	65.377	79.298	68.569	93.001	95.558	72.969	64.884
P62873	GNB1	#N/A	0.02671	101.706	180.519	165.487	64.954	60.079	91.413	75.612	78.387	96.849	78.834	50.488	53.873
P62937	PPIA	#N/A	0.20709	75.366	166.050	126.586	54.281	60.819	70.704	80.033	66.024	83.880	103.161	68.083	66.667
P62979	RPS27A	#N/A	0.85800	51.388	212.950	68.139	19.768	31.070	65.688	51.124	30.305	78.102	161.178	85.925	50.591
P63096	GNAI1	#N/A	0.21123	47.803	74.144	69.301	117.732	98.401	94.000	93.064	96.855	85.674	64.578	106.365	85.112
P63104	YWHAZ	#N/A	0.02965	125.680	218.519	173.018	39.980	54.493	65.127	66.403	57.359	85.840	101.258	52.473	46.893
P68036	UBE2L3	#N/A	0.05684	92.969	51.073	48.693	74.147	93.297	80.360	97.777	79.865	64.907	105.142	110.087	96.322
P78371	CCT2	#N/A	0.11281	69.981	51.915	75.021	93.683	92.650	93.145	84.457	96.568	90.885	73.734	118.531	94.131
P78417	GSTO1	#N/A	0.10552	84.729	345.579	236.916	21.088	49.737	32.177	25.504	32.330	74.833	106.475	36.418	25.392
P84085	ARF5	#N/A	0.08119	84.117	56.567	62.191	89.345	86.671	88.197	95.334	93.512	90.531	82.900	110.103	90.940
Q00577	PURA	#N/A	0.62623	178.617	66.805	67.373	113.066	87.268	66.233	112.822	84.250	89.401	74.613	86.871	87.595

ProteinID	Gene	Cluster	pvalue GST vs GST-Fascin1	GST			GST-Fascin1+BTA-EG4			GST-Fascin1+BTA-EG4			GST-Fascin1		
				Trial 1	Trial 2	Trial 3	Trial 1	Trial 2	Trial 3	Trial 1	Trial 2	Trial 3	Trial 1	Trial 2	Trial 3
Q01082	SPTBN1	#N/A	0.13157	72.513	71.832	77.030	97.505	82.949	94.367	91.562	91.135	95.717	75.626	84.141	95.414
Q01518	CAP1	#N/A	0.05905	129.684	142.592	199.889	70.115	68.549	71.935	69.011	83.869	75.953	70.140	73.881	75.445
Q01995	TAGLN	#N/A	0.28342	63.573	98.746	88.823	68.500	71.162	78.178	75.584	73.090	77.984	103.074	97.906	91.117
Q02750	MAP2K1	#N/A	0.06674	81.720	56.232	45.059	102.743	98.210	90.473	100.995	88.926	83.362	81.295	99.115	92.921
Q02790	FKBP4	#N/A	0.06594	98.876	99.415	120.157	69.603	79.465	83.808	78.244	77.181	72.820	91.066	85.217	87.863
Q03013	GSTM4	#N/A	0.20730	329.306	98.585	146.872	91.658	85.675	88.660	77.842	103.833	90.791	55.462	69.998	62.203
Q04695	KRT17	#N/A	0.17855	191.142	109.067	53.045	57.869	251.696	92.412	192.347	69.040	67.156	43.984	35.224	30.072
Q04917	YWHAH	#N/A	0.02037	108.305	138.348	118.344	67.035	73.138	82.009	84.034	71.048	84.196	92.814	74.217	66.885
Q06124	PTPN11	#N/A	0.17566	89.537	52.636	49.178	104.641	81.925	92.833	105.097	109.272	96.092	74.606	98.935	90.553
Q06830	PRDX1	#N/A	0.00245	178.169	212.571	214.631	38.752	45.607	61.095	64.186	51.996	81.545	97.707	49.283	48.499
Q08209	PPP3CA	#N/A	0.00156	189.349	184.823	150.555	72.147	78.862	68.880	72.227	75.269	83.600	78.082	55.997	51.328
Q12765	SCRN1	#N/A	0.06513	116.368	328.895	252.506	16.606	24.845	38.565	26.227	31.401	73.999	115.652	41.933	24.089
Q12860	CNTN1	#N/A	0.07374	140.059	147.690	237.058	70.587	59.529	77.599	80.616	52.080	90.886	68.001	68.169	64.486
Q12906	ILF3	#N/A	0.05281	120.263	108.582	NA	NA	NA	72.951	70.823	NA	NA	NA	84.408	90.121
Q12931	TRAP1	#N/A	0.64003	42.382	109.671	64.284	92.239	89.961	95.331	76.115	98.454	84.031	80.671	83.276	84.850
Q13153	PAK1	#N/A	0.05268	102.790	164.921	121.363	64.409	71.939	74.764	80.843	69.948	88.854	92.087	65.586	62.105
Q13177	PAK2	#N/A	0.12810	90.773	182.366	114.524	65.711	73.304	69.878	70.161	67.304	88.528	93.825	61.001	64.188
Q13228	SELENBP1	#N/A	0.69412	27.846	18.359	160.265	46.708	55.117	135.225	129.858	71.076	88.368	96.094	82.521	90.389
Q13310	PABPC4	#N/A	0.49035	64.670	84.538	111.736	90.779	112.646	99.371	99.971	102.801	68.328	63.207	79.852	83.701
Q13363	CTBP1	#N/A	0.52277	226.704	75.228	58.780	105.702	87.704	83.496	91.102	101.035	88.090	74.942	83.335	79.266
Q13630	TSTA3	#N/A	0.23408	49.631	53.168	104.267	85.777	99.749	84.324	80.210	91.733	70.562	75.793	117.090	104.330
Q14019	COTL1	#N/A	0.09245	57.625	83.756	81.019	84.878	73.644	86.427	92.306	74.467	76.230	97.426	90.495	91.162
Q14103	HNRNPD	#N/A	0.08379	68.590	84.528	53.284	96.642	82.137	87.126	84.804	93.575	85.874	86.123	91.324	92.338
Q14194	CRMP1	#N/A	0.01061	154.290	239.579	216.627	37.002	48.541	51.017	50.773	46.440	80.672	98.798	54.141	45.954
Q14195	DPYSL3	#N/A	0.01012	173.049	248.723	196.481	36.022	44.562	54.323	46.604	45.670	79.520	107.249	46.280	42.303
Q14203	DCTN1	#N/A	0.78884	146.693	61.472	NA	NA	NA	86.290	90.819	NA	NA	NA	86.794	95.208
Q14204	DYNC1H1	#N/A	NA	NA	NA	36.410	101.730	78.301	NA	NA	71.107	74.370	102.389	NA	NA
Q14247	CTTN	#N/A	0.84251	135.052	71.001	NA	NA	NA	87.786	73.940	NA	NA	NA	95.080	94.796
Q14894	CRYM	#N/A	0.36411	66.873	126.536	104.840	78.424	74.388	82.861	86.049	81.800	92.710	84.131	76.066	77.133
Q14914	PTGR1	#N/A	0.36568	72.807	178.440	104.479	57.360	60.934	63.321	70.000	65.276	89.802	105.734	86.321	59.587
Q14974	KPNB1	#N/A	0.42332	232.833	64.527	111.329	85.028	94.105	85.053	68.558	71.069	85.048	77.529	86.752	94.148
Q15075	EEA1	#N/A	0.21374	301.945	128.137	105.716	40.960	81.922	50.764	97.891	91.958	123.019	80.827	53.635	68.235
Q15149	PLEC	#N/A	0.33719	108.828	96.762	77.121	87.558	86.044	90.855	78.700	93.508	89.517	80.229	89.316	81.583
Q15181	PPA1	#N/A	0.15644	67.378	240.666	156.668	50.654	67.047	75.384	58.421	51.661	85.624	97.679	47.155	42.591
Q15257	PTPA	#N/A	0.06075	90.360	63.231	68.781	79.343	89.797	69.953	84.655	87.640	83.018	88.967	107.507	103.766
Q15286	RAB35	#N/A	0.00550	124.873	108.792	114.792	64.793	68.192	74.266	90.026	77.139	93.469	91.133	80.232	80.588
Q15365	PCBP1	#N/A	0.57783	76.863	69.310	85.861	103.462	91.408	96.216	95.064	104.757	83.438	67.464	91.531	89.502
Q15366	PCBP2	#N/A	0.63029	76.667	69.719	85.861	103.462	91.408	96.017	98.233	104.757	83.438	67.464	89.326	88.877

ProteinID	Gene	Cluster	pvalue GST vs GST-Fascin1	GST			GST-Fascin1+BTA-EG4			GST-Fascin1+BTA-EG4			GST-Fascin1		
				Trial 1	Trial 2	Trial 3	Trial 1	Trial 2	Trial 3	Trial 1	Trial 2	Trial 3	Trial 1	Trial 2	Trial 3
P52907	CAPZA1	#N/A	0.79844	64.954	87.074	94.574	82.038	75.180	97.076	107.047	100.007	90.166	80.125	78.019	80.679
P53041	PPP5C	#N/A	0.13315	133.564	244.719	NA	NA	NA	48.327	50.160	NA	NA	NA	57.670	45.732
P53597	SUCLG1	#N/A	0.66922	103.822	57.332	75.675	92.894	81.816	89.550	96.167	106.660	98.779	72.103	87.895	98.247
P54577	YARS	#N/A	0.62102	126.300	58.121	97.162	87.326	88.970	100.357	111.792	86.378	77.472	80.770	84.727	81.748
P54578	USP14	#N/A	0.74950	136.214	80.859	50.982	103.982	92.167	93.709	91.775	85.972	97.329	77.056	79.670	83.878
P54652	HSPA2	#N/A	0.82351	81.242	80.764	78.401	96.824	87.363	99.847	98.979	89.754	87.875	77.254	81.417	83.131
P55786	NPEPPS	#N/A	0.17371	60.168	271.370	203.359	33.212	43.838	47.536	37.005	41.608	80.489	107.806	57.618	47.211
P55809	OXCT1	#N/A	0.04586	105.928	215.456	199.798	44.196	49.852	65.958	54.438	62.918	77.985	95.479	51.703	57.723
P60174	TPI1	#N/A	0.11242	85.550	346.686	230.033	20.967	31.678	37.361	26.469	34.320	77.567	114.584	31.560	23.632
P60201	PLP1	#N/A	0.14993	71.115	192.015	189.493	66.756	61.424	79.114	79.205	63.605	104.693	72.510	57.407	52.762
P60763	RAC3	#N/A	0.00937	120.480	124.252	110.322	80.496	68.215	93.014	93.970	73.698	120.886	75.612	85.984	55.803
P60953	CDC42	#N/A	0.15358	74.858	146.709	108.031	70.251	81.323	90.444	89.878	79.042	100.246	81.519	74.453	58.274
P60981	DSTN	#N/A	0.05271	77.875	59.859	58.488	96.087	90.727	94.020	100.788	96.504	91.982	77.694	89.261	94.493
P60983	GMFB	#N/A	0.34378	32.383	184.053	198.749	45.567	52.331	60.016	69.250	55.287	75.426	97.653	73.237	70.964
P61020	RAB5B	#N/A	0.10018	216.847	144.322	116.335	76.716	85.785	65.243	60.438	97.457	93.348	71.267	81.201	67.072
P61026	RAB10	#N/A	0.01075	136.117	120.981	106.575	73.365	82.115	71.952	79.080	77.219	88.328	85.710	80.369	78.802
P61081	UBE2M	#N/A	0.42619	239.560	84.692	NA	NA	NA	80.715	75.497	NA	NA	NA	93.500	76.367
P61160	ACTR2	#N/A	0.08942	91.479	33.671	46.966	39.938	53.284	107.983	109.614	36.827	90.663	141.409	97.007	91.482
P61204	ARF3	#N/A	0.07394	81.693	54.247	58.324	91.027	88.135	88.158	97.981	93.983	90.965	82.277	112.922	89.800
P61266	STX1B	#N/A	0.24990	46.367	198.464	150.549	52.330	73.723	62.639	77.032	71.632	87.178	88.517	60.681	61.315
P61328	FGF12	#N/A	0.29129	352.641	104.976	NA	NA	NA	92.002	101.449	NA	NA	NA	58.783	46.565
P61586	RHOA	#N/A	0.78528	47.558	127.747	91.011	87.716	82.420	80.844	85.583	70.572	96.006	82.817	89.392	73.453
P61604	HSPE1	#N/A	0.50637	69.148	247.129	80.752	27.192	44.221	53.752	51.635	37.814	91.169	140.955	74.337	40.370
P61981	YWHAG	#N/A	0.08001	96.983	197.948	139.884	57.954	65.699	63.954	74.809	68.153	81.879	95.898	60.010	55.460
P62258	YWHAE	#N/A	0.12296	82.162	277.516	189.567	33.582	44.227	49.147	48.315	49.601	80.023	108.846	45.838	39.750
P62714	PPP2CB	#N/A	NA	NA	NA	68.529	58.686	70.773	NA	NA	91.142	104.128	96.419	NA	NA
P62760	VSNL1	#N/A	NA	NA	NA	110.532	76.102	103.235	NA	NA	87.972	87.912	70.811	NA	NA
P62820	RAB1A	#N/A	0.00453	149.379	153.721	130.568	63.170	56.621	65.377	79.298	68.569	93.001	95.558	72.969	64.884
P62873	GNB1	#N/A	0.02671	101.706	180.519	165.487	64.954	60.079	91.413	75.612	78.387	96.849	78.834	50.488	53.873
P62937	PPIA	#N/A	0.20709	75.366	166.050	126.586	54.281	60.819	70.704	80.033	66.024	83.880	103.161	68.083	66.667
P62979	RPS27A	#N/A	0.85800	51.388	212.950	68.139	19.768	31.070	65.688	51.124	30.305	78.102	161.178	85.925	50.591
P63096	GNAI1	#N/A	0.21123	47.803	74.144	69.301	117.732	98.401	94.000	93.064	96.855	85.674	64.578	106.365	85.112
P63104	YWHAZ	#N/A	0.02965	125.680	218.519	173.018	39.980	54.493	65.127	66.403	57.359	85.840	101.258	52.473	46.893
P68036	UBE2L3	#N/A	0.05684	92.969	51.073	48.693	74.147	93.297	80.360	97.777	79.865	64.907	105.142	110.087	96.322
P78371	CCT2	#N/A	0.11281	69.981	51.915	75.021	93.683	92.650	93.145	84.457	96.568	90.885	73.734	118.531	94.131
P78417	GSTO1	#N/A	0.10552	84.729	345.579	236.916	21.088	49.737	32.177	25.504	32.330	74.833	106.475	36.418	25.392
P84085	ARF5	#N/A	0.08119	84.117	56.567	62.191	89.345	86.671	88.197	95.334	93.512	90.531	82.900	110.103	90.940
Q00577	PURA	#N/A	0.62623	178.617	66.805	67.373	113.066	87.268	66.233	112.822	84.250	89.401	74.613	86.871	87.595

ProteinID	Gene	Cluster	pvalue GST vs GST-Fascin1	GST			GST-Fascin1+BTA-EG4			GST-Fascin1+BTA-EG4			GST-Fascin1		
				Trial 1	Trial 2	Trial 3	Trial 1	Trial 2	Trial 3	Trial 1	Trial 2	Trial 3	Trial 1	Trial 2	Trial 3
Q96QK1	VPS35	#N/A	0.21887	69.024	49.607	NA	NA	NA	84.619	63.676	NA	NA	NA	81.610	131.129
Q99447	PCYT2	#N/A	0.35450	108.806	48.254	49.219	96.223	92.476	90.578	101.664	86.979	79.669	87.588	94.332	96.120
Q99497	PARK7	#N/A	0.16749	59.744	287.726	187.343	33.297	41.109	51.334	55.497	48.748	91.685	106.472	41.493	33.864
Q99714	HSD17B10	#N/A	0.05154	74.477	45.528	52.263	99.055	105.388	98.230	94.237	97.835	77.993	76.984	88.627	104.951
Q99832	CCT7	#N/A	0.11913	97.919	46.449	45.603	90.981	99.314	93.210	78.838	89.782	74.780	88.891	103.529	104.451
Q99962	SH3GL2	#N/A	0.19088	359.817	130.425	146.805	60.249	70.439	61.390	72.608	80.371	97.932	80.355	67.371	58.930
Q9BPU6	DPYSL5	#N/A	NA	NA	NA	167.134	69.844	75.300	NA	NA	60.261	81.576	81.813	NA	NA
Q9BUT1	BDH2	#N/A	0.95878	140.583	52.796	54.678	96.251	99.957	101.063	95.980	103.941	93.806	71.433	97.060	84.494
Q9BY11	PACSIN1	#N/A	NA	NA	NA	216.064	35.135	42.722	NA	NA	52.379	88.660	97.088	NA	NA
Q9BYE2	TMPRSS13	#N/A	0.30846	308.103	101.381	NA	NA	NA	83.438	96.371	NA	NA	NA	73.768	54.635
Q9C040	TRIM2	#N/A	0.16020	198.662	81.935	108.133	90.419	83.338	107.868	142.191	122.798	118.500	50.164	52.886	53.722
Q9GZP4	PITHD1	#N/A	0.39746	32.432	122.394	177.085	49.743	64.960	107.277	108.627	67.282	96.029	83.957	59.858	66.628
Q9GZV7	HAPLN2	#N/A	0.00402	99.151	106.770	114.103	84.684	69.414	84.435	86.940	90.804	91.099	78.784	82.220	79.985
Q9H0E2	TOLLIP	#N/A	NA	NA	NA	113.089	58.219	71.864	NA	NA	122.081	83.840	81.929	NA	NA
Q9H479	FN3K	#N/A	0.07958	80.223	46.597	66.265	87.968	98.990	82.621	74.272	85.387	89.052	80.232	127.300	102.870
Q9H492	MAP1LC3A	#N/A	0.66344	127.756	61.975	82.204	94.397	79.752	95.505	100.485	101.539	101.124	71.294	83.727	88.597
Q9H9S4	CAB39L	#N/A	0.10115	69.599	52.855	NA	NA	NA	76.426	72.872	NA	NA	NA	135.884	100.393
Q9HB71	CACYBP	#N/A	0.13909	340.901	122.261	190.661	80.430	66.480	71.249	77.122	71.751	81.356	70.986	56.392	64.068
Q9NP79	VTA1	#N/A	NA	NA	NA	54.360	109.451	100.201	NA	NA	102.437	83.257	70.590	NA	NA
Q9NR45	NANS	#N/A	0.04646	180.807	165.888	NA	NA	NA	45.446	68.212	NA	NA	NA	71.340	71.637
Q9NRN7	AASDHPPT	#N/A	0.21062	90.971	45.040	56.332	107.483	96.354	94.533	101.391	106.606	83.789	70.984	106.678	91.830
Q9NSD9	FARSB	#N/A	0.85043	150.021	50.461	76.071	100.065	94.893	91.165	96.770	95.752	81.363	73.896	91.246	93.031
Q9NUJ1	ABHD10	#N/A	0.46166	123.228	52.116	63.071	90.030	87.801	69.401	88.710	100.126	81.783	83.262	109.053	103.312
Q9NUQ9	FAM49B	#N/A	0.36096	64.289	88.952	98.473	71.201	80.172	88.243	66.748	85.928	81.752	89.540	105.362	91.812
Q9NZR1	TMOD2	#N/A	0.13590	31.316	41.895	64.895	99.374	92.606	116.785	133.146	115.738	115.867	57.621	68.012	92.396
Q9UBB6	NCDN	#N/A	0.57950	129.644	49.656	67.309	97.296	87.369	87.879	78.066	83.688	76.834	86.617	102.733	102.115
Q9UBW8	COPS7A	#N/A	NA	NA	NA	80.011	83.879	109.616	NA	NA	104.792	76.414	72.283	NA	NA
Q9UEY8	ADD3	#N/A	0.25751	53.099	77.574	81.405	95.968	88.940	99.762	89.341	96.814	84.497	75.152	84.859	92.266
Q9UHD1	CHORDC1	#N/A	NA	NA	NA	104.134	86.886	98.018	NA	NA	90.094	78.666	73.350	NA	NA
Q9UHY7	ENOPH1	#N/A	NA	NA	NA	172.385	43.793	56.183	NA	NA	43.397	74.204	108.411	NA	NA
Q9UI15	TAGLN3	#N/A	0.03733	156.196	267.830	170.795	33.038	42.472	45.890	43.426	45.146	82.561	115.464	50.008	37.750
Q9UIC8	LCMT1	#N/A	0.57803	168.570	66.692	69.182	113.842	101.394	90.903	84.944	104.014	83.174	63.618	90.485	87.552
Q9UIJ7	AK3	#N/A	0.07308	84.467	39.065	54.260	91.989	110.240	85.146	91.138	100.190	69.125	80.156	110.229	105.380
Q9UJ70	NAGK	#N/A	0.36646	213.837	100.666	NA	NA	NA	72.967	60.102	NA	NA	NA	102.190	78.395
Q9UJC5	SH3BGRL2	#N/A	0.41719	61.747	130.351	NA	NA	NA	108.228	94.999	NA	NA	NA	49.988	69.710
Q9UJU6	DBNL	#N/A	NA	NA	NA	52.504	88.513	77.296	NA	NA	107.504	106.595	78.885	NA	NA
Q9UKG1	APPL1	#N/A	NA	NA	NA	148.216	70.361	86.033	NA	NA	110.309	66.272	71.880	NA	NA
Q9ULP0	NDRG4	#N/A	0.88507	100.144	88.791	NA	NA	NA	61.865	94.606	NA	NA	NA	103.262	88.695

ProteinID	Gene	Cluster	pvalue GST vs GST-Fascin1	GST			GST-Fascin1+BTA-EG4			GST-Fascin1+BTA-EG4			GST-Fascin1		
				Trial 1	Trial 2	Trial 3	Trial 1	Trial 2	Trial 3	Trial 1	Trial 2	Trial 3	Trial 1	Trial 2	Trial 3
Q9ULP9	TBC1D24	#N/A	0.23998	80.432	64.218	102.999	85.952	85.749	80.048	78.648	74.420	66.335	89.638	110.036	100.498
Q9UPY8	MAPRE3	#N/A	0.52668	107.109	51.298	71.787	95.170	84.639	99.838	108.176	77.949	77.782	88.986	90.953	87.431
Q9Y281	CFL2	#N/A	0.57877	53.227	111.373	100.553	74.536	76.449	87.888	109.444	83.840	95.025	84.450	73.793	73.964
Q9Y2T3	GDA	#N/A	0.09334	102.361	314.414	196.786	38.955	43.885	46.971	30.575	43.793	74.426	108.910	40.059	28.501
Q9Y376	CAB39	#N/A	0.12234	110.101	54.297	42.773	81.521	78.285	69.937	75.063	71.062	78.360	107.633	123.201	103.283
Q9Y570	PPME1	#N/A	0.81943	137.132	61.466	63.374	85.550	88.102	87.828	80.198	89.062	84.433	87.516	99.245	94.709
Q9Y5X2	SNX8	#N/A	0.89884	76.831	124.210	NA	NA	NA	68.759	54.498	NA	NA	NA	108.244	85.222
Q9Y617	PSAT1	#N/A	0.50488	58.667	138.394	115.936	64.358	72.267	76.308	71.357	64.762	81.354	98.231	80.841	80.233
Q9Y696	CLIC4	#N/A	NA	NA	NA	37.221	87.280	100.407	NA	NA	96.699	91.441	83.226	NA	NA
A0A087WZT3	BOLA2	#N/A	NA	NA	NA	22.914	107.615	95.848	NA	NA	97.181	68.314	89.797	NA	NA
A0A0A0MT35	PRXL2B	#N/A	NA	NA	NA	63.447	96.732	75.160	NA	NA	82.501	86.649	89.669	NA	NA
A0A286YEY4	IGHG2	#N/A	NA	NA	NA	163.820	54.581	61.840	NA	NA	79.098	79.822	89.654	NA	NA
C9JIZ6	PSAP	#N/A	NA	NA	NA	83.838	74.722	71.571	NA	NA	94.219	90.820	89.429	NA	NA
E7EMB3	CALM2	#N/A	NA	NA	NA	70.491	32.177	20.223	NA	NA	48.269	108.385	141.733	NA	NA
E9PF18	HADH	#N/A	NA	NA	NA	119.008	48.993	64.177	NA	NA	79.259	79.260	103.562	NA	NA
F6TLX2	GLOD4	#N/A	NA	NA	NA	230.807	11.086	50.058	NA	NA	20.968	87.221	110.965	NA	NA
F8VXU5	VPS29	#N/A	NA	NA	NA	49.970	99.069	98.546	NA	NA	106.443	106.653	66.085	NA	NA
G8JLH6	CD9	#N/A	NA	NA	NA	259.356	27.980	49.089	NA	NA	57.062	81.417	86.799	NA	NA
H0YB34	RIDA	#N/A	NA	NA	NA	169.861	53.612	51.688	NA	NA	48.326	78.482	103.530	NA	NA
I3L0M9	ELOB	#N/A	NA	NA	NA	73.978	82.144	73.305	NA	NA	117.175	96.374	78.407	NA	NA
I3L504	EIF5A	#N/A	NA	NA	NA	119.615	85.809	77.657	NA	NA	56.595	106.784	78.021	NA	NA
K7ES00	H3F3B	#N/A	NA	NA	NA	429.798	73.020	47.534	NA	NA	75.363	48.236	28.741	NA	NA
O00178	GTPBP1	#N/A	NA	NA	NA	70.750	93.387	106.511	NA	NA	130.403	106.020	51.642	NA	NA
O60784	TOM1	#N/A	NA	NA	NA	113.039	52.680	72.599	NA	NA	68.178	82.077	102.440	NA	NA
O94856	NFASC	#N/A	NA	NA	NA	169.963	79.674	27.455	NA	NA	89.622	113.467	75.170	NA	NA
O94985	CLSTN1	#N/A	NA	NA	NA	48.390	111.558	91.333	NA	NA	94.749	111.888	66.081	NA	NA
O95372	LYPLA2	#N/A	NA	NA	NA	43.538	83.295	87.247	NA	NA	87.503	80.389	96.493	NA	NA
O95425	SVIL	#N/A	NA	NA	NA	92.218	104.639	88.639	NA	NA	104.255	94.479	62.082	NA	NA
O95989	NUDT3	#N/A	NA	NA	NA	131.177	42.862	70.182	NA	NA	58.072	93.666	101.270	NA	NA
P13010	XRCC5	#N/A	NA	NA	NA	66.500	86.975	91.804	NA	NA	86.097	82.806	86.059	NA	NA
P14324	FDPS	#N/A	NA	NA	NA	185.635	71.868	75.404	NA	NA	58.227	53.056	88.104	NA	NA
P16298	PPP3CB	#N/A	NA	NA	NA	127.468	75.800	78.423	NA	NA	82.735	68.152	86.942	NA	NA
P21579	SYT1	#N/A	NA	NA	NA	89.091	75.096	74.968	NA	NA	109.338	119.077	69.819	NA	NA
P28066	PSMA5	#N/A	NA	NA	NA	127.766	62.298	54.660	NA	NA	53.179	79.548	108.120	NA	NA
P30084	ECHS1	#N/A	NA	NA	NA	188.877	39.724	45.502	NA	NA	57.681	84.338	101.441	NA	NA
P35612	ADD2	#N/A	NA	NA	NA	71.020	87.093	85.478	NA	NA	77.087	104.483	81.657	NA	NA
P54725	RAD23A	#N/A	NA	NA	NA	83.653	65.912	80.943	NA	NA	77.750	106.415	88.174	NA	NA
P58546	MTPN	#N/A	NA	NA	NA	86.130	39.465	44.073	NA	NA	58.785	83.935	130.357	NA	NA

ProteinID	Gene	Cluster	pvalue GST vs GST-Fascin1	GST			GST-Fascin1+BTA-EG4			GST-Fascin1+BTA-EG4			GST-Fascin1		
				Trial 1	Trial 2	Trial 3	Trial 1	Trial 2	Trial 3	Trial 1	Trial 2	Trial 3	Trial 1	Trial 2	Trial 3
P61970	NUTF2	#N/A	NA	NA	NA	228.087	25.271	29.257	NA	NA	40.882	84.222	109.476	NA	NA
P62942	FKBP1A	#N/A	NA	NA	NA	96.756	77.565	66.407	NA	NA	75.288	88.099	94.258	NA	NA
Q04760	GLO1	#N/A	NA	NA	NA	168.516	16.897	32.061	NA	NA	42.520	76.028	131.069	NA	NA
Q12792	TWF1	#N/A	NA	NA	NA	74.381	105.782	92.558	NA	NA	116.213	109.573	54.705	NA	NA
Q12959	DLG1	#N/A	NA	NA	NA	63.080	92.708	111.121	NA	NA	75.283	118.580	65.041	NA	NA
Q13619	CUL4A	#N/A	NA	NA	NA	43.031	84.338	100.292	NA	NA	89.454	80.083	89.945	NA	NA
Q15056	EIF4H	#N/A	NA	NA	NA	129.524	95.782	90.244	NA	NA	91.623	100.694	56.468	NA	NA
Q3ZCW2	LGALSL	#N/A	NA	NA	NA	186.147	28.069	46.690	NA	NA	50.858	88.307	107.263	NA	NA
Q5CZC0	FSIP2	#N/A	NA	NA	NA	170.117	76.754	77.188	NA	NA	108.875	90.986	57.377	NA	NA
Q5SQ11	PTGDS	#N/A	NA	NA	NA	132.407	7.876	18.342	NA	NA	50.968	82.207	145.605	NA	NA
Q5T6V5	C9orf64	#N/A	NA	NA	NA	35.013	119.399	79.955	NA	NA	157.790	102.679	54.440	NA	NA
Q7L5N1	COPS6	#N/A	NA	NA	NA	65.437	81.907	83.413	NA	NA	109.824	64.694	91.779	NA	NA
Q7Z4W1	DCXR	#N/A	NA	NA	NA	133.738	108.515	93.541	NA	NA	110.973	80.394	50.349	NA	NA
Q86TB3	ALPK2	#N/A	NA	NA	NA	26.113	119.781	102.942	NA	NA	113.294	110.731	58.003	NA	NA
Q8TBC4	UBA3	#N/A	NA	NA	NA	72.502	101.855	81.726	NA	NA	81.966	88.590	81.487	NA	NA
Q96S19	METTL26	#N/A	NA	NA	NA	19.026	117.709	78.802	NA	NA	79.163	115.881	80.572	NA	NA
Q9H0Q0	FAM49A	#N/A	NA	NA	NA	106.935	56.871	89.200	NA	NA	94.776	77.247	88.270	NA	NA
Q9H1K1	ISCU	#N/A	NA	NA	NA	84.066	94.701	85.478	NA	NA	99.047	102.864	68.246	NA	NA
Q9NQR4	NIT2	#N/A	NA	NA	NA	210.579	49.495	53.822	NA	NA	83.936	69.473	85.058	NA	NA
Q9NUB1	ACSS1	#N/A	NA	NA	NA	55.959	81.742	118.567	NA	NA	91.757	85.751	76.387	NA	NA
Q9ULU8	CADPS	#N/A	NA	NA	NA	65.130	101.638	78.480	NA	NA	88.928	83.670	84.757	NA	NA
Q9Y223	GNE	#N/A	NA	NA	NA	14.567	100.748	114.367	NA	NA	137.773	124.869	50.457	NA	NA
Q9Y3D6	FIS1	#N/A	NA	NA	NA	94.914	63.326	72.696	NA	NA	98.117	79.127	94.219	NA	NA

References

(1) ALZHEIMER, A. Uber Eine Eigenartige Erkrankung Der Hirnrinde. *Zentralbl Nervenh Psych* **1907**, *18*, 177–179 https://doi.org/10.1002/ca.980080612

(2) Stelzmann, R. A.; Schnitzlein, H. N.; Murtagh, F. R. An English Translation of Alzheimer's 1907 Paper, "Über Eine Eigenartige Erkankung Der Hirnrinde." *Clin. Anat.* **1995**, *8* (6), 429–431. https://doi.org/10.1002/ca.980080612.

(3) Merriam, A. E.; Miriam, K. A.; Gaston, P.; Wey, S. L.; Katz, I. The Psychiatric Symptoms of Alzheimer's Disease *J. Amer. Geriatrics Soc.* **1988**, 7-22, https://doi.org/10.1111/j.1532-5415.1988.tb03427.x

(4) Reisberg, B.; Borenstein, J.; Salob, S. P.; Ferris, S. H.; Franssen, E.; Georgotas, A. Behavioral Symptoms in Alzheimer's Disease: Phenomenology and Treatment. *J. Clin. Psychiatry* **1987**, *48* (5, Suppl), 9–15. PMID: 3553166

(5) Lyketsos, C. G.; Carrillo, M. C.; Ryan, J. M.; Khachaturian, A. S.; Trzepacz, P.; Amatniek, J.; Cedarbaum, J.; Brashear, R.; Miller, D. S. Neuropsychiatric Symptoms in Alzheimer's Disease. *Alzheimers Dement.* **2011**, *7* (5), 532–539. https://doi.org/10.1016/j.jalz.2011.05.2410.

(6) 2021 Alzheimer's Disease Facts and Figures. *Alzheimers Dement.* **2021**, *17* (3), 327–406. https://doi.org/10.1002/alz.12328.

(7) Katzman, R. The Prevalence and Malignancy of Alzheimer Disease: A Major Killer. *Arch. Neurol.* **1976**, *33* (4), 217–218. https://doi.org/10.1001/archneur.1976.00500040001001.

(8) Hardy, J. A.; Higgins, G. A. Alzheimer's Disease: The Amyloid Cascade Hypothesis. *Science* **1992**, *256* (5054), 184–185. https://doi.org/10.1126/science.1566067.

(9) McGeer, P. L.; McGeer, E. G. The Amyloid Cascade-Inflammatory Hypothesis of Alzheimer Disease: Implications for Therapy. *Acta Neuropathol. (Berl.)* **2013**, *126* (4), 479–497. https://doi.org/10.1007/s00401-013-1177-7.

(10) Iversen, L. L.; Mortishire-Smith, R. J.; Pollack, S. J.; Shearman, M. S. The Toxicity in Vitro of Beta-Amyloid Protein. *Biochem. J.* **1995**, *311* (Pt 1), 1–16. https://doi.org/10.1042/bj3110001

(11) Milton, N. G. Amyloid-Beta Binds Catalase with High Affinity and Inhibits Hydrogen Peroxide Breakdown. *Biochem. J.* **1999**, *344* (Pt 2), 293–296. PMID: 10567208

(12) Gibson Wood, W.; Eckert, G. P.; Igbavboa, U.; Müller, W. E. Amyloid Beta-Protein Interactions with Membranes and Cholesterol: Causes or Casualties of Alzheimer's Disease. *Biochim. Biophys. Acta BBA - Biomembr.* **2003**, *1610* (2), 281–290. https://doi.org/10.1016/S0005-2736(03)00025-7.

(13) Wilkinson, K.; Boyd, J. D.; Glicksman, M.; Moore, K. J.; El Khoury, J. A High Content Drug Screen Identifies Ursolic Acid as an Inhibitor of Amyloid β Protein Interactions with Its Receptor CD36*,. *J. Biol. Chem.* **2011**, *286* (40), 34914–34922. https://doi.org/10.1074/jbc.M111.232116.

(14) Herrup, K. The Case for Rejecting the Amyloid Cascade Hypothesis. *Nat. Neurosci.* **2015**, *18* (6), 794–799. https://doi.org/10.1038/nn.4017.

(15) Hardy, J. Alzheimer's Disease: The Amyloid Cascade Hypothesis: An Update and Reappraisal. *J. Alzheimers Dis.* **2006**, *9* (s3), 151–153. https://doi.org/10.3233/JAD-2006-9S317.

(16) Pimplikar, S. W. Reassessing the Amyloid Cascade Hypothesis of Alzheimer's Disease. *Int. J. Biochem. Cell Biol.* **2009**, *41* (6), 1261–1268. https://doi.org/10.1016/j.biocel.2008.12.015.

(17) Karran, E.; Strooper, B. D. The Amyloid Cascade Hypothesis: Are We Poised for Success or Failure? *J. Neurochem.* **2016**, *139* (S2), 237–252. https://doi.org/10.1111/jnc.13632.

(18) Coleman, P. D.; Yao, P. J. Synaptic Slaughter in Alzheimer's Disease. *Neurobiol. Aging* **2003**, *24* (8), 1023–1027. https://doi.org/10.1016/j.neurobiolaging.2003.09.001.

(19) Selkoe, D. J. Alzheimer's Disease Is a Synaptic Failure. *Science* **2002**, *298* (5594), 789–791. https://doi.org/10.1126/science.1074069.

(20) Terry, R. D.; Masliah, E.; Salmon, D. P.; Butters, N.; DeTeresa, R.; Hill, R.; Hansen, L. A.; Katzman, R. Physical Basis of Cognitive Alterations in Alzheimer's Disease: Synapse Loss Is the Major Correlate of Cognitive Impairment. *Ann. Neurol.* **1991**, *30* (4), 572–580. https://doi.org/10.1002/ana.410300410.

(21) Dillon, C.; Goda, Y. THE ACTIN CYTOSKELETON: Integrating Form and Function at the Synapse. *Annu. Rev. Neurosci.* **2005**, *28* (1), 25–55. https://doi.org/10.1146/annurev.neuro.28.061604.135757.

(22) Small, J. V.; Rottner, K.; Kaverina, I.; Anderson, K. I. Assembling an Actin Cytoskeleton for Cell Attachment and Movement. *Biochim. Biophys. Acta BBA - Mol. Cell Res.* **1998**, *1404* (3), 271–281. https://doi.org/10.1016/S0167-4889(98)00080-9.

(23) Stevens, C. F. The Neuron. *Sci. Am.* **1979**, *241* (3), 54–65. htpps://doi.org/ 10.1038/scientificamerican0979-54

(24) Jessen, K. R. Glial Cells. *Int. J. Biochem. Cell Biol.* **2004**, *36* (10), 1861–1867. https://doi.org/10.1016/j.biocel.2004.02.023.

(25) Konietzny, A.; Bär, J.; Mikhaylova, M. Dendritic Actin Cytoskeleton: Structure, Functions, and Regulations. *Front. Cell. Neurosci.* **2017**, *11*. https://doi.org/10.3389/fncel.2017.00147.

(26) Geraldo, S.; Gordon-Weeks, P. R. Cytoskeletal Dynamics in Growth-Cone Steering. *J. Cell Sci.* **2009**, *122* (20), 3595–3604. https://doi.org/10.1242/jcs.042309.

(27) Ziv, N. E.; Smith, S. J. Evidence for a Role of Dendritic Filopodia in Synaptogenesis and Spine Formation. *Neuron* **1996**, *17* (1), 91–102. https://doi.org/10.1016/S0896-6273(00)80283-4.

(28) Fiala, J. C.; Feinberg, M.; Popov, V.; Harris, K. M. Synaptogenesis Via Dendritic Filopodia in Developing Hippocampal Area CA1. *J. Neurosci.* **1998**, *18* (21), 8900–8911. https://doi.org/10.1523/JNEUROSCI.18-21-08900.1998.

(29) Portera-Cailliau, C.; Pan, D. T.; Yuste, R. Activity-Regulated Dynamic Behavior of Early Dendritic Protrusions: Evidence for Different Types of Dendritic Filopodia. *J. Neurosci.* **2003**, *23* (18), 7129–7142. https://doi.org/10.1523/JNEUROSCI.23-18-07129.2003.

(30) Sekino, Y.; Kojima, N.; Shirao, T. Role of Actin Cytoskeleton in Dendritic Spine Morphogenesis. *Neurochem. Int.* **2007**, *51* (2), 92–104. https://doi.org/10.1016/j.neuint.2007.04.029.

(31) Inbar, P.; Li, C. Q.; Takayama, S. A.; Bautista, M. R.; Yang, J. Oligo(Ethylene Glycol) Derivatives of Thioflavin T as Inhibitors of Protein–Amyloid Interactions. *ChemBioChem* **2006**, *7* (10), 1563–1566. https://doi.org/10.1002/cbic.200600119.

(32) Ps, V.; Cf, C. Fluorescent Stains, with Special Reference to Amyloid and Connective Tissues. *Arch. Pathol.* **1959**, *68*, 487–498. PMID: 13841452

(33) Biancalana, M.; Koide, S. Molecular Mechanism of Thioflavin-T Binding to Amyloid Fibrils. *Biochim. Biophys. Acta BBA - Proteins Proteomics* **2010**, *1804* (7), 1405–1412. https://doi.org/10.1016/j.bbapap.2010.04.001.

(34) Yang, N. J.; Hinner, M. J. Getting Across the Cell Membrane: An Overview for Small Molecules, Peptides, and Proteins. In *Site-Specific Protein Labeling: Methods and Protocols*; Gautier, A., Hinner, M. J., Eds.; Methods in Molecular Biology; Springer: New York, NY, 2015; pp 29–53. https://doi.org/10.1007/978-1-4939-2272-7_3.

(35) Veber, D. F.; Johnson, S. R.; Cheng, H.-Y.; Smith, B. R.; Ward, K. W.; Kopple, K. D. Molecular Properties That Influence the Oral Bioavailability of Drug Candidates. *J. Med. Chem.* **2002**, *45* (12), 2615–2623. https://doi.org/10.1021/jm020017n.

(36) Hamidi, M.; Azadi, A.; Rafiei, P. Pharmacokinetic Consequences of Pegylation. *Drug Deliv.* **2006**, *13* (6), 399–409. https://doi.org/10.1080/10717540600814402.

(37) Kang, J. S.; DeLuca, P. P.; Lee, K. C. Emerging PEGylated Drugs. *Expert Opin. Emerg. Drugs* **2009**, *14* (2), 363–380. https://doi.org/10.1517/14728210902907847.

(38) Kubetzko, S.; Sarkar, C. A.; Plückthun, A. Protein PEGylation Decreases Observed Target Association Rates via a Dual Blocking Mechanism. *Mol. Pharmacol.* **2005**, *68* (5), 1439–1454. https://doi.org/10.1124/mol.105.014910.

(39) Pfister, D.; Morbidelli, M. Process for Protein PEGylation. *J. Controlled Release* **2014**, *180*, 134–149. https://doi.org/10.1016/j.jconrel.2014.02.002.

(40) Habib, L. K.; Lee, M. T. C.; Yang, J. Inhibitors of Catalase-Amyloid Interactions Protect Cells from β-Amyloid-Induced Oxidative Stress and Toxicity*,. *J. Biol. Chem.* **2010**, *285* (50), 38933–38943. https://doi.org/10.1074/jbc.M110.132860.

(41) Olsen, J. S.; Brown, C.; Capule, C. C.; Rubinshtein, M.; Doran, T. M.; Srivastava, R. K.; Feng, C.; Nilsson, B. L.; Yang, J.; Dewhurst, S. Amyloid-Binding Small Molecules Efficiently Block SEVI (Semen-Derived Enhancer of Virus Infection)- and Semen-Mediated Enhancement of HIV-1 Infection*. *J. Biol. Chem.* **2010**, *285* (46), 35488–35496. https://doi.org/10.1074/jbc.M110.163659.

(42) Song, J. M.; DiBattista, A. M.; Sung, Y. M.; Ahn, J. M.; Turner, R. S.; Yang, J.; Pak, D. T. S.; Lee, H.-K.; Hoe, H.-S. A Tetra(Ethylene Glycol) Derivative of Benzothiazole Aniline Ameliorates Dendritic Spine Density and Cognitive Function in a Mouse Model of Alzheimer's Disease. *Exp. Neurol.* **2014**, *252*, 105–113. https://doi.org/10.1016/j.expneurol.2013.11.023.

(43) Megill, A.; Lee, T.; DiBattista, A. M.; Song, J. M.; Spitzer, M. H.; Rubinshtein, M.; Habib, L. K.; Capule, C. C.; Mayer, M.; Turner, R. S.; Kirkwood, A.; Yang, J.; Pak, D. T. S.; Lee, H.-K.; Hoe, H.-S. A Tetra(Ethylene Glycol) Derivative of Benzothiazole Aniline Enhances Ras-Mediated Spinogenesis. *J. Neurosci.* **2013**, *33* (22), 9306–9318. https://doi.org/10.1523/JNEUROSCI.1615-12.2013.

(44) Yoshihara, Y.; De Roo, M.; Muller, D. Dendritic Spine Formation and Stabilization. *Curr. Opin. Neurobiol.* **2009**, *19* (2), 146–153. https://doi.org/10.1016/j.conb.2009.05.013.

(45) Yuste, R. The Discovery of Dendritic Spines by Cajal. *Front. Neuroanat.* **2015**, *9*. https://doi.org/10.3389/fnana.2015.00018.

(46) Cifelli, J. L.; Dozier, L.; Chung, T. S.; Patrick, G. N.; Yang, J. Benzothiazole Amphiphiles Promote the Formation of Dendritic Spines in Primary Hippocampal Neurons. *J. Biol. Chem.* **2016**, *291* (23), 11981–11992. https://doi.org/10.1074/jbc.M115.701482.

(47) Cifelli, J. L.; Berg, K. R.; Yang, J. Benzothiazole Amphiphiles Promote RasGRF1-Associated Dendritic Spine Formation in Human Stem Cell-Derived Neurons. *FEBS Open Bio* **2020**, *10* (3), 386–395. https://doi.org/10.1002/2211-5463.12788.

(48) Sibucao, K. Photoaffinity Labeling Studies on a Promoter of Dendritic Spine Formation, UC San Diego, **2017**. Doctoral dissertation, University of California San Diego.

(49) Hashimoto, M.; Hatanaka, Y. Recent Progress in Diazirine-Based Photoaffinity Labeling. *Eur. J. Org. Chem.* **2008**, *2008* (15), 2513–2523. https://doi.org/10.1002/ejoc.200701069.

(50) Ge, S.-S.; Chen, B.; Wu, Y.-Y.; Long, Q.-S.; Zhao, Y.-L.; Wang, P.-Y.; Yang, S. Current Advances of Carbene-Mediated Photoaffinity Labeling in Medicinal Chemistry. *RSC Adv.* **2018**, *8* (51), 29428–29454. https://doi.org/10.1039/C8RA03538E.

(51) Sedeh, R. S.; Fedorov, A. A.; Fedorov, E. V.; Ono, S.; Matsumura, F.; Almo, S. C.; Bathe, M. Structure, Evolutionary Conservation, and Conformational Dynamics of Homo Sapiens Fascin-1, an F-Actin Crosslinking Protein. *J. Mol. Biol.* **2010**, *400* (3), 589–604. https://doi.org/10.1016/j.jmb.2010.04.043.

(52) Zhang, F.-R.; Tao, L.-H.; Shen, Z.-Y.; Lv, Z.; Xu, L.-Y.; Li, E.-M. Fascin Expression in Human Embryonic, Fetal, and Normal Adult Tissue. *J. Histochem. Cytochem.* **2008**, *56* (2), 193–199. https://doi.org/10.1369/jhc.7A7353.2007.

(53) Vignjevic, D.; Kojima, S.; Aratyn, Y.; Danciu, O.; Svitkina, T.; Borisy, G. G. Role of Fascin in Filopodial Protrusion. *J. Cell Biol.* **2006**, *174* (6), 863–875. https://doi.org/10.1083/jcb.200603013.

(54) Yang, S.; Huang, F.-K.; Huang, J.; Chen, S.; Jakoncic, J.; Leo-Macias, A.; Diaz-Avalos, R.; Chen, L.; Zhang, J. J.; Huang, X.-Y. Molecular Mechanism of Fascin Function in Filopodial Formation *. *J. Biol. Chem.* **2013**, *288* (1), 274–284. https://doi.org/10.1074/jbc.M112.427971.

(55) Claessens, M. M. a. E.; Semmrich, C.; Ramos, L.; Bausch, A. R. Helical Twist Controls the Thickness of F-Actin Bundles. *Proc. Natl. Acad. Sci.* **2008**, *105* (26), 8819–8822. https://doi.org/10.1073/pnas.0711149105.

(56) Winkelman, J. D.; Suarez, C.; Hocky, G. M.; Harker, A. J.; Morganthaler, A. N.; Christensen, J. R.; Voth, G. A.; Bartles, J. R.; Kovar, D. R. Fascin- and α-Actinin-Bundled Networks Contain Intrinsic Structural Features That Drive Protein Sorting. *Curr. Biol.* **2016**, *26* (20), 2697–2706. https://doi.org/10.1016/j.cub.2016.07.080.

(57) Pelosi, G.; Pastorino, U.; Pasini, F.; Maissoneuve, P.; Fraggetta, F.; Lannucci, A.; Sonzogni, A.; De Manzoni, G.; Terzi, A.; Durante, E.; Bresaola, E.; Pezzella, F.; Viale, G. Independent Prognostic Value of Fascin Immunoreactivity in Stage I Nonsmall Cell Lung Cancer. *Br. J. Cancer* **2003**, *88* (4), 537–547. https://doi.org/10.1038/sj.bjc.6600731.

(58) Rodrigues, P. C.; Sawazaki-Calone, I.; Ervolino de Oliveira, C.; Soares Macedo, C. C.; Dourado, M. R.; Cervigne, N. K.; Miguel, M. C.; Ferreira do Carmo, A.; Lambert, D. W.; Graner, E.; Daniela da Silva, S.; Alaoui-Jamali, M. A.; Paes Leme, A. F.; Salo, T. A.; Coletta, R. D. Fascin Promotes Migration and Invasion and Is a Prognostic Marker for Oral Squamous Cell Carcinoma. *Oncotarget* **2017**, *8* (43), 74736–74754. https://doi.org/10.18632/oncotarget.20360.

(59) Gun, B. D.; Bahadir, B.; Bektas, S.; Barut, F.; Yurdakan, G.; Kandemir, N. O.; Ozdamar, S. O. Clinicopathological Significance of Fascin and CD44v6 Expression in Endometrioid Carcinoma. *Diagn. Pathol.* **2012**, *7* (1), 80. https://doi.org/10.1186/1746-1596-7-80.

(60) Valkov, A.; Sorbye, S. W.; Kilvaer, T. K.; Donnem, T.; Smeland, E.; Bremnes, R. M.; Busund, L.-T. The Prognostic Impact of TGF-B1, Fascin, NF-KB and PKC-ζ Expression in Soft Tissue Sarcomas. *PLOS ONE* **2011**, *6* (3), e17507. https://doi.org/10.1371/journal.pone.0017507.

(61) Machesky, L. M.; Li, A. Fascin. *Commun. Integr. Biol.* **2010**, *3* (3), 263–270. https://doi.org/10.4161/cib.3.3.11556.

(62) Van Audenhove, I.; Denert, M.; Boucherie, C.; Pieters, L.; Cornelissen, M.; Gettemans, J. Fascin Rigidity and L-Plastin Flexibility Cooperate in Cancer Cell Invadopodia and Filopodia*. *J. Biol. Chem.* **2016**, *291* (17), 9148–9160. https://doi.org/10.1074/jbc.M115.706937.

(63) Li, A.; Dawson, J. C.; Forero-Vargas, M.; Spence, H. J.; Yu, X.; König, I.; Anderson, K.; Machesky, L. M. The Actin-Bundling Protein Fascin Stabilizes Actin in Invadopodia and Potentiates Protrusive Invasion. *Curr. Biol.* **2010**, *20* (4), 339–345. https://doi.org/10.1016/j.cub.2009.12.035.

(64) Lin, S.; Taylor, M. D.; Singh, P. K.; Yang, S. How Does Fascin Promote Cancer Metastasis? *FEBS J.* **2021**, *288* (5), 1434–1446. https://doi.org/10.1111/febs.15484.

(65) Jacquemet, G.; Hamidi, H.; Ivaska, J. Filopodia in Cell Adhesion, 3D Migration and Cancer Cell Invasion. *Curr. Opin. Cell Biol.* **2015**, *36*, 23–31. https://doi.org/10.1016/j.ceb.2015.06.007.

(66) Jayo, A.; Malboubi, M.; Antoku, S.; Chang, W.; Ortiz-Zapater, E.; Groen, C.; Pfisterer, K.; Tootle, T.; Charras, G.; Gundersen, G. G.; Parsons, M. Fascin Regulates Nuclear Movement and Deformation in Migrating Cells. *Dev. Cell* **2016**, *38* (4), 371–383. https://doi.org/10.1016/j.devcel.2016.07.021.

(67) Pfisterer, K.; Jayo, A.; Parsons, M. Control of Nuclear Organization by F-Actin Binding Proteins. *Nucleus* **2017**, *8* (2), 126–133. https://doi.org/10.1080/19491034.2016.1267093.

(68) Zanet, J.; Jayo, A.; Plaza, S.; Millard, T.; Parsons, M.; Stramer, B. Fascin Promotes Filopodia Formation Independent of Its Role in Actin Bundling. *J. Cell Biol.* **2012**, *197* (4), 477–486. https://doi.org/10.1083/jcb.201110135.

(69) Oak, Y. Filopodia-Independent Roles of the Actin Bundling Protein Fascin in Promoting Cell Motility. **2014**. Doctoral dissertation, Harvard University

(70) Lamb, M. C.; Tootle, T. L. Fascin in Cell Migration: More Than an Actin Bundling Protein. *Biology* **2020**, *9* (11), 403. https://doi.org/10.3390/biology9110403.

(71) Elkhatib, N.; Neu, M. B.; Zensen, C.; Schmoller, K. M.; Louvard, D.; Bausch, A. R.; Betz, T.; Vignjevic, D. M. Fascin Plays a Role in Stress Fiber Organization and Focal Adhesion Disassembly. *Curr. Biol.* **2014**, *24* (13), 1492–1499. https://doi.org/10.1016/j.cub.2014.05.023.

(72) Zhang, J.; Fonovic, M.; Suyama, K.; Bogyo, M.; Scott, M. P. Rab35 Controls Actin Bundling by Recruiting Fascin as an Effector Protein. *Science* **2009**, *325* (5945), 1250–1254. https://doi.org/10.1126/science.1174921.

(73) Beghein, E.; Devriese, D.; Van Hoey, E.; Gettemans, J. Cortactin and Fascin-1 Regulate Extracellular Vesicle Release by Controlling Endosomal Trafficking or Invadopodia Formation and Function. *Sci. Rep.* **2018**, *8* (1), 15606. https://doi.org/10.1038/s41598-018-33868-z.

(74) Saad, A.; Bijian, K.; Qiu, D.; da Silva, S. D.; Marques, M.; Chang, C.-H.; Nassour, H.; Ramotar, D.; Damaraju, S.; Mackey, J.; Bismar, T.; Witcher, M.; Alaoui-Jamali, M. A. Insights into a Novel Nuclear Function for Fascin in the Regulation of the Amino-Acid Transporter SLC3A2. *Sci. Rep.* **2016**, *6* (1), 36699. https://doi.org/10.1038/srep36699.

(75) Korobova, F.; Svitkina, T. Molecular Architecture of Synaptic Actin Cytoskeleton in Hippocampal Neurons Reveals a Mechanism of Dendritic Spine Morphogenesis. *Mol. Biol. Cell* **2009**, *21* (1), 165–176. https://doi.org/10.1091/mbc.e09-07-0596.

(76) Doudna, J. A.; Charpentier, E. The New Frontier of Genome Engineering with CRISPR-Cas9. *Science* **2014**, *346* (6213). https://doi.org/10.1126/science.1258096.

(77) Hsu, P. D.; Lander, E. S.; Zhang, F. Development and Applications of CRISPR-Cas9 for Genome Engineering. *Cell* **2014**, *157* (6), 1262–1278. https://doi.org/10.1016/j.cell.2014.05.010.

(78) Ran, F. A.; Hsu, P. D.; Wright, J.; Agarwala, V.; Scott, D. A.; Zhang, F. Genome Engineering Using the CRISPR-Cas9 System. *Nat. Protoc.* **2013**, *8* (11), 2281–2308. https://doi.org/10.1038/nprot.2013.143.

(79) Wang, J.; Lu, Z.; Wientjes, M. G.; Au, J. L.-S. Delivery of SiRNA Therapeutics: Barriers and Carriers. *AAPS J.* **2010**, *12* (4), 492–503. https://doi.org/10.1208/s12248-010-9210-4.

(80) Gunawardane, L. S.; Saito, K.; Nishida, K. M.; Miyoshi, K.; Kawamura, Y.; Nagami, T.; Siomi, H.; Siomi, M. C. A Slicer-Mediated Mechanism for Repeat-Associated SiRNA 5' End Formation in Drosophila. *Science* **2007**, *315* (5818), 1587–1590. https://doi.org/10.1126/science.1140494.

(81) Altschul, S. F.; Madden, T. L.; Schäffer, A. A.; Zhang, J.; Zhang, Z.; Miller, W.; Lipman, D. J. Gapped BLAST and PSI-BLAST: A New Generation of Protein Database Search Programs. *Nucleic Acids Res.* **1997**, *25* (17), 3389–3402. https://doi.org/10.1093/nar/25.17.3389.

(82) Zhang, Z.; Schwartz, S.; Wagner, L.; Miller, W. A Greedy Algorithm for Aligning DNA Sequences. *J. Comput. Biol. J. Comput. Mol. Cell Biol.* **2000**, *7* (1–2), 203–214. https://doi.org/10.1089/10665270050081478.

(83) Thomsen, D. R.; Stenberg, R. M.; Goins, W. F.; Stinski, M. F. Promoter-Regulatory Region of the Major Immediate Early Gene of Human Cytomegalovirus. *Proc. Natl. Acad. Sci.* **1984**, *81* (3), 659–663. https://doi.org/10.1073/pnas.81.3.659.

(84) Pol, A. N. van den; Ghosh, P. K. Selective Neuronal Expression of Green Fluorescent Protein with Cytomegalovirus Promoter Reveals Entire Neuronal Arbor in Transgenic Mice. *J. Neurosci.* **1998**, *18* (24), 10640–10651. https://doi.org/10.1523/JNEUROSCI.18-24-10640.1998.

(85) Dalby, B.; Cates, S.; Harris, A.; Ohki, E. C.; Tilkins, M. L.; Price, P. J.; Ciccarone, V. C. Advanced Transfection with Lipofectamine 2000 Reagent: Primary Neurons, SiRNA, and High-Throughput Applications. *Methods* **2004**, *33* (2), 95–103. https://doi.org/10.1016/j.ymeth.2003.11.023.

(86) Kingston, R. E.; Chen, C. A.; Rose, J. K. Calcium Phosphate Transfection. *Curr. Protoc. Mol. Biol.* **2003**, *Chapter 9*, Unit 9.1. https://doi.org/10.1002/0471142727.mb0901s63.

(87) Das, K. P.; Freudenrich, T. M.; Mundy, W. R. Assessment of PC12 Cell Differentiation and Neurite Growth: A Comparison of Morphological and Neurochemical Measures. *Neurotoxicol. Teratol.* **2004**, *26* (3), 397–406. https://doi.org/10.1016/j.ntt.2004.02.006.

(88) Guroff, G. PC12 Cells as a Model of Neuronal Differentiation. In *Cell Culture in the Neurosciences*; Bottenstein, J. E., Sato, G., Eds.; Current Topics in Neurobiology; Springer US: Boston, MA, 1985; pp 245–272. https://doi.org/10.1007/978-1-4613-2473-7_8.

(89) Radio, N. M.; Breier, J. M.; Shafer, T. J.; Mundy, W. R. Assessment of Chemical Effects on Neurite Outgrowth in PC12 Cells Using High Content Screening. *Toxicol. Sci.* **2008**, *105* (1), 106–118. https://doi.org/10.1093/toxsci/kfn114.

(90) Westerink, R. H. S.; Ewing, A. G. The PC12 Cell as Model for Neurosecretion. *Acta Physiol.* **2008**, *192* (2), 273–285. https://doi.org/10.1111/j.1748-1716.2007.01805.x.

(91) Schindelin, J.; Arganda-Carreras, I.; Frise, E.; Kaynig, V.; Longair, M.; Pietzsch, T.; Preibisch, S.; Rueden, C.; Saalfeld, S.; Schmid, B.; Tinevez, J.-Y.; White, D. J.; Hartenstein, V.; Eliceiri, K.; Tomancak, P.; Cardona, A. Fiji: An Open-Source Platform for Biological-Image Analysis. *Nat. Methods* **2012**, *9* (7), 676–682. https://doi.org/10.1038/nmeth.2019.

(92) Goldstein, J. I.; Newbury, D. E.; Michael, J. R.; Ritchie, N. W. M.; Scott, J. H. J.; Joy, D. C. ImageJ and Fiji. In *Scanning Electron Microscopy and X-Ray Microanalysis*; Goldstein, J. I., Newbury, D. E., Michael, J. R., Ritchie, N. W. M., Scott, J. H. J., Joy, D. C., Eds.; Springer: New York, NY, 2018; pp 187–193. https://doi.org/10.1007/978-1-4939-6676-9_13.

(93) Kocsis, E.; Trus, B. L.; Steer, C. J.; Bisher, M. E.; Steven, A. C. Image Averaging of Flexible Fibrous Macromolecules: The Clathrin Triskelion Has an Elastic

Proximal Segment. *J. Struct. Biol.* **1991**, *107* (1), 6–14. https://doi.org/10.1016/1047-8477(91)90025-r.

(94) Cartier, A. E.; Djakovic, S. N.; Salehi, A.; Wilson, S. M.; Masliah, E.; Patrick, G. N. Regulation of Synaptic Structure by Ubiquitin C-Terminal Hydrolase L1. *J. Neurosci. Off. J. Soc. Neurosci.* **2009**, *29* (24), 7857–7868. https://doi.org/10.1523/JNEUROSCI.1817-09.2009.

(95) Schwarz, L. A.; Hall, B. J.; Patrick, G. N. Activity-Dependent Ubiquitination of GluA1 Mediates a Distinct AMPA Receptor Endocytosis and Sorting Pathway. *J. Neurosci. Off. J. Soc. Neurosci.* **2010**, *30* (49), 16718–16729. https://doi.org/10.1523/JNEUROSCI.3686-10.2010.

(96) Djakovic, S. N.; Schwarz, L. A.; Barylko, B.; DeMartino, G. N.; Patrick, G. N. Regulation of the Proteasome by Neuronal Activity and Calcium/Calmodulin-Dependent Protein Kinase II. *J. Biol. Chem.* **2009**, *284* (39), 26655–26665. https://doi.org/10.1074/jbc.M109.021956.

(97) Schneider, C. A.; Rasband, W. S.; Eliceiri, K. W. NIH Image to ImageJ: 25 Years of Image Analysis. *Nat. Methods* **2012**, *9* (7), 671–675. https://doi.org/10.1038/nmeth.2089

(98) The UniProt Consortium. UniProt: The Universal Protein Knowledgebase in 2021. *Nucleic Acids Res.* **2021**, *49* (D1), D480–D489. https://doi.org/10.1093/nar/gkaa1100.

(99) Zhang, L.; Elias, J. E. Relative Protein Quantification Using Tandem Mass Tag Mass Spectrometry. In *Proteomics: Methods and Protocols*; Comai, L., Katz, J. E., Mallick, P., Eds.; Methods in Molecular Biology; Springer: New York, NY, 2017; pp 185–198. https://doi.org/10.1007/978-1-4939-6747-6_14.

(100) Edwards, R. A.; Bryan, J. Fascins, a family of actin bundling proteins. *Cell Motil.* **1995**, *32* (1), 1–9. https://doi.org/10.1002/cm.970320102.

(101) Asanuma, K.; Kim, K.; Oh, J.; Giardino, L.; Chabanis, S.; Faul, C.; Reiser, J.; Mundel, P. Synaptopodin Regulates the Actin-Bundling Activity of α-Actinin in an Isoform-Specific Manner. *J. Clin. Invest.* **2005**, *115* (5), 1188–1198. https://doi.org/10.1172/JCI23371.

(102) Meyer, R. K.; Aebi, U. Bundling of Actin Filaments by Alpha-Actinin Depends on Its Molecular Length. *J. Cell Biol.* **1990**, *110* (6), 2013–2024. https://doi.org/10.1083/jcb.110.6.2013.

(103) Otto, J. J. Actin-Bundling Proteins. *Curr. Opin. Cell Biol.* **1994**, *6* (1), 105–109. https://doi.org/10.1016/0955-0674(94)90123-6.

(104) Honda, K.; Yamada, T.; Endo, R.; Ino, Y.; Gotoh, M.; Tsuda, H.; Yamada, Y.; Chiba, H.; Hirohashi, S. Actinin-4, a Novel Actin-Bundling Protein Associated with Cell Motility and Cancer Invasion. *J. Cell Biol.* **1998**, *140* (6), 1383–1393. https://doi.org/10.1083/jcb.140.6.1383.

(105) Burridge, K.; Chrzanowska-Wodnicka, M.; Zhong, C. Focal Adhesion Assembly. *Trends Cell Biol.* **1997**, *7* (9), 342–347. https://doi.org/10.1016/S0962-8924(97)01127-6.

(106) Sun, Z.; Lambacher, A.; Fässler, R. Nascent Adhesions: From Fluctuations to a Hierarchical Organization. *Curr. Biol.* **2014**, *24* (17), R801–R803. https://doi.org/10.1016/j.cub.2014.07.061.

(107) Geiger, T.; Zaidel-Bar, R. Opening the Floodgates: Proteomics and the Integrin Adhesome. *Curr. Opin. Cell Biol.* **2012**, *24* (5), 562–568. https://doi.org/10.1016/j.ceb.2012.05.004.

(108) Tojkander, S.; Gateva, G.; Lappalainen, P. Actin Stress Fibers – Assembly, Dynamics and Biological Roles. *J. Cell Sci.* **2012**, *125* (8), 1855–1864. https://doi.org/10.1242/jcs.098087.

(109) Pring, M.; Weber, A.; Bubb, M. R. Profilin-Actin Complexes Directly Elongate Actin Filaments at the Barbed End. *Biochemistry* **1992**, *31* (6), 1827–1836. https://doi.org/10.1021/bi00121a035.

(110) Neuhaus, J. M.; Wanger, M.; Keiser, T.; Wegner, A. Treadmilling of Actin. *J. Muscle Res. Cell Motil.* **1983**, *4* (5), 507–527. https://doi.org/10.1007/BF00712112.

(111) Rust, M. B. ADF/Cofilin: A Crucial Regulator of Synapse Physiology and Behavior. *Cell. Mol. Life Sci.* **2015**, *72* (18), 3521–3529. https://doi.org/10.1007/s00018-015-1941-z.

(112) Choi, C. K.; Vicente-Manzanares, M.; Zareno, J.; Whitmore, L. A.; Mogilner, A.; Horwitz, A. R. Actin and α-Actinin Orchestrate the Assembly and Maturation of Nascent Adhesions in a Myosin II Motor-Independent Manner. *Nat. Cell Biol.* **2008**, *10* (9), 1039–1050. https://doi.org/ 10.1038/ncb1763

(113) Oakes, P. W.; Beckham, Y.; Stricker, J.; Gardel, M. L. Tension Is Required but Not Sufficient for Focal Adhesion Maturation without a Stress Fiber Template. *J. Cell Biol.* **2012**, *196* (3), 363–374. https://doi.org/10.1083/jcb.201107042.

(114) Kovac, B.; Teo, J. L.; Mäkelä, T. P.; Vallenius, T. Assembly of Non-Contractile Dorsal Stress Fibers Requires α-Actinin-1 and Rac1 in Migrating and Spreading Cells. *J. Cell Sci.* **2013**, *126* (1), 263–273. https://doi.org/10.1242/jcs.115063.

(115) Pavalko, F. M.; Burridge, K. Disruption of the Actin Cytoskeleton after Microinjection of Proteolytic Fragments of Alpha-Actinin. *J. Cell Biol.* **1991**, *114* (3), 481–491. https://doi.org/10.1083/jcb.114.3.481.

(116) Hu, S.; Dasbiswas, K.; Guo, Z.; Tee, Y.-H.; Thiagarajan, V.; Hersen, P.; Chew, T.-L.; Safran, S. A.; Zaidel-Bar, R.; Bershadsky, A. D. Long-Range Self-Organization of Cytoskeletal Myosin II Filament Stacks. *Nat. Cell Biol.* **2017**, *19* (2), 133–141. https://doi.org/10.1038/ncb3466.

(117) Fukumoto, M.; Kurisu, S.; Yamada, T.; Takenawa, T. α-Actinin-4 Enhances Colorectal Cancer Cell Invasion by Suppressing Focal Adhesion Maturation. *PLOS ONE* **2015**, *10* (4), e0120616. https://doi.org/10.1371/journal.pone.0120616.

(118) Kemp, J. P.; Brieher, W. M. The Actin Filament Bundling Protein α-Actinin-4 Actually Suppresses Actin Stress Fibers by Permitting Actin Turnover. *J. Biol. Chem.* **2018**, *293* (37), 14520–14533. https://doi.org/10.1074/jbc.RA118.004345.

(119) Lilja, J.; Ivaska, J. Integrin Activity in Neuronal Connectivity. *J. Cell Sci.* **2018**, *131* (jcs212803). https://doi.org/10.1242/jcs.212803.

(120) Moeller, M. L.; Shi, Y.; Reichardt, L. F.; Ethell, I. M. EphB Receptors Regulate Dendritic Spine Morphogenesis through the Recruitment/Phosphorylation of Focal Adhesion Kinase and RhoA Activation*. *J. Biol. Chem.* **2006**, *281* (3), 1587–1598. https://doi.org/10.1074/jbc.M511756200.

(121) Shi, Y.; Pontrello, C. G.; DeFea, K. A.; Reichardt, L. F.; Ethell, I. M. Focal Adhesion Kinase Acts Downstream of EphB Receptors to Maintain Mature

Dendritic Spines by Regulating Cofilin Activity. *J. Neurosci.* **2009**, *29* (25), 8129–8142. https://doi.org/10.1523/JNEUROSCI.4681-08.2009.

(122) Collins, B. M.; McCoy, A. J.; Kent, H. M.; Evans, P. R.; Owen, D. J. Molecular Architecture and Functional Model of the Endocytic AP2 Complex. *Cell* **2002**, *109* (4), 523–535. https://doi.org/10.1016/S0092-8674(02)00735-3.

(123) Piguel, N. H.; Fievre, S.; Blanc, J.-M.; Carta, M.; Moreau, M. M.; Moutin, E.; Pinheiro, V. L.; Medina, C.; Ezan, J.; Lasvaux, L.; Loll, F.; Durand, C. M.; Chang, K.; Petralia, R. S.; Wenthold, R. J.; Stephenson, F. A.; Vuillard, L.; Darbon, H.; Perroy, J.; Mulle, C.; Montcouquiol, M.; Racca, C.; Sans, N. Scribble1/AP2 Complex Coordinates NMDA Receptor Endocytic Recycling. *Cell Rep.* **2014**, *9* (2), 712–727. https://doi.org/10.1016/j.celrep.2014.09.017.

(124) Fiuza, M.; Rostosky, C. M.; Parkinson, G. T.; Bygrave, A. M.; Halemani, N.; Baptista, M.; Milosevic, I.; Hanley, J. G. PICK1 Regulates AMPA Receptor Endocytosis via Direct Interactions with AP2 α-Appendage and Dynamin. *J. Cell Biol.* **2017**, *216* (10), 3323–3338. https://doi.org/10.1083/jcb.201701034.

(125) Kittler, J. T.; Delmas, P.; Jovanovic, J. N.; Brown, D. A.; Smart, T. G.; Moss, S. J. Constitutive Endocytosis of GABAA Receptors by an Association with the Adaptin AP2 Complex Modulates Inhibitory Synaptic Currents in Hippocampal Neurons. *J. Neurosci.* **2000**, *20* (21), 7972–7977. https://doi.org/10.1523/JNEUROSCI.20-21-07972.2000.

(126) De Franceschi, N.; Arjonen, A.; Elkhatib, N.; Denessiouk, K.; Wrobel, A. G.; Wilson, T. A.; Pouwels, J.; Montagnac, G.; Owen, D. J.; Ivaska, J. Selective Integrin Endocytosis Is Driven by Interactions between the Integrin α-Chain and AP2. *Nat. Struct. Mol. Biol.* **2016**, *23* (2), 172–179. https://doi.org/10.1038/nsmb.3161.

(127) Villari, G.; Jayo, A.; Zanet, J.; Fitch, B.; Serrels, B.; Frame, M.; Stramer, B. M.; Goult, B. T.; Parsons, M. A Direct Interaction between Fascin and Microtubules Contributes to Adhesion Dynamics and Cell Migration. *J. Cell Sci.* **2015**, *128* (24), 4601–4614. https://doi.org/10.1242/jcs.175760.

(128) Gu, J.; Zheng, J. Q. Microtubules in Dendritic Spine Development and Plasticity. *Open Neurosci. J.* **2009**, *3*, 128–133. https://doi.org/10.2174/1874082000903020128.

(129) Dent, E. W. Dynamic Microtubules at the Synapse. *Curr. Opin. Neurobiol.* **2020**, *63*, 9–14. https://doi.org/10.1016/j.conb.2020.01.003.

(130) Jaworski, J.; Kapitein, L. C.; Gouveia, S. M.; Dortland, B. R.; Wulf, P. S.; Grigoriev, I.; Camera, P.; Spangler, S. A.; Di Stefano, P.; Demmers, J.; Krugers, H.; Defilippi, P.; Akhmanova, A.; Hoogenraad, C. C. Dynamic Microtubules Regulate Dendritic Spine Morphology and Synaptic Plasticity. *Neuron* **2009**, *61* (1), 85–100. https://doi.org/10.1016/j.neuron.2008.11.013.

(131) Lapek, J. D.; Lewinski, M. K.; Wozniak, J. M.; Guatelli, J.; Gonzalez, D. J. Quantitative Temporal Viromics of an Inducible HIV-1 Model Yields Insight to Global Host Targets and Phospho-Dynamics Associated with Protein Vpr*. *Mol. Cell. Proteomics* **2017**, *16* (8), 1447–1461. https://doi.org/10.1074/mcp.M116.066019.

(132) Huang, J.; Dey, R.; Wang, Y.; Jakoncic, J.; Kurinov, I.; Huang, X.-Y. Structural Insights into the Induced-Fit Inhibition of Fascin by a Small-Molecule Inhibitor. *J. Mol. Biol.* **2018**, *430* (9), 1324–1335. https://doi.org/10.1016/j.jmb.2018.03.009.

(133) Francis, S.; Croft, D.; Schüttelkopf, A. W.; Parry, C.; Pugliese, A.; Cameron, K.; Claydon, S.; Drysdale, M.; Gardner, C.; Gohlke, A.; Goodwin, G.; Gray, C. H.; Konczal, J.; McDonald, L.; Mezna, M.; Pannifer, A.; Paul, N. R.; Machesky, L.; McKinnon, H.; Bower, J. Structure-Based Design, Synthesis and Biological Evaluation of a Novel Series of Isoquinolone and Pyrazolo[4,3-c]Pyridine Inhibitors of Fascin 1 as Potential Anti-Metastatic Agents. *Bioorg. Med. Chem. Lett.* **2019**, *29* (8), 1023–1029. https://doi.org/10.1016/j.bmcl.2019.01.035.

(134) Jansen, S.; Collins, A.; Yang, C.; Rebowski, G.; Svitkina, T.; Dominguez, R. Mechanism of Actin Filament Bundling by Fascin. *J. Biol. Chem.* **2011**, *286* (34), 30087–30096. https://doi.org/10.1074/jbc.M111.251439.

(135) Chen, L.; Yang, S.; Jakoncic, J.; Zhang, J. J.; Huang, X.-Y. Migrastatin Analogues Target Fascin to Block Tumour Metastasis. *Nature* **2010**, *464* (7291), 1062–1066. https://doi.org/10.1038/nature08978.

(136) Dessau, M. A.; Modis, Y. Protein Crystallization for X-Ray Crystallography. *JoVE J. Vis. Exp.* **2011**, No. 47, e2285. https://doi.org/10.3791/2285.

(137) Kabsch, W. XDS *Acta Crystallogr D Biol Crystallogr.* **2010** Feb;66(Pt 2):125-32. https://doi.org/10.1107/S0907444909047337.

(138) McCoy, A. J.; Grosse-Kunstleve, R. W.; Adams, P. D.; Winn, M. D.; Storoni, L. C.; Read, R. J. Phaser Crystallographic Software. *J. Appl. Crystallogr.* **2007**, *40* (Pt 4), 658–674. https://doi.org/10.1107/S0021889807021206.

(139) Emsley P, Lohkamp B, Scott WG, Cowtan K. Features and development of Coot. *Acta Crystallogr D Biol Crystallogr.* **2010** Apr;66(Pt 4):486-501. https://doi.org/10.1107/S0907444910007493.

(140) Adams, P. D.; Afonine, P. V.; Bunkóczi, G.; Chen, V. B.; Davis, I. W.; Echols, N.; Headd, J. J.; Hung, L.-W.; Kapral, G. J.; Grosse-Kunstleve, R. W.; McCoy, A. J.; Moriarty, N. W.; Oeffner, R.; Read, R. J.; Richardson, D. C.; Richardson, J. S.; Terwilliger, T. C.; Zwart, P. H. PHENIX: A Comprehensive Python-Based System for Macromolecular Structure Solution. *Acta Crystallogr. D Biol. Crystallogr.* **2010**, *66* (Pt 2), 213–221. https://doi.org/10.1107/S0907444909052925.

(141) Cavanagh, J.; Fairbrother, W. J.; III, A. G. P.; Skelton, N. J. *Protein NMR Spectroscopy: Principles and Practice*; Elsevier, 1995.

(142) M, I.; Le, K.; A, B. A Novel Approach for Sequential Assignment of 1H, 13C, and 15N Spectra of Proteins: Heteronuclear Triple-Resonance Three-Dimensional NMR Spectroscopy. Application to Calmodulin. *Biochemistry* **1990**, *29* (19), 4659–4667. https://doi.org/10.1021/bi00471a022.

(143) Farmer, B. T.; Venters, R. A.; Spicer, L. D.; Wittekind, M. G.; Müller, L. A Refocused and Optimized HNCA: Increased Sensitivity and Resolution in Large Macromolecules. *J. Biomol. NMR* **1992**, *2* (2), 195–202. https://doi.org/10.1007/BF01875530.

(144) Grzesiek, S.; Bax, A. An Efficient Experiment For Sequential Backbone Assignment of Medium-Sized Isotopically Enriched Proteins. *J. Magn. Reson.* **1992**, *Vol. 99, H. 1*, 201–207.

(145) Pervushin, K.; Riek, R.; Wider, G.; Wüthrich, K. Attenuated T2 Relaxation by Mutual Cancellation of Dipole–Dipole Coupling and Chemical Shift Anisotropy Indicates an Avenue to NMR Structures of Very Large Biological Macromolecules in Solution. *Proc. Natl. Acad. Sci.* **1997**, *94* (23), 12366–12371. https://doi.org/10.1073/pnas.94.23.12366.

(146) F, D.; S, G.; Gw, V.; G, Z.; J, P.; A, B. NMRPipe: A Multidimensional Spectral Processing System Based on UNIX Pipes. *J. Biomol. NMR* **1995**, *6* (3), 277–293. https://doi.org/10.1007/bf00197809.

(147) Riek, R.; Pervushin, K.; Wüthrich, K. TROSY and CRINEPT: NMR with Large Molecular and Supramolecular Structures in Solution. *Trends Biochem. Sci.* **2000**, *25* (10), 462–468. https://doi.org/10.1016/S0968-0004(00)01665-0.

(148) Kay, L. E.; Ikura, M.; Tschudin, R.; Bax, A. Three-Dimensional Triple-Resonance NMR Spectroscopy of Isotopically Enriched Proteins. *J. Magn. Reson. 1969* **1990**, *89* (3), 496–514. https://doi.org/10.1016/0022-2364(90)90333-5.

(149) Ulrich, E. L.; Akutsu, H.; Doreleijers, J. F.; Harano, Y.; Ioannidis, Y. E.; Lin, J.; Livny, M.; Mading, S.; Maziuk, D.; Miller, Z.; Nakatani, E.; Schulte, C. F.; Tolmie, D. E.; Kent Wenger, R.; Yao, H.; Markley, J. L. BioMagResBank. *Nucleic Acids Res.* **2008**, *36* (suppl_1), D402–D408. https://doi.org/10.1093/nar/gkm957.

(150) A, B.; M, I. An Efficient 3D NMR Technique for Correlating the Proton and 15N Backbone Amide Resonances with the Alpha-Carbon of the Preceding Residue in Uniformly 15N/13C Enriched Proteins. *J. Biomol. NMR* **1991**, *1* (1), 99–104. https://doi.org/10.1007/bf01874573.

(151) Nanda, A.; Nasker, S. S.; Mehra, A.; Panda, S.; Nayak, S. Inteins in Science: Evolution to Application. *Microorganisms* **2020**, *8* (12), 2004. https://doi.org/10.3390/microorganisms8122004.

(152) Stevens, A. J.; Brown, Z. Z.; Shah, N. H.; Sekar, G.; Cowburn, D.; Muir, T. W. Design of a Split Intein with Exceptional Protein Splicing Activity. *J. Am. Chem. Soc.* **2016**, *138* (7), 2162–2165. https://doi.org/10.1021/jacs.5b13528.

(153) Stevens, A. J.; Sekar, G.; Shah, N. H.; Mostafavi, A. Z.; Cowburn, D.; Muir, T. W. A Promiscuous Split Intein with Expanded Protein Engineering Applications. *Proc. Natl. Acad. Sci.* **2017**, *114* (32), 8538–8543. https://doi.org/10.1073/pnas.1701083114.

(154) Vikström, D.; Schlegel, S.; DeGier, J.-W. Production of Routine and Difficult Targets. *Genet. Eng. Biotechnol. News* **2013**, *33* (13), 37–37. https://doi.org/10.1089/gen.33.13.20.

(155) Gupta, S.; Tycko, R. Segmental Isotopic Labeling of HIV-1 Capsid Protein Assemblies for Solid State NMR. *J. Biomol. NMR* **2018**, *70* (2), 103–114. https://doi.org/10.1007/s10858-017-0162-1.